UNIVERSITY OF OKLAHOMA

GRADUATE COLLEGE

LITHOFACIES AND SEQUENCE STRATIGRAPHIC FRAMEWORK OF THE

BARNETT SHALE, NORTHEAST TEXAS

A DISSERTATION

SUBMITTED TO THE GRADUATE FACULTY

in partial fulfillment of the requirements for the

Degree of

DOCTOR OF PHILOSOPHY

By

PRERNA SINGH
Norman, Oklahoma
2008

LITHOFACIES AND SEQUENCE STRATIGRAPHIC FRAMEWORK OF
THE BARNETT SHALE, NORTHEAST TEXAS

A DISSERTATION APPROVED FOR THE
SCHOOL OF GEOLOGY AND GEOPHYSICS

By

_____
Dr. Roger M. Slatt, Chair

_____
Dr. James M. Forgotson, Jr.

_____
Dr. R. Douglas Elmore

_____
Dr. Chandra S. Rai

_____
Dr. William Coffey

Acknowledgments

I feel immense pleasure in expressing my deepest sense of gratitude to my advisor, Dr. Roger M. Slatt for his guidance, instruction, counsel, tireless patience, and for having trust in me.

Dr. James M. Forgotson, Dr. Doug Elmore, Dr. Chandra Rai, and Dr. Bill Coffey are acknowledged for their reviews and all the efforts they put into serving on my Ph.D. committee.

I would also like to give special thanks to the professors Dr. Roger Slatt, Dr. John Piggott, Dr. James Forgotson, Dr. Chandra Rai, and Dr. Roger Young for their eloquent teachings during this degree program and helping me hone my skills and learn the process of 'investigation and researching'. A number of individuals have provided analytical support to this study. I would like to thank Dr. Robert Loucks, Kitty Milliken, Tony D'Agostino, George Pemberton, Eric Eslinger, and Kevin Bohacs for their constructive discussion and help during my learning process of the fine-grained rocks. I would like to thank Dr. Bob Wright for providing insightful details on macrofossils of the Barnett Shale. I would also like to acknowledge Bill Coffey, Mike Cameron, and Chris Stamm for their willingness to help me in retrieving data for my research.

Presentation and interaction with other researchers at professional meetings was very helpful. I thank those who contributed to make these travel possible and I highly

Contents

List of Tables

List of Figures

List of Plates

Abstract

The Barnett Shale, Northeast Texas, is a self-contained petroleum system (Jarvie, 2005). The Newark East field (Barnett Shale, TX) is the second largest producing field of natural gas in the U.S (EIA 2006 Annual Reserve Reports) and the Barnett Shale, Fort Worth Basin is projected for 374 bcf of annual production by 2010 (EIA, 2004). The depositional history and sequence stratigraphy of the Barnett Shale is not fully known. This dissertation establishes Barnett Shale sequence stratigraphy based on observations of continuous cores and wireline logs, integrated with analytical data.

Four continuous long cores from Denton, Wise, and Parker counties, Texas have been studied to document the detailed internal stratigraphy and architecture of the Barnett Shale. Visual, petrographic and mineralogic analysis reveals nine distinct lithofacies within the Barnett Shale in the study area. The study indicates significance of depositional processes which have constrained the vertical facies successions and cyclicity in the study area.

The identification of a systematic and cyclic stratal stacking pattern of the lithofacies coupled with the gamma-ray log patterns led to identification of three parasequence types: upward-increasing Gamma Ray Parasequence, upward-decreasing Gamma Ray Parasequence and intervals of constant Gamma Ray Parasequence. A typical upward-decreasing Gamma ray parasequence is composed of upward-decreasing amounts of clay and phosphatic sediments accompanied by increasing allochthonous calcite

grains, and capped with a reworked shelly deposit. This pattern is indicative of upward-shoaling of the depositional environment during a very gradual fall in relative sea level. An upward-increasing Gamma Ray Parasequence consists of upward-decreasing amounts of calcareous sediments and increasing amounts of clay and phosphatic sediments which are indicative of a rise in relative sea level. These parasequences stack systematically to form parasequence sets which constitute systems tracts.

The Lower Barnett Shale is composed of nine and the Upper Barnett Shale is composed of five Gamma Ray parasequences and parasequence sets in the 'core area'. Their comparison and correlation between different locations suggests the lateral facies variability which has been explained as a function of sediment source area distance and accommodation space. Thickness maps of these Gamma Ray parasequences and parasequence sets reveal changing thickness trends.

Thus, by integrating several attributes and scales of observations, from logs to subsurface cores to thin sections and incorporating geochemical parameters, this study establishes the sequence stratigraphy of the Barnett Shale. The study also provides a workflow for systematically constructing a sequence stratigraphic framework for mudstones of similar setting.

Chapter 1

Introduction

1.1 Geology of Gas Shale

Gas Shales are defined as continuous type of unit that commonly have high organic richness and widespread gas saturation. They are geographically extensive accumulations, lack buoyancy related, well-defined oil/water or gas/water contacts, and hence the assessment methodology and production practices differ from those used in conventional resources (USGS webpage). Due to their widespread geographical occurrence and organic richness, the total in-place gas volume is commonly large. However, the overall recovery factor is relatively low due to their low matrix permeability. These low matrix permeability gas shales are known to produce gas by creation of flow paths by artificially fracturing the formation.

1.1.1 Lithology

Shale is defined as a fine-grained detrital sedimentary rock, formed by the consolidation of clay, silt, or mud (O'Brien and Slatt, 1990). The term shale is highly descriptive and is used for the smallest grain size in the classification of sedimentary rocks. It is not based on the mineralogy, but on particle size finer than 0.004mm. Shale is commonly composed

of a mixture of clay minerals, quartz, feldspars, carbonate particles, organic material and small amounts of other minerals. Shale can vary in color from red to green to gray to black depending upon the amount of organic carbon (Potter et al., 1980) and Fe^{3+}/Fe^{2+} ratio (Tomlinson, 1916).

1.1.2 Organic geochemistry

The accumulation of organic matter in marine sediments has been widely studied (Potter, 1980; Demaison and Moore, 1980; Stein, 1991). It is found that the degree of accumulation of organic matter in marine shales mainly depends on the rate of productivity of the organic matter and the rate of preservation of the organic matter. The increase in productivity of organic matter occurs due to an increase in nitrate and phosphate (Shelley, 1998) e.g. during times of upwelling of deeper water. Preservation of the organic matter requires rapid burial, development of anoxic bottom conditions and reduced dilution by terrestrial sediments.

With the burial of the organic matter, the evolution of the organic matter begins, which transforms it into kerogen. Kerogen is a complex hydrocarbon formed at low temperature by biogenic decay and abiogenic reactions of the organic matter. During this diagenetic phase methane, carbon dioxide and water are released (described by Tissot, 1977). Three main types of kerogen: Type I (algal), II (liptinic) and III (humic) have been identified by the workers at the French Petroleum Institute depending on the different organic chemical characteristics of the source material. Subsequent work added Type IV kerogen which includes oxidized and decomposed organic matter devoid of hydrogen; and with virtually no petroleum potential.

Various studies have been done on the evolution of organic matter with burial into kerogen and subsequently to oil and gas (Tissot, 1977; Tissot and Welte 1978). The gas can be generated as biogenic or thermogenic gas. The biogenic gas forms by the action of anaerobic micro-organisms during the early diagenetic phase of burial or during recent invasion of bacteria-laden meteoric water. The thermogenic gas originates by thermal breakdown of kerogen and hydrocarbons at greater depths and temperature during the catagenesis phase of the evolution of organic matter (described by Tissot, 1977).

Rocks that are classified as gas shales have high organic richness with the TOC values very commonly being over 20 wt.%. However, gas shales with as low as 2% are economically viable (e.g. Lewis Shale, San Juan Basin). The nature of the organic matter controls the type of kerogen and hence its hydrocarbon generative capacity. Type III kerogen which is formed from terrestrial plant matter generates mainly gas. Thus, the shale gas can be sourced from gas prone Type III kerogen. Shale gas is commonly generated by cracking the oil sourced by other kerogen types. Gas storage in gas shales may occur in three forms: as free gas in natural fractures and intergranular porosity, as sorbed gas on kerogen and clay-particle surfaces, or as dissolved gas in bitumen (Curtis, 2002).

1.1.3 Petrophysics of gas shale

The unique petrophysical quality of these continuous type gas reservoirs is that they have extremely low permeability and porosity. The permeability value is in nanodarcies. The porosity of gas shales can be as low as 4.5% (e.g. Ohio Shale) to as high as 14% (e.g. New Albany Shale). Pore size distribution in shale gas is generally on the order of 0.3-60 nm with unimodal size distribution (Best and Kastube, 1995). Some previous studies on shale to evaluate its potential as a good seal have illuminated the factors that might preserve better porosity and permeability in these rocks (Dewhurst and Alpin, 1998; Krushin, 1997; Sutton et al. 2004). The mineralogy and the textural characteristics, including the clay fabric orientation pattern, the ratio of fine to coarse grained particles and so forth are a few factors which have been documented to affect the petrophysical properties of shales. Dewhurst and Alpin (1998) in their experimental study showed the response of clay-rich and silt-rich samples to the effect of compaction. The permeability of silt rich samples was much higher than clay rich samples possibly due to greater range of pore throat size and presence of bottle-shaped pores (Hildenbrand et al. 2003) around silt grains. Gipson (1966) found from statistical analysis on Pennsylvanian shales of western Kentucky that there was a decrease in porosity with increasing depth, illite content and preferred clay mineral orientation. With the increase in depth of burial and compaction pressures, the illite content in shales gradually increases and becomes increasingly oriented resulting in a loss of porosity unless there are relatively coarse quartz grains to withstand the compaction pressures.

Organic richness in shale has also been related to the porosity. Krushin (1997) found that organic-rich shale has larger pore throats. Similarly, Ross and Bustin (2007)

showed that thermally mature Devonian and Jurassic gas shales of Western Canada have greater micropore volumes associated with the organics, and hence more gas adsorbed per wt% TOC.

Due to the low porosity and permeability of gas shales, it is often thought that the presence of natural fractures in the system will aid the gas flow and hence the producibility of the gas shale systems. However, the significance of pre-existing natural fractures to production is questionable; some studies suggest the existence of natural fractures in the gas shales impede fracture stimulation and are not good or does not affect production (Gonzalez, 2004 and Borges, 2007), whereas other studies suggest that natural fractures could be effective in enhancing and connecting the artificial fracture network in gas shale plays (Fisher, 2006 and Gale et al. 2007). The work of Davies and Vessel (2003) suggest that the combination of fracture, pores, and organics may help identify shales as gas reservoirs.

1.1.4 Paleoenvironment and Paleoecology

Shales vary significantly compositionally, texturally and in organic richness depending on their continental, transitional or marine depositional setting. Table 1.1 show that most of the gas shale plays in the US (Fig. 1.1) are marine and Devonian-Mississippian in age (Fig. 1.2). Thus, hereafter the sections deal mostly with discussions of marine shales.

Table 1.1 Major gas shale formations of North America with their depositional setting.

Gas Shale	Basin	Age	Setting
Ohio Shale	Appalachian	Late Devonian	Marine –Devonian Epicontinental sea (Provo et al. 1978)
Antrim Shale	Michigan	Late Devonian	Marine – Eastern Interior seaway (Dorr et al. 1970)
New Albany Shale	Illinois	Middle Devonian to Early Mississippian	Marine – Broad Epeiric sea (Cluff, 1980)
Floyd Shale	Black Warrior	Mississippian	Marginal marine (Pashin, 1994)
Barnett Shale	Fort Worth	Mississippian	Marine – Mississippian Interior sea (Craig and Connor, 1979)
Fayetteville Shale	Arkoma	Upper Mississippian	Marine (Handford, 1984)
Woodford Shale	Anadarko	Devonian	Marine – Devonian Epicontinental sea (Over, 1992)
Barnett and Woodford Shale	Delaware	Devonian-Mississippian	Marine – Epicontinental sea (Stucker, 2008)
Excello Shale	Cherokee	Pennsylvanian	Marine (Ece, 1987)
Cane Creek	Paradox	Pennsylvanian	Marine (Morgan and Chidsey, 1991)
Monterey	Santa Maria	Miocene	Marine (Bramlette, 1946)
Green River	Uinta, Piceance	Eocene	Lacustrine (Dyni, 2005)
Lewis and Mancos	San Juan	Cretaceous	Marine – Western Interior seaway (Lorenz, 1982)
Bakken Shale	Williston	Devonian-Mississippian	Marine – Epicontinental sea (Halabura et al. 2007)
Marcellus Shale	Appalachian	Devonian	Marine Epicontinental sea (Ruedemann, 1935)
Haynesville Shale	Louisiana	Upper Jurassic	Shallow marine (Obid, 2008)
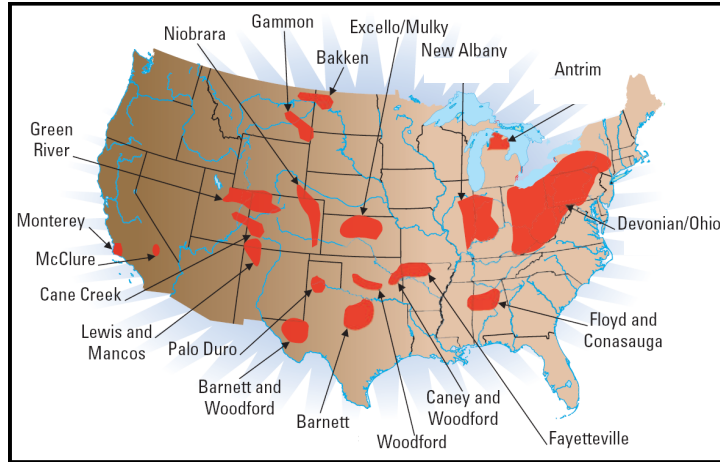
Figure1.1 Major Gas Shale basins in the United States (After Frantz and Jochen, 2005)
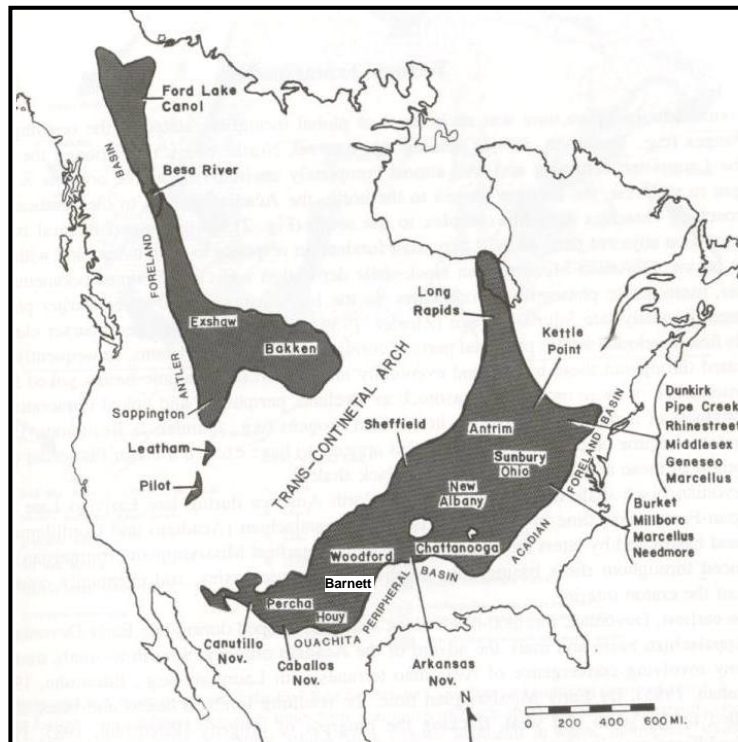
Figure 1.2. Distribution of Devonian-Mississippian black shales of North America deposited in the epicontinental sea (Modified after Ettensohn, 1998).

The first observation that is made on any rock is its color. This simple characteristic can be an informative attribute for describing shales. Like other rocks, the color of marine shales depends on primary depositional process and later secondary

burial changes. The shelf to basin transition can be reflected by color transition from greenish-gray to more widespread black shales. Potter (1980) suggests that the colors of shales are significantly controlled by organic matter which in turn is preserved depending upon the level of dissolved oxygen in the water.

Rhoads and Morse (1971) made an immense contribution in understanding of oxygen deficient environments. They proposed the lower limit of dissolved oxygen in the aerobic water and the concept of a dysaerobic zone (Fig. 1.3). The reduction of the oxygen level in the water (Fig. 1.4) is generally a result of density stratification (Olausson, 1961). Density stratification could result from the difference in temperature and salinity which inhibits aerated water circulation.
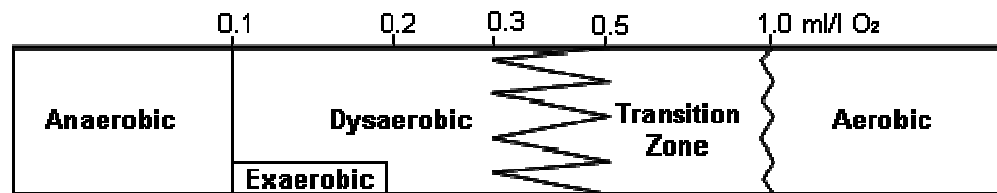
Figure 1.3 shows the level of dissolved oxygen values giving rise to varying biofacies. (After Rhoads et al. 1991)

The increase of water depth and decrease in bottom water oxygen levels affects the faunal assemblage. As the oxygen levels are reduced, the benthos become less abundant, diverse, smaller, less heavily calcified, and more dominated by infauna. There is a gradational loss of shelly fauna with a transition from aerobic to the dysaerobic zone, although echinoderms, protobranch brachiopods and pleurotomariid gastropods can withstand rigorous conditions (Fig. 1.5). With the declining oxygen gradient, deposit feeders become dominant while suspension feeders become rare (Edwards, 1985). Infaunal organisms are commonly more tolerant to a wide range of oxygen levels than are epifaunal organisms (Theede, 1973).
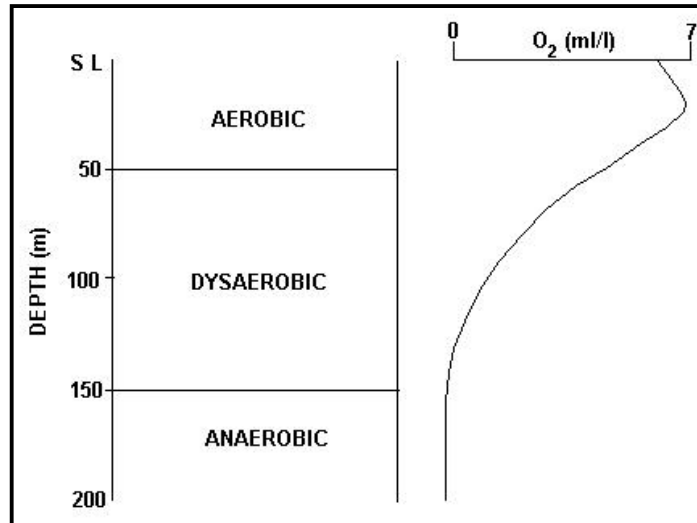
Figure 1.4 Water stratification/layering due to dissolved oxygen content. (After Caspers, 1957)

In the anaerobic realm, though no macrofauna can survive, some foraminifera can survive. Due to high pH values commonly found in low oxygen environments, calcium carbonate secretion by dysaerobic foraminifera becomes difficult. Like other organisms, foraminifera in this environment are thin shelled, poorly ornamented (Bernhard, 1986) and very commonly agglutinated (Koutsoukos et al., 1990). Byers (1977) suggests that such change of facies according to oxygenation conditions - aerobic-dysaerobic-anaerobic - can be indicative of the basin slope direction (Byers, 1977). He also suggests that in a deeper marine basin which is far from the coastal sediment source supply, the lithologic changes might not be very distinctive. However, the lateral changes in sedimentary fabric from dysaerobic to anaerobic could be suggestive of the basinward direction. O'Brien and Slatt (1990) suggest that well-developed lamination is preserved in a low energy, anaerobic depositional environment where bioturbation of the sediments by benthic organisms does not occur due to poor bottom oxygenation conditions.

9
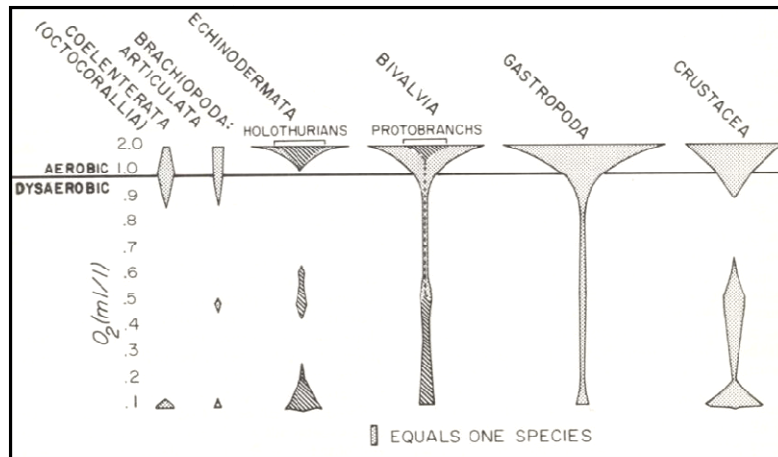
Figure 1.5 shows the shrinking diversity of the species in oxygen restricted environments. (After Byers, 1977)

1.1.5 Sequence Stratigraphy

Sequence stratigraphy is the interplay between sediment supply and accommodation space wherein the accommodation space is controlled by differential tectonic subsidence and eustatic sea level change. Establishing sequence stratigraphy in fine grained rocks is challenging and certainly not as straightforward as in more energetic marine environments and their coarser-grained facies. However, the key to understanding the sequence framework in marine shale depositional systems is to understand the character of the sediment supply. The mode of delivery, rate of deposition and the type of sediment (carbonates vs. clastic, coarse vs. fine, detrital vs. biogenic) can make a difference in the record of depositional sequences in these kinds of depositional systems (Bohacs and Schwalbach, 1992).

The various systems tracts within a sequence contain different shales which can be identified by their predictable characteristics (Schutter, 1998). Schutter (1998) points out that the *lowstand fans shales* are deposited during the waning period of more proximal fan deposition and includes the allochthonous waning turbidite fine grained

10

sediments and autochthonous hemipelagic sediments between turbidites. Lowstand fan shales can be rich or poor in organic content depending upon the bottom oxygen levels. These shales generally act as a seal because they are typically interbedded with coarse siliciclastics or carbonates whereas *lowstand wedge shales* are relatively high in mud and terrestrial organic matter compared to lowstand fan shales (Schutter, 1998). Bohacs and Schwalbach (1992) suggest some critera to identify a sequence boundary in such a setting includes higher bottom energy levels, micropaleontology data that reflects maximum numbers of shallower-water and reworked fauna.

Transgressive shales are deposited during rising sea level. The transgressive shale can vary in thickness and facies depending upon the rate of relative sea level rise. If the relative sea level rise is rapid, thin and discontinuous shale would be deposited, while a slow relative sea level rise promotes deposition of thicker, more complete and well developed transgressive shales (Schutter, 1998). Commonly trangressive shales overlie shallow water sediments such as coals and shallow water limestone (Coveney et al., 1991) mantled by a thin layer of coarse material including phosphatized fecal pellets, and glauconite often with reworked conodonts (Leckie et al., 1990). In terms of general large scale variability, Macquaker et al. (1998) suggest that upward-fining successions in Kimmeridge Clay Formation can be interpreted as a transgressive systems tract candidate. They further state that the top of these upward-fining successions indicate many characteristics of condensed sections such as the presence of concretions. A similar origin of concretionary carbonates is argued by Raiswell (1998) who said that concretions are precipitated early and close to the sediment-water interface during periods of either complete break in sedimentation or low sedimentation.

Glauconite along with phosphate grains can be very commonly associated with condensed sections; however, Amorosi (1995) shows that glauconites can be common in other system tracts and its usage in a sequence stratigraphic framework should be carefully backed and analyzed by its maturity, spatial distribution and genetic attributes. Bohacs and Schwalbach (1992) suggest that the flooding surface or turnaround point of litho-stratigraphic stacking patterns is characterized by low sediment-accumulation rates and can be recorded as a change of lithofacies from calcareous shale or siliceous shale to phosphatic shale or clay shale with minimal levels of bottom energy conditions and no reworked fauna.

Highstand shales are produced when highstand systems tract sediments aggrade (early highstand deposition) and prograde. Schutter (1998) suggests that there will be a coarsening upward trend; noncalcareous shales will be associated with high siliciclastic component, whereas calcareous shales will be associated with a high amount of carbonates. The organic matter in highstand shales will be low and degraded with terrestrial influxes. The clay minerals are variable and frequently very immature (Schutter, 1998). Other detrital grains, e.g. muscovite, commonly mark the detritus influx. Schutter (1998) points out that the interdigitation of shale with other lithologies is particularly significant in highstand shales. Shales interfingering with carbonates can be very fossiliferous. In general the paleontological characteristics of these shales reflect the process of shoaling and progradation (Schutter, 1998). However, they are poorly fossiliferous if diluted by high terrigenous influx. In the Shell Beach outcrop of Monterey Shale studied by Bohacs and Schwalbach (1992), the highstand shales are dominated by phosphatic shale with slightly more silica than phosphatic shales of a transgressive

deposit within the same section. They suggest two sources of silica: biosiliceous productivity and detrital silt. The internal geometry of a sequence demands proper and complete identification of its smaller units called parasequences and their bounding surfaces. Bohacs (1998) has summarized the characteristics of important bounding surfaces in various environments of muddy basins (Table 1.2. modified after Potter, 2005).

Bohacs and Schwalbach (1992) summarize the procedure for establishing a sequence-stratigraphic framework with special reference to fine-grained rocks as (I) establish and familiarize with regional geology, (II) record the lithological and stratal characteristics and (III) locate the position of lithologic stacking patterns in depositional sequences to establish the sequence stratigraphy. Fig. 1.6 shows an example of the procedure for progression from lithologic characterization to systems tracts identification.

Table 1.2 Characteristics for recognition of sequence boundary and flooding surface in marine muddy environments (Modified after Bohacs 1998).

Environment	Sequence boundaries (SB)	Flooding surface (FS)
Marine Basins	**More hemipelagics and biogenic debris** and lower total gamma-ray counts.	**Minimal bottom energy and terrigenous input;** high total gamma-ray counts, more deep water microfossils at or just above surface; **phosphatic concretions and lowest terrestrial organic matter above surface**
Marine shelf	Greater terrigenous input with more and coarser typically resedimented sandstone, thicker beds, wavy laminations, and lower total gamma ray, more terrestrial organic matter. Beds below boundary are regionally moderately truncated and onlapped; more shallow-water fossils *above* than *below* boundary.	Minimal bottom energy and terrigenous input, more concretions, fine-grained pelagics and more marine organic matter at or just above surface; possible concentrates of bones, fish scales at surface. Both total gamma-ray and deepwater fossils are maximal; phosphatic, siliceous or calcareous shales at or above surface.
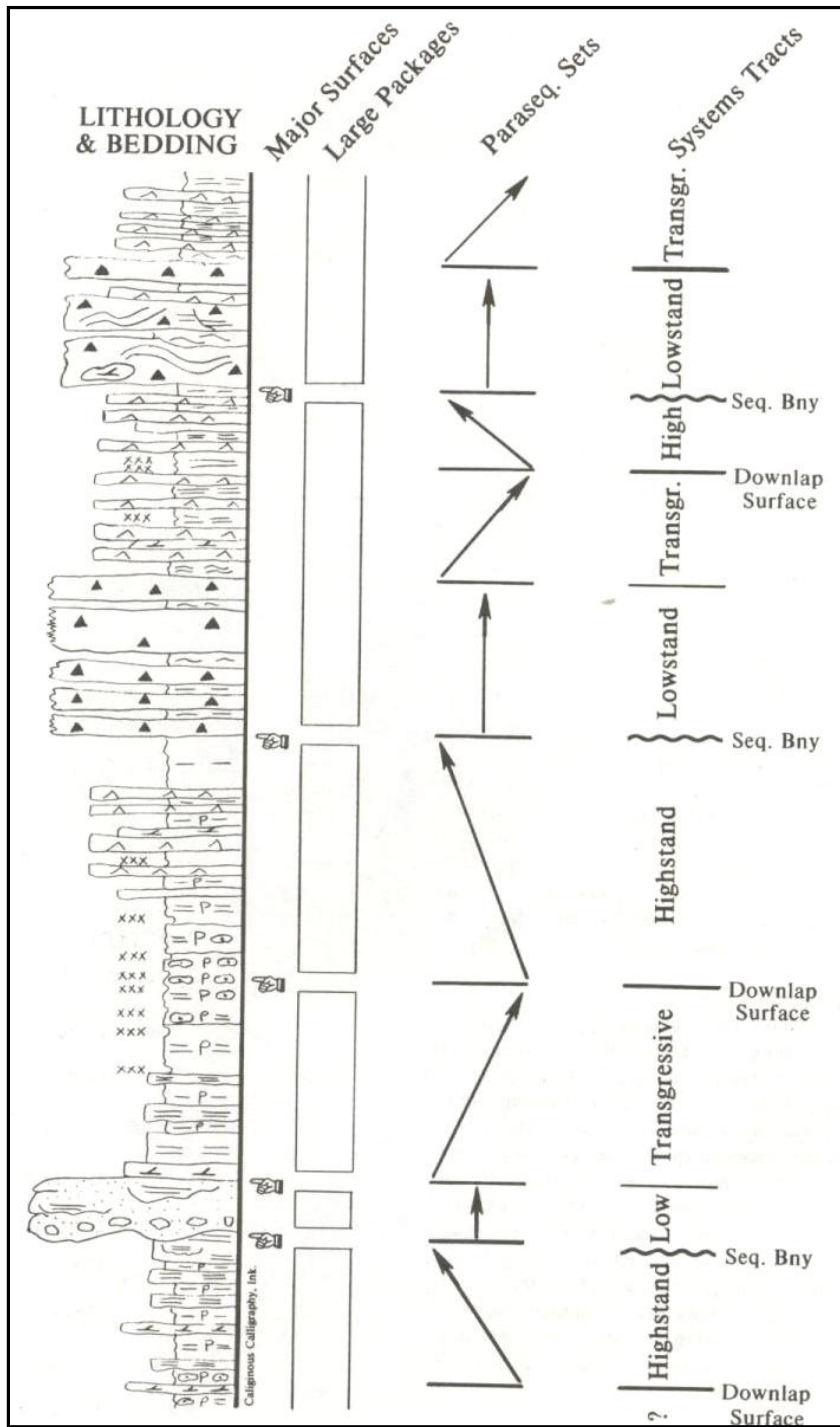
Figure 1.6 Stratal stacking pattern and interpreted sequence stratigraphy for a distal setting muddy environment (Monterey Formation). 'P's represent phosphatic shales and triangles represent chert beds. (After Bohacs and Schwalbach, 1992)

15

1.1.6 Application

Generation of a sequence stratigraphic framework for gas shales is imperative not just to comprehend the history of basin development, but also to predict the zones of organic richness, mineralogical affinity, and fracture potential. As discussed previously, the amount of organic matter and mineralogy plays an important role not only in controlling the porosity and permeability of gas shale, but also its capacity to retain gas in the system. Accumulation of organic matter depends on the dilution affect by inorganic sediments. Thus organic carbon will be higher in condensed sections and will decrease in abundance as the system grades into a highstand systems tract (Fig. 1.7). However, if the bottom oxygen level is not low, the condensed section will be characterized by bioturbation and benthic activity, thus lowering the organic matter content.
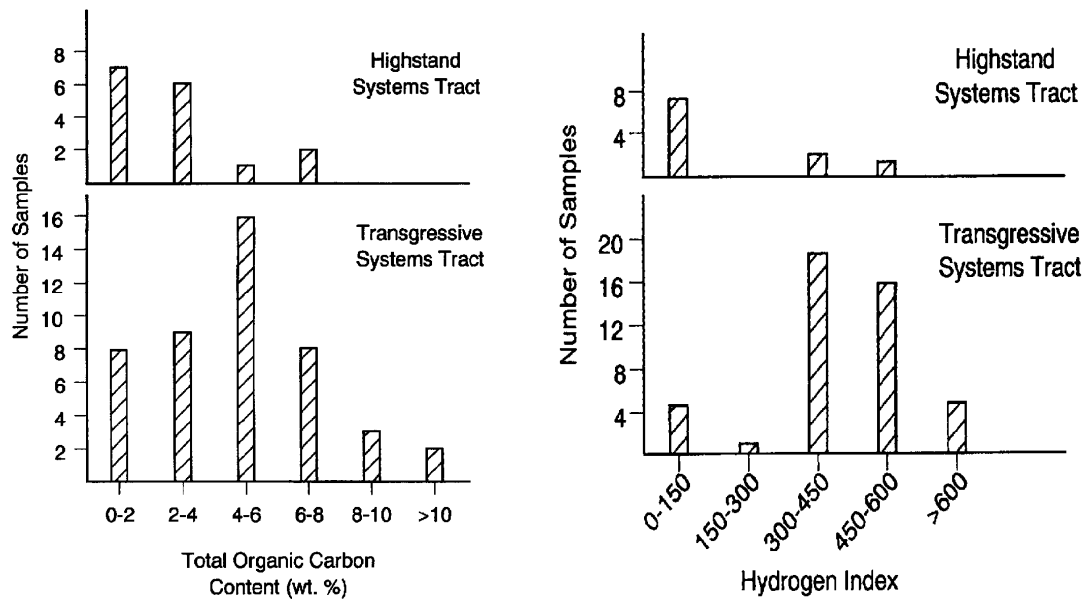
Figure 1.7 shows the distribution of organic carbon content and hydrogen index values for a set of samples from a North East Africa source rock. (After Robinson and Engel, 1992)

16

It is well known that the quantity of petroleum generated depends on the quantity of hydrogen in the organic matter contained within the sediment. Chandra et al. (1993) observed that the best organic-rich shales coupled with hydrogen enrichment in the Cauvery Basin of India were associated with early transgressive events of the basin.

The style of depositional succession and stacking pattern can also effect production. Apart from other factors, the producibility of gas shales depends significantly on the lithology. Quartz-rich strata, due to their brittleness and relative ease of fracture stimulation, can be excellent reservoir intervals. Thus, knowledge of the positioning of the systems tracts within a sequence will provide a generalized distribution of the quartz content in the section, which in turn can be helpful to decipher more fracture-prone intervals (Fig. 1.8).
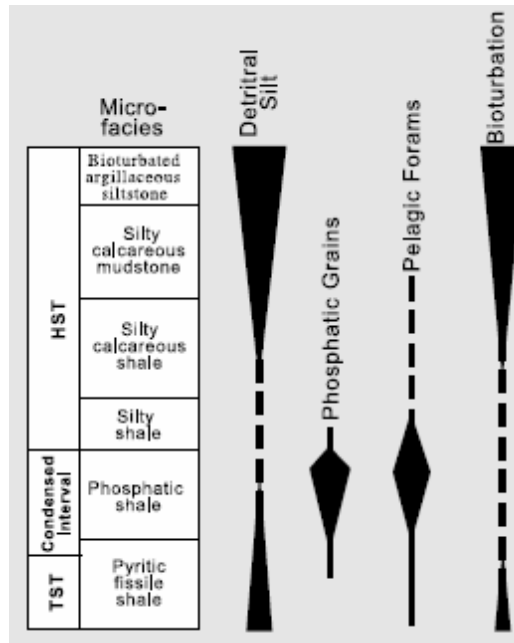
Figure 1.8 shows the varying lithology and biogenic component within the different systems tracts. (Modified after Almon et al. 2002)

1.2 Problem Statement

Shales constitute two-thirds of the sedimentary rock record in relatively continuous successions. Ironically, shale sedimentology is one of the least explored aspects of sedimentary geology. Schieber, et al. (1999) found that for the years 1980 to 1995 on average there were 1332 papers per year on sandstone and carbonate sedimentology and only 22 with shales being the focus of study. A major reason for the poor understanding and documentation of these rocks is their fine-grained nature. As stated by Bohacs (1998), the perception "they all look the same" and the real challenge in studying these rocks - the subtle expressions of surfaces and not so easily seen changes in lithology - has caused shale to be the least studied of sedimentary rocks. The fine grained nature of shale demands much beyond the macroscopic and mesoscopic hand sample examination. This fine grain size makes analysis difficult and creates a paucity of knowledge compared to conventional sandstone and carbonate rocks and reservoirs.

Shale is often considered to be very homogeneous and deposited in calm and stagnant marine water under very low energy conditions. However, closer examination reveals a wide range of properties which indicate considerable variability in depositional and diagenetic environments. Just like sandstones and carbonates, shales also reveal systematic vertical successions and cyclic sedimentation patterns indicating systematic, often predictable changes in depositional environment (Macquaker et. al., 1998). Very little work has been done along these lines. However, there is no doubt that detailed studies, such as this dissertation, will reveal that cyclic successions and complex sedimentation are equally common in gas shales such as the Barnett Shale. Bohacs (1998) has shown that there can be contrasting variation of depositional sequences in mudrocks

in settings varying from marine to non marine environments. Within marine environments, depending upon the different settings for organic productivity (Demaison and Moore, 1980), the shale can vary in terms of facies building blocks and organic content. Potter et al. (1980) devoted a whole book *Sedimentology of Shale* to questions and unsolved problems related to these rocks. Several such topics related to shale geology are yet unsolved.

Being able to extend sequence stratigraphy to the marine shale environment can be challenging, but a detailed sequence-set scale study can be very critical. As shown by Bohacs (1993) and Dawson (2000), systematic variations in source quality occur in sequences and sequence sets of the source rocks of the Miocene Monterey Formation. He has extended the relation of the depositional sequences to variations in rock properties (Bohacs and Lazar, 2008). Bouma, (2005) states that we are not in a position to indicate what parameters are the most useful for these rocks to serve as seal, source rock and/or reservoir rocks and that interested universities and companies will have to work together to be able to do so.

1.3 Objective and Scope

The Barnett Shale is considered to be one of the largest unconventional resource plays and the most prolific shale gas play in North America. Current natural gas production from the Barnett Shale is estimated to be 2 Bcf/d from approximately 5,500 wells with more than 60 operators involved (Tubb, 2007). The United States Geological Survey, in a study, stated "the Barnett Shale play has total resource potential of approximately 26 trillion cubic feet of natural gas." As big as the play is, bigger is the gap in the

understanding of various reservoir properties determined from detailed sedimentological study, facies analyses of the superficially homogenous mudstone successions, and general rock unit/facies behavior. This dissertation has been pursued in order to address these subjects.

This dissertation is intended to document the variation of depositional processes and environments of the Barnett Shale. This variation is investigated for clues about oxic/anoxic conditions, provenance area, cyclicity and relative sea level. The vertical succession and lateral continuity are studied to document the temporal and spatial distribution of the internal components of the Barnett Shale.

Objective of the dissertation is concisely represented in the following:

- The primary building block of a depositional system is 'facies'. Facies may be defined as a body of rock characterized by a particular combination of lithology, physical and biological structures that makes it different from the rock unit above and below it (Walker and James, 1992). Facies identification is done based on the observations made on internal characteristics including lithology, mineralogy and sedimentary and biologic structures.

- Facies identification accompanied by the identification of processes that controlled their depositional geometries and cyclicity will lead to understanding of the depositional systems within the Barnett Shale.

- The interpretation of depositional environment, identification of vertical facies successions followed by lateral correlation of the genetically related facies successions will provide a sequence stratigraphic framework for the Barnett Shale.

The database/resources and funds required for the accomplishments of this Ph.D. dissertation were provided by Devon Energy Corp. as part of the Devon-OU Barnett Shale Project. The dataset provided includes several whole cores, related core measured geochemical data and wireline log suites.

In an era when the world's energy demand outstrips supply, the unconventional reservoirs have soaring prospects. Other active shale gas plays in the U.S. include the Fayetteville Shale of the Arkoma Basin, Barnett and Woodford Shale of the Delaware Basin, Floyd Shale of Black Warrior Basin, Haynesville Shale in Louisiana, Marcellus Shale and the Utica Shale in the Appalachian basin. In addition to increasing knowledge of the Barnett Shale, this dissertation also provides a workflow for investigating other shale gas plays.

Chapter 2

General Geology of the Fort Worth Basin

2.1 Study Area

Barnett Shale of the Fort Worth basin has been considered to be 'homogeneous, undifferentiated black shale'. Our studies, in addition to other recent studies in the area (Loucks et al. 2007, Hickey et al. 2007, Bowker, 2007), show significant variation exists in the internal stratigraphy of the Barnett Shale. This variable lithologic nature underscores the need to better understand depositional conditions prevalent during deposition of these fine grained rocks.

Barnett Shale is organic rich, marine shale which is the source rock for numerous conventional clastic and carbonate reservoirs including the Pennsylvanian Bend, Strawn, and Canyon groups of the Fort Worth basin (Pollastro et al, 2007). It is now considered a fully self-contained petroleum system, whereby it serves as the source, seal and the reservoir rock (Jarvie, 2005). It is considered to be one of the largest unconventional resource plays and the most prolific shale gas play in North America. It has produced >2.6TCF of gas in recent years (Durham, 2007). Success with this play has been instrumental in initiating active pursuits of other Mississippian and Devonian shales in North America to find possible Barnett-like plays.

This integrated core and wireline log study addresses the sedimentology, internal geometry, and lateral, vertical and cyclical depositional patterns in the Newark East field and adjoining areas, Fort Worth Basin of Texas (Fig. 2.1).
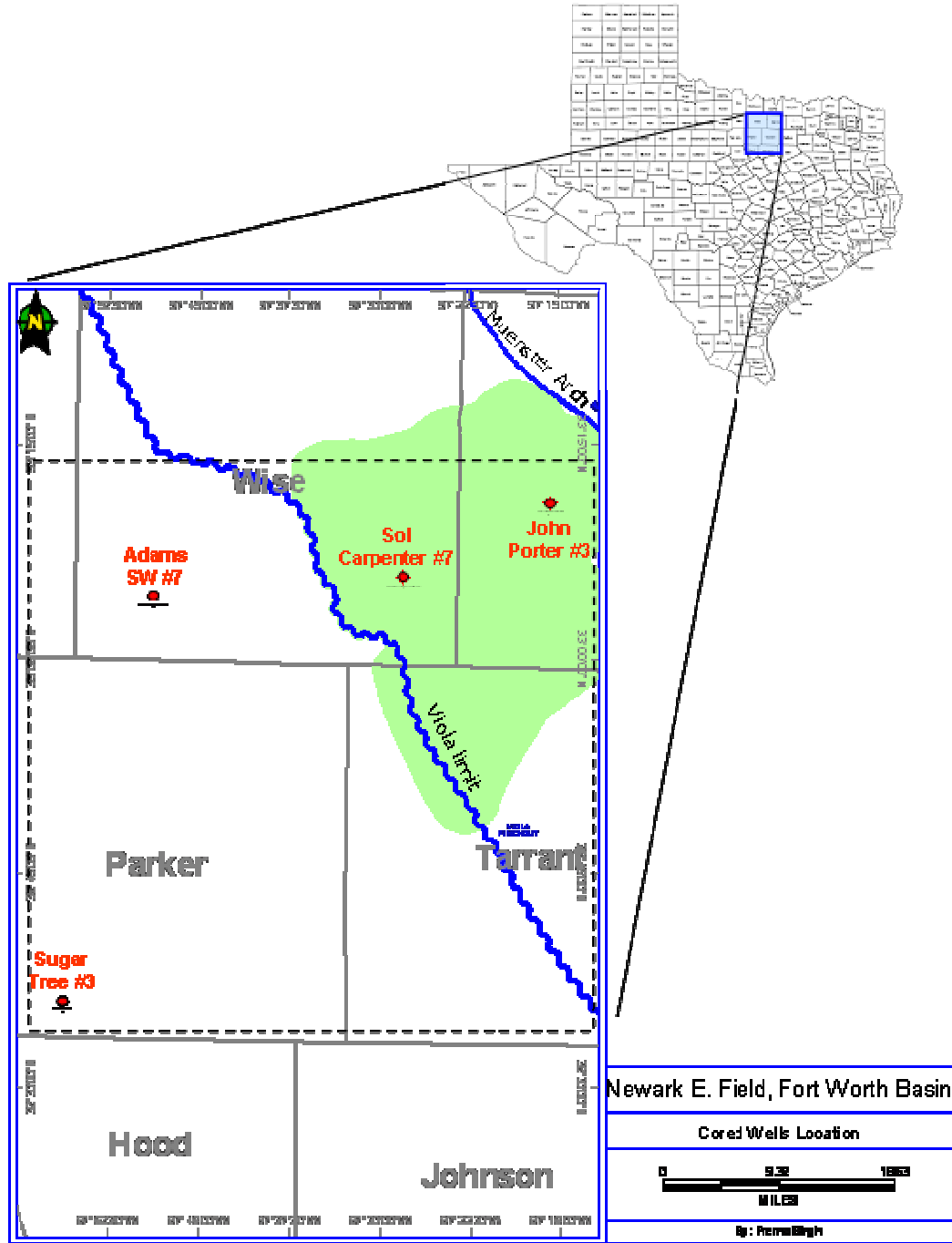
Figure 2.1: Map showing the study area. The dots are the approximate locations of the study wells John Porter #3 (JP) in Denton County, Sol Carpenter H#7 (SC) and Adams

SW#7 (ASW) in Wise County and Sugar Tree #1 (ST) in Parker County. The black box with dashed line represents the approximate limit of the wireline well logs data used in this study.

2.2 Previous Studies

Regional stratigraphic relationships for the Barnett Shale are fairly well established (Fig. 2.2A). Stratigraphic subdivisions within the Barnett Shale are less well established (Fig 2.2B). Plummer and Scott (1937) and Cheney (1940) were among the first to discuss the Barnett Shale. Cloud and Barnes, (1948) suggested that the term "Barnett Shale" be replaced by Barnett Formation. Cheney and Gloss (1952) discussed the tectonics associated with the Llano Uplift and other related principal structural features in central Texas. Craig and Connor (1979) have discussed the Mississippian deposits of the United States. Kier et al. (1979) have summarized Carboniferous geology in central, north-central and west-central Texas. The geosynclinal model has been put into a plate tectonic perspective by Walper (1982). Meckel et al. (1992) discussed the tectonics, paleogeography and facies of the foredeep basins associated with the Ouachita thrust belt system.

Most of the previous works were largely concerned with surface outcrops in the Llano area of Central Texas. Henry (1982) attempted detailed analysis of Barnett Shale subsurface stratigraphy in north-central Texas, especially in the deeper parts of the Fort Worth basin. Henry's comment on the stratigraphic studies of the subsurface Barnett as "modestly represented in the literature" (Henry, 1982) still seems to be correct.

Many studies have been more recently published as a result of the growing interest in the Barnett Shale. Pollastro (2003) attempted to assess the Barnett-Paleozoic Total Petroleum System resources. The regional thickness trends of the Barnett Shale and

intermediate Forestburg limestone have been mapped by Gonzalez, (2004). Montgomery (2005) has compiled the basic reservoir characteristics including the lithology, log character and petrophysical properties and traditional information on the Barnett Shale. Most recent work by Loucks et al. (2007), Hickey et al. (2007) and Bowker, (2007) has provided significant new knowledge of Barnett Shale lithologies. Javier (2006) has provided a significant contribution towards the characterization of the Barnett Shale internal stratigraphy by cluster analysis method wherein the Barnett Shale lithofacies were translated to electrofacies based on similar log response. They were further discriminated on high resolution seismic data.

SYSTEM AND SERIES		STAGE	GROUP or FORMATION
CRETACEOUS	LOWER	COMANCHEAN	
PERMIAN		OCHOAN - GUADALUPIAN	
		LEONARDIAN	
		WOLFCAMPIAN	CISCO GROUP
PENNSYLVANIAN		VIRGILIAN	
		MISSOURIAN	CANYON GROUP
		DESMOINESIAN	STRAWN GROUP
		ATOKAN	BEND GROUP
		MORROWAN	MARBLE FALLS LIMESTONE
MISSISSIPPIAN		CHESTERIAN- -MERAMECIAN	BARNETT SHALE
		OSAGEAN	CHAPPEL LIMESTONE
ORDOVICIAN	U		VIOLA LIMESTONE
	M		SIMPSON GROUP
	L		ELLENBURGER GROUP
CAMB	UPPER		WILBERNS - RILEY - HICKORY FORMATIONS
PRE- CAMB			GRANITE - DIORITE - METASEDIMENTS
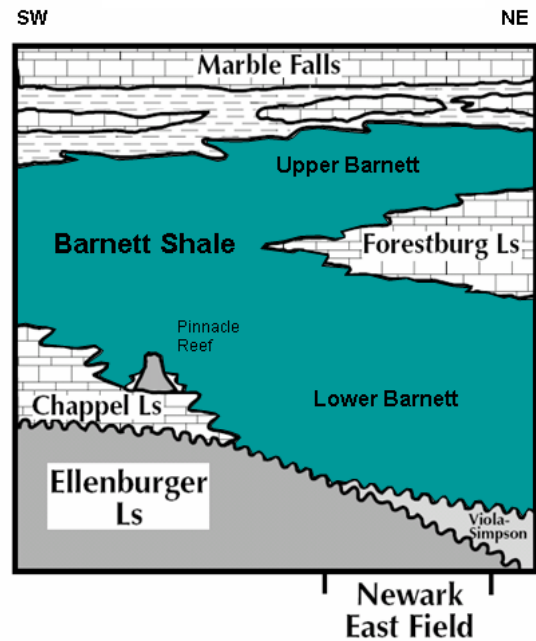
(A) (B)

Figure 2.2 (A) Generalized stratigraphic column of the Bend Arch-Fort Worth basin Province. Modified after Pollastro (2003). (B) Stratigraphic subdivisions within Middle Paleozoic units in Newark East Field and areas to the west, Fort Worth Basin-Bend Arch. Modified after Montgomery (2005).

2.3 Regional Geology

The Fort Worth basin is a north-south elongated basin in north-central Texas encompassing roughly 15,000 square miles (24,140.2 sq. km). It is one of seven late Paleozoic basins associated with the Ouachita fold and overthrust belt (Meckel et. al., 1992). The basin extends for approximately 200 miles (321.8 km) along this foldbelt. The

26

basin is bounded on the northeast by the Muenster Arch, on the north by the Red River

Arch, on the west by the Bend Arch and on the south by the Llano uplift (Figure 2.3).

The presence of the basin is related to the formation of the Muenster arch to the

northeast, the Ouachita system to the southeast (Bowker, 2007) and Llano uplift in the

south (Turner, 1957)
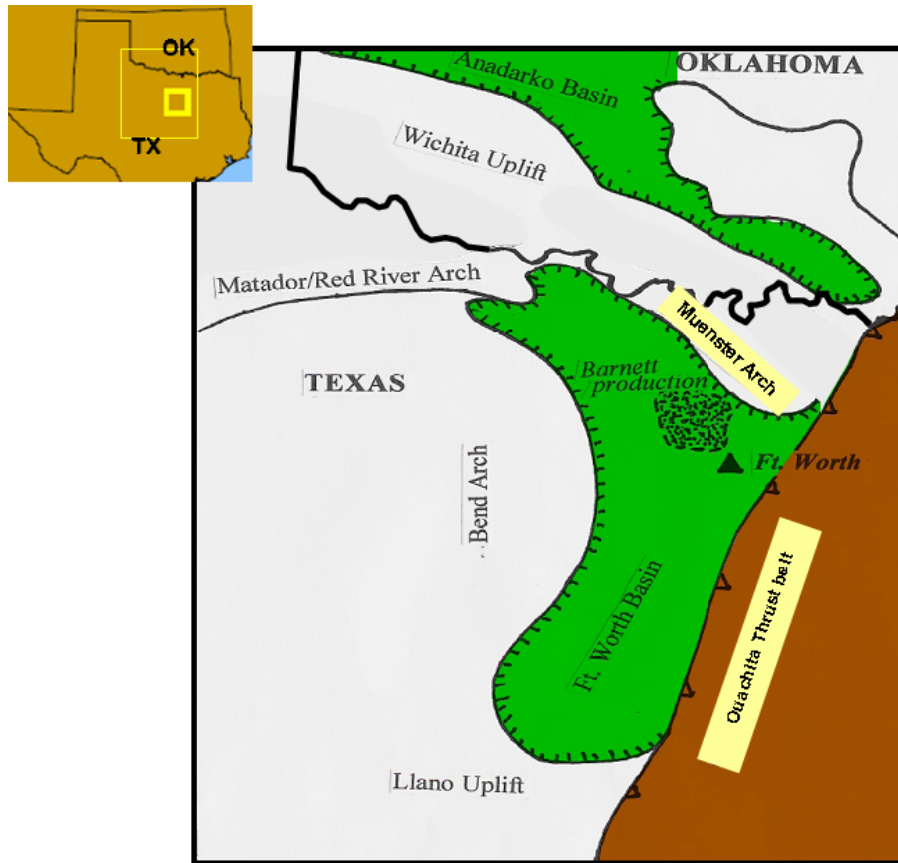
Figure 2.3. Regional setting of Fort Worth Basin. Modified after Bowker (2007).

2.3.1 Tectonic-Sedimentary Evolution

The complete history of the Fort Worth basin records the Wilson cycle of the opening

and subsequent closing of an ocean basin (Walper, 1982). The continental breakup of the

North American part of Laurentia in early Paleozoic time gave rise to several aulocogens

in nearby areas (Walper, 1977). As the margin of southern North America subsided and retreated from a spreading ridge, the Paleozoic sea, the Iapetus Ocean advanced. This invasion of the warm tropical sea is marked by widespread carbonate shelf deposition such as the Ellenburger Group of rocks. By Early Ordovician time the Iapetus Oceanic lithosphere began to subduct beneath the eastern margin of North America to form a marginal ocean basin between them (Walper, 1982). Similar configuration existed along the ancient southern margin of North America.

During the Middle Paleozoic, a period of tectonic activity resulted in erosion or non-deposition of sediments in the Fort Worth basin area. It is believed that this tectonism marks the onset of the closure of the marginal ocean basin and reversal of the subduction polarity. With the onset of closure of the continents to form Pangaea, the formation of the Ouachita fold belt began, which represents the suture zone of the collision of the North America and the Afro-South American plates. The Ouachita fold-thrust belt grew and evolved as the subduction complex - composed of the Ouachita facies strata which were deposited in the marginal ocean basin - was scraped from the subducting oceanic crust.

As the North American plate continued to underthrust the subduction complex, its outer arch migrated westward so that the hinge line continued to retreat into the continental or cratonic interior. A widespread marine transgression resulted with the formation of younger strandlines towards the craton. Hoffman et al. (1974) suggests that dormant aulacogens, which are zones of structural weaknesses, were reactivated by subsequent collision of the North American and South American plates to eventually subside and become inundated by the sea.

By Late Paleozoic time, the Fort Worth foreland basin formed in front of the advancing Ouachita structural belt. The basin was submerged and the Barnett Shale and Comyn Limestone formations were deposited over the area of the Fort Worth basin (Walper, 1982). The carbonates thickened westward towards the shelf and shales thickened eastward toward a modest detrital source in the growing subduction complex.

As the Ouachita fold-thrust belt continued to grow and migrate farther west, it forced a similar shift of the shelf hinge line of the Fort Worth basin. Thus the basin matured more and more as a ramp dipping into and under the Ouachita thrust. This structural belt was not present as a significant source area until middle Atokan time. Morrowan and Atokan times marked the greatest basin subsidence as thick terrigenous clastics were shed from both the Ouachita belt on the east and from the Wichita mountain system from the north. Figure 2.4 shows the paleogeographic reconstruction of the study area in Late Mississippian period.

Figure 2.4. Paleogeographic reconstruction of the study area during Late Mississippian period. (Modified after Blakey, 2006: http://jan.ucc.nau.edu/~rcb7/nam.html)

2.3.2 Stratigraphy

The generalized stratigraphy of the Fort Worth basin is shown in Figure 2.2. The following section discusses the stratigraphy of the Fort Worth Basin from pre-Mississippian through Pennsylvanian age.

Pre-Mississippian System: The Precambrian and Lower Paleozoic rocks exposed at the Llano Uplift area in Central Texas provide a unique opportunity in the south to study the pre-Mississippian deposits. The Riley and Wilberns Formation constitute the Middle and

Upper Cambrian sedimentary rocks. The Ordovician System is represented by the Ellenburger, Viola and Simpson Groups. The Ellenburger Group is believed to extend over the entire Fort Worth basin. In Lower Ordovician time a broad, shallow, limestone-depositing shelf sea extended from east Oklahoma to northern Mexico. A landmass of low relief existed to the northwest and the deep ocean was present to the southeast. The El Paso-Ellenburger-Arbuckle dolomite-limestone wedge was deposited on this shelf (Adams, 1954). These widespread carbonate shelf deposits thickened from a feather edge at the northwest to a massive limestone to more than 2000 ft. (609.6 m) thick at the base of continental shelf. Cloud and Barnes (1957) studied the lithic features of Ellenburger Group of rocks of Central Texas and documented an increasing abundance of disseminated quartz-sand grains, which is believed to be wind blown, toward the southern and eastern parts of the Llano region indicating that land lay to the south and east of the Ellenburger marine province.

An unconformity exists between the Ellenburger and younger strata. The overlying Simpson and Viola Groups are generally crystalline limestone and dolomitic limestone which occur only in the northeastern part of the basin. The Simpson Group thickens from 0 ft. to 500 ft. in the northeast direction and the Viola thickens to the northeast from 0 ft. to over 200 feet (Souders, 1975).

Middle Paleozoic: The top of Ordovician strata is an erosional surface upon which sit the younger Mississippian Chappel Formation, Barnett Shale and lower Marble Falls Formation (Montgomery et al. 2005). Along the margins of the Llano Uplift, the Ellenburger Group is overlain by transitional strata across the Devonian–Mississippian

boundary, the Houy Formation (Kier et al., 1979) which includes Ives Breccia and the Doublehorn Shale, and several unnamed members. The Ives Breccia crops out on the eastern, western and northern sides of the Llano uplift as angular to subangular chert breccia. The offshore equivalent of Ives may be the Doublehorn Shale (Kier, 1972). Kier (1972) suggests that at least part of the Ives Breccia may have been deposited contemporaneously with the Chappel Limestone. The Chappel Formation comprises several isolated carbonate buildups and associated debris (Ruppel, 1989). Hass (1959) gave the age of the Chappel as late Kinderhookian to early Osagean. The lower Chappel is bedded and forms the base upon which crinoidal bioherms developed (Peppard-Souders, 1975). The overlying Barnett Shale documents major Mississippian marine transgressions (Zackry, 1969; Kier, 1972). The Barnett mostly consists of organic rich, black shale. The interval of the Barnett Formation and its equivalent formations in western Oklahoma, north-central and western Texas and southeastern New Mexico were marked by a rapid sinking of a structural and topographic trough, the Ouachita Geosyncline or Llanoria trough (Mapel et al., 1979) (Fig. 2.5). Mapel et al., (1979) suggest that during the early depositional period, as the axial part of the trough sank, the flanking cratonic margin, which included the areas of the present Fort Worth, Kerr, Val Verde and Marfa basins, was also carried down below sea level, and the sediments began to accumulate. He also suggests that the increase in thickness of the Barnett Formation in the easterly direction indicates that the source of the mudstone in these formations remained to the east or northeast and that the muds were mostly deposited in the east and were intermittently and broadly deposited in shallower flanking parts in the westward or southwestward directions.

Provenance area of the terrigenous material that constitutes the Barnett Shale are the Ouachita thrust sheets and the reactivation of the older Muenster Arch (Pollastro et al. 2003) in the northeast. The Muenster Arch, which comprises a zone of steep dips and faults, is believed to be a positive area throughout most of the Paleozoic time (Clark and Bybee, 1951). The depositional patterns of the Barnett Shale - which was deposited on the southwestern flank of the Southern Oklahoma aulacogen - reflect the general northwest-southeast trend of the aulacogen axis, whereas the burial patterns reflect the subsequent depositional and structural influence of the present day Fort Worth basin (Schmoker et al., 1996). The Barnett Shale is about 1000 ft. (300 m) thick near the south-west fault of the aulacogen. However, it thins to 30 -50 ft. (9 m. – 15.2 m.) to the southwest (Fig. 2.6) where it crops out over the Chappel formation along the Llano Uplift (Henry, 1982).
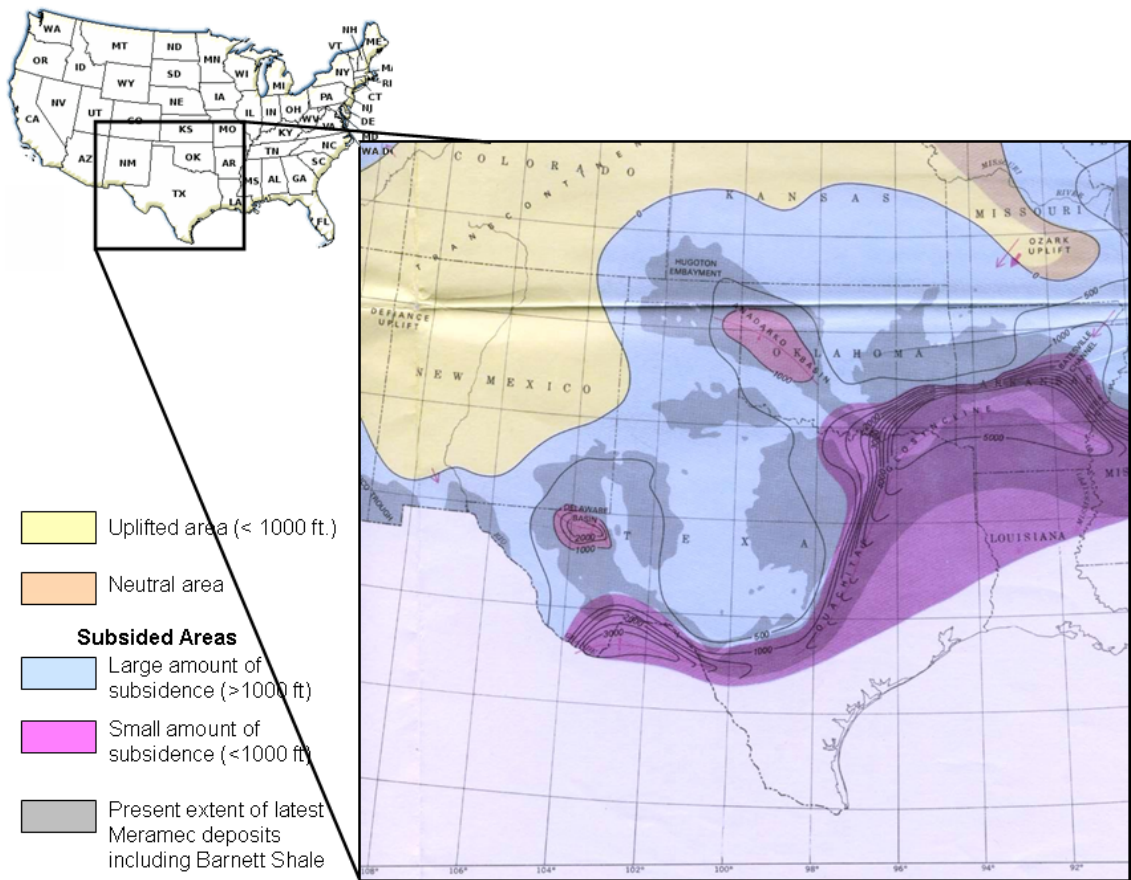
Figure 2.5. Map showing the structural and topographic features including Transcontinental Arch, the Ouachita gosyncline or Llanoria trough during the late Mississippian period. (Modified after Mapel et al., 1979; and

http://npic.orst.edu/countyext.htm).
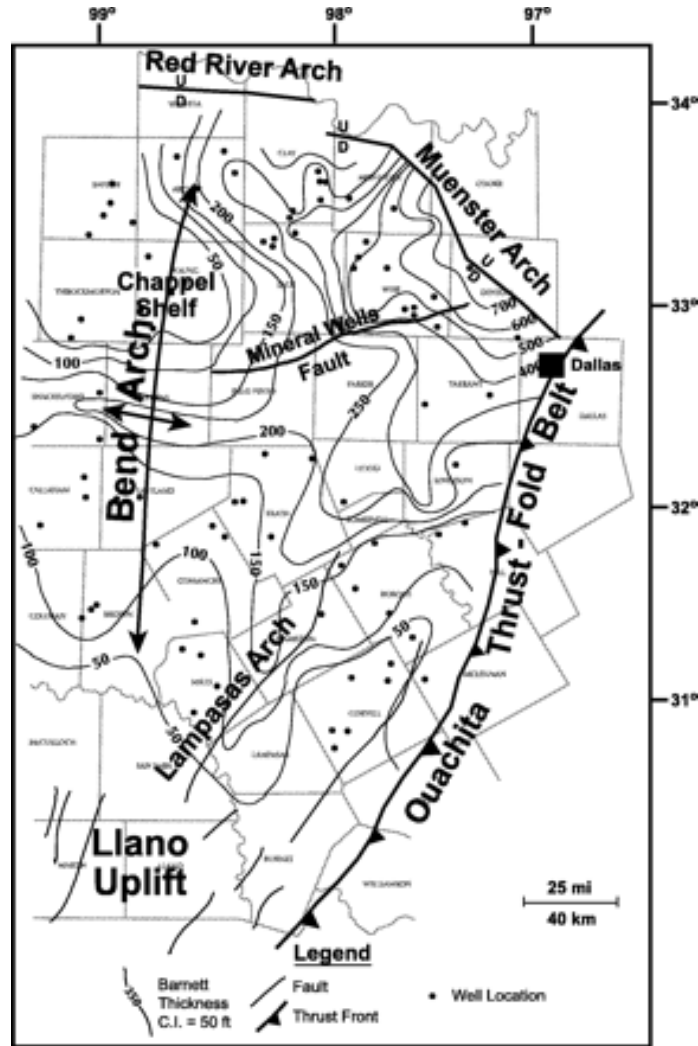
Figure 2.6. Isopach map of the Barnett Shale. (Modified after Montgomery et al., 2005).

This thinning or absence of the Chappel and Barnett locally in the Marble Falls district and generally over the Concho arch region is related to uplift and local tectonic features trending north to northwest in the Llano-Concho arch region (Cheney and Gloss, 1952). Mapel et al. (1979) suggest that a low broad arch, called by Adams (1952) the Texas Peninsula or Texas Arch, which extended from central Texas northwestward into northwestern New Mexico, as the dominant structural feature at the beginning of Mississippian time (Fig. 2.7).
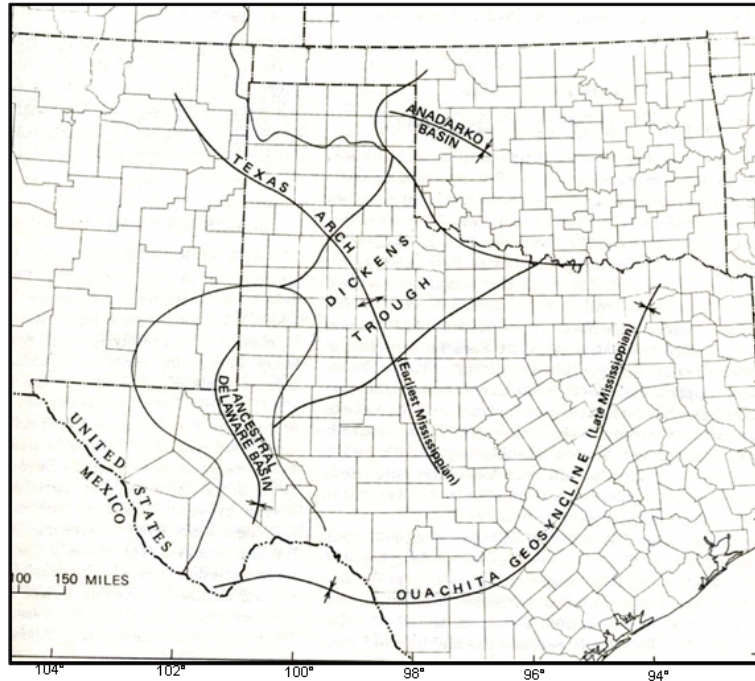
Fig. 2.7: Map showing the location of the Texas Arch in the Southern Midcontinent region during Mississippian age (modified after Mapel et al., 1979).

In Newark East field, the Barnett Shale is divided into lower and upper intervals by a carbonate unit called the Forestburg limestone. This limestone is over 250 feet thick in the north, close to the Muenster Arch. However, it thins to extinction in the southern and western part of the basin. The Barnett Shale becomes undifferentiated where the Forestburg Limestone is absent (Fig. 2.2B). The Barnett Shale is conformable with the overlying Mississippian age Lower Marble Falls Formation. The Marble Falls records reestablishment of a carbonate platform, normal marine conditions and widespread limestone environments of deposition (Kier et al., 1979). Marble Falls strata in Central Texas were deposited on a southeast-sloping shelf as part of the Texas craton (Namy, 1982) and range from platform to open marine to shelf-edge carbonate deposits.

36

Pennsylvanian: The Pennsylvanian system consists of the Upper part of the Marble Falls, Atoka etc (Montgomery, et. al., 2005). The Upper part of the Marble Falls is Morrowan in age. Various names and stratigraphic ranks have been proposed for the Marble Falls of central, north-central and west-central Texas, for example the Comyn Limestone and Big Saline Limestone (Cheney, 1940). The Ouachita structural belt was a major source for the thick terrigenous clastics of the Atoka and Strawn Groups which forms several conventional oil and gas reservoirs in the Fort Worth basin.

Chapter 3

Lithofacies

3.1 **Lithofacies characterization**

Continuous, long cores of Barnett Shale have been studied from four wells (Fig. 3.1) to understand the depositional processes and environment, style of vertical stacking pattern and lateral continuity. Visual core description, extensive petrography and mineralogy, integrated with wire-line log data analysis, has led to the identification of nine lithofacies within the Barnett Shale which takes into account their 1) physical characteristics, including mineralogy, grain size, texture and sedimentary structures, 2) chemical features, including diagenetic alteration, and 3) some biogenic features, including ichnofabrics and fossil assemblages. Lithofacies are described below along with their systematic stacking patterns. The format follows such that it first discusses muddy facies deposited for the most part under low energy conditions *viz.* s*iliceous non-calcareous mudstone, siliceous calcareous mudstone* and *micritic/ limy mudstone*. The next three facies discussed represent relatively high energy facies *viz. bottom current calcareous laminae deposit, reworked shelly deposit* and *silty-shaly (wavy) interbedded mudstone*; next the two diagenetic facies are discussed viz: *concretions and dolomitic mudstone*, followed by *phosphatic lithofacies* which was deposited in both low energy and high energy environments.

Siliceous non-calcareous mudstone: The *siliceous non-calcareous mudstone* facies is black, massive mudstone, which does not react with dilute hydrochloric acid. Petrography and mineralogic measurement indicates quartz and clays are the most dominant mineral components. Pyrite, phosphate peloids, calcite, dolomite, and ferroan dolomite are the minor components. The silica content is of both biogenic and detrital nature. Detrital quartz grains are of silt and finer sizes (Fig. 3.1A). Detrital quartz grains are often bound organically as agglutinated arenaceous forams (Papazis, 2005, Milliken et al. 2007) (Fig. 3.1B). The common biogenic components are agglutinated forams and sponge spicules, which occur in variable abundance. The small sized, flattened shaped and large pore - bearing forms of forams are indicative of deposition in oxygen - poor habitats (Kaminski et al., 1995).
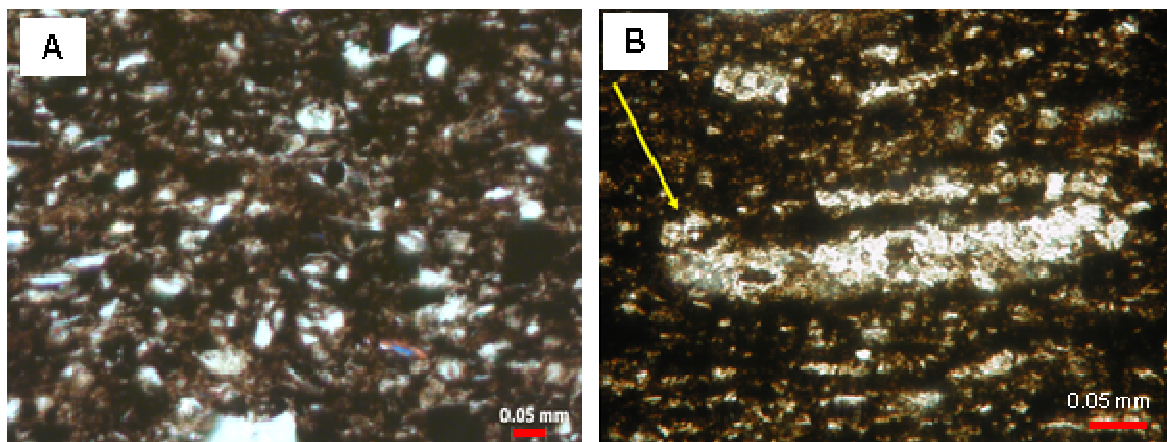
Figure 3.1. Photomicrographs showing A) the high amount of detrital quartz often found in *siliceous non-calcareous mudstone*, B) Agglutinated forams in s*iliceous non-calcareous mudstone.* Scale bar is 0.05 mm.

Analysis of the samples in the Scanning Electron Micropscope (Fig. 3.2) shows horizontal alignment of the minerals, suggesting compaction. The lack of any

bioturbation and micro-sedimentary structures suggests a quiet water environment of deposition, dominated for the most part by suspension settling of the pelagic and hemipelagic grains. This unique association of phosphatic fecal pellets, and calcareous laminae deposits indicates that this lithofacies could be indirectly suggestive of an oxygen depleted paleoenvironment.
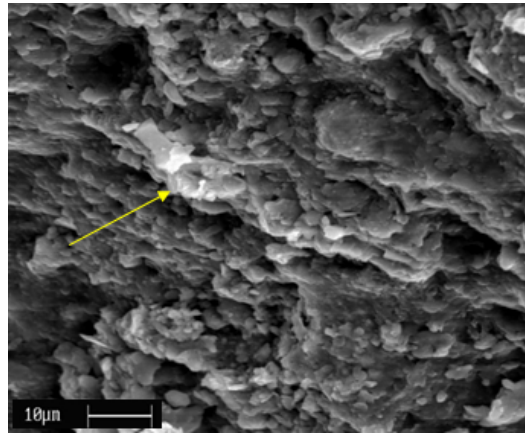
Figure 3.2. SEM image of *siliceous non-calcareous mudstone* section which reveals the fabric, parallel orientation of the clays. The arrow points to an agglutinated foram.

Siliceous calcareous mudstone: The *siliceous calcareous mudstone facies* is black, massive mudstone which effervesences with dilute hydrochloric acid. The *calcareous mudstone* facies has a composition very close to that of the *siliceous non-calcareous mudstone*, except that calcite occurs in a sufficient proportion (Fig. 3.3A and B) to produce effervescence with dilute HCl acid. The calcite content varies from 4% to 40% of the total composition. Based on the amount of calcite present, this facies can be further subdivided into *siliceous calcareous mudstone with low calcite* (less than 10%) and *siliceous calcareous mudstone with high calcite* (10%-40%). The *siliceous calcareous mudstone with high calcite* occurs associated with *reworked shelly deposits;* however, not all depths of *reworked shelly deposits* are accompanied by *siliceous calcareous mudstone*

40

with high calcite. Calcite very often occurs as sparry calcite fillings in probable burrows (Fig. 3.3B), or as tiny broken skeletal fragments.
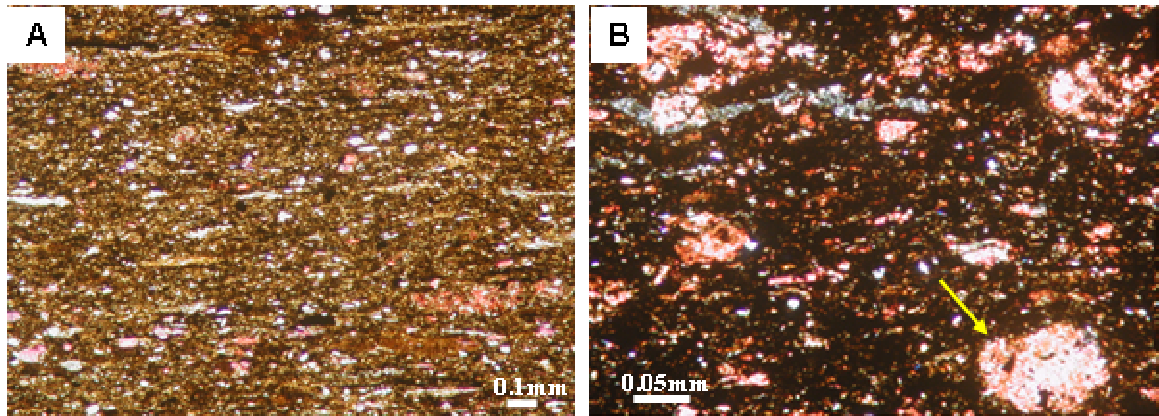
Figure 3.3. A) Relative abundance of calcite (pink color stained grains) in *Siliceous calcareous mudstone*, B) Calcite (pink stained grains) fill the probable burrows (yellow arrow) in *siliceous calcareous mudstone.*

Micritic/Limy mudstone: The *micritic/limy mudstone* facies is composed of autocthonous calcite mud (Fig. 3.4A and B) with low abundance of microfossils and small amounts of scattered invertebrate fauna, shell fragments and detrital silt size grains (Table 3.1). There are several secondary diagenetic features including compactional stylolites. This facies represents a change of depositional environment to relatively shallow water conditions. The widespread micrite forming the matrix suggests that the depositing water was relatively warm to provide autochthonous chemical precipitate of calcite and skeletal calcite sediments. The horizontal lamination and lack of significant bioturbation suggests that the lime was being deposited in a quiet water setting, though shallower than the preceeding two muddy facies.
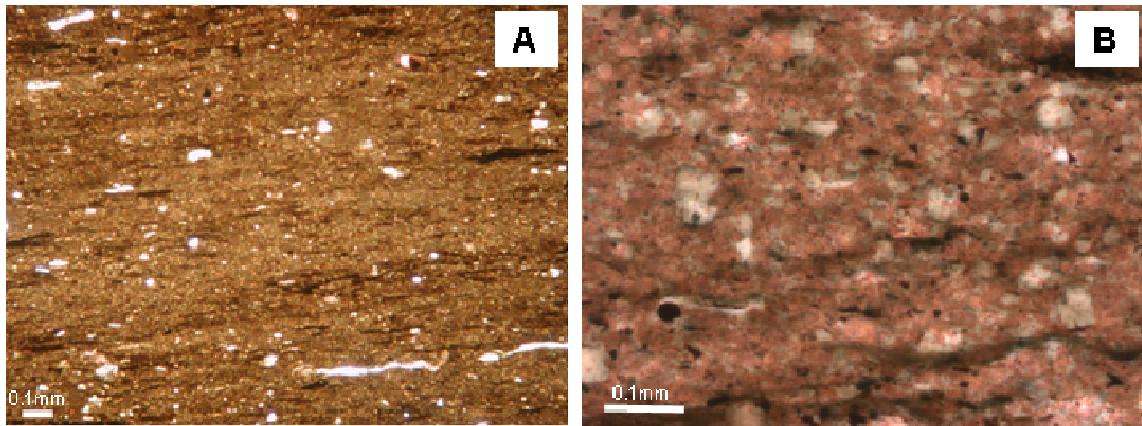
Figure 3.4. Photomicrograph of (A) *Micritic/Limy Mudstone*, (B) Close up showing the high detrital quartz (white grains) in micritic, calcite matrix stained pink. The scale bar is 0.1 mm.

Bottom current calcareous laminae deposit: This facies is composed of calcite rich laminae, which are horizontal and parallel to bedding. Very often they exhibit ripples and cross lamination (Fig. 3.5), suggesting bottom current activity. Often, such fine-grained sediments that were primarily deposited by hemipelagic accumulation can become subjected to reworking (Fig. 3.6A) by bottom currents which are expressions of oceanic thermohaline circulation (Stow et al. 1996, Stow et al. 2001). These features are very commonly lenticular in shape which could either be the actual form of the deposit i.e. thick where currents allow sediment to settle and thin where currents winnow it away, or it could be a result of diagenesis, hence forming secondary lensoid-shapes (Fig. 3.6B). This facies is bioturbated and contains the trace fossil *Chondrites, Teichichnus, Phycosiphon, Cosmoraphe, Asterosoma* and *Planolites,* indicating low oxygenation. Possibly the short-lived, oxygenation prevalent during deposition of this facies was conducive for organisms to dwell only for a short time and to be restricted only within this facies. Petrography reveals a high amount of calcite, pyrite, marcasite, minor quartz and clay minerals (Table 3.1). Amrishaw (1999) suggests that high sea level with

diminished sediment supply and strong bottom current activity can lead to the development of such deposits. The analysis of the vertical succession of the lithofacies and the anoxic/oxic conditions associated with these facies (discussed in the next chapter) support this suggestion.
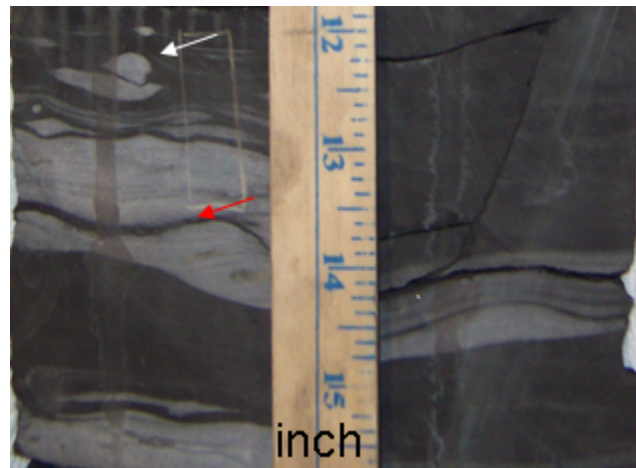
Figure 3.5. Core photo of *Bottom current calcareous laminae deposit*: white arrow shows *Teichichnus* trace fossil, red arrows shows the current lamination and ripple structures.
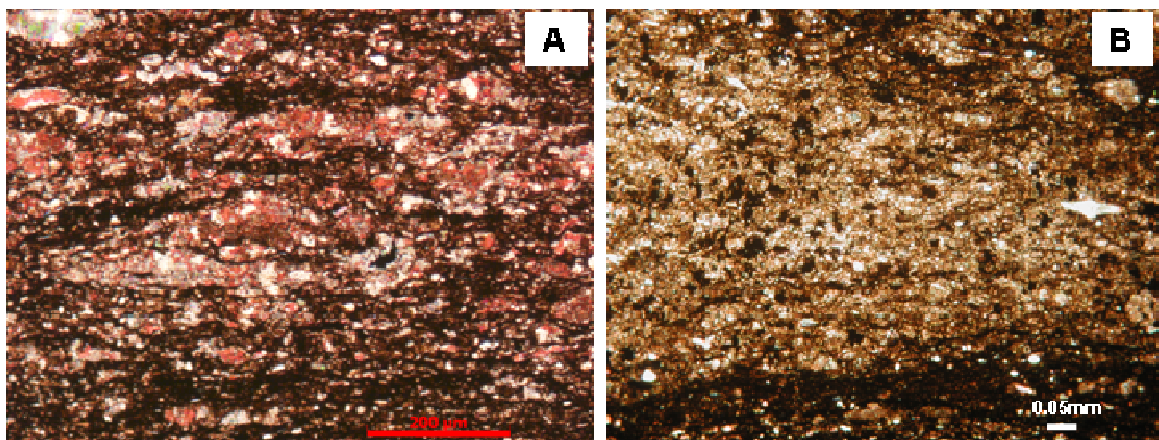
Figure 3.6. Photomicrograph of *Bottom current calcareous laminae deposit* showing: A) concentration of forams possibly by winnowing, B) Reworked spicules and the lenticular shape of the calcareous laminae.

Reworked shelly deposit: The *reworked shelly deposit* refers to thin laminae of broken macrofossil shell fragments (Fig. 3.7A), often in imbricated and coalesced forms, perhaps

43

as a result of post-depositional compaction. Laminae are finely interlayered with *siliceous*

calcareous mudstone (Fig 3.8). The thin-walled, shell fragments, which include

brachiopods, filibranch mollusks and echinoderms, are commonly accompanied with

surficially coated phosphatic grains/ooids (Fig. 3.7B) and intraclasts. Overall, shelly

material consists of fragments and disarticulated shells. Disarticulated shells lay parallel

to the bedding mostly in concave down and a few with concave up position. Rippled

upper surfaces are often present on individual shelly laminae (Fig 3.8). Sharply defined

top and basal surfaces are noted. The mixing and sorting of the different grains and

rippled surfaces suggest that they have been deposited under relatively high energy

conditions. The concave down orientation of the shells also suggest current action

(Embry 1968, Clifton, 1971). Winnowing currents could possibly have reworked and

deposited these shelly fragments. These intervals are typically widely traceable as

stratigraphic units. Calcite is the dominant mineral (Table 3.1).
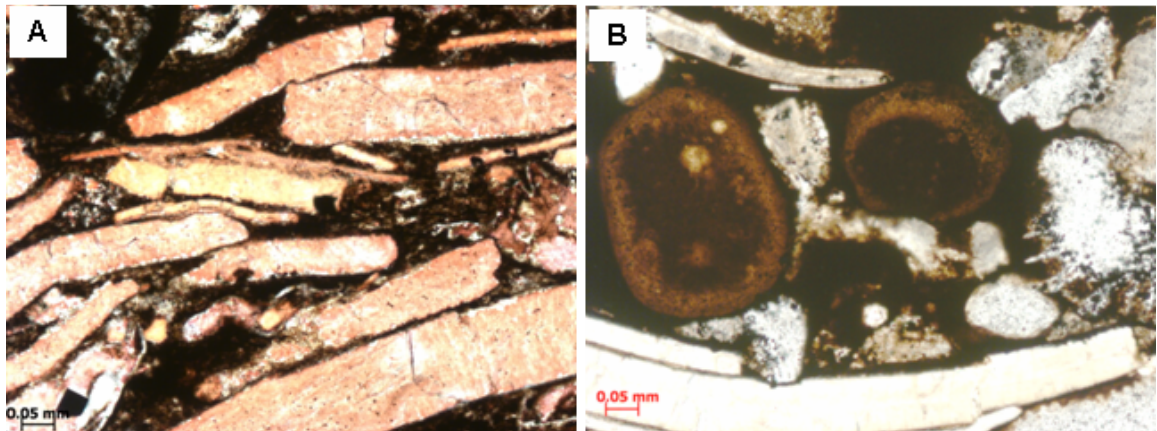
Figure 3.7. (A) Photomicrograph showing the macrofossil shell fragments (calcite is stained pink) and (B) Surficially coated phosphatic ooids mixed in *reworked shelly deposit*.
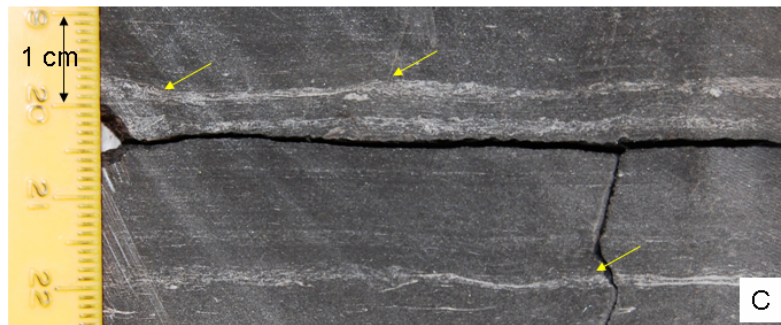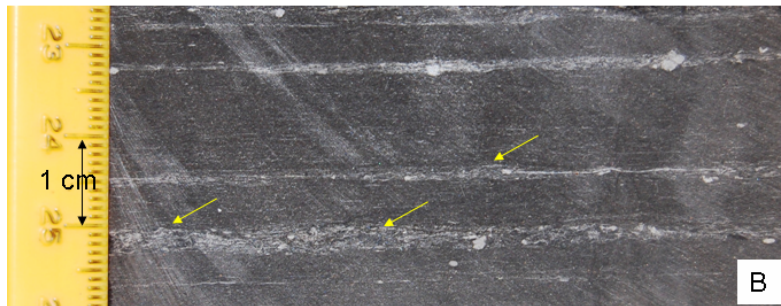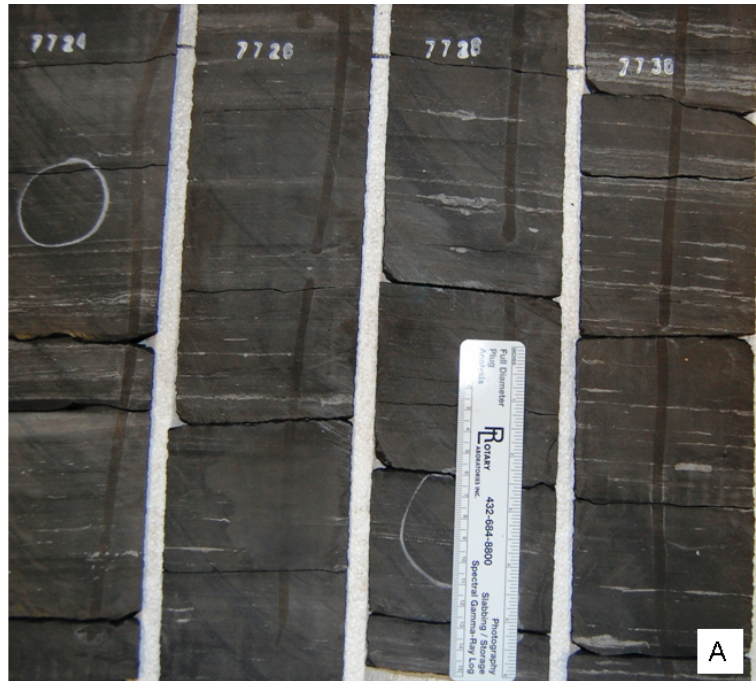
Figure 3.8. Core photo showing the shell fragments in coquina intervals (A) from Sol Carpenter H#7 well. (B) 8454.8 feet (2577 m) and (C) 8455.9 ft (2577.4 m) in John Porter #3 well shows close up of few of these laminae highlighting the ripples. Also note there is no graded bedding.

Silty-shaly (wavy) interlaminated deposit: The *silty-shaly (wavy) interlaminated deposit* is not a common facies of the Barnett Shale, and occurs mostly in the Upper Barnett and in the Lower Barnett at depths close to the Forestburg limestone. Internally, this facies consists of alternate and continuous laminae of silt and mud (Fig. 3.9A and B) which indicates frequent alternation of energy conditions. The oscillatory or repetitive nature of these interbeds indicates periodic high-energy events that resulted in the deposition of detrital silt sized layers followed by periods of low-energy deposition. The silts are composed of detrital quartz, calcite and glauconite grains. The average grain size is 0.05mm. Broken shell fragments and a few arenaceous, agglutinated forams are prevalent. Ripples and cross laminations are common sedimentary structures (Fig. 3.9A and 10). The relatively larger burrows associated with this facies, the subrounded to angular nature of the detrital grains and ripple cross lamination suggests a close proximity to a source/marginal basin setting and relatively shallow water conditions and high current activity.
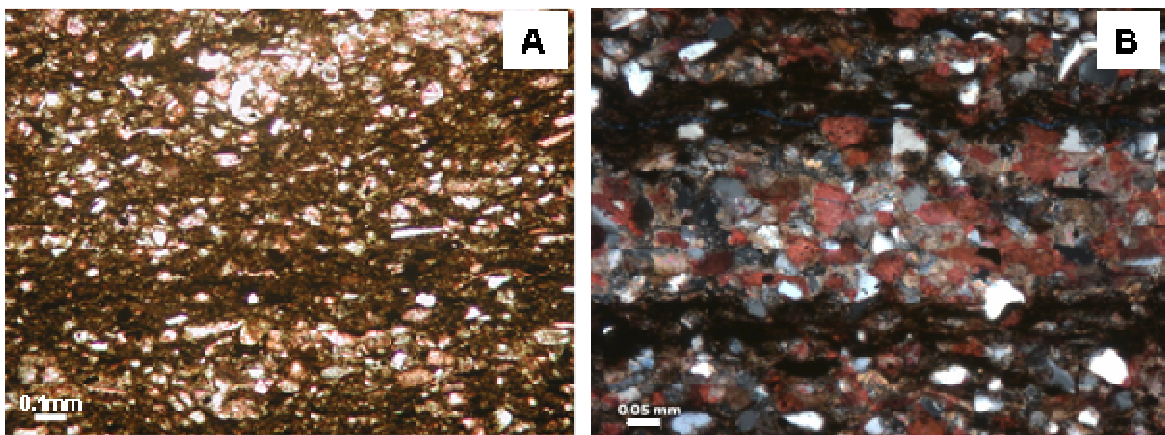
Figure 3.9. *Silty-shaly (wavy) interlaminated deposits*: (A) Photomicrograph showing the high amount of detritus and the cross laminae nature of detritus laminae. (B) Photomicrograph showing the abundant silt size quartz and calcite grains (pink stained grains) interlaminated with clay.

Figure 3.10. Core photograph of *silty-shaly (wavy) interlaminated deposit.* Zoom in view shows a large vertical burrow (circled).

Concretion: *Concretions* within the Barnett Shale are calcareous in nature. They range from < 2 inches (5.08 cm) to 1.5 ft (0.46 m) in thickness. They are found in equal abundance in both the Upper and Lower Barnett. Concretions are common diagenetic products and generally are thought to be syngenetic (early diagenetic) as well as epigenetic (late diagenetic) in origin. Carbonate concretions are common in shales

(Weeks, 1953). When developed in their early stages and when the enveloping mud was still unlithified, the concretions tend to preserve full bodied, uncompressed microfossils (Fig. 3.11) within them and the enveloping shales are bent and compacted around the nodular form. Well preserved burrows are also present (Fig. 12). However, when developed in later stages (epigenetic), concretions generally exhibit continuous bedding through them (Fig.13). This lithofacies uniquely contains most of the natural fractures present in the core sections studied.
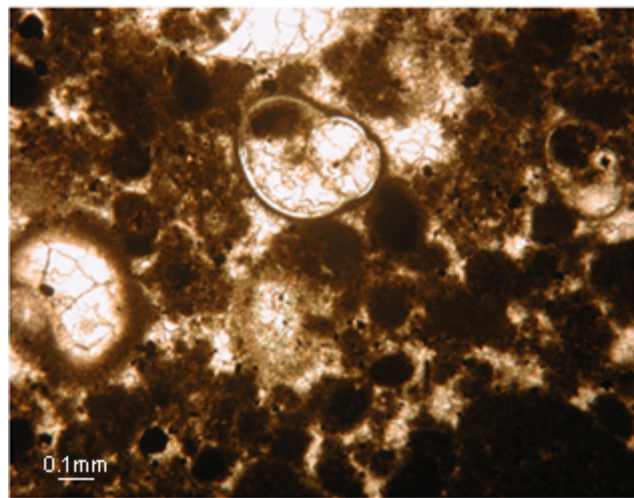
Figure 3.11. Photomicrograph of well preserved microgastropods and pelloids in *concretion*.
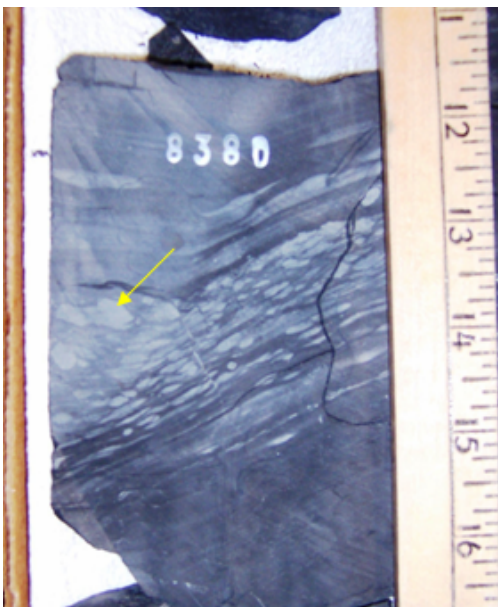
Figure 3.12. Core photograph of *concretion* which has preserved internal burrows (arrow) at 8380 ft (2554.2 m) in John Porter #3 well.
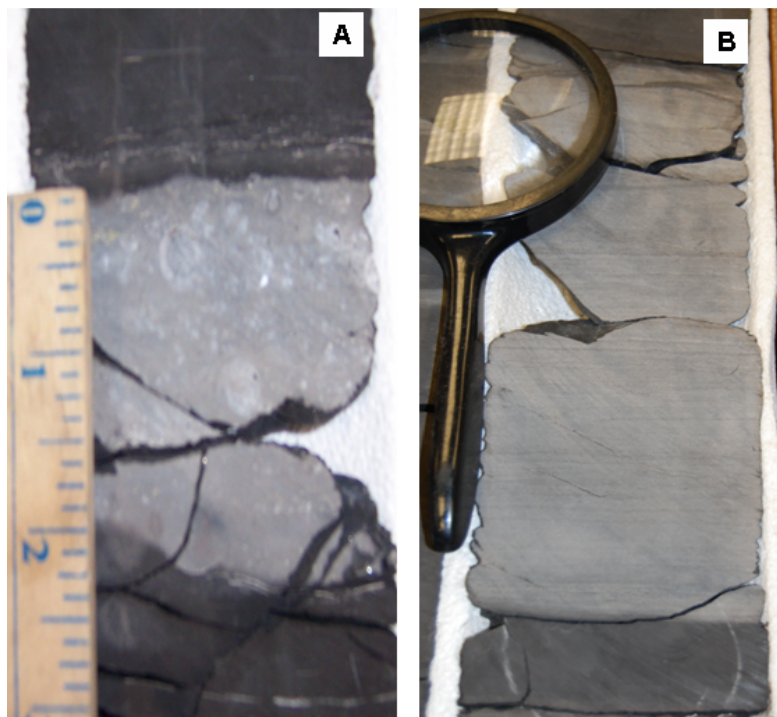
Figure 3.13. Core photograph of *concretions* at (A) 7490.5 ft (2283.1 m) in Sol Carpenter H#7 well showing nodular shape and preserving fossils within and (B) 7668.2 ft (2337.2 m) in Sol Carpenter H#7 well showing continuous bedding and parallel to bedding outline.

Dolomitic mudstone: *Dolomitic mudstone* is composed mostly of rhombohedral dolomite crystals. In core view, this lithofacies appears light grey in color. This facies can be subdivided into two subtypes depending upon the proportion of dolomite in the matrix i.e. about 20 - 25 % and >40 % (Fig. 3.14). The *dolomitic mudstone* with 20-25% dolomite commonly contains finely disseminated dolomite with high amount of calcite shell fragments, suggesting secondary, diagenetic dolomitization of initially *reworked shelly deposit*. The *dolomitic mudstone* containing over 40% dolomite commonly occurs with dolomite as the most dominant mineral phase, embedded in a clayey matrix. Land (1985) suggests that a large amount of magnesium required for a massive dolomitization is sourced by sea water. Baker and Kastner (1981) demonstrate that modifying sea water chemistry by reducing the dissolved sulfate concentration as a result of microbial sulphate reduction can speed dolomitization in anoxic environments. These dolomites are hence, thought to be a result of direct precipitation in the early depositional history.
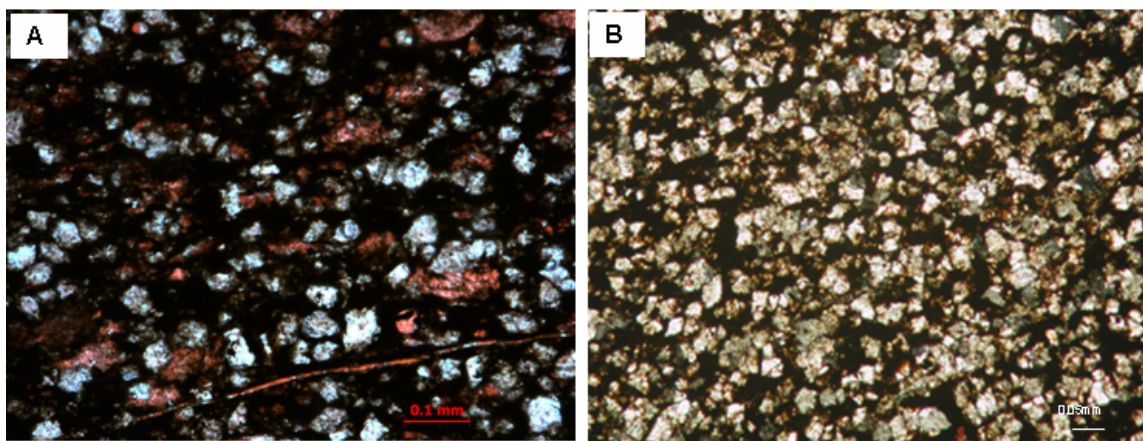
Figure 3.14: Photomicrograph of *dolomitic mudstone* with (A) less than 20 - 25 % dolomite and (B) 40 % or greater dolomite in the matrix.

Phosphatic deposit: The *phosphatic* intervals occur as thin lamina of less than about 0.5 inch (1.27 cm) each. However, very often several laminae stack vertically for a foot or so in *siliceous non-calcareous mudstone* (Fig. 3.15). The phosphatic deposit mostly consists of pellets and less commonly of ooid forms. The phosphatic pellets occur in several forms and shapes ranging from subrounded to elongate to irregular (Fig. 3.16A). Very commonly the elongated pellets incorporate terrigenous grains of quartz and mica flakes, as well as microfossils. Wignall (1994) suggested that phosphatic fecal pellets are good agents for removal of both terrigenous and biogenic material through the water column (Fig. 3.16B). He noted that they are commonly preserved in low energy environments. Other common forms include poorly developed pelloid-like structures, often with surficial concentric ring. Sometimes, these are accompanied with clumped aggregates of three to four pelloids to form irregular shaped intraclasts (Fig. 3.17A). These forms suggest minor reworking. Other reworked phosphatic deposit forms are good concentric cortex ooids (Fig. 3.17B). Phosphatic nodules are not very common features in the studied cored wells in the north (Adams SW #7, Sol Carpenter H#7 and John Porter #3) however, the southern well (Sugar Tree #1) has several nodules which are composed of phosphatic cement concurrently occurring with other authigenic minerals in significant proportions e.g. very commonly Fe-dolomite, pyrite and sometimes microcrystalline silica. This phosphatic nodule type ranges in shape from circular to irregular to parallel to bedding.
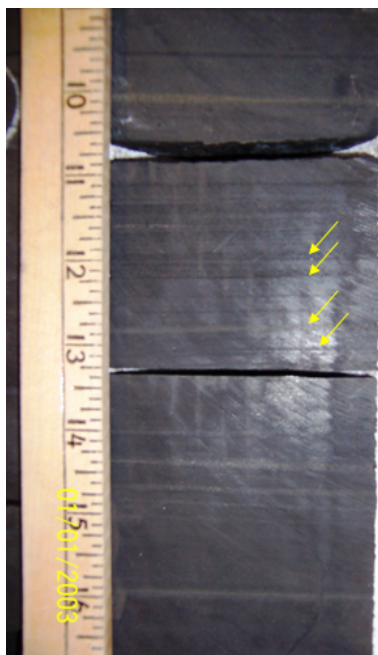
Figure 3.15. Core photograph of several phosphatic laminae (few marked by yellow arrow) stacked together at 7702.2 – 7702.6 ft (2347.6 m – 2347.7 m) in Sol Carpenter H#7 well.
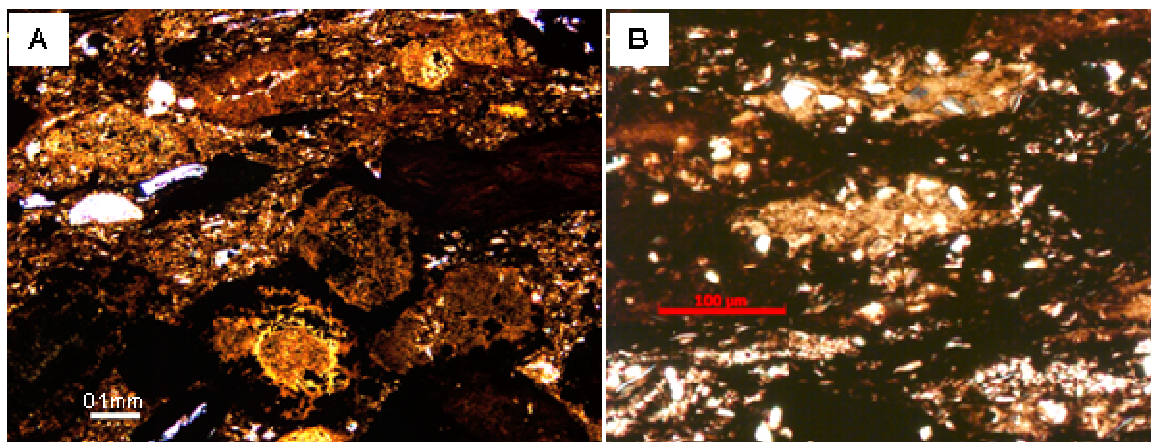
Figure 3.16. Photomicrograph of (A) *Phosphatic* pellets at 7709 ft (2349.7) in Sol Carpenter H#7 and (B) Close up of fecal pellets with large amounts of detrital quartz at 8465.7 ft (2580 m) in John Porter #3 well.
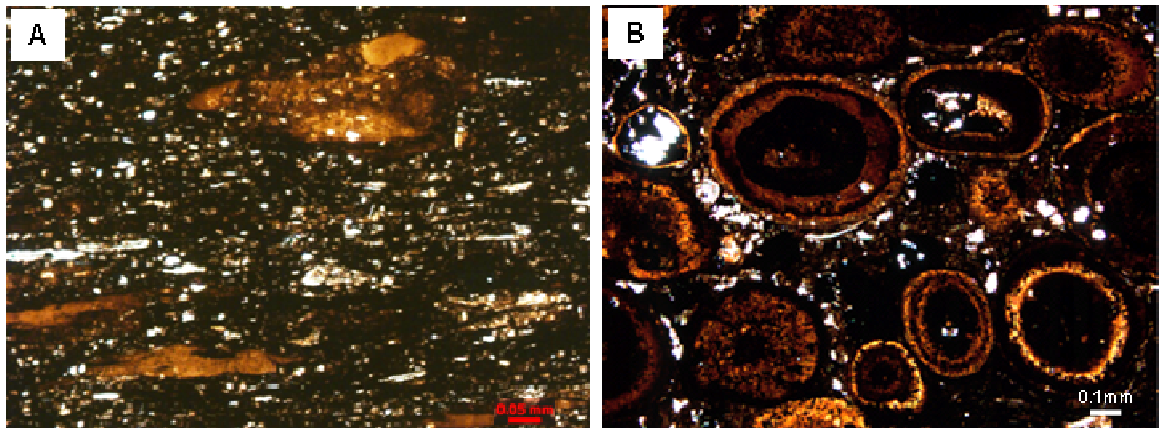
Figure 3.17. Photomicrograph showing (A) phosphatic intraclast at 8444.5 ft. (2573.8 m) in John Porter #3 well. The scale bar is 0.05 mm (B) well-developed *phosphatic* ooids at 7252.8 ft (2210.6 m) in Sol Carpenter #7 well. The scale bar is 0.1mm

The phosphatic deposits provide important Gamma Ray log response because of their highly radioactive nature. This section discusses its origin and cause for high radioactivity. All phosphate in phosphorites occurs as Flourine-carbonate-apatite although chemical variations occur (Deer et al., 1982). The origin and environment of deposition of phosphorite has long been investigated. The ocean water contains on average 70 ppb phosphorous. However, near the sea surface phosphorous is mostly depleted to a few ppb due to biological uptake. In the zone of organic matter regeneration, the concentration of dissolved phosphate rises to 50-100 ppb at a depth of about 200-400 m in the ocean column. From here down to the ocean floor, dissolved oceanic phosphate remains constant or declines very slightly (Bentor, 1980). The solubility of phosphate is higher at low pH. Bentor (1980) made observations which indicate that interstitial water in reducing sediments is the ideal habitat for phosphorite formation in the present ocean. The common association of phosphorite deposits with chert or porcellanite and organic matter suggest the biophile nature of phosphorous. The central idea of upwelling put forth by Kazakov (1934) still holds true. High productivity

of phosphorous is caused by enhanced biological activity which is triggered by the steady replenishing supply of nutrient rich water during upwelling. The high radioactivity of phosphate deposits occurs because of the common association and concentration of uranium with calcium phosphate. The reduced uranium species have lower solubility than the oxidized ones. Thus, reducing conditions, rich organic matter and high sorbtion ability of phosphates plays a significant role in concentrating uranium.

An important hurdle for apatite crystallization from open-sea water is Mg^{2+} ion. Birch (1980) suggests that this could be happening because the Mg^{2+} ions compete for the Ca^{2+} sites in the apatite structure. Mg depletion can occur through dolomitization or diagenetic reactions e.g. Mg^{2+} replacing Fe^{2+} in clays. Gulbrandsen (1960) pointed out the frequent association of dolomite with apatite, but rarely with calcite in the Phosphoria Formation.

Table 3.1. Generalized mineralogy of the lithofacies.

Facies Names	Silica including quartz and authigenic silica		Clay size minerals	Calcite		Dolomite (including Fe-dolomite)		Mica	Phosphate	Glauconite	Pyrite
	*Aver-age	Min-Max		*Average	Min-Max	*Average	Min-Max				
Siliceous non calcareous mudstone	30%	20->50%	30-40%	0-2%	0-5%	2-5%	2-10%	0-5%	0-5%	-	0-3%
Siliceous calcareous mudstone	25%	15-30%	30-40%	10-15%	5-40%	2-5%	2-15%	0-5%	0-5%	-	0-3%
Micrite/limy mudstone	*10%		40%	*30-40%		*5%		-	-	-	5%
Bottom current calcareous	*15%		20-25%	*35-40%		*2-5%		-	0-5%	-	5-7%
Reworked shelly deposit	*2-10%		15-20%	*50%		*1%		-	10%	-	2-10%
Silty-shaly (wavy) interlaminated deposit	*20%		25%	*30%		*15%		-	-	8-10%	-
Phosphatic deposit	*10-15%		35%	*10%		*2-3%		-	20-30%	3-5%	2-5%
Dolomitic mudstone	*10%		20-30%	*2-20%		30-40%	40-80%	-	-	-	-
Concretion	*10-15%		20%	*55-60%		-		-	1%	-	10-15%

55

It is clear that the lithofacies variation depicts a changing depositional environment. Thus, the several lithofacies, on the basis of their different depositional environments, will have varying organic richness due to differences in productivity and preservation in different depositional environments. Table 3.2 shows the varying amounts of total organic carbon for the various lithofacies. Total organic carbon content of a rock is a direct measure of its organic richness. As discussed in the first chapter in this dissertation, accumulation of organic matter will depend on the bottom oxygen levels. Oxygenated strata will be characterized by bioturbation and benthic activity, thus lowering the organic matter content. On the basis of this and noted specific lithofacies association, the lithofacies can be plotted against expected bottom water oxygen conditions (Table 3.3), which controls organic matter preservation.

Other geochemical parameters were also analyzed to determine the depositional environment (Rodriguez, 2007). Samples from two lithofacies – Siliceous, non-calcareous mudstone and siliceous, calcareous mudstone - were tested to determine depositional environments based on the characterization of their biomarkers. Biomarkers are controlled by variations of facies and depositional environment, and are independent of burial modifications including maturity. Figure 3.18 compares the biomarkers: Pristane/Phytane (Pr/Ph) ratio for the two samples (Rodriguez, 2007). The siliceous, non-calcareous mudstone sample which, apart from other differences in content, was richer in agglutinated forams than the siliceous, calcareous mudstone sample. The difference in Pr/Ph ratio between the two samples suggests different depositional environments for the two samples in that the siliceous non-calcareous mudstone sample was deposited in a

more reducing environment than the siliceous calcareous mudstone sample (Rodriguez, 2007).

Table 3.2. TOC (wt%) distribution for the various lithofacies in the four cored wells. Avg – average; Std.D. – Standard deviation

Lithofacies	Sugar Tree #1		Adams SW#7		Sol Carpenter H#7		John Porter #3	
	Avg.	*Std. D.*	*Avg.*	*Std. D.*	*Avg.*	*Std. D.*	*Avg.*	*Std. D.*
Phosphatic deposit	6.2	2	6.08	0.9	6.8	1.6	6	0.7
Siliceous non-calcareous mudstone	6.4	-	5	0.8	5.6	1.3	4.5	0.7
Siliceous calcareous mudstone	-	-	3.7	0.9	4.2	1.3	3.5	0.7
Calcareous laminae	3.7	-	-	-	4.2	1.1	3.5	0.5
Reworked shelly deposit	3.1	0.5	3.9	0.3	2.9	0.9	2.6	0.7
Micritic/Limy mudstone	-	-	1.3	0.1	1.5	0.3	1.2	0.5
Silty-shaly (wavy) interlaminated	-	-	-	-	1.8	0.5	-	-
Concretion	-	-	0.7	-	3.9	0.3	-	-
Dolomitic mudstone	-	-	-	-	2.3	1.2	1.9	-

Table 3.3. Position of the lithofacies (excluding diagenetic lithofacies) in relation to interpreted relative bottom oxygenation and organic richness.

57

(a) Barnett Shale sample rich in agglutinated forams   (b) Barnett Shale sample poor in agglutinated forams

Figure 3.18: Gas chromatograms of the Barnett Shale samples showing the difference in the Pristane (Pr) and Phytane (Ph) content in the two samples (a) from Siliceous non-calcareous mudstone rich in agglutinated forams at 7720 feet (2353.05 m) (b) from Siliceous calcareous mudstone poor in agglutinated foram at 7742.4 feet (2359.8 m). Modified after Rodriguez (2007).

3.2 Gamma Ray response of lithofacies

Some lithofacies have very distinctive log signatures (Fig. 3.19). *Phosphatic deposits* exhibit a characteristic high gamma ray value, due to a high amount of Uranium (detected on a spectral gamma ray log). The association of Uranium with phosphates is common to many other marine shales (Kochenov and Baturin, 2002). The *reworked shelly deposits* like *dolomitic mudstone,* if sufficiently thick, result in low gamma ray values. A sharp contact between a less calcitic facies, such as *siliceous calcareous mudstone*, and overlying more calcitic facies, such as *micritic/limy mudstone*, is represented by an abrupt upward decrease in the log response. Careful identification of the corresponding core-log response is imperative for identification of regional trends of vertical and lateral facies change and correlations in uncored wells.
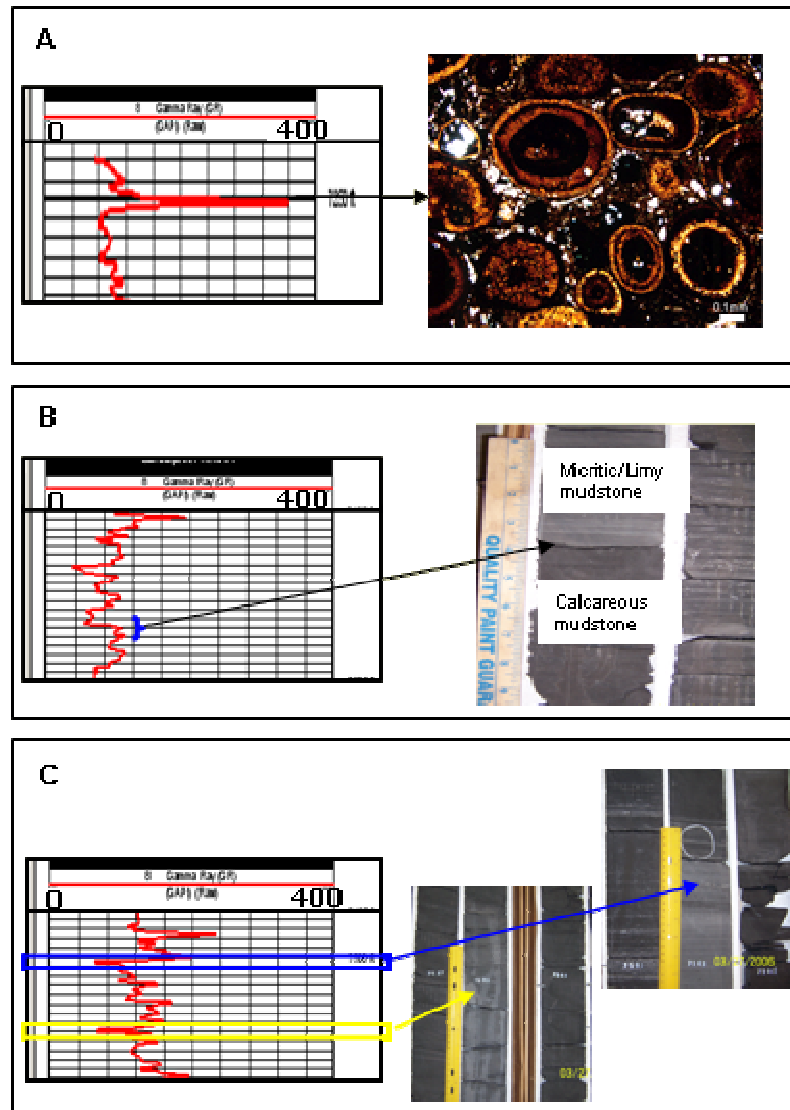
Figure 3.19: Log responses of some lithofacies. A) Phosphatic ooid at 7252.8 ft (2210.6 m) in Sol Carpenter #7 well giving rise to remarkably high Gamma Ray response, B) Abrupt change in Gamma Ray values owing to sharp contact between *Micritic/limy mudstone* and *Siliceous calcareous mudstone* at 7346.5 ft (2239.2 m), and C) *Dolomitic mudstone* at 7503 ft (2286.9 m) and 7539 ft (2297.8 m) in Sol Carpenter H#7 well giving rise to low Gamma Ray values.

Chapter 4

Sequence Stratigraphy

4.1 Introduction

Sequence stratigraphy involves recognition and correlation of time-stratigraphic surfaces that represent changes in the depositional record preserved in the rocks (Embry, 2007). It can be used in combination with facies analysis to provide a framework for interpreting depositional history and paleogeographic evolution (Embry, 2007).

Establishing sequence stratigraphy in fine grained rocks is challenging and certainly not as straightforward as in more energetic marine environments and their coarser-grained facies. The key to understanding the sequence stratigraphic framework in marine shale depositional systems is to understand that the character of the sediment supply, the mode of delivery, rate of deposition and the type of sediment (carbonates vs. clastics, coarse vs. fine, detrital vs. biogenic) can make a difference in the record of depositional sequences in these kinds of depositional systems (Bohacs and Schwalbach, 1992). The association of the mudstones with water depths and bottom oxygen levels is also significant. The deposition of fine grained sediment signifies quiet water conditions which in turn are indicative of higher accommodation. An increase in accommodation would usually mean deeper water (muddy tidal flats are an exception), hence reduction in

oxygen levels at the sea bottom, reduction in fossil abundance and diversity and enhanced organic matter preservation. A study of all these factors collectively brings out the genetic relations of these rocks, thus helping to generate the sequence stratigraphic model for the mudstone deposits.

It is important to bear in mind that in the depositional environment of deeper water Barnett strata (Loucks and Ruppel, 2007) and other similar deposits no single unique feature in a stratigraphic section can be used to make an interpretation. The interpretation is based on several features and characteristics, including the sedimentologic criteria, spectral gamma ray elemental composition, identification of repeated, recognizable patterns in vertically stacked successions, and identification of parasequences and their lateral continuity. Spectral gamma-ray provides the total gamma ray radiation and the relative amounts contributed by potassium, uranium and thorium. These data indicating major lithologic changes in marine shales are incorporated into this interpretation.

The recognition of the cyclical stacking pattern of the lithofacies, coupled with identification of Gamma Ray Parasequences (GRP) from the gamma-ray log patterns was the key to establishing a sequence stratigraphic framework for the Barnett Shale.

4.2 Barnett Shale Parasequences

The gamma ray profile of the cored wells provided identification of *upward-increasing Gamma Ray API (American Petroleum Institute) intervals*, *upward-decreasing API intervals* and *intervals of constant API* (Fig. 4.1). These intervals are bounded by gamma ray kicks i.e. log based flooding surfaces and hence they can be termed Gamma Ray

Parasequences where a parasequence is defined as a relatively conformable succession of genetically related beds or bedsets bounded by marine-flooding surfaces (Van Wagoner et al. 1990). A parasequence boundary records an increase in accommodation and separates strata deposited in deeper water, low energy conditions from those deposited in relatively shallow water, higher energy conditions (Bohacs, 1998). Commonly, most siliciclastic parasequences are progradational and most carbonate parasequences are aggradational (Van Wagoner et al. 1990). Deepening-upward (retrogradational) parasequences which are assumed to be rare in the rock record by Van Wagoner et al. (1990) are common, along with the other types of parasequences in the Barnett Shale marine setting.
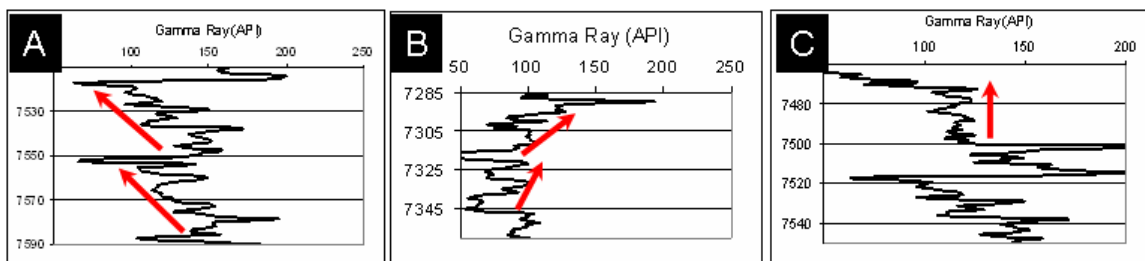
Figure 4.1. Example of (A) upward- decreasing Gamma Ray-API, (B) upward- increasing Gamma Ray-API, and (C) Constant Gamma Ray-API parasequence patterns of the Barnett Shale from the Sol Carpenter H#7 well.

These log parasequences were analyzed in detail in all the cores. They are discussed further in this chapter, but provided below is a synopsis of the general trend of the Barnett rock record with respect to these three kinds of GRP:

1) *Upward-decreasing intervals of API:* A typical upward-decreasing Gamma Ray Parasequence (Fig. 4.1A) is mineralogically represented by upward-decreasing amounts of clay and phosphatic sediments accompanied by increasing calcite content (Fig. 4.2). Lithologically, the lower part of the GRP package is composed of *siliceous non*

62

calcareous mudstone facies with a large amount of compacted phosphatic pellets in the matrix. The lower middle part of this GRP also contains several *bottom current calcareous laminae* deposits suggesting relatively deeper water conditions. Upsection, this GRP is generally capped by *reworked shelly deposit* lithofacies. This GRP pattern could be indicative of either upward-shoaling of the depositional environment during gradual fall in relative sea level or progradation during late stage highstand.
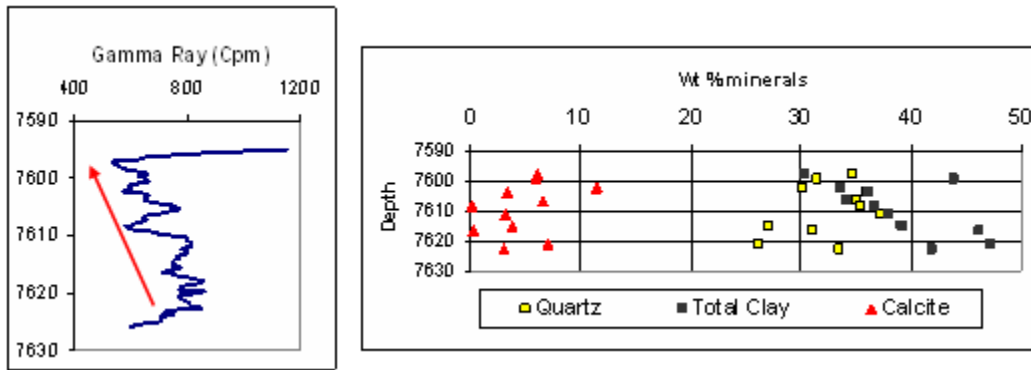
Figure 4.2. The Gamma Ray and mineralogical profile of an upward- decreasing Gamma Ray-API Parasequence. (Also refer to Appendix A.1)

2) *Upward-increasing intervals of API:* A typical upward-increasing Gamma Ray Parasequence (Fig. 4.1B) is mineralogically composed of upward-increasing amounts of clay and upward-decreasing calcite content (Fig. 4.3). Lithologic composition consists of *silty shaly wavy bed* and *micritic/limy mudstone* deposit in the lower part of the package which is followed upward by *siliceous, calcareous mudstone* and *siliceous, non calcareous mudstone deposits* at the top. This GRP pattern could be indicative of a deepening-upward depositional environment during gradual rise in relative sea level.
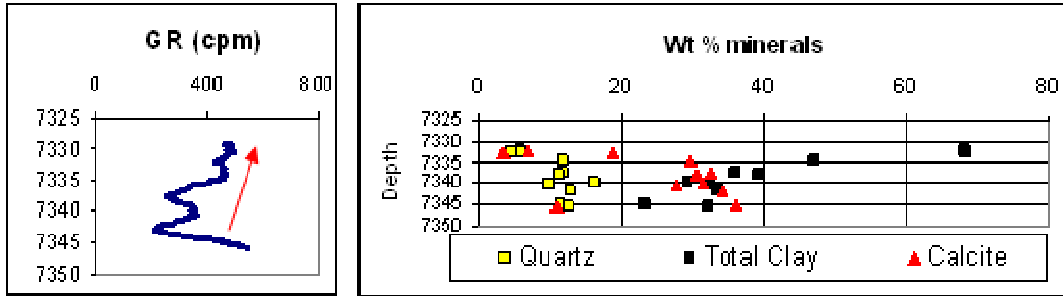
Figure 4.3. The Gamma Ray and mineralogical profile of an upward- increasing Gamma Ray-API parasequence. (Also refer to Appendix A.2)

3) *Intervals of constant API:* A typical constant-Gamma Ray Parasequence (Fig. 4.1C) is mineralogically represented by upward-increasing amounts of clay and quartz and uniformly low calcite content. Lithologically, the GRP generally varies from siliceous, non calcareous mudstone to siliceous, calcareous mudstone.
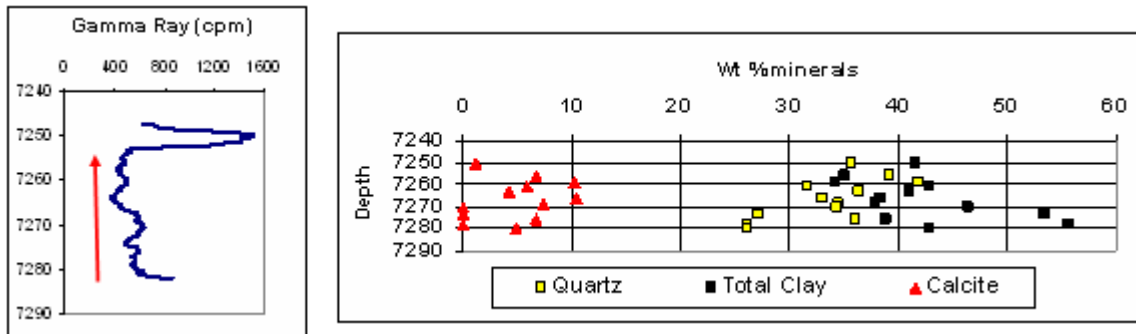
Figure 4.4. The Gamma Ray and mineralogical profile of an interval of constant Gamma Ray API. (Also refer to Appendix A.3)

4.3 Barnett Shale Sequence Framework

This section discusses the vertical succession of the lithofacies within each parasequence in the Sol Carpenter H#7 well. This is followed by a documentation of lateral correlation of the parasequences in the John Porter #3, Adams SW #7 and Sugar Tree #1 cores in

order to evaluate regional parasequence trends. The complete section: 7752.2 ft (2362.8 m) to 7236 ft (2205.5 m) of the Sol Carpenter H#7 - which includes the Upper Barnett Shale, Forestburg Limestone and the Lower Barnett Shale - provides a continuous core to document the evolution of depositional environments, depositional sequences, parasequences and parasequence sets, their bounding surfaces, and other significant stratal surfaces within the Barnett Shale. Figure 4.5 displays the core gamma-ray data, lithostratigraphy and interpreted sequence stratigraphy of Sol Carpenter H #7 which will be discussed in this chapter.
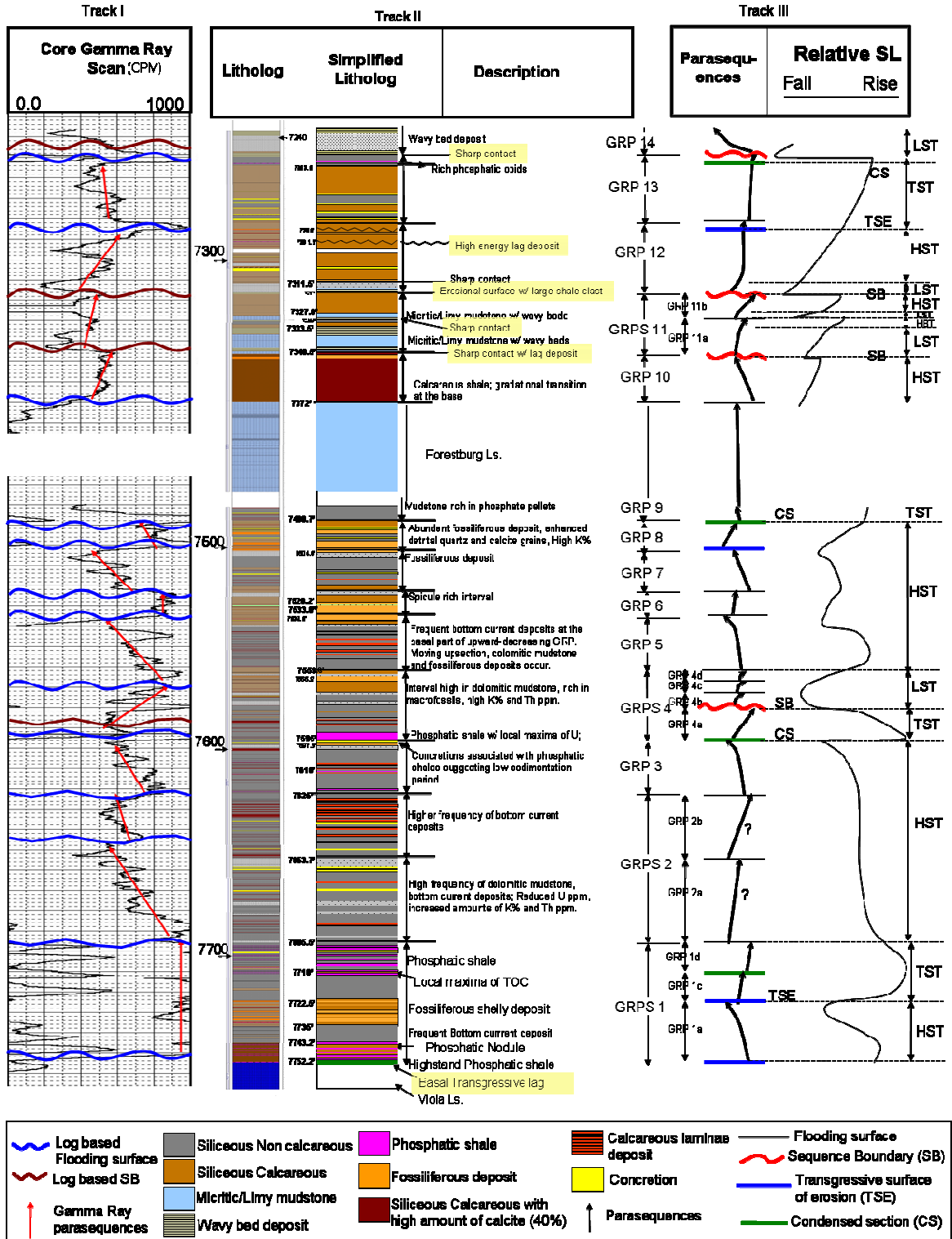
Figure 4.5. Sequence stratigraphic interpretation of the Barnett Shale in Sol Carpenter H#7 well [7752.2 ft (2362.8 m) to 7236 ft (2205.5 m)]. Track I shows the core gamma ray profile, track II is the litholog and core description, track III illustrates the interpreted

parasequences, relative sea level fluctuations; however, the magnitude of fluctuations is not known, so is not shown to scale, and positions of systems tracts.

Note: Each GRP/GRPS description is summarized in the following format:

- Vertical succession of lithofacies within GRP/GRPS in Sol Carpenter H#7 well,

- Lateral Correlation in other wells.

- Interpretation

4.3.1 Lower Barnett Shale

GRPS 1: 7752.2 ft (2362.8 m) – 7695.5 ft (2345.5m)

Vertical succession in Sol Carpenter H#7 well: This Gamma Ray Parasequence Set (GRPS) mostly has remarkably high gamma ray values (>1000 counts per minute in core gamma ray log) (Fig. 4.5). This interval is a Gamma Ray Parasequence Set because it is composed of three parasequences (GRP 1a, c, d) based on the vertical succession of lithofacies (Figures. 4.5 and 4.6). The lowermost parasequence (GRP 1a) displays a typical upward-decreasing gamma ray pattern with *non calcareous siliceous mudstone* and *phosphatic deposits* in the lower part and capped by *reworked shelly deposit* (Fig. 4.6).

This is followed upward by two parasequences (GRP 1c and d) which are separated by a horizon marked by TOC maxima around 7710 ft (2350 m) (Fig. 4.7). The onset of parasequence 1c is marked by a high gamma ray, hot shale which is a correlative conformity equivalent to transgressive surface of erosion. These two parasequences are composed of *siliceous non calcareous mudstone* and *phosphatic deposits.* In addition, the upper parasequence contains few bottom current reworked, *calcareous laminae deposits*

67

and a *concretion.* The TOC maxima horizon indicates low sedimentation and hence a high organic matter preservation. It is a condensed section, which was a regionally significant surface and identified in all other cored wells (Fig. 4.7).
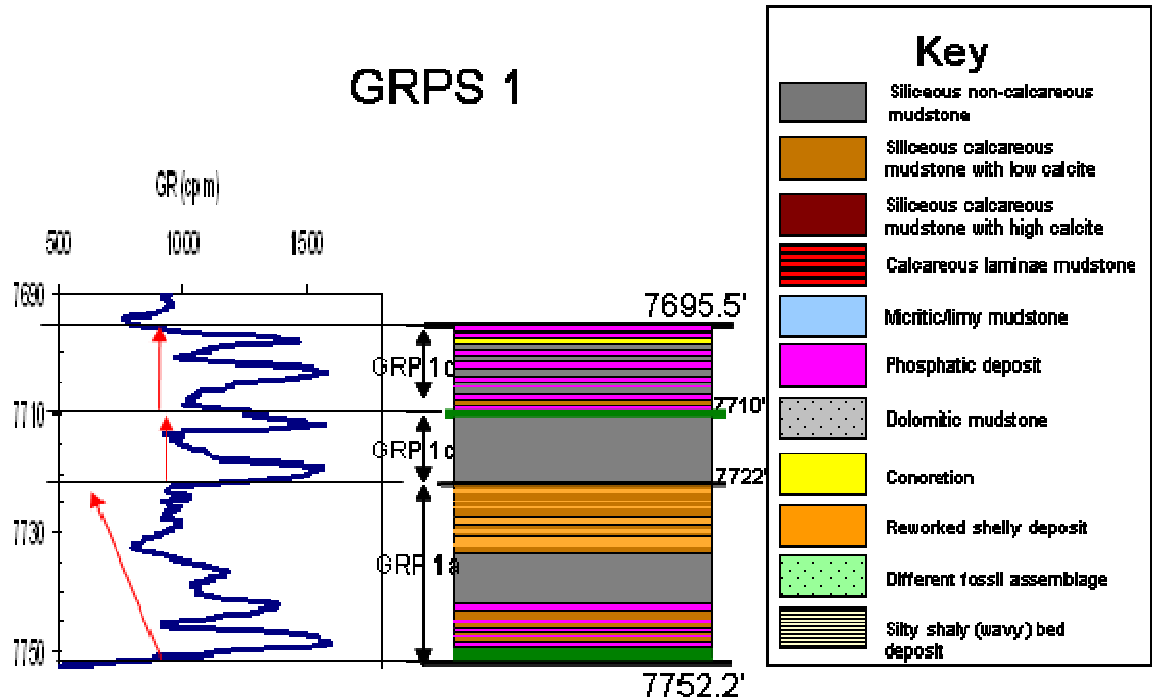
Figure 4.6. GRPS1 - Gamma Ray and lithology profiles of Sol Carpenter H#7. The key provides the lithofacies color code.

Detailed description**:** The base of the lower parasequence is marked by a transgressive lag at 7752.2 ft (2362.8 m). It marks the onset of transgression by the Mississippian sea. The surface immediately underlying the lag is a *glossifungitis* surface (burrow assemblage) which suggests that the horizon underneath was firm and consolidated at the onset of transgression (Fig. 4.8).

The phosphatic deposits of the lowermost parasequence occur in the form of phosphatic pellets which are often irregularly coalesced in several distinct laminae. Agglutinated forams and detrital quartz are very common within this interval. A similar

pattern is observed in the correlative intervals of the John Porter #3, Adams SW#7 and Sugar Tree #1 wells. This interval has high amounts of potassium and thorium, suggestive of terrigenous input (Fig. 4.9). The capping interval of this lowermost parasequence is *reworked shelly deposit* (Fig. 4.10) [from 7735 ft (2357.6 m) to 7722 ft (2353.6 m)] (Fig. 6).
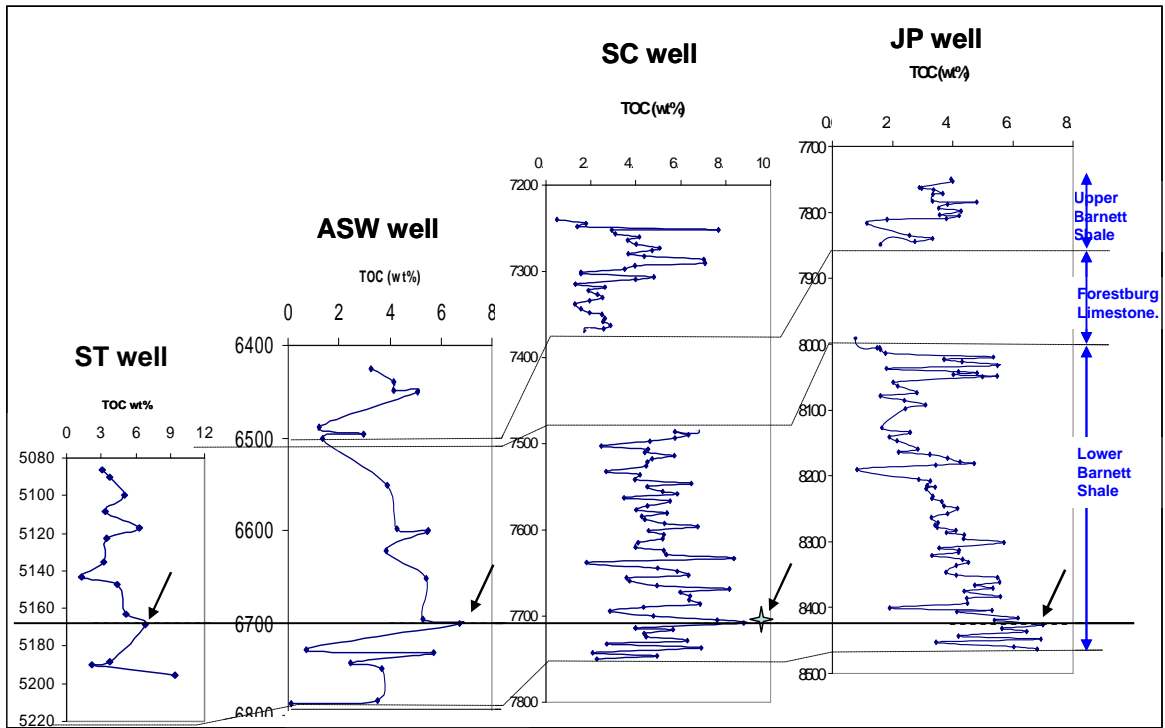
Figure 4.7. Core measured Total Organic Carbon (TOC) for the entire Barnett Shale section in the four wells: Sugar Tree #1 (ST), Adams SW #7 (ASW), Sol Carpenter H#7 (SC) and John Porter #3 (JP). The star marks the position of local maxima of TOC (see text for details) in the Sol Carpenter H#7 well and the arrows mark the correlative depth for this maxima in all cored wells.
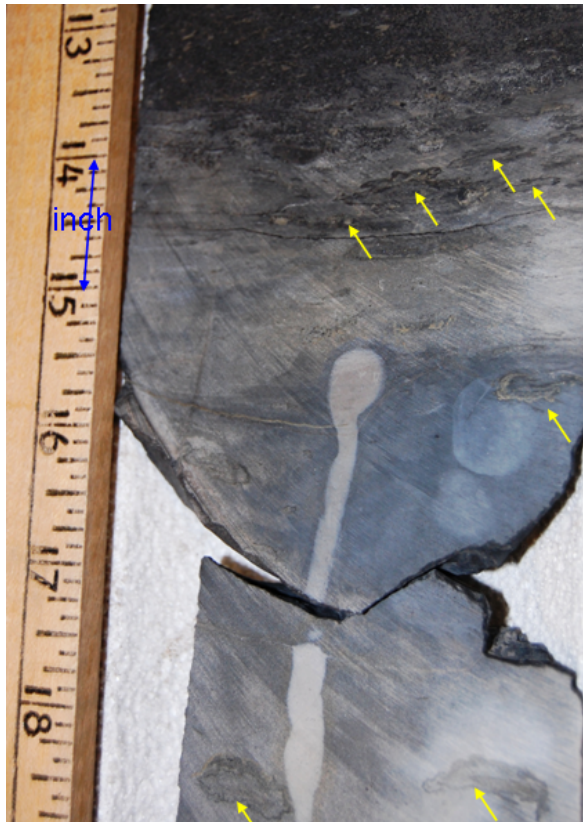
Figure 4.8. Core photograph showing the glossifungitis surface at 7752.3 ft – 7752.4 ft. in Sol Carpenter H#7 well.
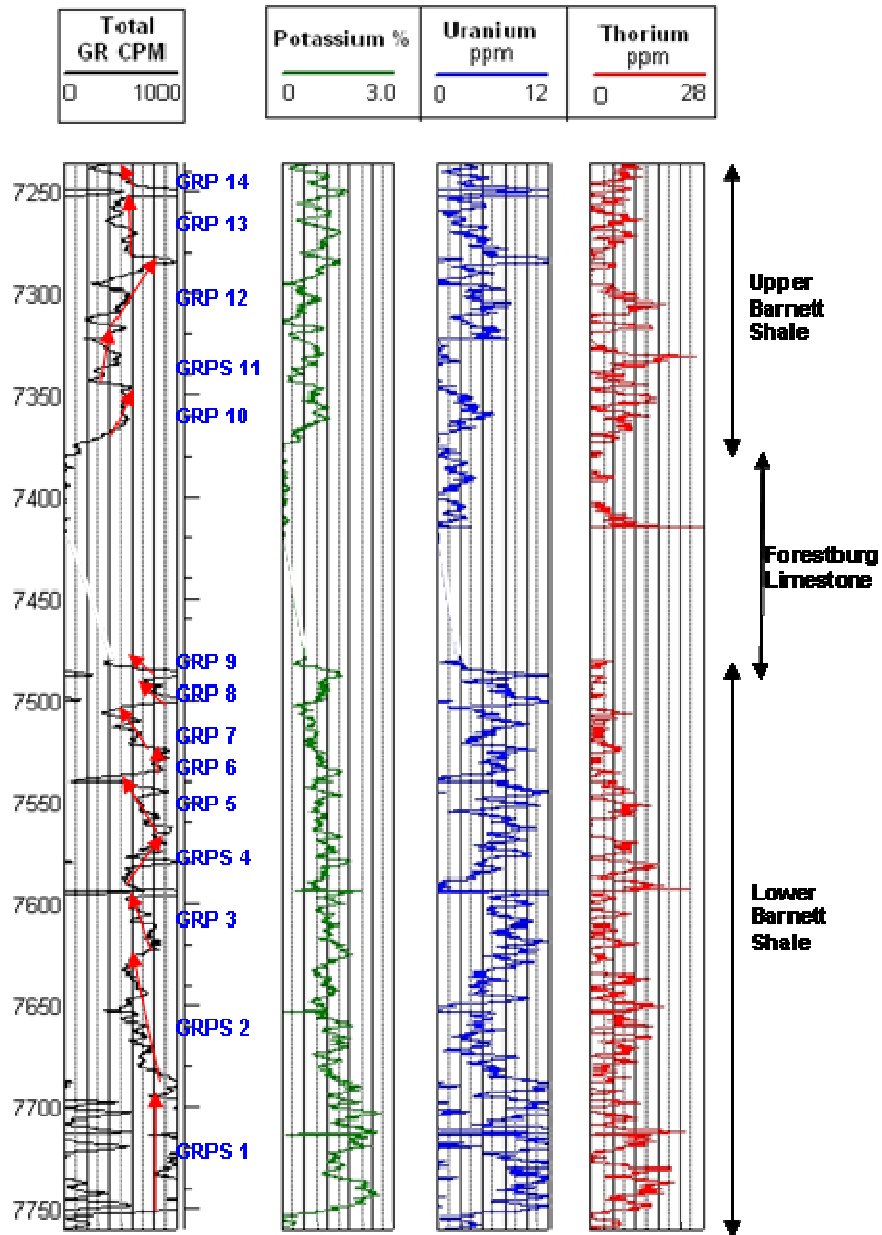
Figure 4.9. Display of the core Gamma Ray scan and the abundances of Potassium, Uranium and Thorium for Sol Carpenter H#7 well - 7752.2 ft (2362.8 m) to 7236 ft (2205.5 m).

71
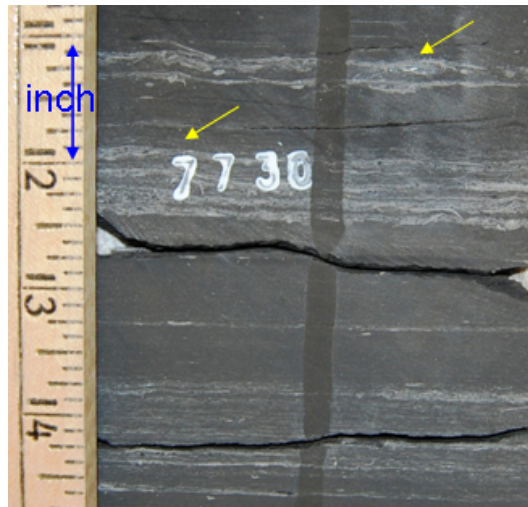
Figure 4.10. Core photo of the reworked shelly deposit at 7730 ft. (2356.1 m). The arrows point to the rippled top surfaces of the shelly deposits.

Lateral Correlation in other wells: Lateral correlation of this GRPS in all the cored wells shows that this GRPS thins in the northeast direction towards John Porter #3 well (Fig. 4.11). The three parasequences that were identified in the Sol Carpenter H#7 were traced to the John Porter #3 well in the northeast. However, towards the west and southwest direction i.e., in Adams SW#7 and Sugar Tree #1 wells, an additional parasequence (GRP 1b) was noted in the vertical succession which occurs at depths corresponding to those between the lowermost and middle parasequences in the Sol Carpenter H#7 and John Porter #3 wells (Fig. 4.11). Overall, the lowermost parasequence (GRP 1a) with capping *reworked shelly deposit* is present in all the wells (Fig. 4.11). The detrital quartz grains present in this parasequence of Adams SW#7 section are much larger compared to those in the John Porter #3 section (Fig. 4.12). The Adams SW#7 section also contains detrital calcite grains - these are not common in the Sol Carpenter H#7 and John Porter #3 sections. Strange burrow-like features were identified in the Adams SW#7 within this quartz rich interval. The increasing abundance of sand to the

72

west and southwest indicates that the land/source area lay towards the west-southwest. The *reworked shelly deposit* capping the lowermost parasequence is present in all the wells; however, it is condensed to a thin interval in the John Porter #3 well. The next parasequence (GRP 1b) has a similar vertical succession of lithofacies, however, it is present only in the Adams SW#7 and Sugar Tree #1 wells and thins out before reaching the Sol Carpenter H#7 and John Porter #3 wells in the northeast (Fig. 4.11). The two uppermost parasequences (GRP 1c and d) in all four wells represent deeper water deposits composed mainly of *non calcareous mudstone* and *phosphatic deposits* (Fig. 4.11).
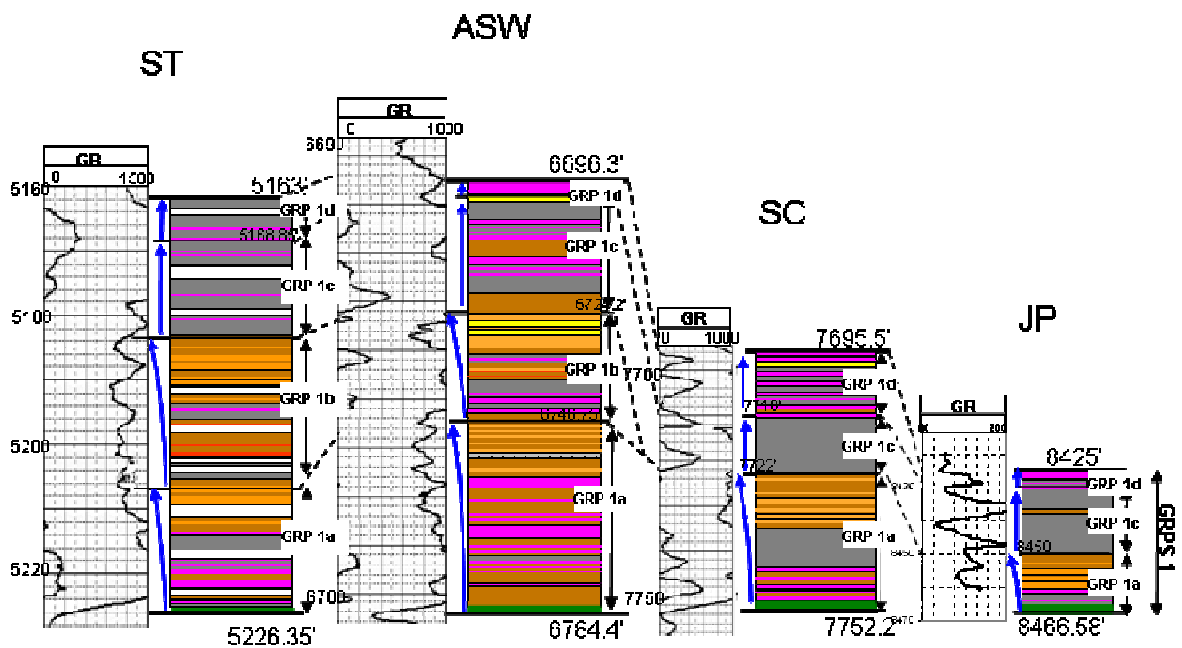
Figure 4.11. Lateral correlation of the GRPS 1 in the four cored wells: Sugar Tree #1 (ST), Adams SW #7 (ASW), Sol Carpenter Heirs #7 (SC) and John Porter #3 (JP). For color index see Figure 4.6.
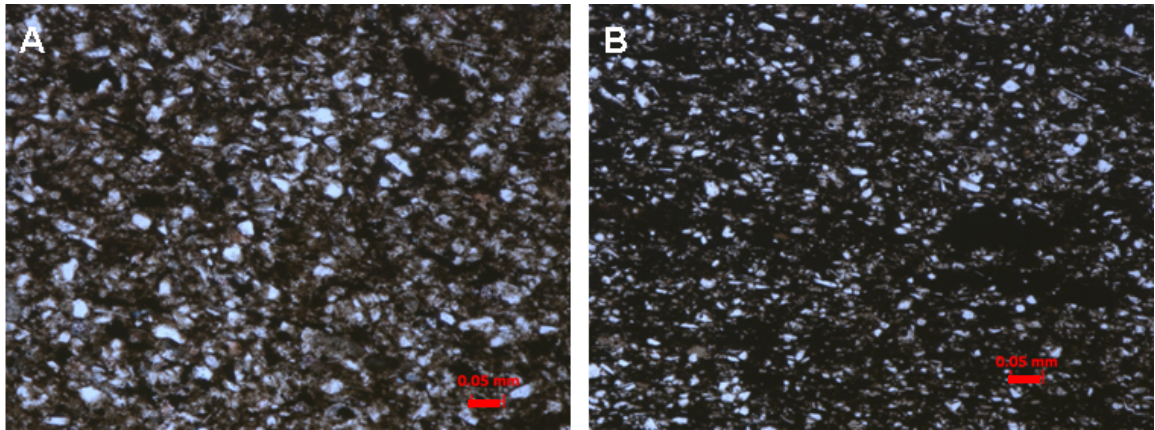
Figure 4.12. The high abundance of detrital quartz in the lowermost parasequence of GRPS 1 is shown in these thin sections. The petrographic image of the two thin sections shows the decrease in quartz grain size from the correlatable interval in the Adams SW#7 and John Porter #3 wells. (A) 6782.2 ft. (2067.2 m) of Adams SW#7 and (B) 8464 ft. (2579.8 m) of John Porter #3. The scale bar is equal to 0.05 mm.

Detailed description: This section gives further details on few aspects of this GRPS. The basal transgressive lag (BTL) is present in all the wells. The *glossifungitis* surface beneath the transgressive lag, as discussed above, was also traced in all the wells. Figure 4.13 shows the photomicrograph of the basal transgressive lag interval in Sugar Tree #1 and Sol Carpenter #7 wells. The dominant components of BTL are phosphate, glauconite and conodont grains. However, there is remarkable variation in the form and proportion of these grains. The BTL in Sugar Tree #1 is rich in detrital glauconite grains, phosphatic grains, also grains that are partially phosphatic and partially glauconitic, and conodonts. The phosphatic grains in Sugar Tree #1 are more elongated with lesser evidence of reworking than at the Sol Carpenter H#7 transgressive surface, which is heavily pyritized, rich in reworked phosphatic grains and relatively low in glauconite and conodont grains. The phosphate grains are more circular in shape with frequent phosphatic intraclast grains, suggesting more reworking during transgression.

74
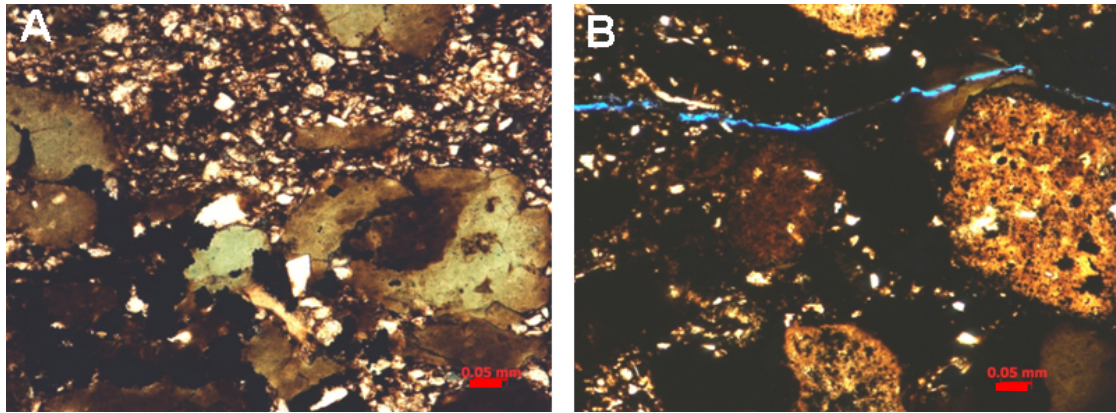
Figure 4.13. Shows the basal transgressive lag at (A) 5226 feet (1592.8 m) in Sugar Tree #1 well which is rich in detrital and in situ glauconite, phosphate, detrital quartz and glauconite grains. The grains have undergone phosphatization and the (B) 7752.3 feet (2362.9 m) in Sol Carpenter Heirs #7 well is heavily pyritized (appears black in optical microscopy), is rich in reworked, subrounded phosphatic grains and contains few detrital quartz grains. Note: Compare the grain size of detrital quartz at the two sites. The detrital quartz grains in Sugar Tree #1 well are relatively abundant and larger. The scale bar is equal to 0.05 mm.

A large proportion of grains that are partially phosphatic and partially glauconitic in the Sugar Tree #1 core were studied to determine the paragenesis of glauconite-phosphorite in these grains. However, no distinct order was identified. It is likely that in some cases glauconitization (glauconitic alteration of phosphates) has occurred and in other cases phosphatization (phosphatic alteration of glauconites) has occurred. Glauconitization, on one hand, is suggested by the presence of phosphate intraclast grains which are partially glauconized, indicating that phosphate is the primary grain. Phosphatization, on the other hand, is supported by the presence of crisp, angular boundaries of some of the partially altered glauconite grains (Fig. 4.13A). The BTL in the Sugar Tree #1 section is unusually rich in detrital quartz and the grains are larger in size as compared to the Sol Carpenter H#7 detrital quartz, suggesting Sugar Tree #1 well lay closer to the land source area. The high amount of pyrite, lesser proportion and smaller

size of detrital quartz and the subrounded, reworked phosphatic grains in Sol Carpenter H#7 suggests that at the time of deposition, the Sol Carpenter H#7 site was more reducing and farther basinward than the Sugar Tree #1 site.

Interpretation: This GRPS begins with the basal transgressive surface of erosion in all the cored wells, and high amount of clastics trapped in the lower part suggesting initial stages of transgression. This GRPS consists of stacked shoaling upward depositional parasequences which appear to be retrograding (Plate 5). The land source area most likely lay to the west or southwest during this period of deposition, which is interpreted by relatively high amounts of clastics in this interval in the west and southwest wells i.e. Adams SW #7 and Sugar Tree #1. On a sequence scale, the lower shoaling upward parasequences (GRP 1a and b) of this GRPS are interpreted to constitute a highstand systems tract. The onset of the third parasequence, 1c is marked by a high gamma ray, hot shale in all the wells which is interpreted as a correlative conformity equivalent to transgressive surface of erosion. The parasequences 1c and d constitute the transgressive systems tract (Fig. 4.5; Plate 5). The later interpretation is based on the presence of phosphate rich *non calcareous mudstone* in these parasequences and the presence of the condensed section (Fig. 4.5, Plate 5).

GRPS 2: 7695.5 ft (2345.5 m) - 7625 ft (2324.1 m)

Vertical succession in Sol Carpenter H#7 well: This GRPS is composed of an upward-decreasing gamma ray pattern (Fig. 4.14). It is considered as one Gamma Ray Parasequence set for mapping purposes because it is divisible into two high resolution

depositional parasequences in the northeastern Sol Carpenter H#7 (Fig. 4.14) and John Porter #3 wells on the basis of lithofacies stacking pattern. They were indistinguishable in the Adams SW#7 well. The two depositional parasequences in Sol Carpenter H#7 section are: GRP 2a: 7695.5 ft (2345.5 m) – 7650 ft (2331.7 m) and GRP 2b: 7650 ft (2331.7 m) - 7625 ft (2324.1 m) (Fig. 4.14).

The lower parasequence 2a: 7695.5 ft (2345.5 m) – 7650 ft (2331.7 m) contains *siliceous non calcareous mudstone* with few *calcareous laminae deposit, concretions* and *dolomitic mudstone* (Fig. 4.14). It has a relatively high amount of thorium and potassium and a reduced amount of uranium (Fig. 4.9). The upper parasequence 2b: 7650 ft (2331.7 m) - 7625 ft (2324.1 m) (Fig. 4.14) records *non calcareous mudstone* with abundant bottom current reworked *calcareous laminae deposits*. The *calcareous laminae deposit* has intensified/high frequency in this interval and several of these laminae consist of pyritic lensoids.
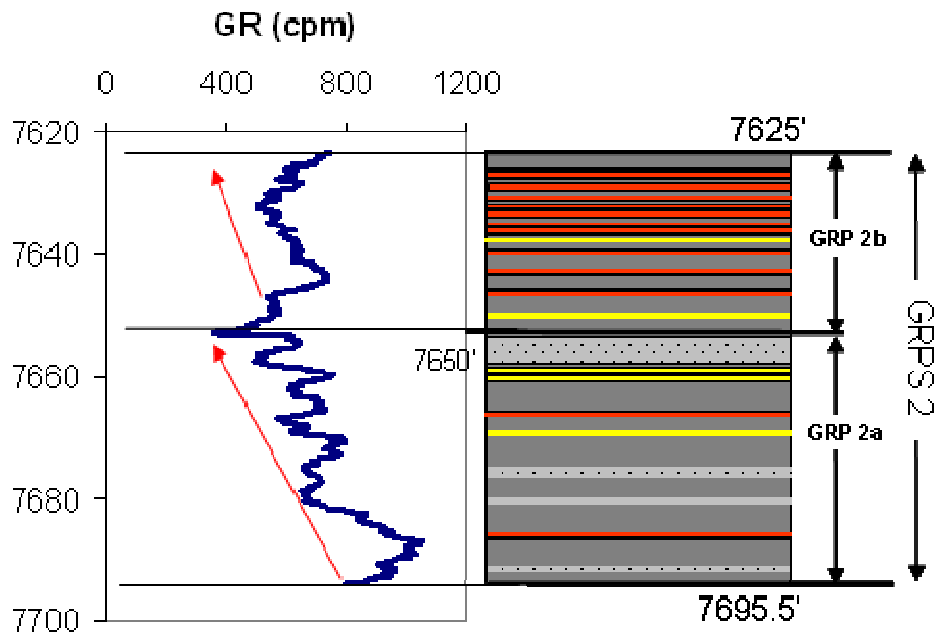
Figure 4.14. GRPS 2 - Gamma Ray and lithology profiles of Sol Carpenter H#7. For color index see Figure 4.6.

Lateral Correlation in other wells: The laterally corresponding interval of the lower parasequence (GRP 2a) in John Porter #3 well consists of a high proportion of *concretions* and almost no *dolomitic mudstone* facies compared to Sol Carpenter H#7 section (Fig 4.15). The *concretions* in the John Porter #3 well are rich in calcareous (replaced?) spicules – which could act as nuclei for the development of *concretions* (Fig 4.16). The upper depositional parasequence of GRPS 2 (GRP 2b) in the John Porter #3 and Sol Carpenter H#7 and the upper part of this GRPS in the Adams SW#7 well record high frequency and most intensified/frequency bottom current reworked *calcareous laminae deposits* in the entire vertical section of all the wells (Fig. 4.15). This interval suggests a highstand period of sea level characterized by minimal sediment input and strong bottom currents (Armishaw et al., 2000, Masson et al., 2002). Adams SW #7 well contains no concretions in the corresponding interval. Rather, it is rich in phosphatic deposits and calcareous laminae suggesting deeper water conditions.

Figure 4.15. Lateral correlation of the GRPS 2 in three cored wells: Adams SW #7 (ASW), Sol Carpenter Heirs #7 (SC) and John Porter #3 (JP). For color index see Figure 4.6.
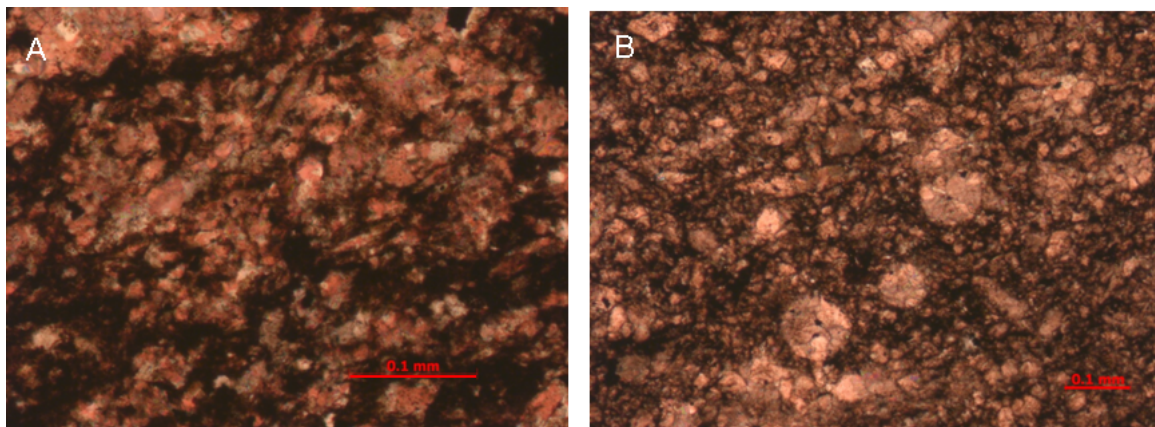
Figure 4.16. Photomicrographs of concretions at - (A) 8380 ft (2554.4 m) in John Porter #3 well and (B) 8413.8 ft. (2564.5 m) in John Porter #3 well - which has a high abundance of calcareous (replaced?) spicules cemented by calcitic spar. Calcite is stained pink in the photo. The scale bar is 0.1mm.

The corresponding interval in Sugar Tree #1 well was not distinguishable from the overlying parasequence.

Interpretation: GRPS 2 was deposited at a highstand of sea level. All the wells have most intensified (abundant) bottom current reworked *calcareous laminae deposits* in this GRPS. Additionally, all the wells excluding John Porter #3 have high abundance of *phosphatic deposits*, confirming the highstand period of sea level with strong bottom currents. The easternmost John Porter #3 well consists of several concretionary carbonates in the lower part of this GRPS, which are rich in calcareous (replaced?) spicules, possibly acting as nuclei for the development of the *concretions*. On a sequence scale, this GRPS is part of the highstand systems tract (Fig. 4.5, Plate 5).

GRP 3: 7625 ft (2324.1 m) - 7595 ft (2314.9 m)

Vertical succession in Sol Carpenter H#7 well: This interval represents an upward-decreasing gamma ray pattern (Fig 4.17). The basal part of the GRP consists of *siliceous, non calcareous mudstone* which is rich in *phosphatic deposits* hence the high gamma ray values at the base (Fig 4.17). Biota content is dominated by agglutinated forams and a few siliceous spicules. Upsection, this GRP is capped by transported *reworked shelly deposit* and *concretion* lithofacies.
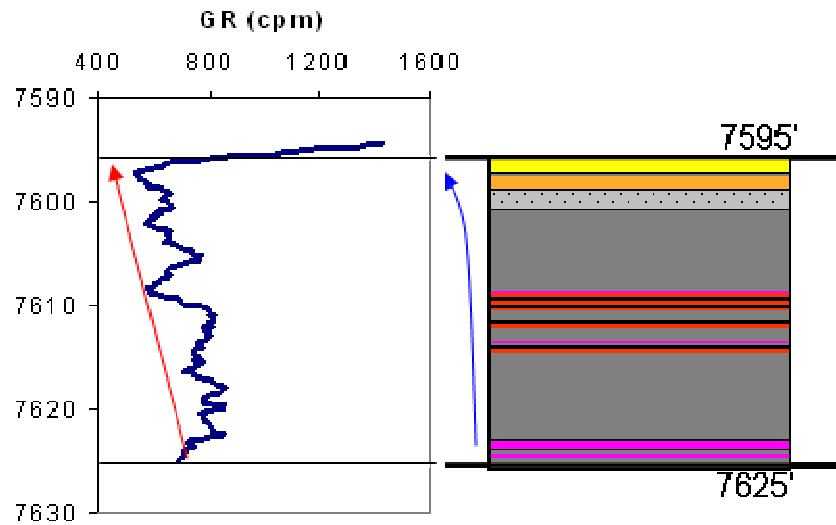
Figure 4.17. GRP3 - Gamma Ray and lithology profiles of Sol Carpenter H#7. For color index see Figure 4.6.

Lateral Correlation in other wells: This GRP is traceable in all the cored wells. All the wells contain *siliceous non calcareous mudstone, calcareous laminae deposit* and *phosphatic deposit* (John Porter #3 has very minimal phosphatic deposit) in the lower part of this GRP; however, the capping *reworked shelly deposit* is absent in Adams SW#7. *Dolomitic mudstone* caps this parasequence in Adams SW#7 (Fig. 4.18). The corresponding interval in the Sugar Tree #1 well contains *concretions* close to the top (details are discussed later).

Detailed description: In Adams SW#7, the lower interval contains higher amount of *phosphatic deposit* than in the Sol Carpenter H#7. John Porter #3 section contains *calcareous laminae* in the lower part with almost no *phosphatic deposit* (Fig. 4.18). *Dolomitic mudstone* towards the top of the parasequence in Sol Carpenter H#7 and Adams SW#7 can be easily distinguished. The individual dolomite grains in the Sol Carpenter H#7 are relatively small in size and abundance as compared to those in the

81

Adams SW#7. The top interval of the John Porter #3 well consists of a different fossil assemblage, which includes calcareous spicules and echinoderm fragments (Fig. 4.19). This fossil assemblage is unique to the John Porter #3 and is not found in other wells suggesting that the John Porter #3 well is close to the source area.

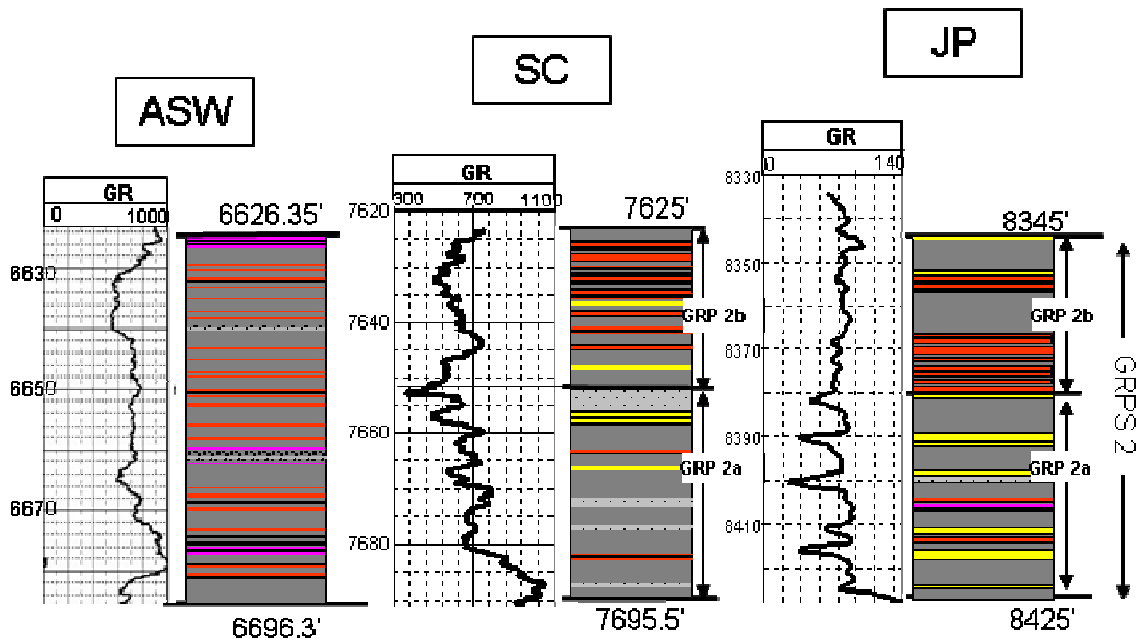Figure 4.18. Lateral correlation of the GRP 3 in three cored wells: Adams SW #7 (ASW), Sol Carpenter Heirs #7 (SC) and John Porter #3 (JP). For color index see Figure 4.6.
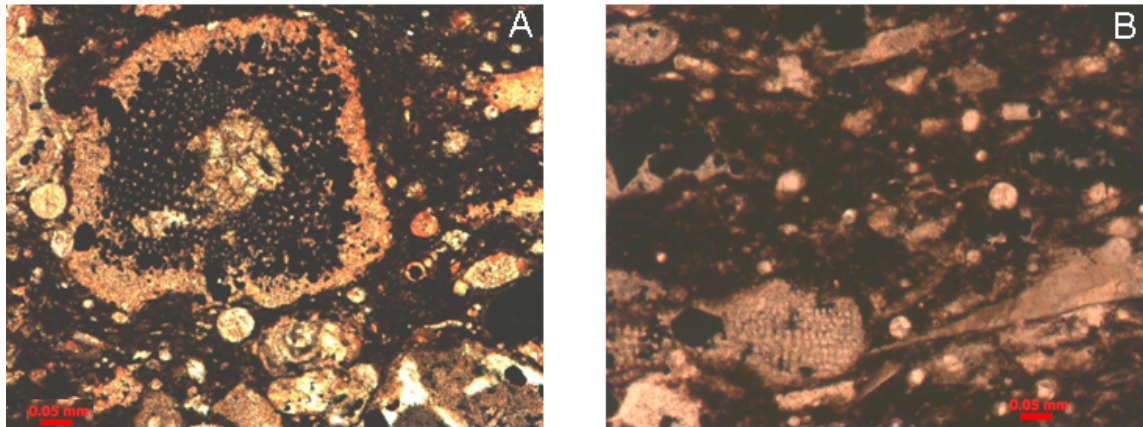

Figure 4.19. Petrographic images of the spicule and echinoderm, fossil-rich interval unique to John Porter #3 in GRP 3 at (A) 8310' and (B) 8315.3'. The scale bar is 0.05mm.

In Sugar Tree #1 well GRP 2 and 3 were indistinguishable by either the gamma ray log profile or lithofacies stacking pattern (Fig. 4.20). The gamma ray profile generally follows an upward decreasing pattern. The interval consists of *siliceous, non calcareous mudstone, phosphatic deposits* and *concretion* towards the top.
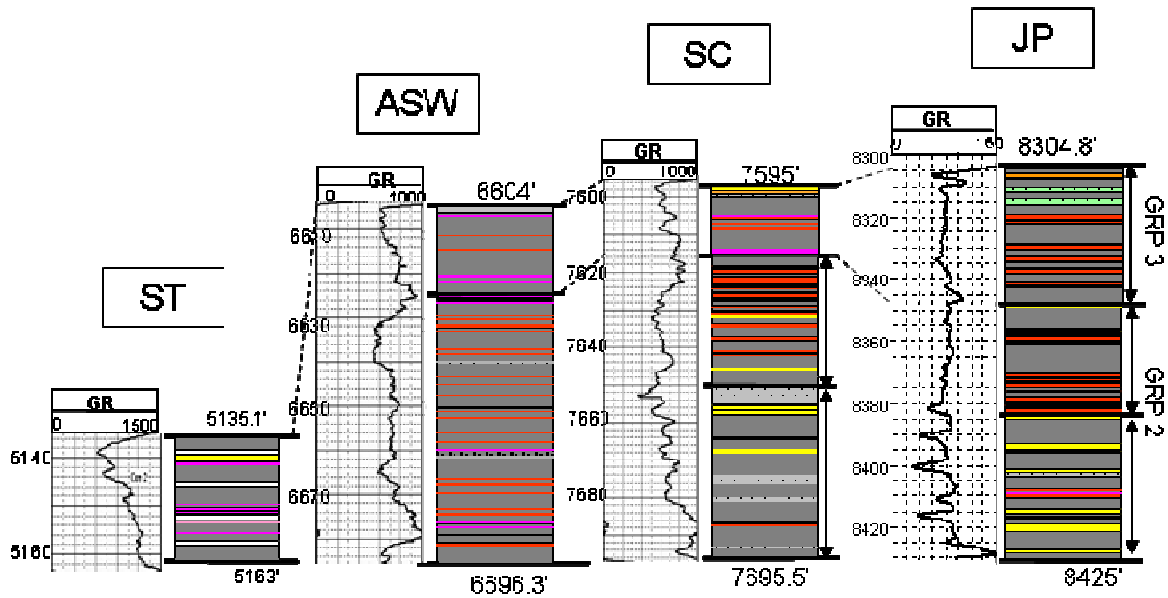
Figure 4.20. Lateral correlation of the GRP 2 and 3 in the cored wells: Sugar Tree #1 (ST), Adams SW #7 (ASW), Sol Carpenter Heirs #7 (SC) and John Porter #3 (JP). For color index see Figure 4.6.

Interpretation: The upward-decreasing gamma ray pattern of this GRP is indicative of either upward-shoaling of the depositional environment during gradual fall in relative sea level or progradation during late stage highstand. Additionally, the several intervals rich in fragments of echinoderms and spicules are present only in the John Porter #3 well (Plate 5), indicating that the John Porter #3 is more proximal to the source area during this period of deposition. Also there are a few *reworked shelly deposits*, in John Porter #3 well and in Sol Carpenter H#7 well which were not recorded in Adams SW #7 and Sugar Tree #1 wells, again suggesting that the eastern wells, i.e. Sol Carpenter H#7 and John

Porter #3 are more proximal to the source area. The abundance of *phosphatic deposits* in the lower part of the GRP in the Adams SW #7 well suggests anoxic water mass. Phosphatic deposits, though less abundant, are recorded in Sol Carpenter H#7 well; however, they are not so common in the John Porter #3 well, indicating that the Adams SW #7 and Sol Carpenter H#7 wells are in the realm of upwelling currents and hence are deeper relative to the easternmost John Porter #3 well. On a sequence scale, this upward-shoaling GRP is part of the highstand systems tract (Fig. 4.5, Plate 5).

GRPS 4: 7595 ft (2314.9 m) – 7559.6 ft (2304.2 m)

Vertical succession in Sol Carpenter H#7 well: The GRPS is an overall upward-increasing gamma ray interval. There are several large gamma ray excursions associated with this pattern (Fig. 4.21). It is composed of four depositional parasequences which are labeled as GRP 4a, b, c and d (Fig. 4.21). The lowermost parasequence (GRP 4a) has a remarkably high gamma ray value at the base. The basal hot shale (Fig. 4.21) can be traced in all the cored wells as well as throughout most of the basin. The hot gamma ray value is due to the presence of abundant *phosphatic deposit* which occurs in the form of concentrated phosphatic pelloids and matrix-hosted compacted, elongated fecal pellets or lenses. It contains maxima of uranium (7595 ft (2314.9 m) -7593 ft (2314.3 m)) (Fig. 4.9) and is a condensed section. The interval above this hot shale to 7578.4 ft (2309.8 m) consists of *siliceous, non calcareous mudstone* with phosphate rich matrix and few *calcareous laminae deposits*. Upsection, there is *dolomitic mudstone* with a high amount of calcite in the form of microfossils such as spicules. This GRPS exhibits cyclic sedimentation.
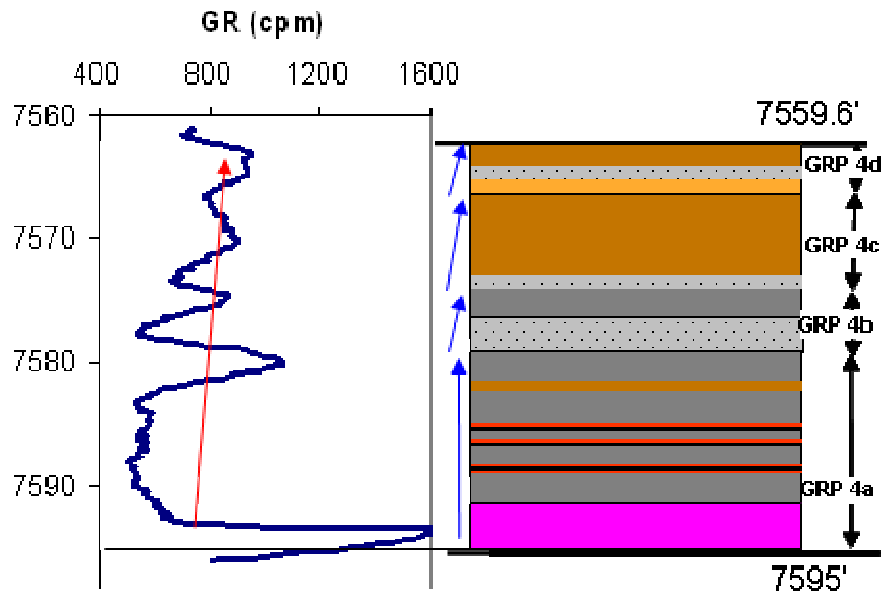
Figure 4.21 GRPS 4 - Gamma Ray and lithology profiles of Sol Carpenter H#7. For color index see Fig. 4.6. Note the high gamma ray kick (over 1600 counts per minute in core gamma ray scan) at the very base. For color index see Figure 4.6.

Lateral Correlation in other wells: All the cored wells studied exhibit an upward increasing gamma ray pattern with a hot gamma ray interval at the base of this GRPS. The basal hot shale, a condensed section, is dominated by *phosphatic deposits* in all the cored wells except Sugar Tree #1 (Fig. 4.22). In Sugar Tree #1 well this interval consists of abundant phosphatic ooids with few shelly fragments. This interval represents a proximal depositional equivalent to a basinal condensed section. Upsection, cyclic sedimentation exhibited by GRP 4b, c, and d, is noted in all the cored wells, and can be laterally correlated. In the lower part, this GRPS contains *siliceous non calcareous mudstone* overlain by *siliceous, calcareous mudstone* facies in all the wells (Fig. 4.22). The basal *siliceous non calcareous mudstone* consists of *calcareous laminae deposit* in all the wells. There is a thick overlying *siliceous calcareous mudstone* lithofacies in John

85

Porter #3 (Fig. 4.22). John Porter #3 contains a *reworked shelly deposit* at 8275.9' which is not present in any other cored wells.
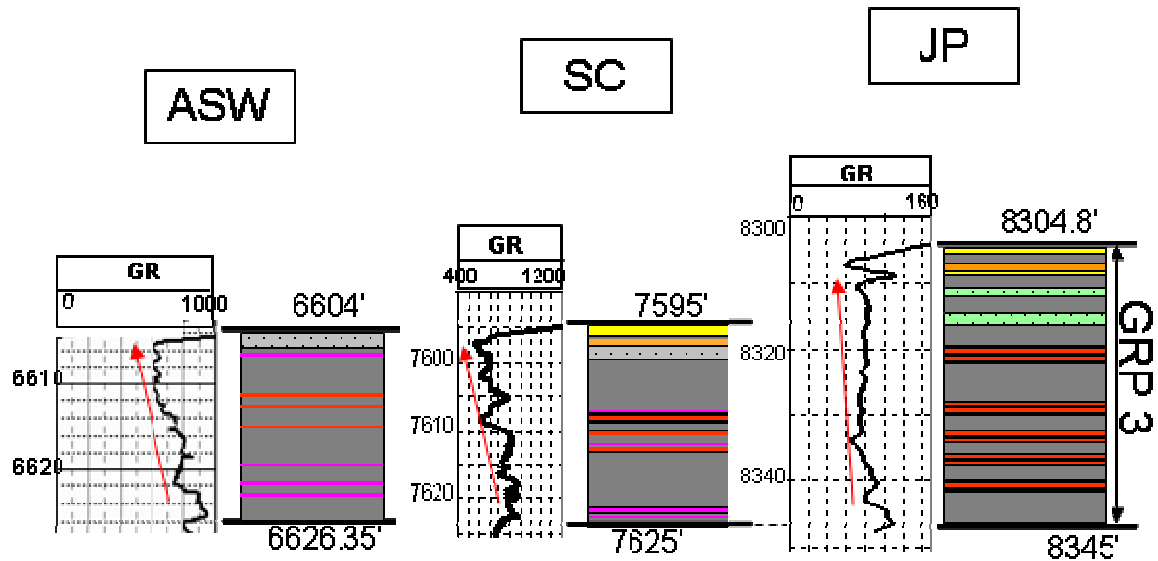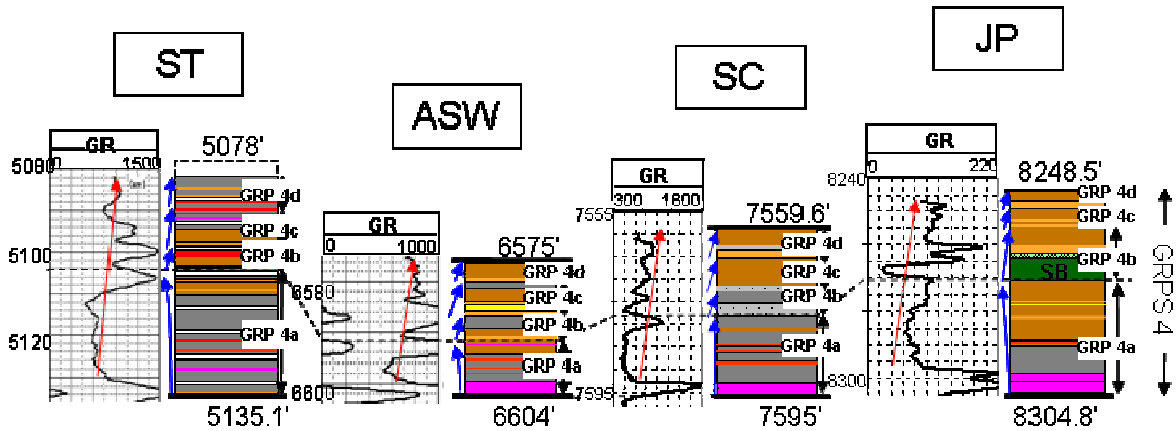

Figure 4.22. Lateral correlation of the GRPS 4 in three cored wells: Adams SW #7 (ASW), Sol Carpenter Heirs #7 (SC) and John Porter #3 (JP). For color index see Figure 4.6.

The onset of GRP 4b is marked by a debris flow deposit in John Porter #3 well. Detailed comparison of this GRPS was completed between the John Porter #3 and Sol Carpenter H#7 wells (Fig. 4.23). This debris flow deposit in John Porter #3 well (marked as 'a' in figure 4.23) occurs as three flow events which are differentiated based on the distinct type and distribution of sediments (Fig. 4.24). The lowermost bed is labeled 1st event bed (Fig 4.24). It is enriched with phosphatic ooids, fragments of echinoderms, spicules, shelly fragments and few intact brachiopods. These grains are randomly oriented and the fabric is preserved from overburden flattening by early calcite and dolomitic cement. The calcitic spar cement is very often replacive resulting in ghost images of the original fabric. This bed has a sharp base (Fig. 4.24). It can be correlated laterally using gamma ray to the *dolomitic mudstone* in Sol Carpenter H#7 well (Figures 4.24 and 4.25) which is

86

marked as 'b' in Figure 4.23. This *dolomitic mudstone* is rich in calcite and calcareous grains, suggesting it is a diagenetically altered deposit.

The 2nd event bed is a matrix supported clast flow deposit which fines upward. The top is rich in fine grained sediments with well developed ripple cross laminae.

The 3rd event bed contains reworked shelly deposit. This bed is subtly reverse graded with a sharp top. The debris flow in the John Porter #3 well is interpreted to be due to shelf instability, probably associated with a falling sea level. Thus, the base of this deposit may be a sequence boundary.

In John Porter #3 well, above the debris flow, a fining upward parasequence (GRP 4c) occurs which is composed of *reworked shelly deposit* at the base, overlain by *calcareous mudstone.* This *reworked shelly deposit* corresponds to the *dolomitic mudstone* in Sol Carpenter H#7 well (Figure 4.23). Thus, the *dolomitic mudstone* in the Sol Carpenter H#7 well may be a diagenetic product of the *reworked shelly deposit*. Event beds 1 and 2 thins out before reaching the Sol Carpenter H#7 well (Fig. 4.23). Further upsection towards the top, another deepening upward parasequence (GRP 4d) is noted in John Porter #3 and Sol Carpenter H#7 wells (Fig. 4.23) thus exhibiting a cyclic sedimentation pattern.
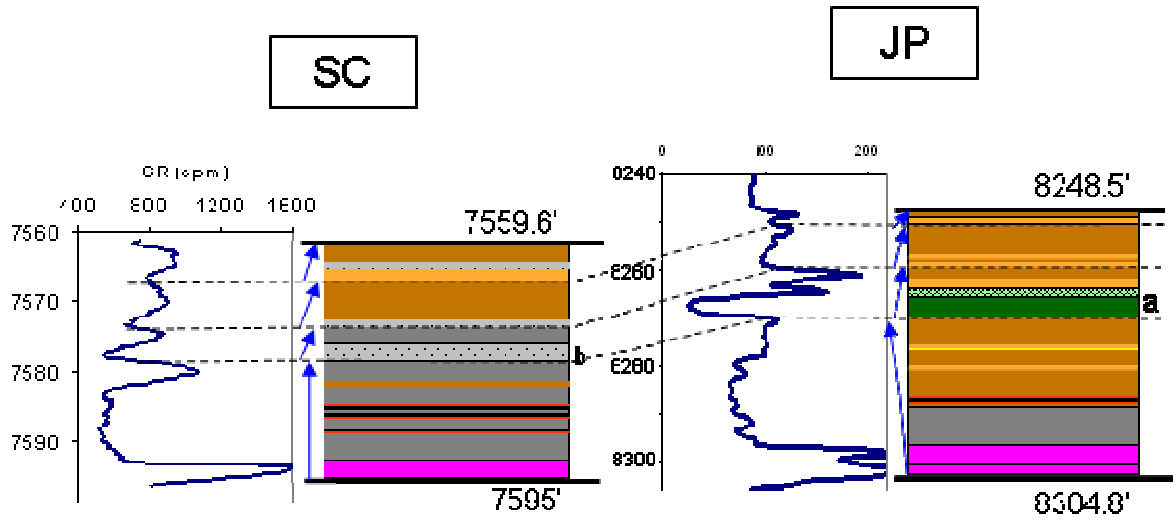
Figure 4.23. Gamma Ray and lithology profiles comparison of Sol Carpenter H#7 (SC) and John Porter #3 (JP) wells. For color index see Figure 4.6. See text for details.
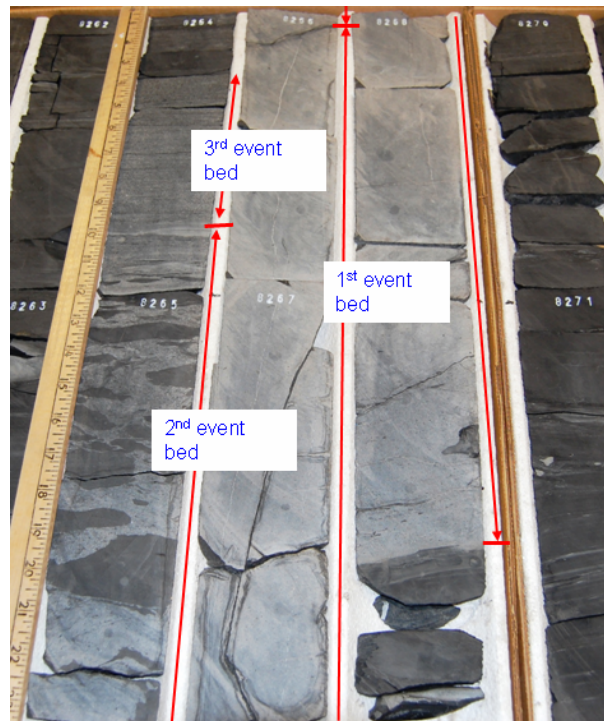
Figure 4.24. Core photograph of the debris flow in the John Porter #3 well in GRP 4. See text for details.

Figure 4.25. Core photograph showing the dolomitic mudstone in Sol Carpenter H#7 well which is correlative to the debris flow deposit in John Porter #3 well. This interval is marked as 'b' in Figure 4.23.

Further to the west similar deepening upward parasequences (GRP 4b, c, and d) are present in the Adams SW#7 and Sugar Tree #1 wells (Fig. 4.22). However, the lowermost parasequence in Adams SW #7 and Sugar Tree #1 wells contains *reworked shelly deposit* with abundant phosphatic pelloids, which is not present in the Sol Carpenter H#7 well. This suggests the presence of a paleo shelf to the west during deposition of this deposit.

Interpretation: The GRPS consists of a condensed section at the base of the lowermost GRP 4a. The overlying parasequences GRP 4b was deposited on a sequence boundary which marks the onset of the lowstand systems tract. The sequence boundary is interpreted on the basis of the significantly thick debris flow in the John Porter #3 well.

This debris flow deposit suggests tectonic instability of the source area, which is thought to be in the east as this debris flow is recorded only in the easternmost John Porter #3 well. It is interpreted that at this time, falling stage of sea level prevailed at least the study area wide and perhaps basin wide on the basis of enhanced influx of sediment not only from east/northeast direction but also west/southwest. Influx from the west/southwest direction is documented by the presence of thick *reworked shelly deposits* in the corresponding intervals in the western, Sugar Tree #1 and Adams SW #7 wells. However, the Sol Carpenter H#7 well records only dolomitic mudstone at the corresponding interval. It is interpreted that simultaneous source areas lay to the east and west and that a falling stage of sea level prevailed at this time of deposition. On a sequence scale, the lowermost GRP 4a, which consists of the condensed section, is interpreted as a transgressive systems tract and the rest of the upper parasequences 4b, c, and d, which exhibits a deepening upward pattern and a basal sequence boundary is interpreted to be a lowstand systems tract (Fig. 4.5, Plate 5).

GRP 5: 7559.6 ft (2304.2 m) - 7534 ft (2296.3 m)

Vertical succession in Sol Carpenter H#7 well: This interval exhibits an upward-decreasing gamma ray pattern capped by a sharp drop in gamma ray values (Fig. 4.26). The lower part of the parasequence is composed of *siliceous, non calcareous mudstone* and *calcareous laminae deposits* which are rich in compacted phosphatic fecal pellets and agglutinated forams (Fig. 4.26). The top part consists of *dolomitic mudstone* overlain by *reworked shelly deposit* (Fig. 4.26). This capping interval is rich in potassium and poor in uranium content, underscoring the detrital influx (Fig. 4.9).

Figure 4.26. GRP5 - Gamma Ray and lithology profiles of Sol Carpenter H#7. For color index see Figure 4.6.

Lateral Correlation in other wells: This GRP is mostly composed of *siliceous non calcareous mudstone* and *calcareous laminae deposits* in all the cored wells (Fig. 4.27) However, there is no core available for the rest of the Barnett Shale section in the Sugar Tree #1 well. Close to the top, the John Porter #3 well consists of a debris flow which is composed of thin platy clasts overlain by calcite-spar cemented phosphatic ooid, echinoderm and shelly fragments (figure 4.28). This is overlain by *reworked shelly deposit* to its top. This interval correlates laterally with *dolomitic mudstone* in the Sol Carpenter H#7 well and perhaps also in the Adams SW #7 well (Fig. 4.27). The top of this GRP consists of *reworked shelly deposit* in the John Porter #3, Sol Carpenter H#7 and Adams SW #7 wells. However, this *shelly deposit* thins in the east towards the Adams SW #7 well (Fig. 4.27).

91

Figure 4.27. Lateral correlation of the GRP 5 in three cored wells: Adams SW #7 (ASW), Sol Carpenter Heirs #7 (SC) and John Porter #3 (JP). For color index see Figure 4.6.
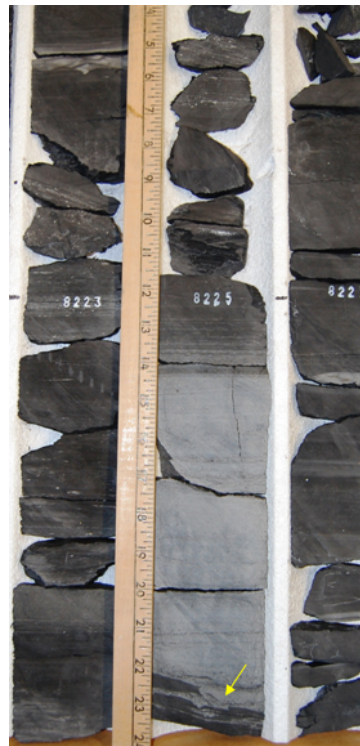
Figure 4.28. Core photograph displaying the debris flow deposit in John Porter #3 well at 8225 ft. (2506.9 m) to 8226 ft. (2507.3 m). The arrow marks the platy clast at the base of the deposit.

Interpretation: The upward-decreasing gamma ray pattern of this GRP is indicative of

either upward-shoaling of the depositional environment during gradual fall in relative sea

92

level or progradation during late stage highstand. Additionally, it is interpreted that at the time of deposition of this GRP, a tectonically active area lay to the east closer to the John Porter #3 well. The Adams SW #7 is located in the quieter part of the basin. This interpretation is based on the presence of a debris flow deposit exclusively in the John Porter #3 well and the *reworked shelly deposit,* in all the wells which thins to the west in the Adams SW #7 well. On a sequence scale, the GRP is part of a highstand systems tract which constitutes most of the rest of the Lower Barnett that consists of vertically stacked cycles of non calcareous mudstone and calcareous mudstone rich in reworked shelly deposits (Fig. 4.5, Plate 5).

GRP 6: 7534 ft (2296.3 m) - 7522 ft (2292.7 m)

Vertical succession in Sol Carpenter H#7 well: This GRP displays a constant Gamma Ray pattern. The lower part of the parasequence, up to 7528.2 ft (2294.5 m), consists of *calcareous mudstone* rich in *reworked shelly deposit* and the upper part consists of *calcareous mudstone* which is capped by *dolomitic mudstone* (Fig. 4.29). The *calcareous mudstone* contains calcareous spicules (Wendt, 1980) or calcite-replaced? spicules and calcite-replaced radiolarians with abundant smaller broken shell fragments scattered in the matrix.
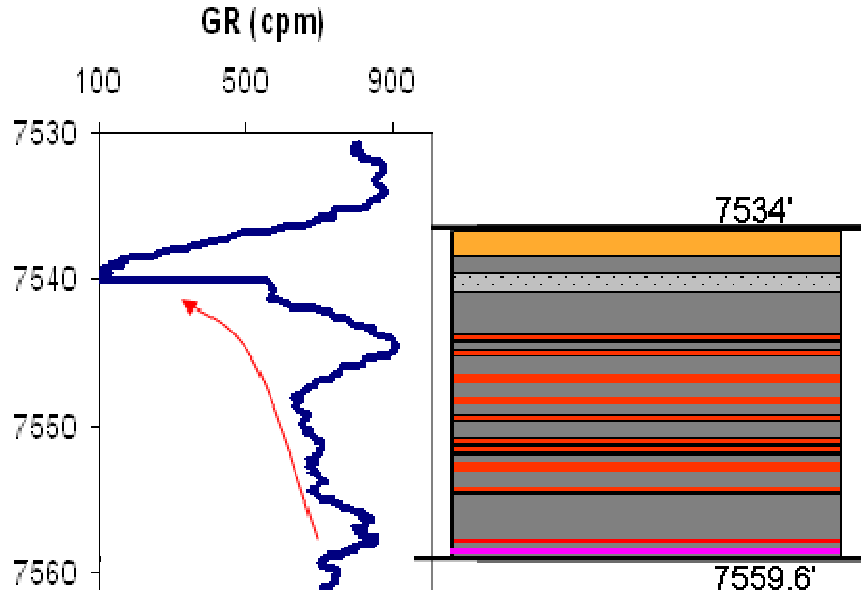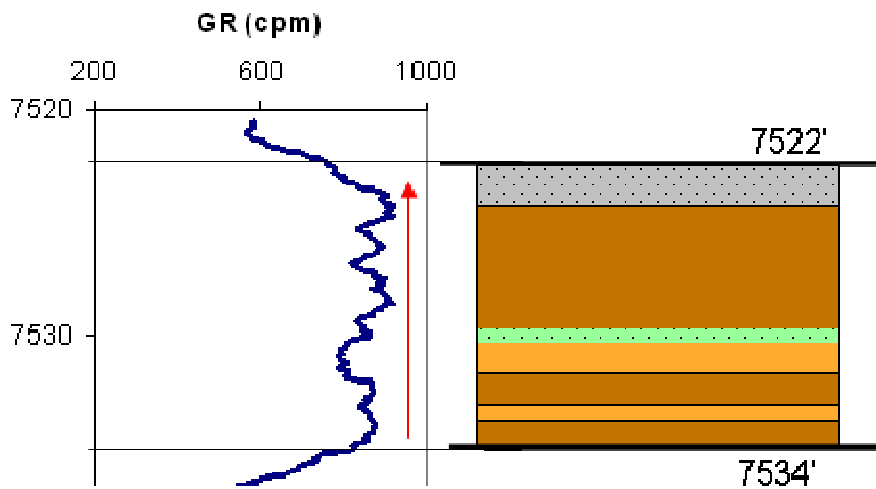
Figure 4.29. GRP6 - Gamma Ray and lithology profiles of Sol Carpenter H#7. For color index see Figure 4.6.

Lateral Correlation in other wells: This interval is composed of varying amounts of *reworked shelly deposit* and *siliceous, calcareous mudstone* facies in the three wells (Fig. 4.30). The base of the parasequence has only a few *reworked shelly deposits* in the Adams SW#7 and Sol Carpenter H#7 wells; however, the John Porter #3 has a relatively thicker *reworked shelly deposit* at the base. Towards the middle of this parasequence, Adams SW #7 contains *reworked shelly deposits* which were absent in the Sol Carpenter H#7 and John Porter #3 wells. Towards the top of the GRP in the John Porter #3, there are high amounts of *reworked shelly deposit* and echinoderms and spicules. Thus, there was a high influx of *reworked shelly deposit* at the top in the John Porter #3 well, whereas *siliceous calcareous mudstone* and *dolomitic mudstone* are common in the Sol Carpenter H#7 well and only *siliceous calcareous mudstone* occurs towards the top in the Adams SW#7 well. The lateral and vertical stacking style of the lithofacies in this GRP suggests that while there is an active source to the east, there was a lesser source towards the west.
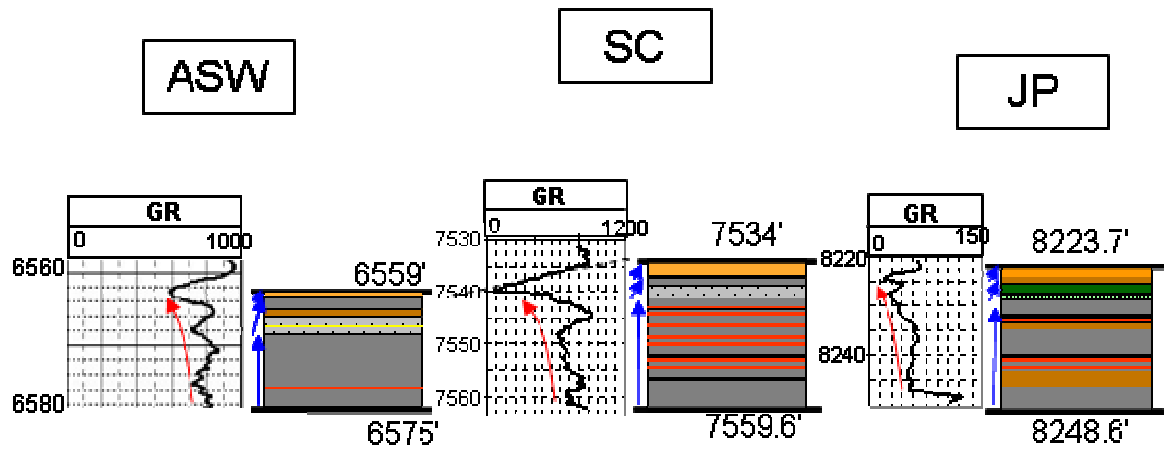
94
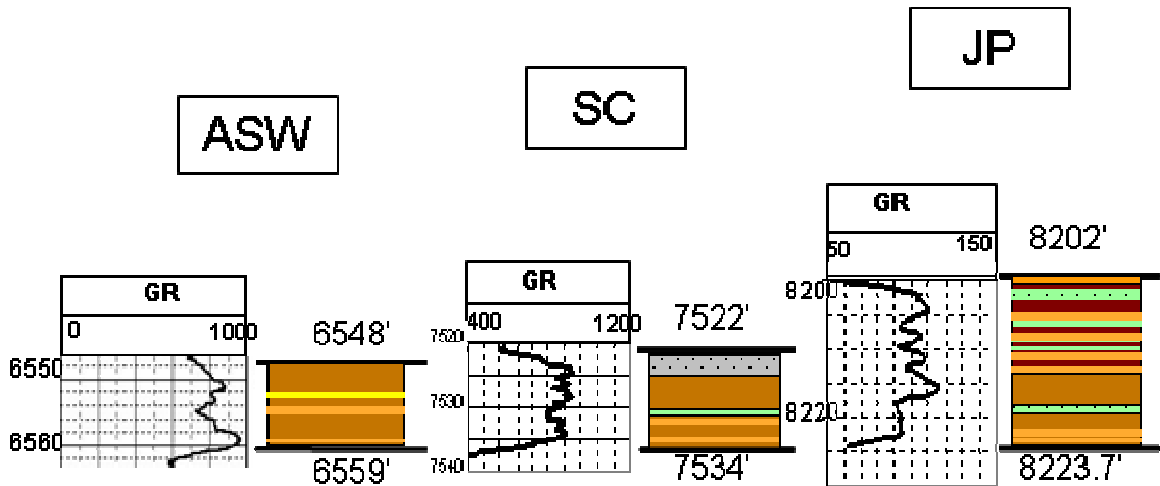
Figure 4.30. Lateral correlation of the GRP 6 in three cored wells: Adams SW #7 (ASW), Sol Carpenter Heirs #7 (SC) and John Porter #3 (JP). For color index see Figure 4.6.

Interpretation: This GRP suggests that at about midsection, Adams SW #7 well is close to the source area that provided *reworked shelly deposit.* This deposit is absent in the eastern, Sol Carpenter H#7 and John Porter #3 wells indicating that periodically the Adams SW #7 well is close to a source in the west where periodic tectonic upliftment occurred. Towards the top of this GRP, an echinoderm rich interval and a few shelly deposits occur in John Porter #3, which are not present in the Sol Carpenter H#7 and Adams SW #7 wells. This capping deposit in the John Porter #3 well suggests a source close to the east at this time of deposition.

GRP 7: 7522 ft (2292.7 m) - 7502 ft (2286.6 m)

Vertical succession in Sol Carpenter H#7 well: This interval exhibits an overall upward-decreasing gamma ray pattern; however, thin couplet with upward increasing gamma ray pattern occurs at the base (Fig. 4.31) which corresponds to the stacking of basal *calcareous mudstone* overlain by *siliceous, non calcareous mudstone.* This GRP is

95

capped by *dolomitic mudstone* and *reworked shelly deposit* (Fig. 4.31). The *dolomitic mudstone* lithofacies at this depth has a high fossil content (Fig. 4.32). The dolomite is diagenetic in origin.

Figure 4.31. GRP7 - Gamma Ray and lithology profiles of Sol Carpenter H#7. For color index see Figure 4.6.
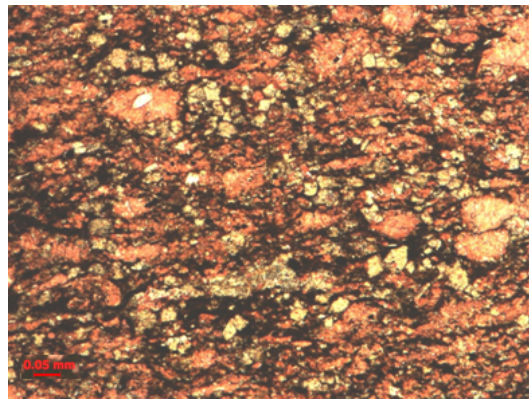
Figure 4.32. Photomicrograph of dolomitic mudstone with high amount of calcite (stained pink) at 7503.4' in the Sol Carpenter H#7 well.

Lateral Correlation in other wells: The basal deepening upward succession recorded in the Sol Carpenter H#7 is also present in the Adams SW #7 well and the John Porter #3 well (Fig. 4.33). However, in the John Porter #3 well, the lower interval is thicker with a

dominant influx of macrofossils. The basal concentration of shells in the John Porter #3 well has led to the development of several concretions (Fig. 4.34). Upsection, *calcareous mudstone* is the predominant lithofacies in the John Porter #3 well. However, in the Sol Carpenter H#7 and Adams SW #7 wells, the corresponding interval consists of *siliceous, non-calcareous mudstone* as the most dominant lithofacies (Fig. 4.33). This lateral transition of lithofacies from *calcareous mudstone* to *non calcareous mudstone* suggests the deepening of water towards the Adams SW#7. The GRP is capped by *reworked shelly deposit* in all three wells; however, the deposit is thickest in the Adams SW #7 well (Fig. 4.35), suggesting the Adams SW #7 well was proximal to the basin margin at this time.
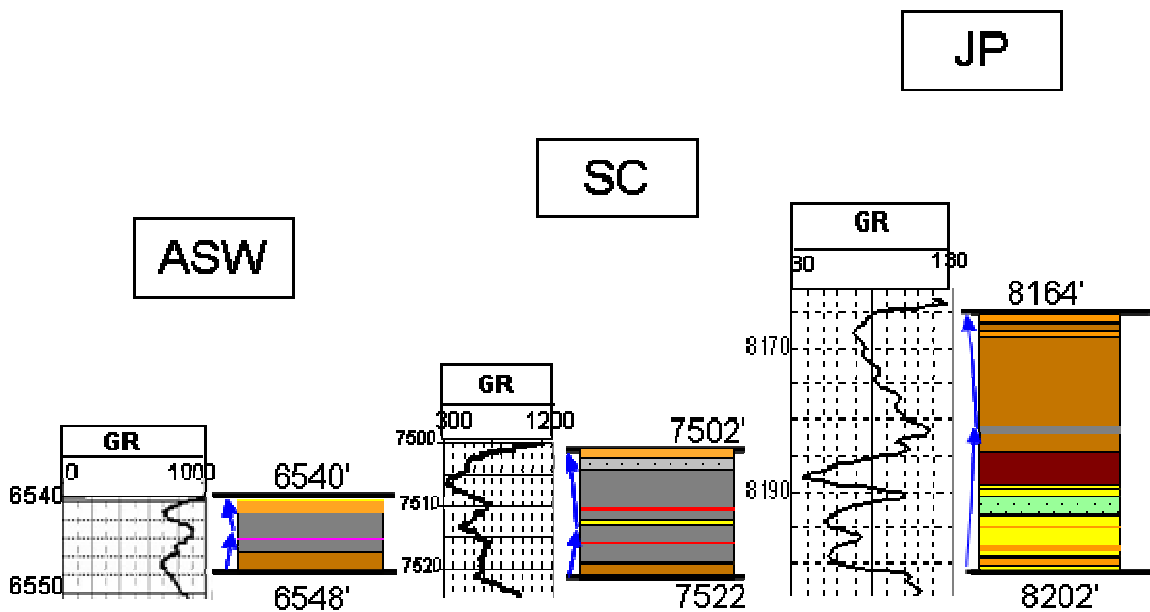
Figure 4.33. Lateral correlation of the GRP 7 in three cored wells: Adams SW #7 (ASW), Sol Carpenter Heirs #7 (SC) and John Porter #3 (JP). For color index see Figure 4.6.

Interpretation: During the deposition of lower interval of GRP 7, it is interpreted that the easternmost John Porter #3 well, is close to the source area where several debris flows were deposited. These deposits are not recorded in the other cored wells, underscoring

the presence of an eastern source area. The overlying interval of decreasing gamma ray pattern is capped by reworked shelly deposit, which is thickest in the Adams SW #7 well and less prominent in the eastern wells. This indicates that Adams SW #7 well site was relatively shallower at the time of deposition. On a sequence scale, this upward decreasing GRP is interpreted to be part of a highstand systems tract (Fig. 4.5, Plate 5).
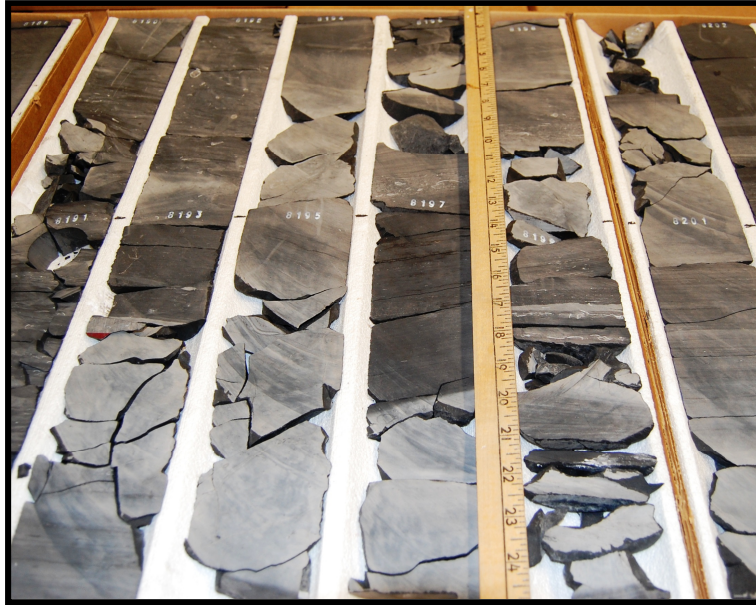
Figure 4.34: Core photograph 8190 ft. (2496.3 m) to 8202 ft. (2499.9 m) showing the high abundance of shelly deposit and concretionary carbonates in the lower part of GRP 7 in the John Porter #3 well.
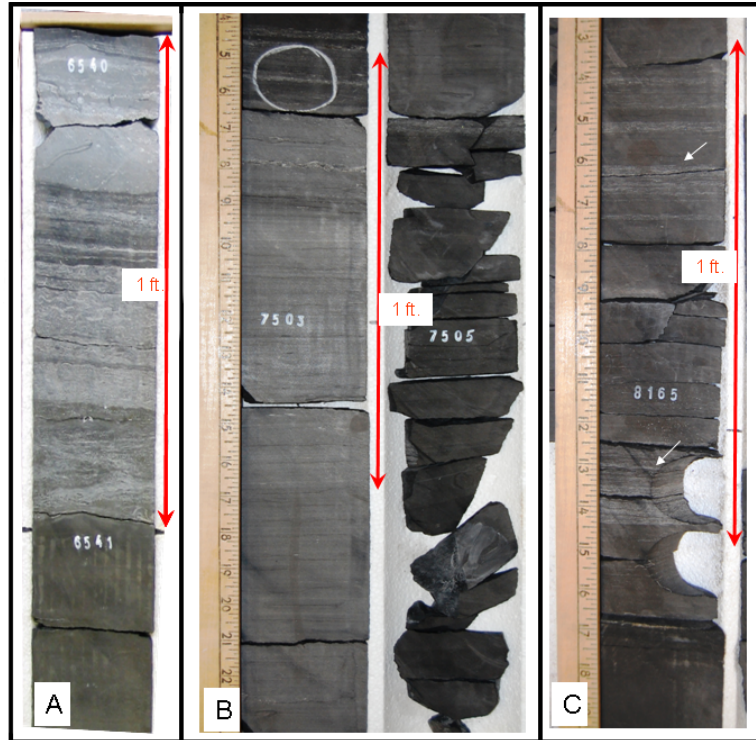
Figure 4.35. Core photograph comparing the deposit at the top of the GRP 7 in the three cored wells: (A) Thick and condensed *reworked shelly deposit* in Adams SW #7 (B) a

99

thinner interval of reworked shelly deposit and diagenetic dolomitic mudstone in Sol Carpenter H#7 and (C) much thinner interval of shelly deposit in John Porter #3 well.

GRP 8: 7502 ft (2286.6 m) - 7487 ft. (2282 m)

Vertical succession in Sol Carpenter H#7 well: This GRP consists of a basal high gamma ray interval which is followed upward by an upward decreasing gamma ray response interval. The interval is composed mostly of *reworked shelly deposit*, *calcareous mudstone* and *concretionary* carbonates (Figures 4.36 and 37). The high gamma ray values at the very base are due to the abundance of phosphatic ooids in the *reworked shelly deposit* (Figures 4.37 and 4.38). The phosphatic content is probably responsible for the high uranium count (14 ppm) at this depth (Fig. 4.9). This suggests that the winnowing and reworking of the shelly deposit took place in anoxic water conditions, thus resulting in a high concentration of preserved uranium. Thus, suggesting that the onset of this deposit as initiation of transgression.
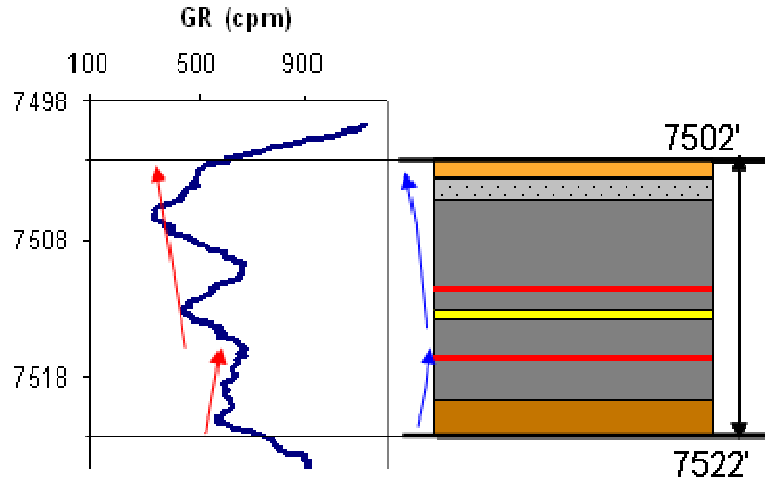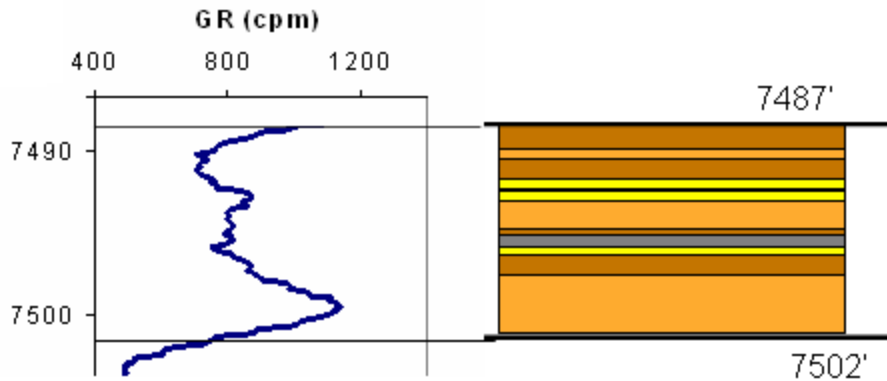

Figure 4.36. GRP8 - Gamma Ray and lithology profiles of Sol Carpenter H#7. For color index see Figure 4.6.
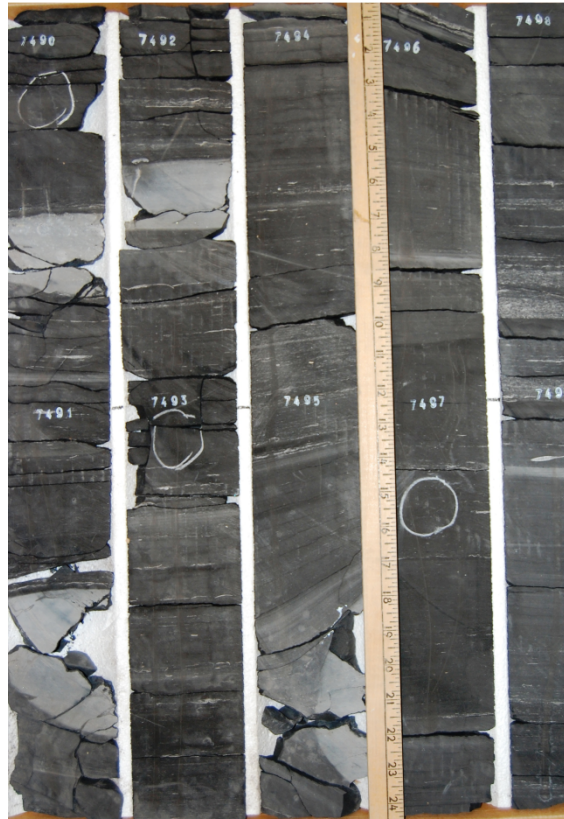
Figure 4.37: Core photograph 7490 ft. (2282.9 m) to 7500 ft. (2286 m) showing the abundance of shelly deposit and concretionary carbonates in GRP 8 of the Sol Carpenter H#7 well.
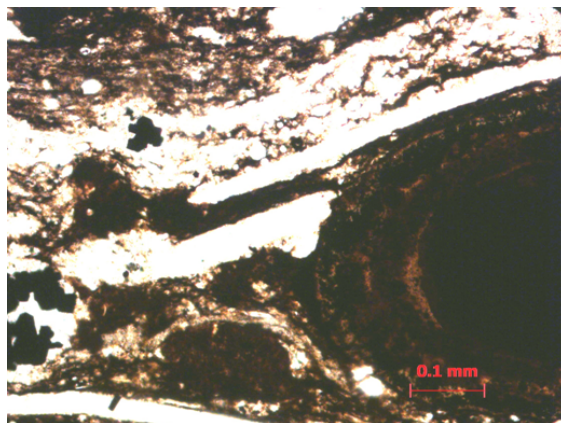
Figure 4.38. Photomicrograph at 7488.9 ft. (2282.6 m) in the Sol Carpenter H#7 showing the shelly deposit and a large phosphatic ooid on the right side in the picture.

Lateral Correlation in other wells: This GRP consists of an overall upward-decreasing gamma ray pattern bounded by very high gamma ray values at the base. This hot gamma ray value at the base is prominent and can be used as a marker bed which can be traced in most of the basin; however, it becomes less prominent in the eastern part of the basin (Fig. 4.39). This basal hot gamma ray interval is due to the presence of uranium in reworked phosphatic ooids within the *reworked shelly deposit.* In the John Porter #3 well this interval consists of less *shelly deposits.*

This entire GRP is composed of amalgamated *reworked shelly deposit* in the Adams SW #7 wherein the *reworked shelly deposit* is thick and condensed with very less interbedded mudstone deposits (Fig. 4.40) compared to the other two cored wells. In the Sol Carpenter H#7, this GRP is mostly composed of *reworked shelly deposit* and *calcareous mudstone*. Towards the top of this GRP, unusually high amounts of detrital quartz are present in the Adams SW #7 and Sol Carpenter H#7 wells (Figure 4.41) suggesting the high flux of terrigenous input during this time. This interval thickens dramatically from the Sol Carpenter H#7 to the John Porter #3 well (Fig. 4.39). In the John Porter #3 well there are several couplets of shale and carbonate rich zones (Fig. 4.42), starting from the base of the GRP up to 8118 ft. Therefore this interval exhibits several gamma ray excursions. The section above this interval to the top in the John Porter #3 well is very fissile (Fig. 4.43). *Calcareous mudstone with high calcite* is the dominant lithofacies in this fissile interval and the presence of several macrofossil shells scattered in the matrix is also unique to this interval. This interval also has reduced organic richness (avg. 2 wt% TOC) compared to overlying, underlying and lateral strata

(avg. 3.5 wt% TOC). This interval also has relatively high amounts of mixed clays in both John Porter #3 and Sol Carpenter H#7 wells.

This lateral correlation of the lithofacies suggests that the Adams SW #7 well is most proximal to the basin margin as compared to the other two wells and that John Porter #3 well while being further from basin margin at this period of deposition, was heavily sourced from a northeast direction.

Figure 4.39. Lateral correlation of GRP 8 in three cored wells: Adams SW #7 (ASW), Sol Carpenter Heirs #7 (SC) and John Porter #3 (JP). For color index see Figure 4.6.
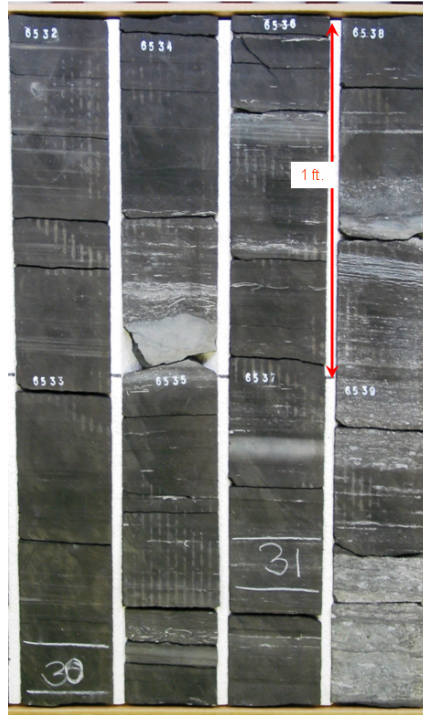
Figure 4.40. Core photograph showing GRP 8 in the Adams SW #7 well.
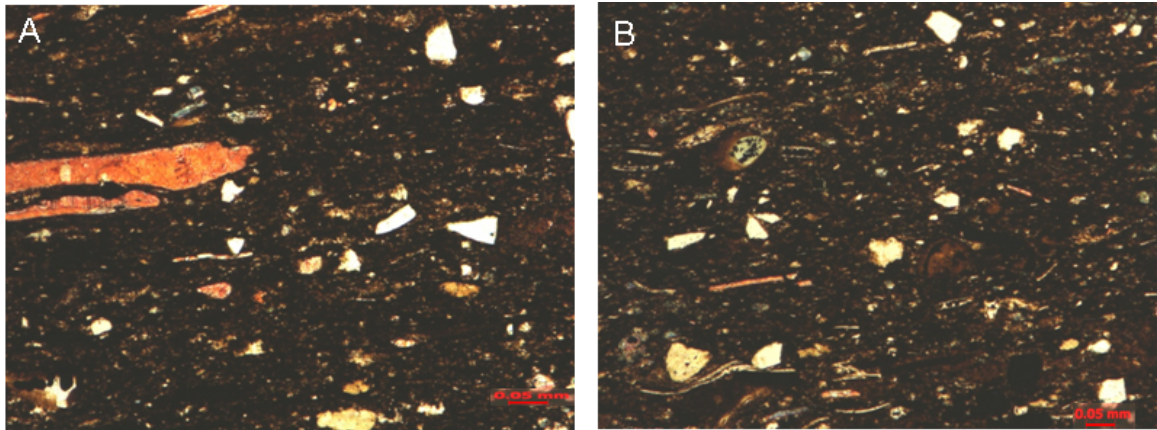
Figure 4.41. Photomicrographs of section at (A) 6538.1 in Adams SW well and (B) 7487.85 in Sol Carpenter H#7 well showing abundant, unusually large detrital quartz grains close to the top of GRP 8. The scale bar is 0.05mm.
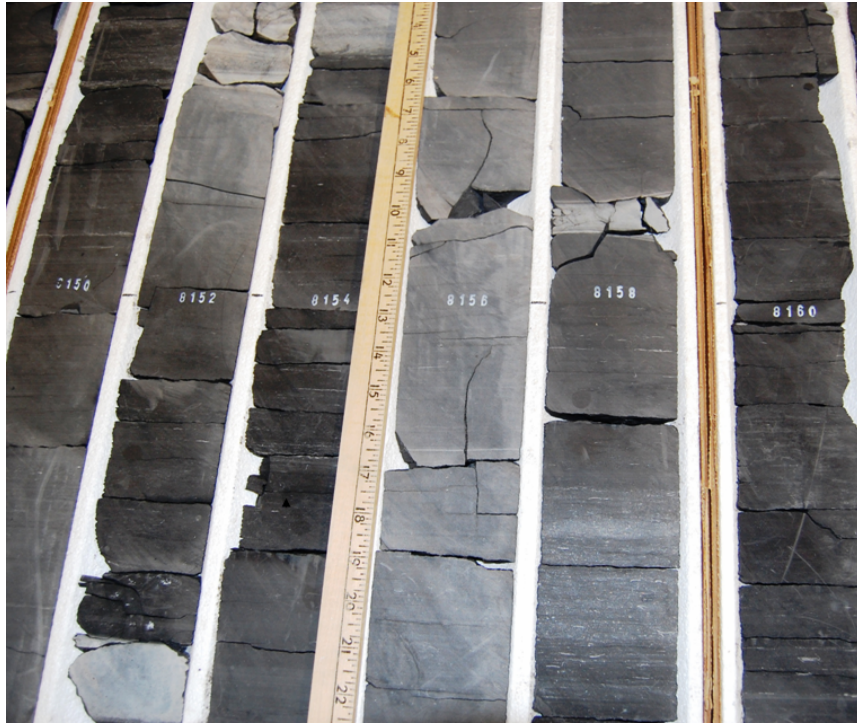
Figure 4.42. Core photograph 8149 ft (2483.8m) to 8162 ft. (2487.7 m) in the John Porter #3 well. See text for details.
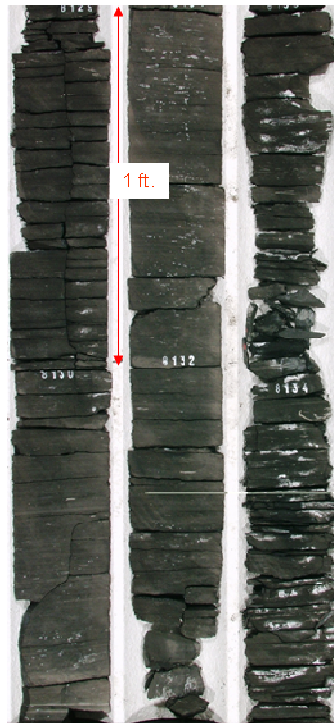
Figure 4.43. Core photographs (8129 feet (2477.7 m) to 8135 feet (2479.5 m)) of part of the 40 feet fissile shale interval of GRP 8 in the John Porter#3 well showing the friable nature of the *calcareous mudstone with high calcite* lithofacies.

Interpretation: The basal surface marking the onset of GRP 8 is interpreted as a transgressive surface of erosion in Adams SW#7 and Sol Carpenter H#7 wells because of the presence of reworked shelly deposit, and phosphatic ooids which are rich in uranium. The high uranium concentration (14 ppm in Sol Carpenter H#7 and 20 ppm in Adams SW#7 well) suggests that a reducing environment prevailed while the winnowing occurred during initial stages of transgression. This GRP thickens dramatically in the John Porter #3 well and is less amalgamated with more frequent interbedded mudstone deposits between the shelly deposits. This suggests that the interval in Adams SW #7 well was deposited in relatively shallower water than in other wells at this time, and that the basin deepened in the direction of the John Porter #3 well; however, John Porter #3 well receives abundant allochthonous calcareous input in the form of macrofossils and detrital calcite grains from a source in the northeast.

GRP 9: 7487 ft. (2282 m) - 7462 ft (2274.4 m)

Vertical succession in Sol Carpenter H#7 well: This GRP has high gamma ray values at the bottom which is followed by an upward-decreasing gamma ray pattern. The cored interval for this GRP in the Sol Carpenter H#7 well is not complete (Fig. 4.44). The available interval - 7487 ft (2282 m) to 7480 ft (2273.9 m) - is composed of *siliceous, non calcareous mudstone* which is rich in phosphates and detrital quartz grains. Core is missing from 7480 ft. (2279.9m) up to the base of the Forestburg limestone at 7462 ft (2274.4 m).

Figure 4.44. GRP9 - Gamma Ray and lithology profiles of Sol Carpenter H#7. For color index see Figure 4.6.

Lateral Correlation in other wells: Adams SW #7 and John Porter #3 wells have complete core sections of this GRP whereas the Sol Carpenter H#7 well contains only the lower part (Fig. 4.45). This GRP exhibits an upward decreasing gamma ray pattern with very hot gamma ray values at the base.

The upper half of two available core sections exhibit an upward increase in calcite content. In the John Porter #3 section, *siliceous non-calcareous mudstone* transitions upward to *calcareous mudstone with low calcite* to *calcareous mudstone with high calcite*. *Silty shaly (wavy) interlaminated deposit* occurs in both the John Porter #3 and Adams SW#7; however, this deposit thins in the Adams SW#7 well.

Interpretation: The basal hot gamma ray shale is interpreted as a condensed section which is present throughout the basin. The rest of upward decreasing gamma ray pattern of this GRP which shoals upward could be a progradational deposit formed during late stage highstand or a deposit resulting from a gradual fall in relative sea level until the deposition of Forestburg limestone begins. On a sequence scale, the lower part

107

of this GRP constitutes a transgressive systems tract which is overlain by a highstand systems tract (Plate 5).
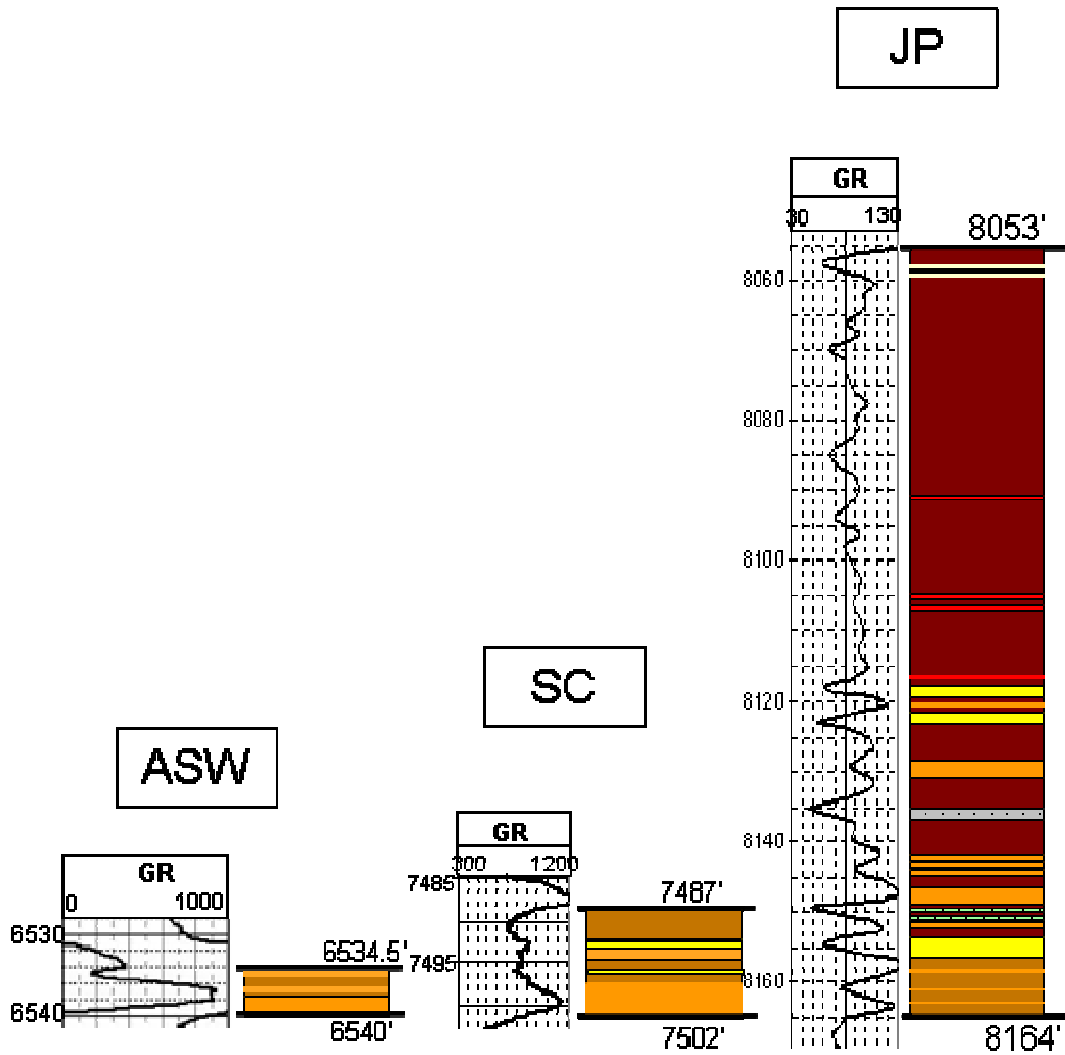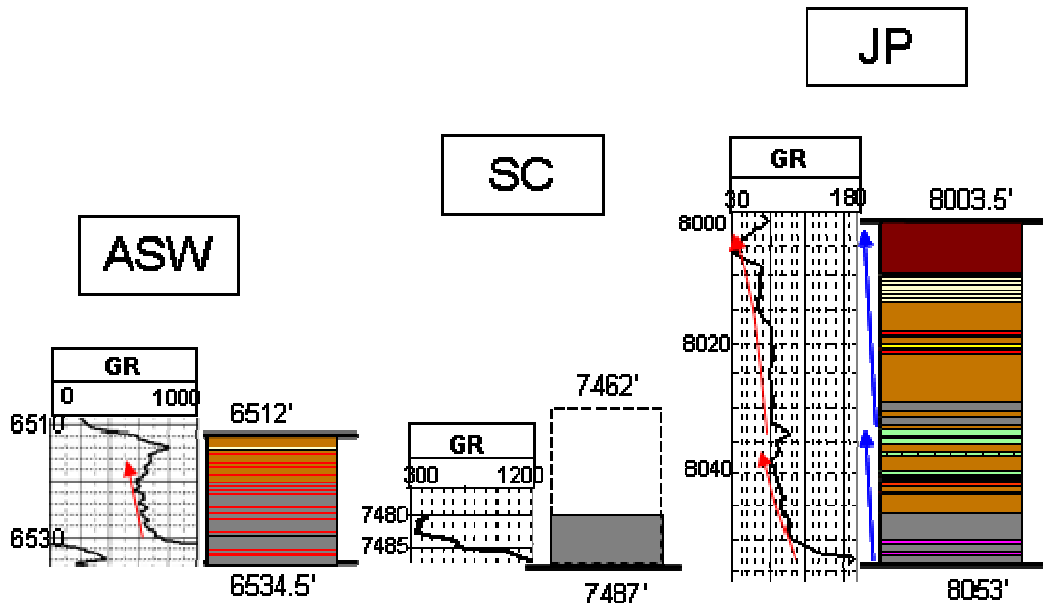

Figure 4.45. Lateral correlation of the GRP 9 in three cored wells: Adams SW #7 (ASW), Sol Carpenter Heirs #7 (SC) and John Porter #3 (JP). For color index see Figure 4.6.

4.3.2 Forestburg Limestone

The Forestburg limestone is dominated by micritic/limy mudstone. For the most part, it is highly laminated. The gamma ray value is lower than that for the Upper and the Lower Barnett Shale. It consists of carbonate-dominated mud as opposed to clay dominated mud of the Lower Barnett Shale. The Forestburg was deposited at a time of sea level rise, or change in seawater chemistry or circulation (Loucks and Ruppel, 2007). The lack of terrigenous input with a rise in sea level is suggested. Very low values of TOC (average 0.01 wt %) indicate that the environment was oxygenated; however, the lack of burrowing and preservation of laminations indicates that the water bottom was relatively anoxic. Hence this suggests that the lack of TOC is more related to lack of organic productivity than organic preservation.

4.3.3 Upper Barnett Shale

The Upper Barnett Shale exhibits a number of lithofacies, significant surfaces and systematic changes in depositional processes and environments as evidenced by a series of parasequences. The presence of several sharp contacts and erosional surfaces present in the Upper Barnett Shale, which are not common in the Lower Barnett Shale, suggests a different general depositional environment during deposition of the Upper and Lower Barnett Shale. Rapid changes in the depositional environment appear to have been particularly common during deposition of the Upper Barnett Shale.

GRP 10: 7372 ft (2246.9 m) - 7346.5 ft (2239.2 m)

Vertical succession in Sol Carpenter H#7 well: This upward-increasing Gamma Ray Parasequence marks the return of siliciclastic clay dominated sedimentation at the onset of Upper Barnett Shale deposition (Fig. 4.46). But the change was gradual as exhibited by the gradational facies change from carbonate-dominated *micritic/limy mudstone* (Forestburg Limestone) to clay-dominated *calcareous mudstone with high calcite* within the interval 7374 ft (2247.5 m) to 7366.5 ft (2245.3 m). The *calcareous mudstone with high calcite* facies has relatively higher TOC (2.47 wt% compared to ~0.01 wt% of Forestburg Limestone) which depicts the return of slow rates of deposition and greater preservation of organic matter. The interval is rich in detrital calcite grains and shelly fragments, which are scattered within the matrix.
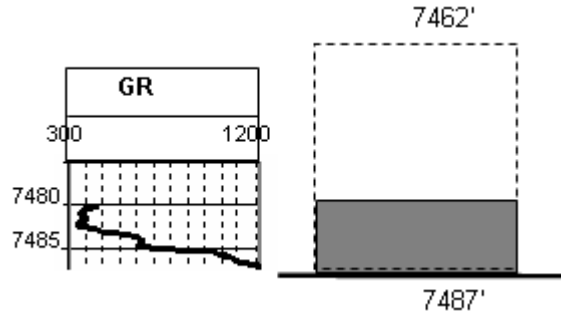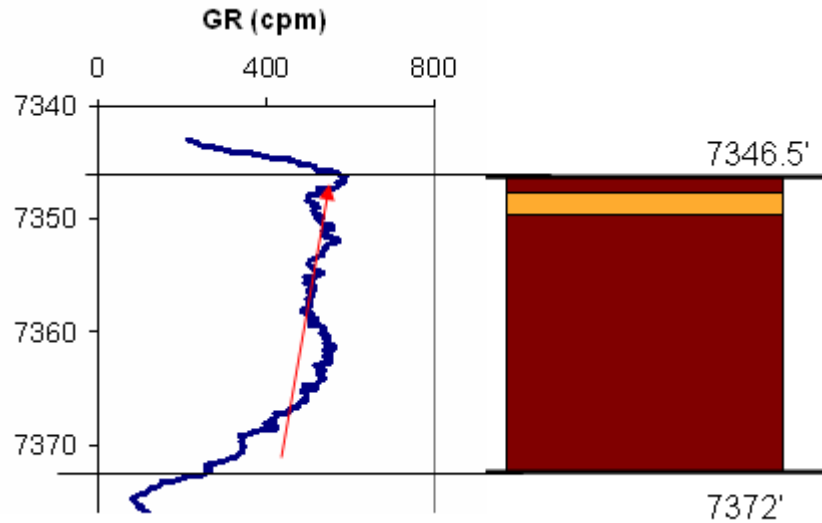
Figure 4.46. GRP10 - Gamma Ray and lithology profiles of Sol Carpenter H#7. For color index see Figure 4.6.

Lateral Correlation in other wells: The core section of John Porter #3 corresponding to this GRP is missing (Fig. 4.47). The section for the Sol Carpenter H#7 and Adams SW#7 contains *calcareous mudstone with high calcite* lithofacies. The lower part of this parasequence in both the Sol Carpenter H#7 and Adams SW#7 wells contains abundant tasmanites (Fig. 4.48). Figure 4.48 also shows the high detrital quartz content in the Sol Carpenter H#7. A fossiliferous deposit occurs close to the top of the parasequence in the Sol Carpenter H#7 well which is absent in the Adams SW#7.

Figure 4.47. Lateral correlation of the GRP 10 of the Upper Barnett Shale in three cored wells: Adams SW #7 (ASW), Sol Carpenter Heirs #7 (SC) and John Porter #3 (JP). For color index see Figure 4.6.
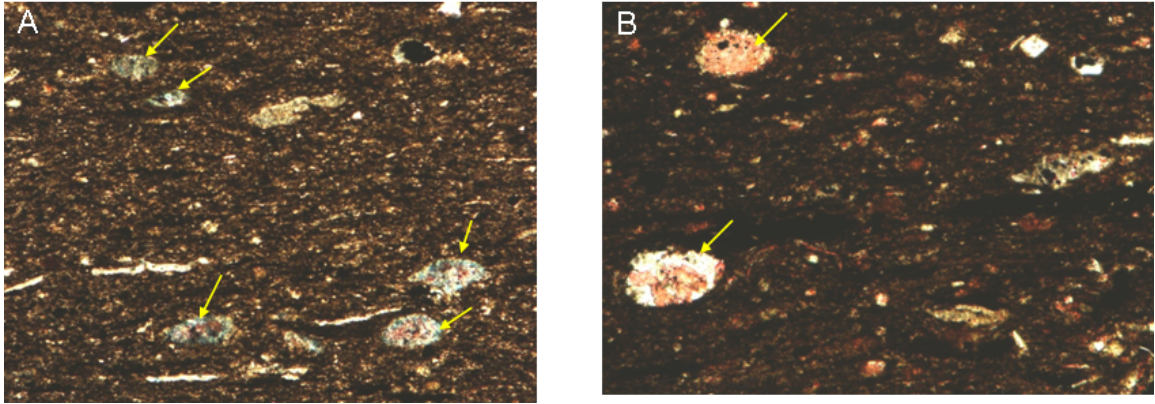
Figure 4.48. Photomicrographs showing the abundance of tasmanites (arrows) in GRP 10 of the Upper Barnett Shale of (A) Adams SW#7 well at 6503.6 and (B) Sol CarpenterH#7 well at 7365'. Calcite is stained pink and Fe-Dolomite is stained blue.

Interpretation: GRP 10, an upward increasing gamma ray interval, marks the beginning of Upper Barnett Shale deposition and the return of a clay mineral-prone environment after the deposition of organic poor Forestburg Limestone. On a sequence scale, this GRP is interpreted as a highstand systems tract (Fig. 4.5).

GRPS 11: 7346.5 ft (2239.2 m) – 7317 ft (2230.2 m)

Vertical succession in Sol Carpenter H#7 well: This GRPS exhibits an overall upward-increasing Gamma Ray pattern comprising two upward deepening parasequences: GRP 11a and b (Fig. 4.49). This interval contains several lithofacies including *micritic/limy mudstone* and *silty-shaly wavy bed deposit.* M*icritic/limy mudstone* is not found at all and

silty-shaly wavy bed deposit was not common in the Lower Barnett Shale, suggesting a change in sediment source or depositional environment.
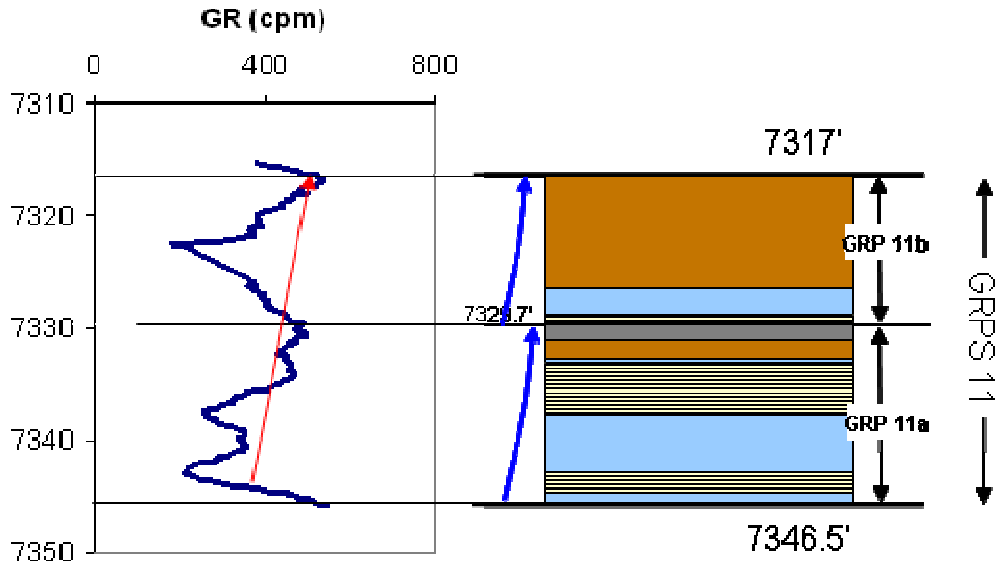
Figure 4.49. GRPS 11 - Gamma Ray and lithology profiles of Sol Carpenter H#7. For color index see Figure 4.6.

The two depositional parasequences consist of *alternate silty shaly wavy bed deposits* and *micritic/limy mudstone* in the lower part of the parasequence which grades upward into *siliceous calcareous mudstone* and/or *siliceous non calcareous mudstone* (Fig. 4.49).

Detailed description: The base of the lower parasequence is marked by a sharp contact overlain by a lag deposit. This sharp contact is interpreted as a sequence boundary. The interval just above this lag from 7346.5 ft (2239.2 m) to 7333.5 ft (2235.2 m) is composed of an interdigitation of *micritic/limy mudstone deposit* and *alternate silty shaly wavy bed deposits* (Fig. 4.49) suggesting frequent change in depositional environment. The *micritic/limy mudstone* is composed of authigenic carbonate-dominated mud, with

112

large detrital quartz grains (~ 0.5mm), and scattered shell fragments. This lower part is interpreted as a lowstand systems tract. The upper part of GRP 11a parasequence, up to 7329.7 ft (2234 m), consists of *siliceous, calcareous* and overlying *non calcareous mudstone* facies. This pattern of vertical stacking of facies suggests a rise in relative sea level with relative shallow water calcareous deposits being overlain by deeper water siliceous deposits. This part is interpreted as a highstand systems tract (Fig. 4.5).

The base of the next parasequence (GRP 11b: 7329.7 ft (2234 m) - 7317 ft (2230.2 m)) is marked by a sharp based *silty shaly wavy bed* deposit. This contact between the underlying lower energy parasequence and the higher energy, coarser grained facies marks the onset of the new parasequence. The *silty shaly wavy bed deposit* is overlain by *micritic/limy mudstone* up to 7327.8 ft (2233.5 m), then by *siliceous calcareous mudstone* to the top (Fig. 4.49).

Lateral Correlation in other wells: This GRPS thins out before reaching the Adams SW#7 well. The lateral correlation of this GRPS in the John Porter #3 could not be done because the core is missing (Fig. 4.50).
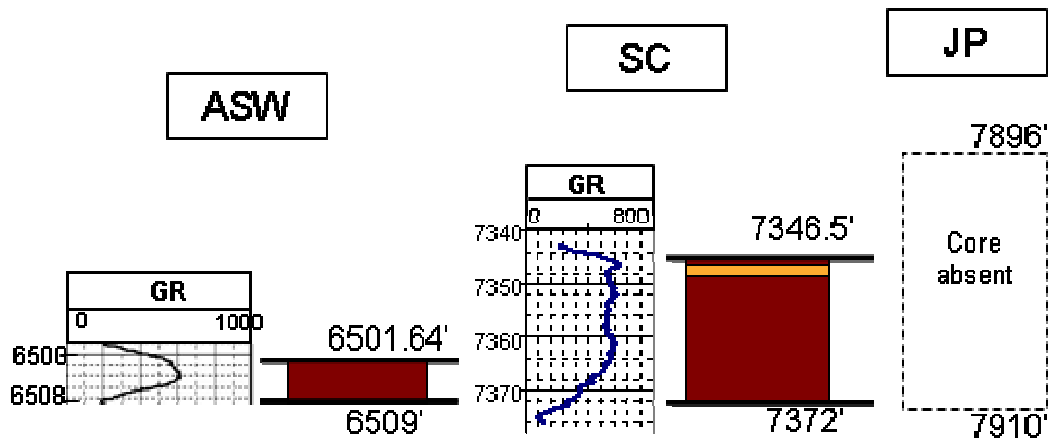
113

Figure 4.50. Lateral correlation of the GRPS 11 of the Upper Barnett Shale in three cored wells: Adams SW #7 (ASW), Sol Carpenter H#7 (SC) and John Porter #3 (JP). For color index see Figure 4.6.

**Interpretation:** GRPS 11, exhibits a frequent change in depositional energy conditions and hence frequent change in lithofacies. On a sequence scale, the lower part of GRP 11a is interpreted as a lowstand systems tract which is overlain by highstand deposits (Fig. 4.5). The upper parasequence, GRP 11b is similar with lowstand deposits at the base followed by highstand deposits (Fig. 4.5).

GRP 12: 7317 ft (2230.2 m) - 7281 ft (2219.2 m)

Vertical succession in Sol Carpenter H#7 well: This GRP consists of an upward-increasing gamma ray pattern (Fig. 4.51). It is composed mostly of *alternate silty shaly wavy bed* and *micritic/limy mudstone* lithofacies in the lower part of the parasequence and *siliceous calcareous mudstone* at the top.

114
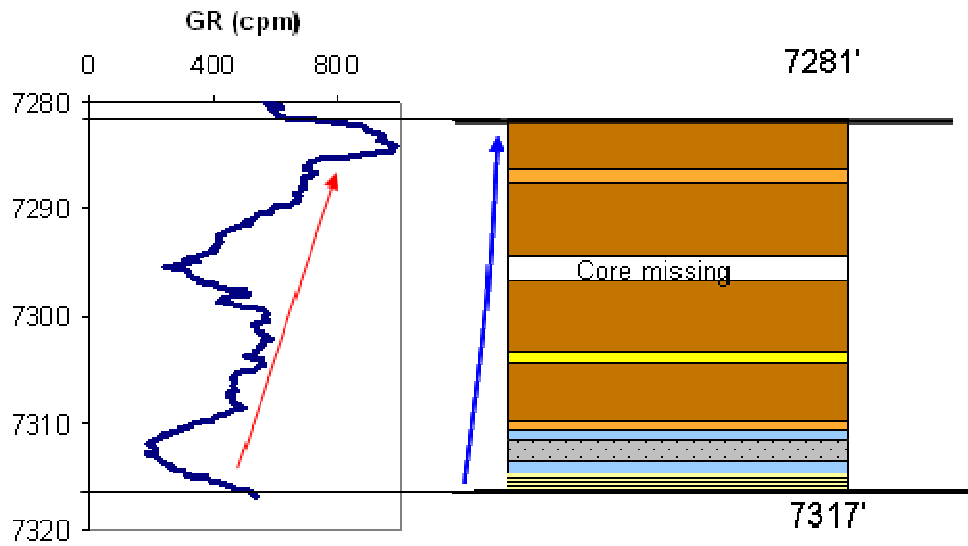
Figure 4.51. GRP12 - Gamma Ray and lithology profiles of Sol Carpenter H#7. For color index see Figure 4.6.

Detailed description: The base of this parasequence is a sharp erosional surface (Fig 4.52). A large clast (Fig. 4.52) at the surface indicates high energy so the erosional surface is a sequence boundary. *Alternate silty shaly wavy bed* deposit overlies the erosional surface. *Micritic/limy mudstone* overlies the *silty shaly wavy bed* deposit. *Dolomitic mudstone* occurs between the *micritic/limy mudstone* (Fig. 4.51).
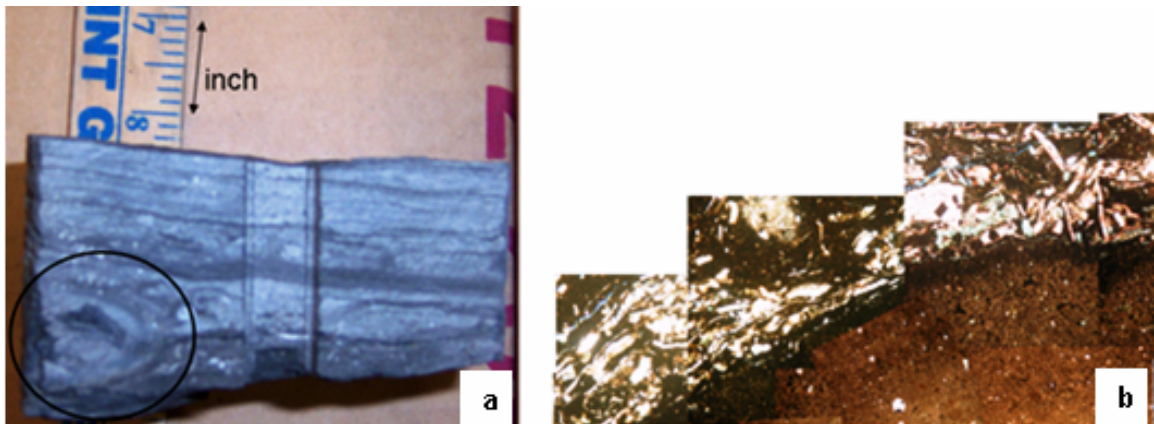
Figure 4.52. (a) Core picture of the erosional surface and the shale clast (circled) at 7317 ft (2230.2 m) and (b) Photomosaic of the thin section picutes of the clast.

The upper part of this parasequence consists of *siliceous, calcareous mudstone*. The calcareous mudstone is rich in detrital quartz. Towards the top of the parasequence, detrital calcite grains become equally abundant (Fig 4.53a) Several reworked phosphatic intervals occur towards the top of this parasequence, including one at 7291.8 ft (2222.5 m) which is a reworked phosphatic ooid deposit (Fig 4.53b) and another at 7285 ft (2220.4 m) which also consists of reworked shelly deposit. This interval is very rich in uranium (14 ppm) (Fig. 4.9) resulting in high gamma ray values. This hot shale can be traced within most of the basin.
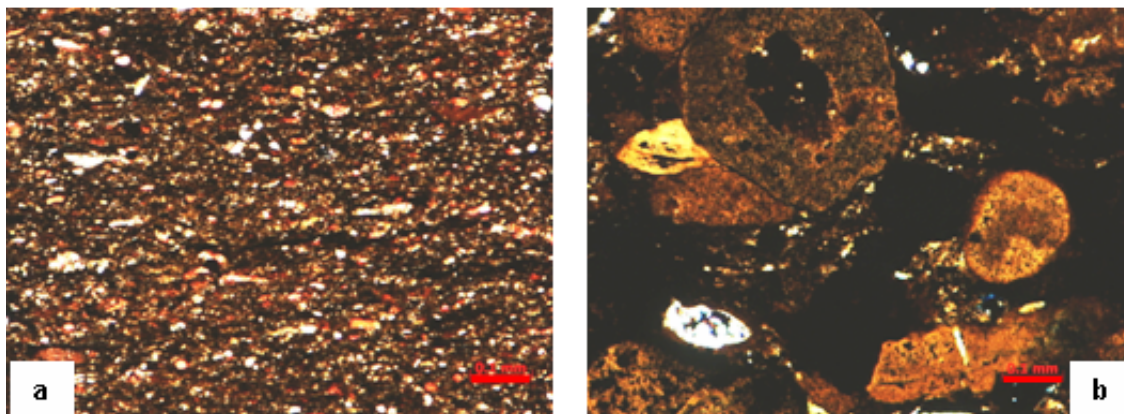
Figure 4.53: Photomicrographs of (a) siliceous, calcareous mudstone at 7281 ft (2219.2 m) showing the high amount of detrital calcite grains (stained pink), (b) phosphatic lag deposit at 7291.8 ft (2222.5 m). The scale bar is equal to 0.1mm.

Lateral Correlation in other wells: Overall, the lateral continuity of this GRP is variable. The vertical facies stacking pattern in all three wells follows a general trend of deepening (Fig. 4.54). The lower part of the parasequence in the Sol Carpenter H#7 and John Porter #3 wells comprise *alternate silty shaly wavy bed* and *micritic/limy mudstone*;

however, only *micritic/limy mudstone* is present in the Adams SW#7. Upsection, there are variable thicknesses of micritic/*limy mudstone* in the John Porter #3 and Adams SW#7 wells. Towards the top of the GRP, hot gamma ray interval occurs which can be traced in all three wells (Fig. 4.54).

Interpretation: GRP 12, an upward increasing gamma ray parasequence, consist of deepening upward succession and is capped by a high gamma ray peak at the top. The base of this GRP is marked by a sequence boundary. On a sequence scale, the lower part of this GRP is interpreted as a lowstand systems tract and the upper part is interpreted as a highstand systems tract (Fig. 4.5, Plate 5). The hot shale at the top consists of reworked phosphatic ooids, shelly deposits and high abundance of uranium concentration. The onset of this interval at the top is interpreted as a transgressive surface of erosion.
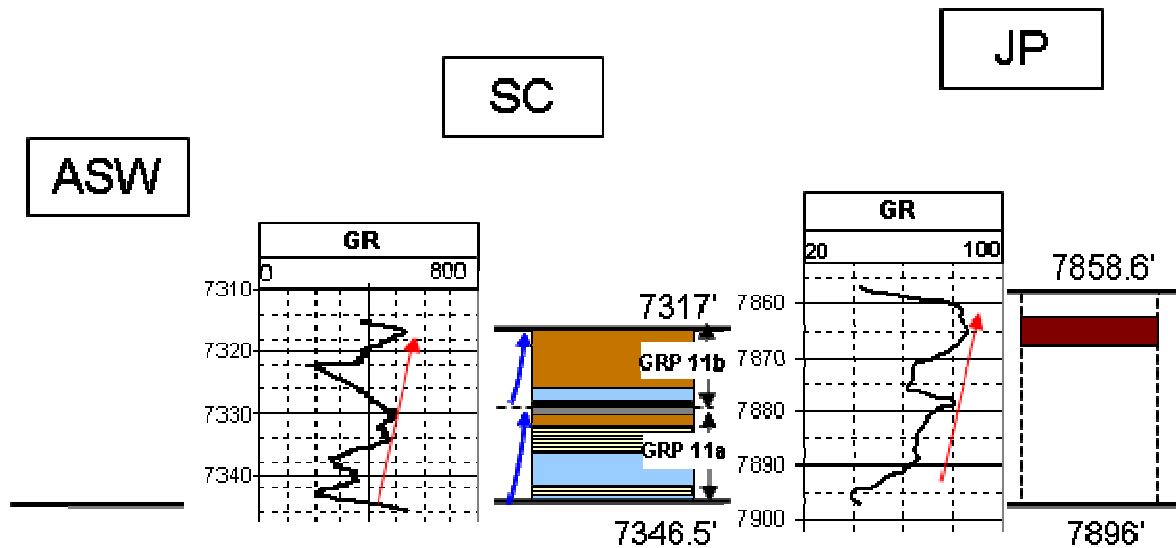
Figure 4.54. Lateral correlation of the GRP 12 of the Upper Barnett Shale in three cored wells: Adams SW #7 (ASW), Sol Carpenter Heirs #7 (SC) and John Porter #3 (JP). For color index see Figure 4.6.

GRP 13: 7281 ft (2219.2 m) - 7249.5 ft (2.209.6 m)

Vertical succession in Sol Carpenter H#7 well: This GRP is an interval with almost

constant Gamma Ray API value capped by a hot gamma ray peak (Fig. 4.55). This

parasequence consists of almost equal proportions of *siliceous non calcareous mudstone*

and *siliceous calcareous mudstone*. The *siliceous, non calcareous mudstone* is rich in

matrix-hosted phosphatic pellets (Fig 4.56a and b). The high gamma ray peak at the top is

due to a phosphate-rich matrix of *siliceous non calcareous mudstone* and partly due to the

presence of a 2.5 inch thick phosphatic ooid deposit (Fig. 4.57).
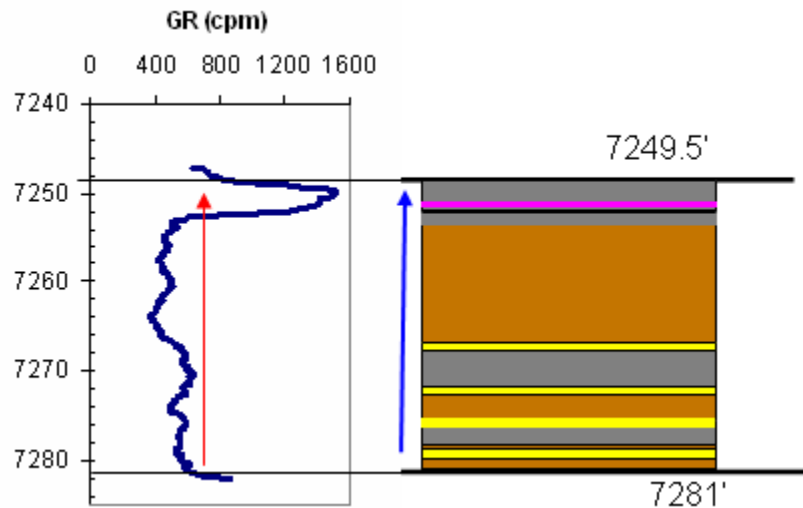
Figure 4.55. GRP13 - Gamma Ray and lithology profiles of Sol Carpenter H#7. For color index see Figure 4.6.
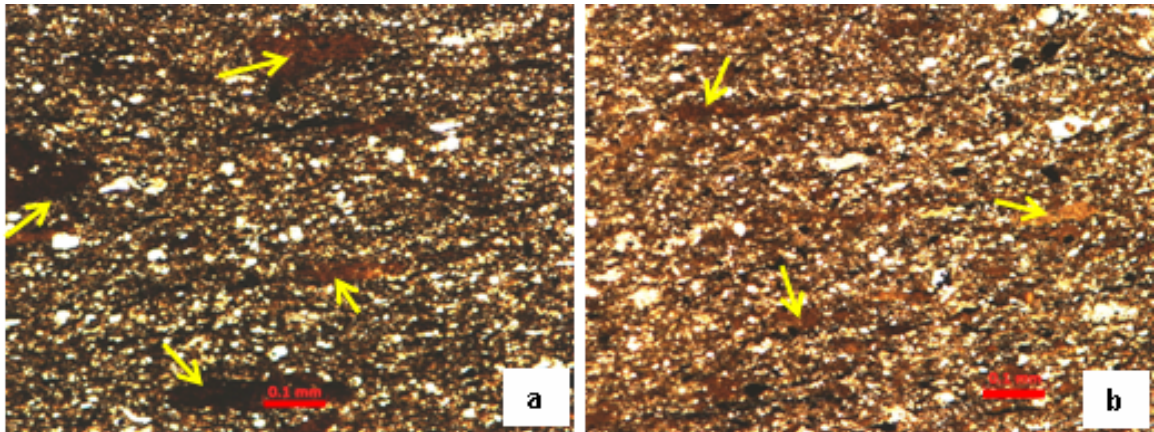
Figure 4.56. Photomicrographs showing the high amount of phosphatic pellets (yellow arrows) in the matrix in GRP 13 at (a) 7279 ft. and (b) 7250 ft. in Sol Carpenter H#7 well. The scale bar is equal to 0.1mm.
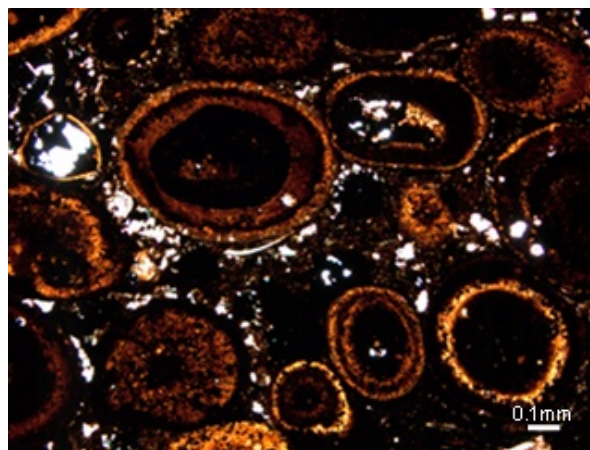
Figure 4.57. Well developed, phosphatic ooid at 7252.5 ft in GRP 13.

Lateral Correlation in other wells: The stacking pattern of the lithofacies of this GRP in the three wells and the reappearance of *non-calcareous mudstone*, *phosphatic* lithofacies suggests a return of deeper conditions (Fig. 4.58). The high gamma ray peak is present in the Adams SW#7 and John Porter#3 well (as noted from the wireline log), however, the core is missing.
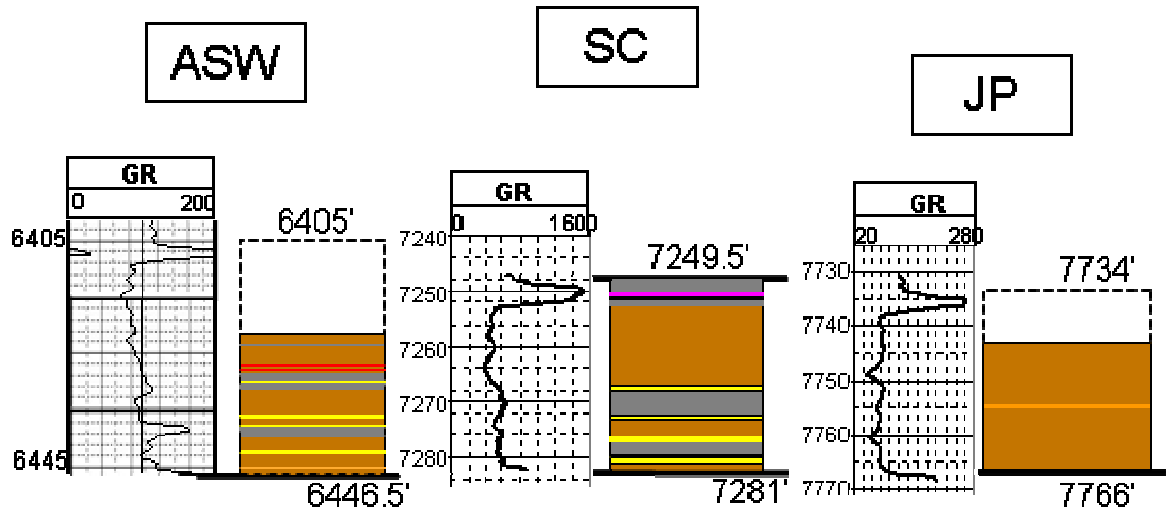
Figure 4.58. Lateral correlation of the GRP 13 of the Upper Barnett Shale in three cored wells: Adams SW #7 (ASW), Sol Carpenter Heirs #7 (SC) and John Porter #3 (JP). For color index see Figure 4.6

Interpretation: GRP 13 overall marks a return of deeper water conditions, more like the depositional environment of the Lower Barnett Shale with the dominant lithofacies being *siliceous, non calcareous mudstone* and *calcareous mudstone*. This GRP, like the Lower Barnett GRP is regionally extensive and is the first parasequence in the Upper Barnett Shale which can be mapped for most of the study area, unlike all the underlying parasequences of the Upper Barnett Shale which thins out towards the south and southwest of the study area. On a sequence scale, this GRP is interpreted as a transgressive systems tract (Fig. 4.5, Plate 5).

GRP 14: 7249.5 ft (2.209.6 m) to 7236 ft (2205.5 m)

Vertical succession in Sol Carpenter H#7 well: This GRP exhibits an upward-decreasing Gamma Ray pattern due to *alternating silty shaly wavy bed deposit* and *dolomitic mudstone* (Fig. 4.59). The sharp contact at the base of this parasequence is

120

interpreted as a sequence boundary. The GRP has increased potassium and thorium

content (Fig. 4.9).
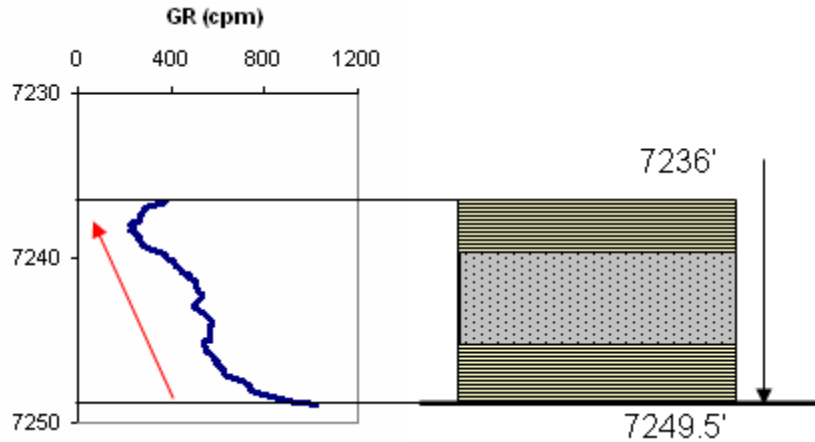
Figure 4.59. GRP14 - Gamma Ray and lithology profiles of Sol Carpenter H#7. For color index see Figure 4.6.

Lateral Correlation in other wells: The core section for this GRP is missing in the

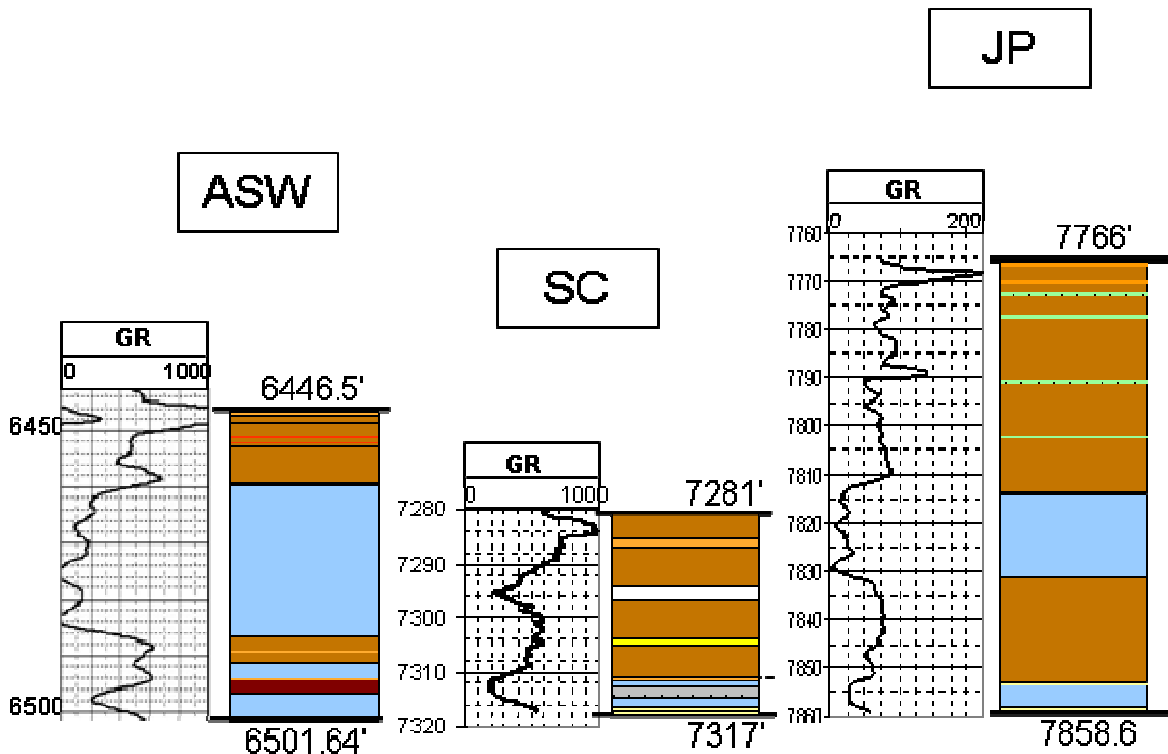Adams SW#7 and John Porter #3 wells (Fig. 4.60).
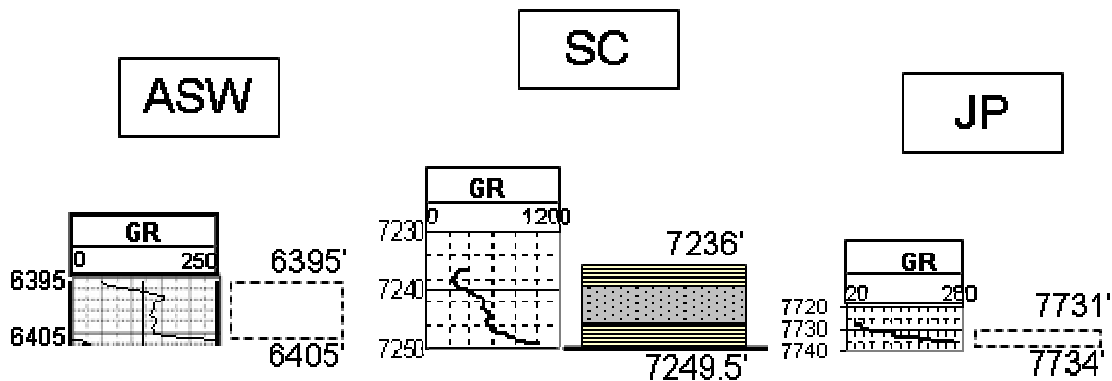
Figure 4.60. Lateral correlation of the GRP 14 of the Upper Barnett Shale in three cored wells: Adams SW #7 (ASW), Sol Carpenter Heirs #7 (SC) and John Porter #3 (JP). For color index see Figure 4.6.

Interpretation: GRP 14, an upward-decreasing gamma ray pattern, is composed mostly

of relatively shallow water silty shaly (wavy) bed deposit and diagenetic dolomitic

mudstone and marks the culmination of the Barnett Shale deposition. On a sequence scale, this GRP is interpreted as a lowstand systems tract (Fig. 4.5, Plate 5).

Summary: In a complete section of the Barnett Shale, one lowstand, three highstand, and three transgressive systems tract were identified in the Lower Barnett Shale whereas four lowstand, four highstand, and one transgressive systems tract were identified in the Upper Barnett Shale (Fig. 4.5). The characteristics of the systems tracts and important stratal surfaces recognized in the Barnett Shale have been summarized (Table 4.1).

Table 4.1. Characteristics for recognition of key surfaces and systems tracts in the Barnett Shale

Key stratal surfaces and systems tracts	Characteristics
Highstand systems tract (HST)	Upward decreasing gamma ray intervals capped by reworked shelly deposits, bottom current reworked calcareous laminae deposits common.
Condensed section	Widespread high gamma ray interval, in situ phosphatic deposits concentrated in laminae, rich in uranium content characterizing low sedimentation and anoxic environment, high in organic carbon.
Transgressive systems tract (TST)	Abundant matrix-hosted phosphatic pellets in siliceous, non calcareous mudstone intervals, overall rich in uranium content, almost no calcareous component
Transgressive surface of erosion	Rich in reworked phosphatic grains, often with winnowed shell fragments, rich in uranium concentration, high gamma ray counts
Lowstand systems tract (LST)	High amounts of terrigenous sediments constituted by silty-shaly (wavy) bed lithofacies and/or debris flows, low in gamma ray counts and organic carbon.
Sequence Boundary	High energy depositional conditions, sharp erosional surface, commonly accompanied by large clasts, or base of debris flows, sharp fall in gamma ray counts

Overall, the Lower Barnett Shale is thought to have been deposited in a more distal part of the basin and hence is dominated by relatively high sea level. The Upper Barnett Shale was deposited in a paralic setting which is characterized by abrupt changes in depositional environment and is more sensitive to sediment accommodation and supply.

4.4 Organic Geochemical Parameters and Gas Content

4.4.1 Organic Richness and RHP

Organic richness, which is measured by TOC content, was compared with the lithology description and the sequence stratigraphic interpretation for the four wells.

The lateral and vertical variation in the organic richness is controlled by changing depositional conditions keeping in mind that the contributing Type II kerogen organic matter is the same for all the Barnett Shale (Pollastro et al. 2003). It is the changing effects of inorganic sediment dilution and bottom oxygen conditions which influence the organic richness of the sediments. Thus, the position of the facies in the depositional sequence will affect the source quality.

Plate 6 is a plot of the TOC wt % of the four wells with their lithofacies distribution. The positions of significant stratigraphic surfaces and systems tracts, interpreted in the earlier section are highlighted. It is noted that major shifts in the TOC values occur at the sequence boundaries, transgressive surface of erosion and condensed sections. A sequence boundary (SB) is marked by a fall in TOC values, transgressive surface of erosion (TSE) is marked by rise in TOC, and condensed section (CS) is represented by maximum TOC content. At the sequence scale, TOC content is low to moderate in lowstand systems tracts, increasing to high TOC in transgressive systems tracts, and low to moderate in highstand systems tracts.

Relative Hydrocarbon Potential (RHP) is a parameter obtained from the Rock-Eval Pyrolysis data - (S1 + S2)/TOC; S1 is the free hydrocarbon, S2 is the hydrocarbon potential, and TOC is the Total Organic Carbon. (S1+S2)/TOC values have been used in

124

the past (Fang et al., 1993; Knies, 2005) to characterize variation in the organic facies and depositional environment. As suggested by Fang et al. (1993), RHP data can be used to determine the organic facies sequence based on the concept that an increasing-upward pattern will suggest vertical change of organic facies from those characteristic of oxic to those of anoxic conditions. In contrast, a decreasing-upward pattern of RHP will suggest vertical change of organic facies from those characteristic of anoxic to those of oxic conditions. Knies (2005) has used similar data to determine climate induced fluctuation in the type of organic matter in interglacial and glacial sediments.

Similar deceasing and increasing patterns of RHP were observed on the RHP data obtained for the Adams SW #7 well. These data were used to compare with the sequence framework interpretations which were based on the sedimentologic characteristics and inorganic constituents of the rock (Fig. 4.61). It was observed that the variation in the degree of oxic to anoxic condition as recorded by the RHP data trend has a good correspondence with the interpreted relative sea level fluctuation and sequence stratigraphic interpretation. The depths with maximum anoxia are the intervals interpreted as condensed section and intervals with highest oxygenation corroborate with the interpreted position of the sequence boundary (Fig. 4.61). At the sequence scale, TOC content is low to moderate in lowstand systems tracts, increasing to high TOC in transgressive systems tracts, and low to moderate in the highstand systems tracts.
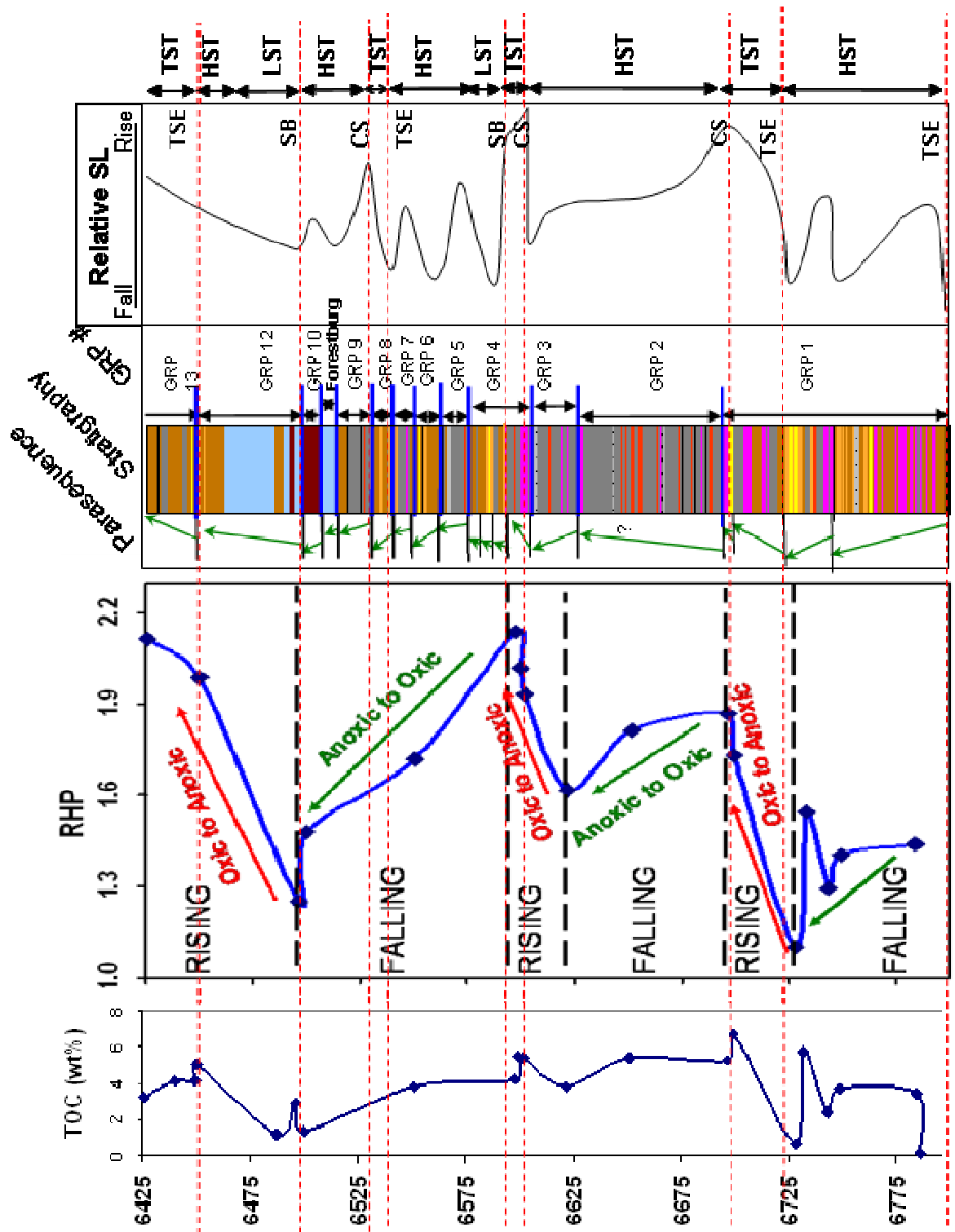
Figure 4.61. The plot shows correlation between the Total Organic Carbon (TOC (wt%), Relative Hydrocarbon Potential (RHP) from Adams SW#7 well core sample measurements and the parasequence, GRP depth assignment, relative sea level curve, and position of the systems tracts for Adams SW#7 well. Good match is obtained for most part. The magnitude of fluctuations of relative sea level is not known, so is not shown to scale. TSE refers to Transgressive surface of erosion, MFS – Maximum flooding surface, SB – Sequence Boundary, LST – Lowstand systems tract, TST – transgressive systems tract, and HST – Highstand systems tract. Major shifts in geochemical parameters tend to occur at maximum flooding surfaces. For color code used in the stratigraphy column see Figure 4.6. RHP data was provided by Gebrehiwet, 2008.

4.4.2 Gas content variation:

Vertical distribution of gas content (total, free, and sorbed) were compared with the vertical distribution of the lithofacies for two cored wells, whose gas content data were available for the Lower Barnett Shale.

Gas in shales are stored as free gas in natural fractures and matrix porosity, or sorbed gas onto kerogen and clay-particle surfaces, or as gas dissolved in kerogen and bitumen (Curtis, 2002). Fracture porosity generally is low (less than 2% of the bulk reservoir volume) (Jenkins and Boyer, 2008). It is important to determine both the sorbed- and free- gas component for shale gas reservoirs. The amount of total gas for gas shales can be obtained by canister desorption measurement in the laboratory (Jenkins and Boyer, 2008). Furthermore, Langmuir isotherm measurements on core can provide direct evaluation of the maximum adsorption capacity of gas by organic matter (Boyer et al., 2006).

However, the gas content data used in this analysis are not obtained by direct measurements but are rather obtained from calculations made for adsorbed gas and free

gas. Combining conventional triple combo and geochemical logs e.g. ELAN, the kerogen thus, organic carbon content can be determined which is utilized to calculate adsorbed gas (Boyer et al., 2006, Bartenhagen, 2006). For free gas evaluation, effective porosity, water saturation measurements from the logs are required.

Appendices A.4 and A.5 shows the Gas content for the Lower Barnett Shale in Sol Carpenter H#7 and John Porter #3 wells. Generally speaking, the variation in the lithology, which ultimately controls the intrinsic porosity, is likely to control the free gas and the variation in the amounts of organic matter will control the sorbed gas. Appendices A.4 and A.5 shows that organic rich shales i.e., non calcareous mudstones rich in phosphatic deposits are the intervals with high gas shows and the intervals composed of high calcite lithofacies i.e. *concretions, reworked shelly deposits,* and *calcareous mudstones with high calcite* lithofacies are the intervals with low gas shows. However, the intervals pointed by red dash arrows in Appendices A.4 and A.5 do not have good correspondence with the above mentioned conclusions.

Chapter 5

Regional Mapping of Gamma Ray Parasequences

The gamma ray profile has been used in the past for regional correlation in several shale formations (Van Buchem et al., 1992, Schieber, 1998). The preceding section shows that systematic vertical stacking pattern of the facies, for the most part, correlates with the cyclical gamma ray profile: i.e. upward-increasing intervals, upward-decreasing intervals and intervals of constant gamma ray API. These Gamma Ray Parasequences thus, provide a means to regionally map these stratigraphic intervals in uncored wells within the study area.

Comprehensive geologic maps of the Barnett Shale have not been published. The available maps are general broad in nature and encompass the geographical extent, total thickness and stratigraphic relations of the Barnett Shale with the underlying and overlying formations. This section provides detailed maps of various parasequences within the Barnett Shale and Forestburg Limestone using the gamma ray wireline logs for Newark East field and the adjoining areas. The total number of control points (vertical wells) selected for mapping was 602. The biggest challenge for the correlations outside Denton and Wise counties is the scarcity of vertical wells in Parker and Tarrant counties. As the play has expanded outside the 'core area' (Hayden and Pursell, 2005) of the basin, more horizontal wells are drilled in preference to vertical wells.

Wireline log cross-sections were also prepared for determining and demonstrating the lateral correlation and variations in interval thicknesses (Figure 5.1). The cross section (Fig. 5.1) and the thickness maps (Fig. 5.2) show that the Lower Barnett Shale thins gradually to the west-southwest; however, most of the Upper Barnett and Forestburg limestone thins out completely to the west-southwest in the study area. Fig. 5.2 A displays the location of faults and graben linear structures related to the Mineral Wells-Newark East fault system. These structural elements were later overlaid on the thickness maps of GRP and GRPS to determine the possible control of structural features on the depositional pattern.

Figure 5.3 shows the Gamma Ray Parasequences composing the Lower and Upper Barnett Shale in Sol Carpenter H#7 well. As stated earlier, the Lower Barnett Shale is composed of 9 parasequences/parasequence sets and the Upper Barnett is composed of 5 parasequences/parasequence sets in most of the 'core' area of the basin. Most of these parasequences/parasequence sets are continuous and mappable over the study area. However, towards the south and west of the 'core' area, most of the Upper Barnett Shale Gamma Ray Parasequences (#10, #11 and #12), Forestburg limestone and the uppermost Gamma Ray Parasequence of the Lower Barnett Shale (#9) thins out (Fig. 5.1). Mapping of these Gamma Ray Parasequences has revealed variations in thickness trends and orientations among them.
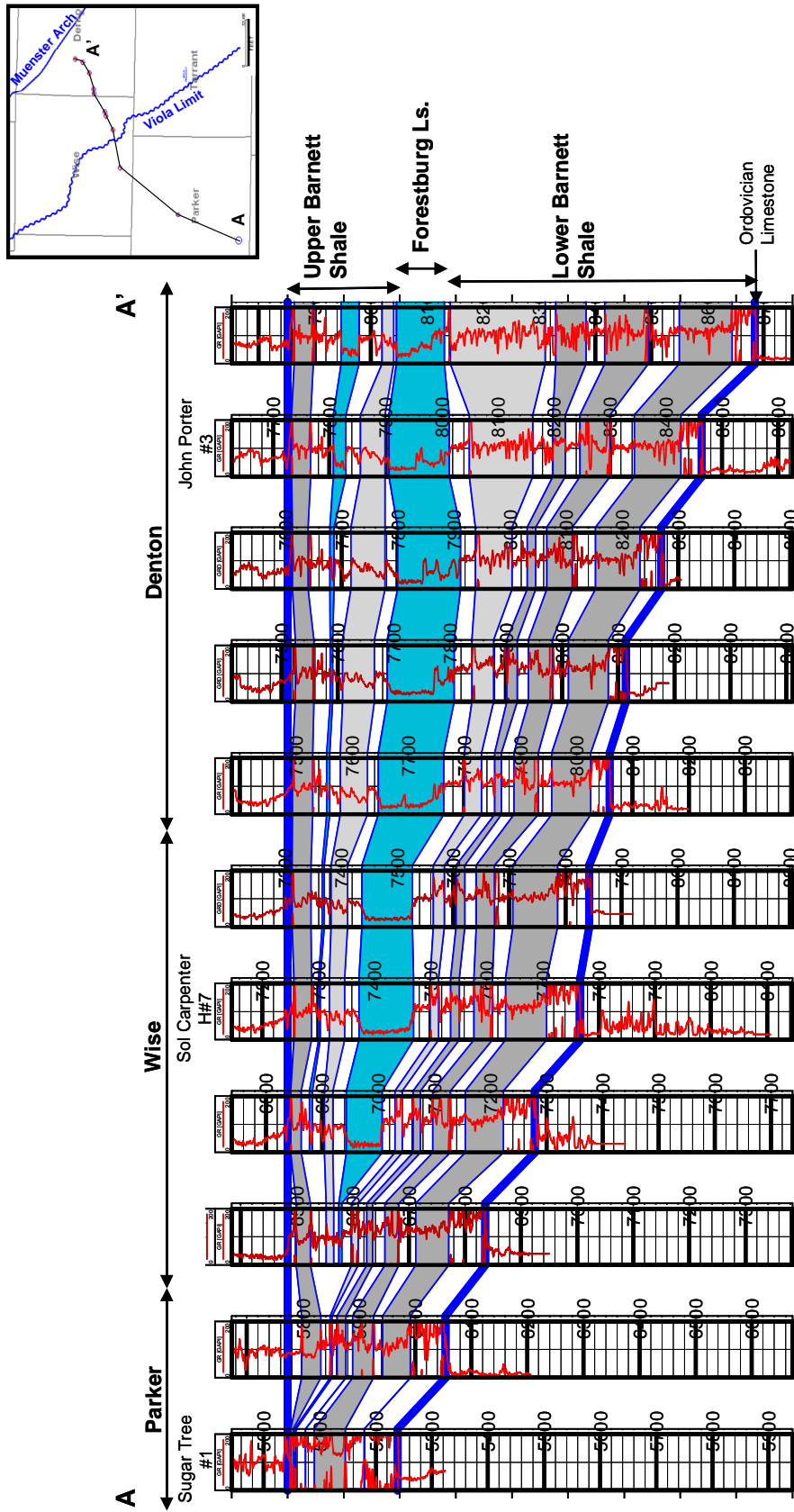
Figure 5.1. Cross section AA' showing subsurface stratigraphic correlation completed using Gamma Ray log. There is a general thinning trend in the Northeast-Southwest direction, however, it is more pronounced for the Upper Barnett Shale and Forestburg Limestone section. Top of Barnett Shale is used as datum. Not to scale horizontally.

131
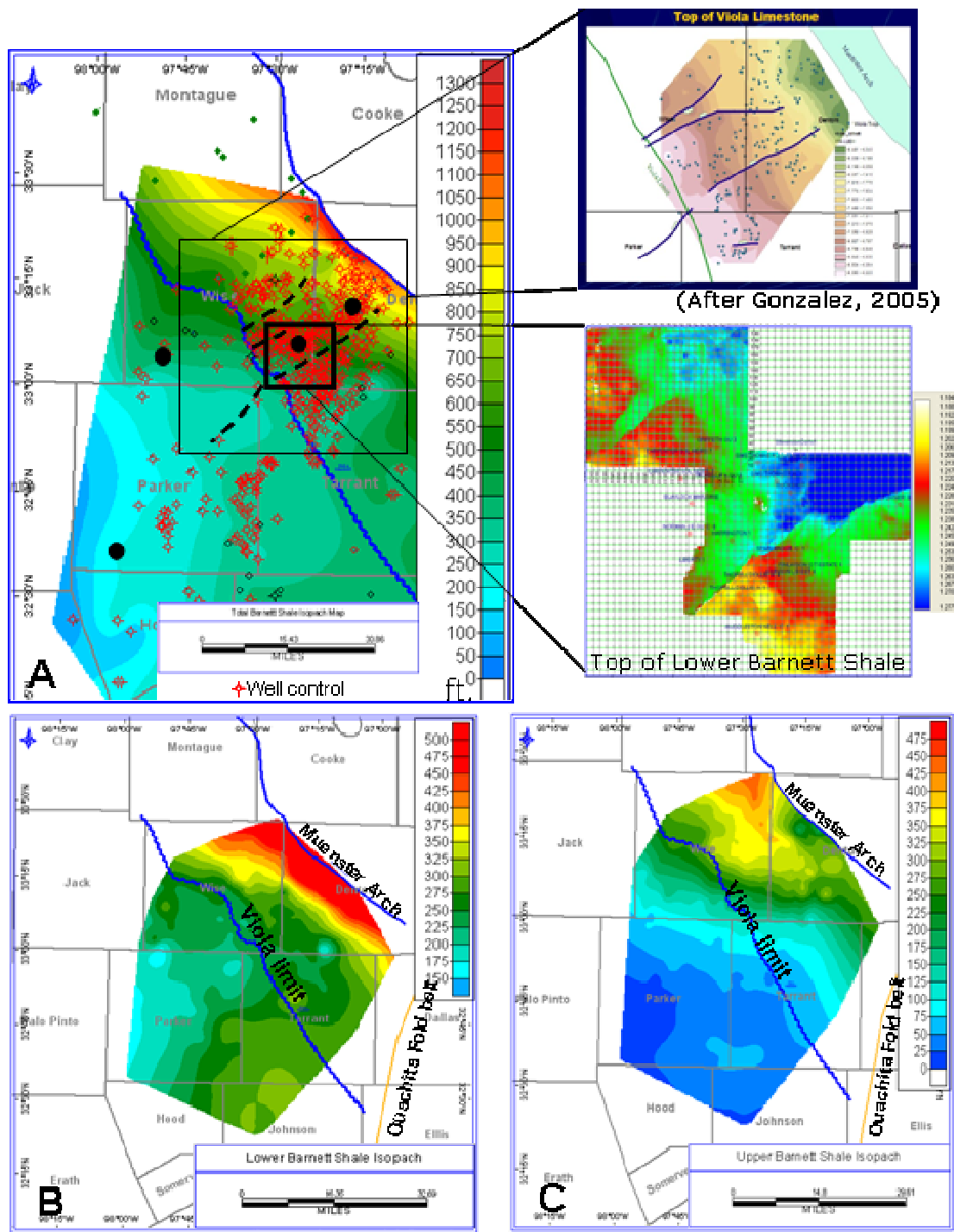
Figure 5.2. (A) Total thickness of the Barnett Shale with the well control locations. The two inset boxes show the locations of the GIS map (Gonzalez, 2005) and time slice of the top of Lower Barnett Shale which were used in order to overlay the fault and graben structures (dashed black lines) onto the thickness maps. (B) Thickness map of the Lower Barnett Shale. (C) Thickness map of Upper Barnett Shale and Forestburg Limestone. Contour intervals are shown in feet.
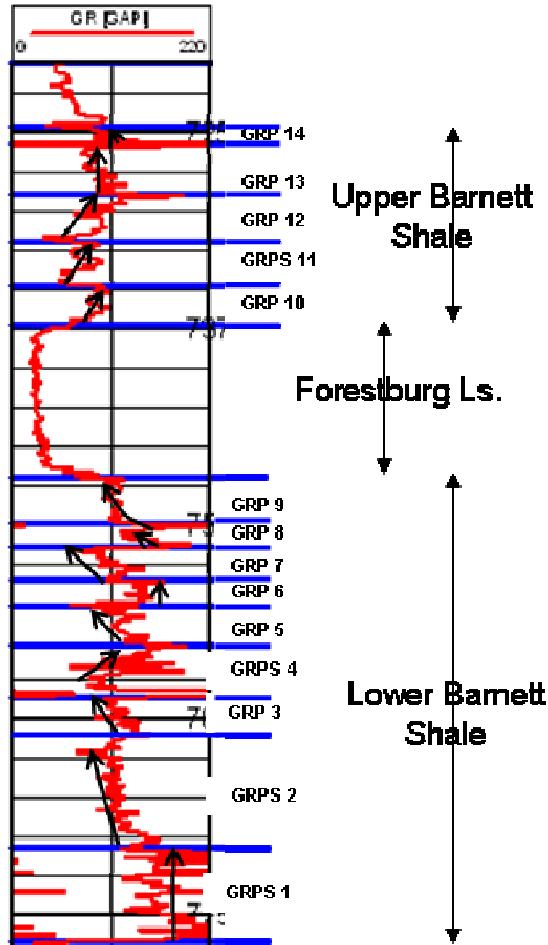
Figure 5.3. Gamma Ray Parasequences of the Upper and Lower Barnett Shale in the Sol Carpenter H#7 well.

The lowermost parasequence set of the Lower Barnett Shale, GRPS 1 (Fig. 5.3) exhibits a northwest-southeast trend of thickness (Fig. 5.4A). This trend has been reinforced by the lithofacies study which suggests that during this time of deposition the land/source area was in the west/southwest direction. GRPS 2 thins in the south direction and exhibits a shifting thickness trend from northwest (observed also in GRPS 1) to northeast (Fig. 5.4 B). This possibly suggests a shifting source area which very well corroborates with the type of sedimentation observed only in the easternmost John Porter

133

#3 well for this interval; here a high number of concretionary intervals rich in calcareous (replaced?) spicules are present. This suggests that this area is possibly proximal to the source area. The younger parasequences (Figures. 5.4 C, D, 5.5 A, B, C, D and 5.6 A) are, in general, thickest in the northeast. However, for GRP #4 and 5 (Figures. 5.4 D and 5.5 A) another thickness trend occurs in the southeast part closer to south Parker and Johnson county. GRP #6 is thickest in the northeast and thins in the northwest and southeast part of the basin (Fig. 5.5 B). GRP #7 is thickest in the northeast and thins in the west and southwest direction (Fig. 5.5 C). It consists of few linear sinuous thickness patterns (oriented northeast-southwest) through the middle of the basin. These linear thickness trends could be due to the periodic accommodation created by reactivation of basement Mineral Wells-Newark East fault system (Pollastro et al. 2007). The northeast-southwest trend of faults in this area (Gonzalez, 2005; Borges, 2007) strongly aligns with the thickness trends. GRP #8 is thickest in the northeast; however, there is a very abrupt decrease in thickness further out (Fig. 5.5 D). This GRP is important because it marks the onset of a dominant northeast sediment source area not only for this parasequence, but for the overlying parasequences (GRP #9, Forestburg Limestone, 10, 11, and 12).

As discussed earlier, studying the sedimentation pattern in the four cored wells, it is thought that the sites of increasing thickness indicate that the sediment source area for those intervals were towards those respective direction. Thus, it is proposed that for GRP 2 through 9, the northeast area was the major sediment source area in this part of the basin (study area). A similar source area was suggested by Borges (2007) for a small area within this dissertation study area. Contribution from a southeast source is also likely

(GRP #4, 5, and 7) but remains to be verified with a cored well in south Tarrant, Johnson counties.
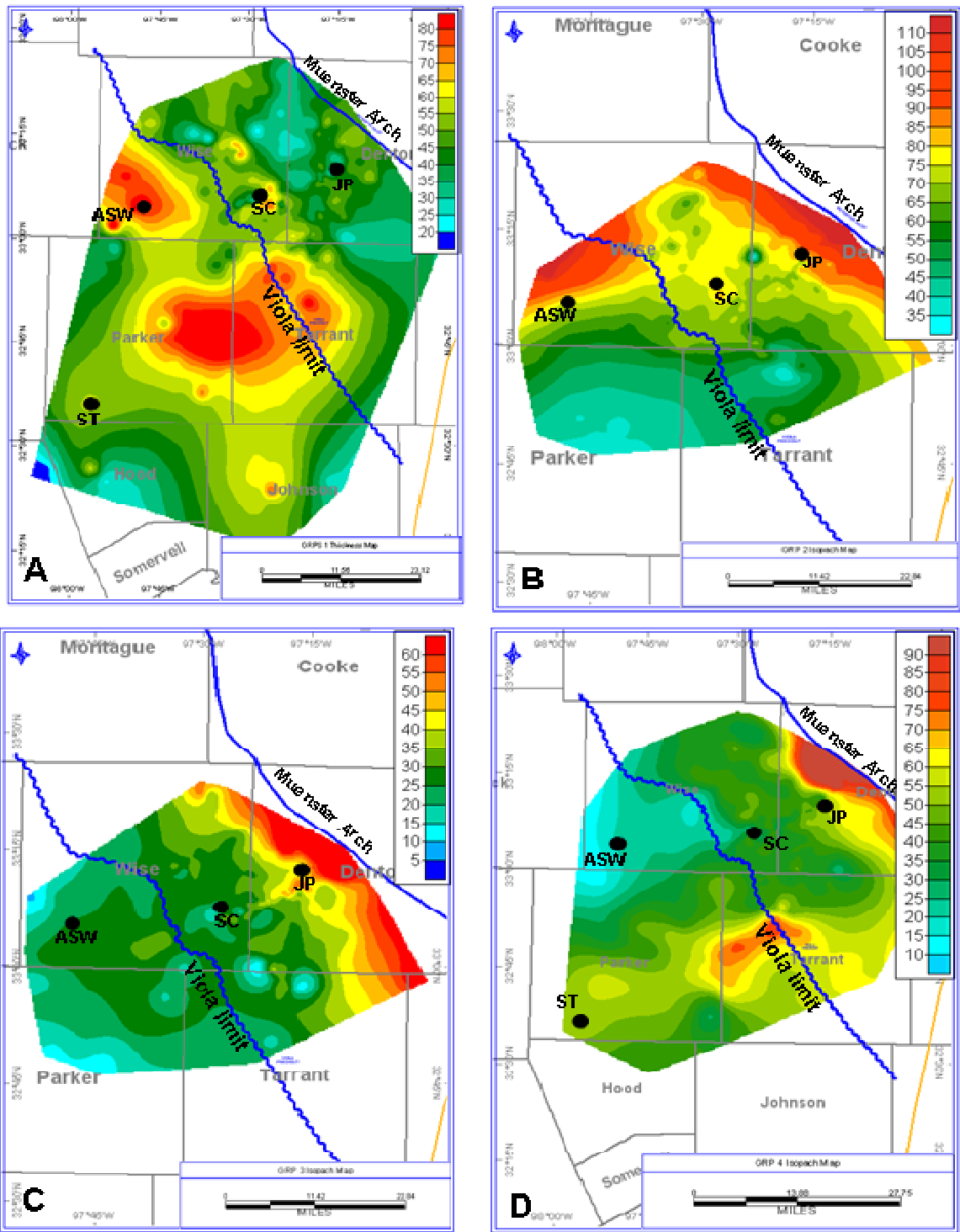
Figure 5.4. Thickness maps of (A) GRPS 1, (B) GRPS 2, (C) GRP 3, and (D) GRPS 4. The cored well locations are marked as ST (Sugar Tree #1), ASW (Adams SW#7), SC

(Sol Carpenter H#7) and JP (John Porter #3). Contour intervals are shown in feet. (Also refer to Appendix A.6)
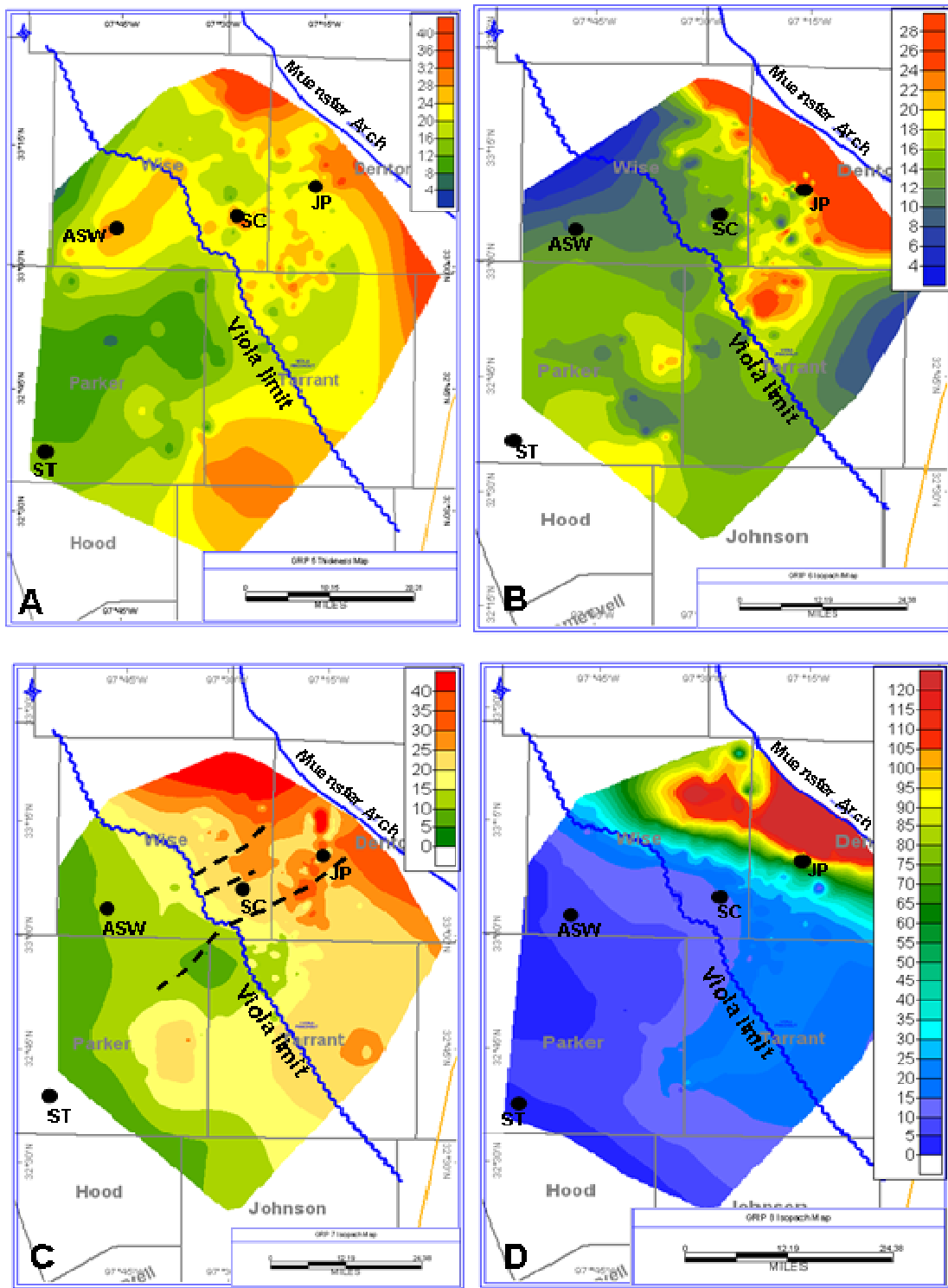
Figure 5.5. Thickness maps of (A) GRP 5, (B) GRP 6, (C) GRP 7, and (D) GRP 8. The cored well locations are marked as ST (Sugar Tree #1), ASW (Adams SW#7), SC (Sol

Carpenter H#7) and JP (John Porter #3). Contour intervals are shown in feet. (Also refer to Appendix A.6)
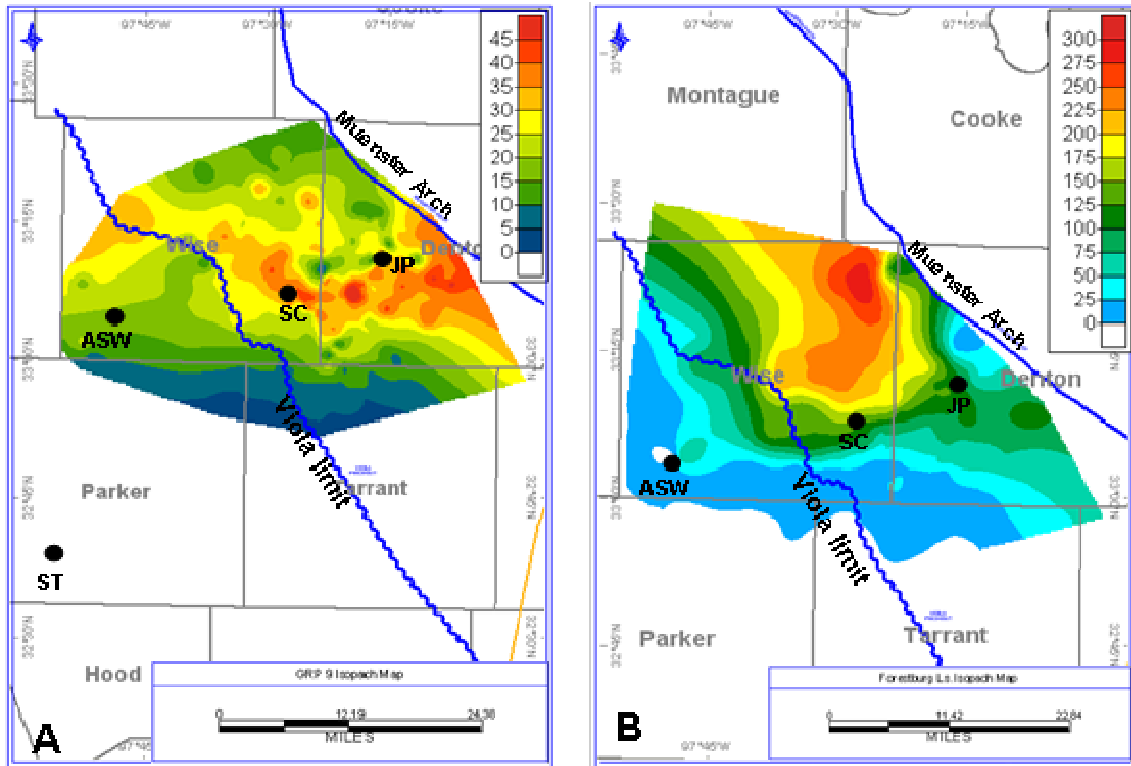
Figure 5.6. Thickness maps of (A) GRP 9, and (B) Forestburg Limestone. The cored well locations are marked as ST (Sugar Tree #1), ASW (Adams SW#7), SC (Sol Carpenter H#7) and JP (John Porter #3). Contour intervals are shown in feet. (Also refer to Appendix A.6)

The Forestburg Limestone reaches a thickness of over 250 feet (76 m) near the Muenster Arch, but thins rapidly south and west of Wise and Denton counties (Fig. 5.6 B). A similar pattern of rapid thinning outside of Wise and Denton counties is observed for most of the Upper Barnett Shale. As mentioned earlier, for the span of GRP 9 through 12, deposition occurred mainly in the Denton and Wise counties with almost no deposition in Parker and Tarrant counties(5.6 A and B, 5.7 A, B, and C). However, the

upper part of the Upper Barnett Shale (GRP # 13 and 14) is regionally extensive (Fig. 5.7 D and E).

GRP 13 exhibits a rough linear thickness trend which thins both in the northwest and southeast directions. The uppermost GRP 14 of the Upper Barnett Shale, which is composed of only lowstand deposits in the Sol Carpenter #7 core, suggests new i.e. northwest-southeast source area direction (Fig. 5.7 E)

Thus, the thickness maps of the parasequences and parasequence sets, constituting the internal stratigraphy of the Barnett Shale, suggests that its depositional history is dynamic and that there has been a reversal in sediment source direction through time, there have been periods of time and areas of non deposition. The linear trends of thickness could be suggestive of the impact of possible recurrent movement of Mineral Wells-Newark East fault system.
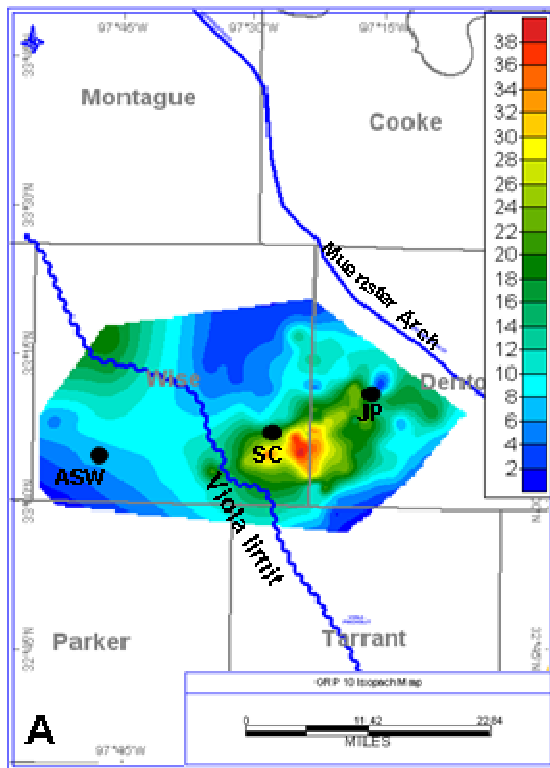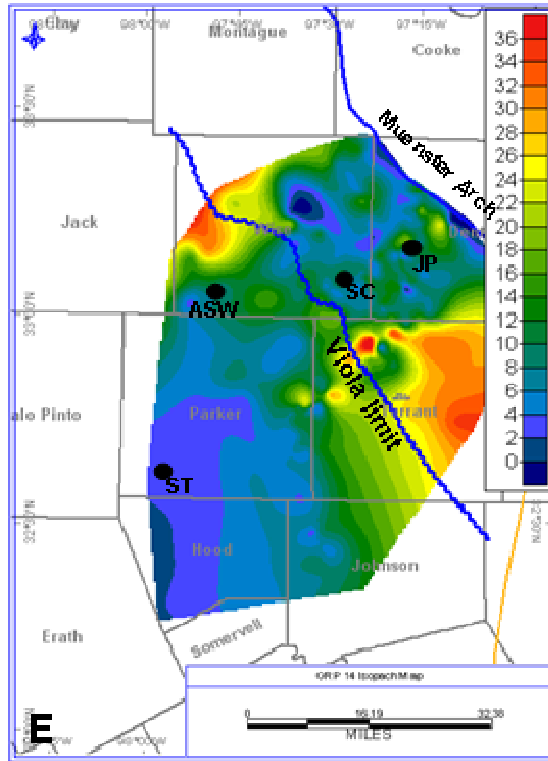
Figure 5.5. Thickness maps of the GRP 10 through 14 (A to E) of the Upper Barnett Shale. The cored well locations are marked as ST (Sugar Tree #1), ASW (Adams SW#7), SC (Sol Carpenter H#7), and JP (John Porter #3). Contour intervals are shown in feet. (Also refer to Appendix A.6)
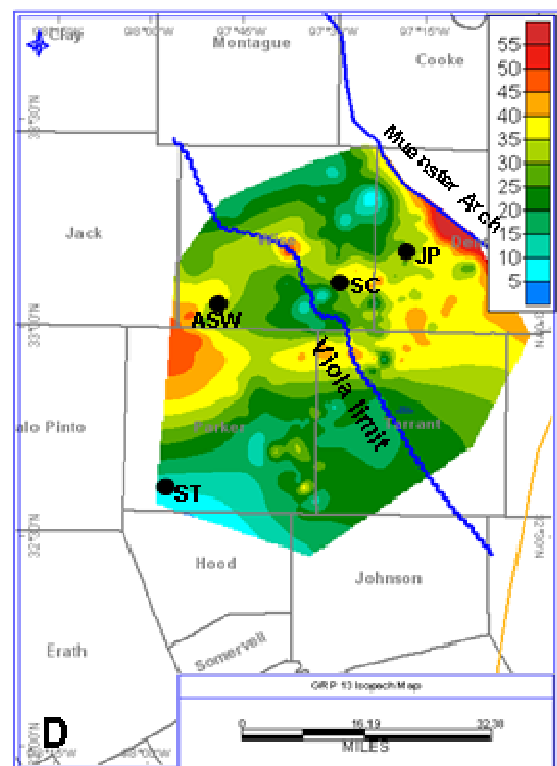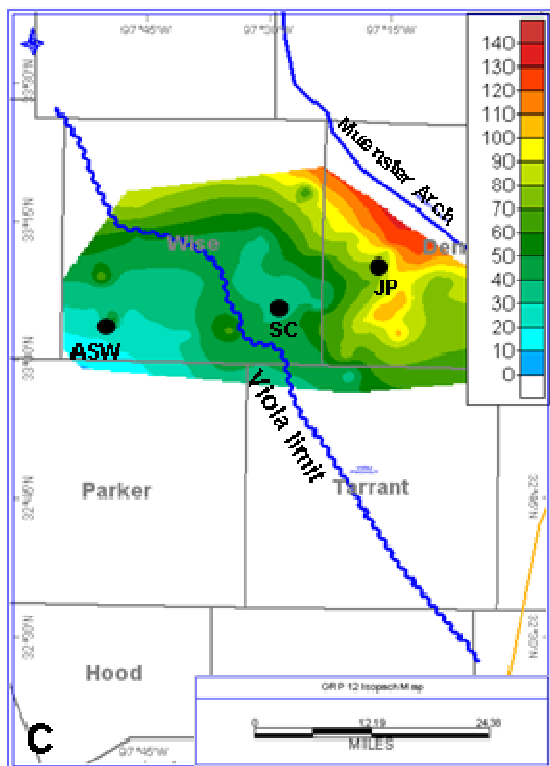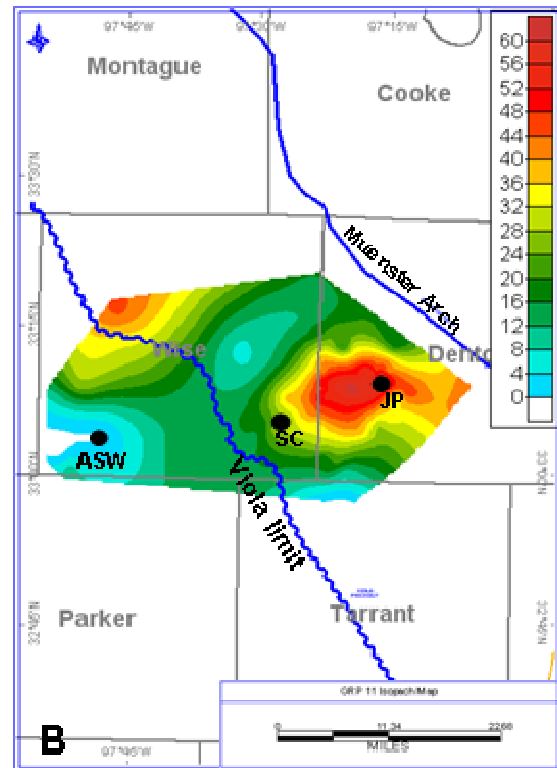
Chapter 6

Discussion, Conclusions and Recommendations

5.1 Discussion and Conclusions

Detailed lithofacies analysis has revealed both complex and cyclic sedimentation patterns indicating systematic changes in depositional environments and processes through the time interval represented by the Barnett Shale. In the past, the heterogeneity in mudstones and shales has been explained only by organic productivity and anoxia changes. However, this dissertation demonstrates that variations in the amounts and type of sediments, variation in accommodation space, etc. also play significant roles in the deposition of gas shale. Equally important is the demonstration that shale successions can be placed within a sequence stratigraphic framework. The following section summarizes the findings of this work:

Lithofacies:

Detailed analysis of physical, mineralogical, chemical and biological characteristics of continuous, long cores has led to the identification of nine lithofacies in the Barnett Shale within the study area: 1) Siliceous, non-calcareous mudstone, 2) Siliceous calcareous mudstone, 3) Micritic/Limy mudstone, 4) Bottom current calcareous laminae deposit, 5)

Reworked shelly deposit, 6) Silty-shaly (wavy) interlaminated deposit, 7) Concretion, 8) Dolomitic mudstone, and 9) Phosphatic deposit. The various components that comprise these facies are allochthonous detrital sediments, autochthonous pelagic sediments, and chemical precipitates. The depositional and diagenetic textures reveal a considerable variation in depositional environments and processes through time, from quiet water deposition of low energy, muddy facies (such as siliceous, non-calcareous mudstone, siliceous calcareous mudstone, and micritic/limy mudstone) to high energy facies (such as phosphatic shelly lags and silty-shaly (wavy) interlaminated mudstones).

The lithofacies exhibit cyclical stacking patterns. Genetically-related lithofacies occur in close association according to their depositional environment. Commonly, *in situ* phosphatic deposits and bottom current calcareous laminae deposits occur with siliceous, non-calcareous mudstone and reworked shelly deposits occur with calcareous mudstone. The earlier assemblage of lithofacies represents relatively deeper water whereas the later assemblage represents relatively shallow water depositional environment.

The wt% TOC values for all the lithofacies in the cored wells were analyzed, and revealed that phosphatic deposits and non calcareous mudstone lithofacies have the highest organic richness and the two diagenetic facies (i.e. concretion and dolomitic mudstone) and silty-shaly (wavy) bed and micritic/limy mudstone are TOC poor lithofacies.

The gamma ray log response of these lithofacies suggests that some of them, including phosphatic deposits, bottom current calcareous laminae deposits, and dolomitic mudstones with reworked shelly deposits have distinctive gamma ray responses. The interval rich in phosphatic deposits exhibits a spike in gamma ray responses with values

142

close to, or over 300 API (wireline gamma ray log); those intervals rich in bottom current calcareous laminae deposit exhibit serrated gamma ray response with values ranging around 80-100 API (wireline gamma ray log). Dolomitic mudstone and reworked shelly deposit exhibit an upward decreasing gamma ray response with values around 60-70 API (wireline gamma ray log).

Parasequences:

The identification of systematic and cyclic stratal stacking patterns of the lithofacies coupled with the gamma-ray log patterns led to identification of three parasequence types: upward-increasing Gamma Ray Parasequence, upward-decreasing Gamma Ray Parasequence and intervals of constant Gamma Ray Parasequence. These intervals are bound by gamma ray kicks or log-based maximum flooding surfaces therefore they are true parasequences (Van Wagoner et al. 1990). A parasequence boundary records an increase in accommodation and separates strata deposited in deeper water, low energy conditions from those deposited in relatively shallow water, higher energy conditions (Bohacs, 1998). The Lower Barnett Shale is composed of nine Gamma Ray Parasequences and the Upper Barnett Shale is composed of five Gamma Ray Parasequences. Unlike siliciclastic and carbonate systems, deepening-upward (upward-increasing) Gamma Ray Parasequences are common, along with the other types of parasequence in this marine setting.

Sequence Stratigraphic Framework:

The stacking pattern of the Gamma Ray Parasequences (GRP) (summarized below) indicates a considerable variation in the depositional history of the Barnett Shale as evidenced by temporal and spatial lithofacies variability and shifting of dominant sediment source areas with time. Systematic, cyclic stacking of parasequences has led to the identification of the parasequence sets which constitute the systems tracts. Upward-decreasing Gamma Ray Parasequences, which are composed of upward-decreasing amounts of clay and phosphatic sediments accompanied by increasing allochthonous calcite grains, capped with reworked shelly deposit are indicative of upward-shoaling of the depositional environment during gradual fall in relative sea level, and thus comprise a highstand systems tract. Lower parts of upward-increasing Gamma Ray Parasequences are underlain by sequence boundaries, representing higher energy conditions, and consist of allochthonous detrital sediments of a lowstand systems tract. Widespread in situ phosphatic rich mudstone intervals, rich in uranium content are associated with widespread slow sedimentation in an anoxic environment representative of transgressive systems tract.

The cyclic pattern indicates sufficient variation in lithofacies and depositional conditions of the Lower and the Upper Barnett Shale so they can be considered in terms of processes that control detrital sediment supply and accommodation. In the past, variations in vertical distribution of successions within shales have been very frequently characterized solely on the basis of variation of organic content and fluctuation of oxygen deficiency (Herbin, et al. 1993; Chandra, et al. 1993). However, there is close correlation between fluctuation of bottom water oxygen concentrations and the variation of detrital

144

sediment accumulation, accommodation which ultimately influences productivity and preservation of organic matter. The strong correspondence between the lithofacies-based interpreted relative sea level curve and the oxic-anoxic variation obtained by the Relative Hydrocarbon Potential (RHP) measurement organic material (Fig. 4.18) supports this relationship. Thus, a sequence framework such as this can be used to predict the source quality of a shale formation.

The Upper Barnett Shale depositional lithofacies exhibit a paralic setting which is characterized by abrupt change in depositional environment, frequent stratigraphic interruption in deposition and/or change in depositional energy conditions. These settings are more sensitive to sediment accommodation and supply (Bohacs, 1998). The Upper Barnett Shale contains more silty-shaly (wavy) beds and micritic/limy mudstone deposits. Three possible sequence boundaries are documented for the Upper Barnett (Fig. 4.5, Plate 5).

Only one sequence boundary was identified in the Lower Barnett Shale. A relatively deeper water setting is interpreted during deposition of the Lower Barnett Shale. Lower Barnett parasequences are best identified by vertically stacked cycles of low energy phosphatic shales with high energy, reworked shelly deposits formed in response to a gradual lowering of relative sea level.

A gradual change in dominant source area from the west-southwest to northeast is recorded primarily by changes in allochthonous detrital sediments including detrital quartz and calcite content, and debris flows through the Lower Barnett Shale. The Upper Barnett appears to have been sourced mostly from the northeast.

Regional distribution of Gamma Ray Parasequences:

The GRP provided means to regionally map these stratigraphic intervals using both cored and uncored wells in the study area. Thickness maps of the nine Gamma Ray parasequences in the Lower Barnett and five in the Upper Barnett Shale, reveal changing thickness patterns and areal extent. Sites of maximum parasequence thickness are indicative of the proximity to the sediment source area.

Thus, by integrating several attributes and scales of observation, from logs to subsurface cores to thin section and incorporating geochemical parameters, this study has illuminated the nature of the Barnett Shale depositional system. The study also provides a workflow (Fig. 6.1) for systematically constructing a sequence stratigraphic framework for mudstones of similar setting.
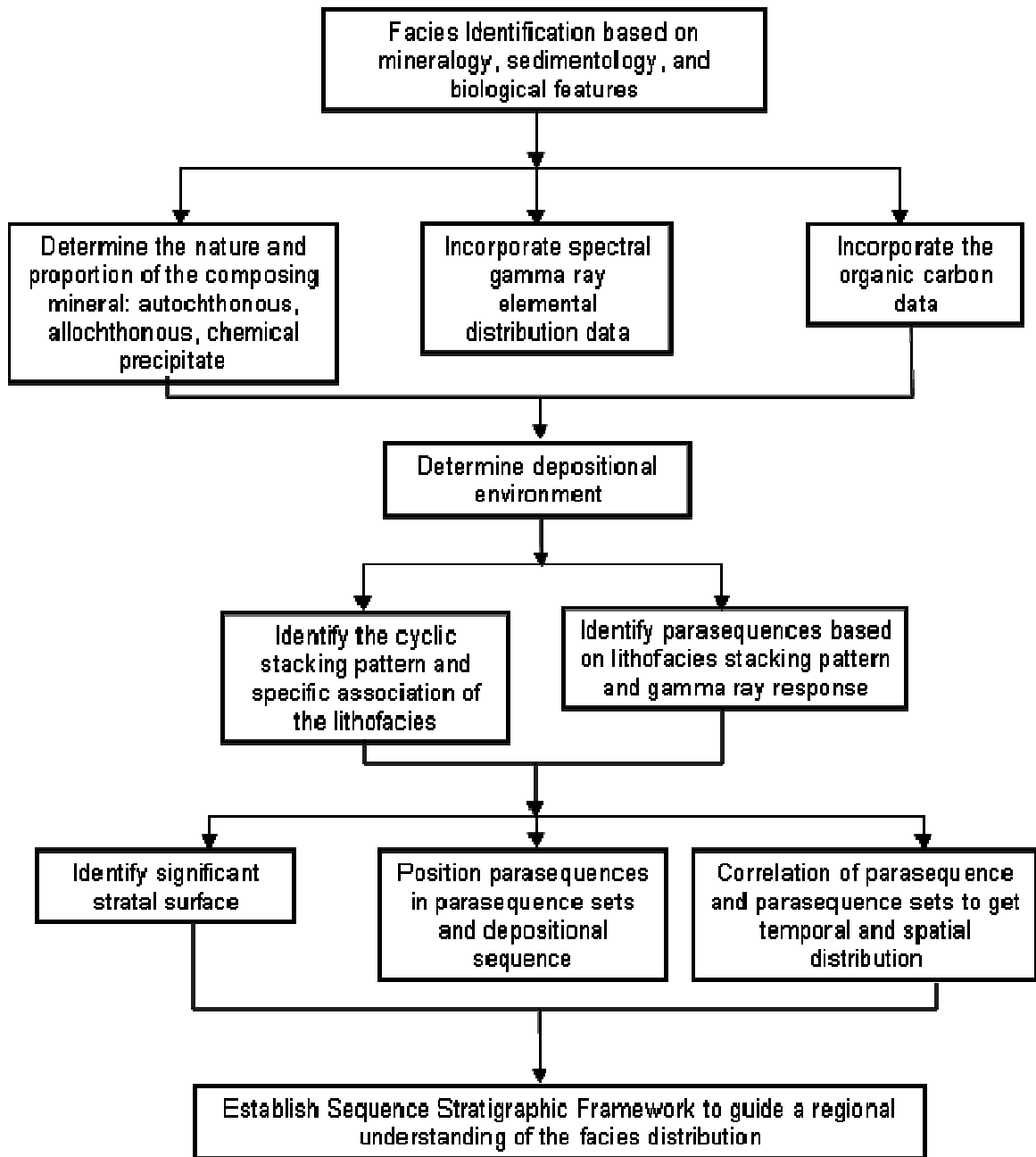
Figure 6.1. Flowchart showing workflow developed for establishing sequence stratigraphy of marine shales.

The study shows that marine shale depositional systems, like other carbonate and siliciclastic systems, are controlled by processes and mechanisms that can be explained within a sequence stratigraphic framework. Such a framework has general application to

identifying source, reservoir, seal rocks as well as predicting organic-richness variation within a depositional sequence.

5.2 Recommendation

1. Suggested future work includes a similar study in the southern Tarrant and Johnson counties to extend the stratigraphic framework and also to help understand the reasons for increased thicknesses of GRP #4, 5, 7 and 14 in these directions. With the exhaustive drilling in the 'core area' and the recognition of Johnson county as another sweet spot (Hayden et al. 2005), the extension will be well worth the effort.

2. Biostratigraphic characterization for the Barnett Shale is recommended. The development of a sequence stratigraphic framework for the Barnett Shale can now provide a structure for construction of a general chronostratigraphic framework by using the significant key surfaces and the time-transgressive nature of lithofacies and surfaces across the basin. Thus, a chronostratigraphic framework will not only help to fine-tune the stratigraphic framework which is currently based on lithofacies vertical successions, but will also address the cyclic pattern of the depositional sequence including possible water depths.

3. This dissertation provides a methodology for geological characterization of other gas shales and mudstones. It is clear that an integration of geochemical characteristics (such as biomarker, RHP, and TOC) reinforces the depositional environment interpreted from lithofacies characterization. It is therefore suggested that for future cored wells, geochemical data be included as part of the characterization.

4. The thickness trends of the GRP above and below Forestburg Limestone follows that of the Forestburg Limestone. It is hence recommended that Forestburg limestone be studied in detail as it might further shed light on depositional conditions during the period of its deposition.

4. The stratigraphy established in this study needs to be integrated with 3D seismic studies to evaluate the level of possible resolution of parasequences for mapping in lightly drilled areas.

5. Construction of models integrating the geologic framework developed in this study and other petrophysical parameters to predict the rock units as flow units and those more susceptible to fracture stimulation is suggested for future research.

References

Adams, J.E., 1954: Mid Paleozoic Paleogeography of Central Texas: Shale Shaker v. 4, no.6, p. 4-9.

Almon WR, Dawson WC, Sutton SJ, Ethridge FG, Castelblanco B 2002: Sequence stratigraphy, facies variation and petrophysical properties in deepwater shales, Upper Cretaceous Lewis Shale, south-central Wyoming. Gulf Coast Association of Geological Socities Transactions 52, p.1041–1053.

Amorosi, A., 1995: Glaucony and sequence stratigraphy: a conceptual framework of distribution in siliciclastic sequences. Journal of Sedimentary Research B65, 419-425.

Baker, P.A., and Kastner, M., 1981: Constraints on the formation of sedimentary dolomite. *Science,* 213:215-216.

Barterhagen, K., 2006: Wireline evaluation techniques of shale gas reservoirs. RPSEA Shale gas forum. http://www.rpsea.org/forums/shale_bartenhagen.pdf (accessed on 19th September 2008).

Bentor, Y.K., 1980: Phosphorites-the unsolved problems. SEPM Special Publication, no. 29, p 3-18.

Bernhard, J.M. 1986 Characteristic assemblages and morphologies of benthic foraminifera from anoxic, organic- rich deposits: Jurassic through Holocene. Journal of Foraminiferal Research, 16, 207-215.

Best, M.E. and Kastube, T.J. 1995: Shale permeability and its significance in hydrocarbon exploration. The Leading Edge, March, 165-170.

Birch, G. F., 1980: A model of penecontemporaneous phosphatization by diagenetic and authigenic mechanisms from the western margin of Southern Africa. SEPM Special Publication No. 29, p 79-100.

Bohacs, K. and Schwalbach, J., 1992: Sequence stratigraphy of fine-grained rocks with special reference to the Monterey Formation. In Schwalbach, J. and Bohacs, K., eds., Sequence Stratigraphy in Fine-Grained Rocks: Examples form the Monterey Formation, Soc. Econ. Paleontol. Pacific Section Vol. 70, p 7-19.

Bohacs, K. M, 1993: Source Quality Variations tied to Sequence Development in the Monterey and Associated Formations, Southwestern California: AAPG Special Volumes, Vol SG 37, p. 177-204.

Bohacs, K. M., 1998: Introduction: Mudrock Sedimentology and Stratigraphy-Challenges at the Basin to Local Scales. In: J. Schieber, W. Zimmerle, and P. Sethi (editors), Shales and Mudstones (vol. 1): Basin Studies, Sedimentology and Paleontology, Schweizerbart'sche Verlagsbuchhandlung, Stuttgart, p.13-20.

Borges, G., 2007, Seismic Sequence Stratigraphic Interpretation of Barnett Shale at Newark East Field in Fort Worth Basin, Texas: Unpublished Master's thesis, University of Oklahoma, Norman, Oklahoma, 72 p.

Bouma, A. 2005: Shales, Siltstones and Mudstone in our Future: Am. Assoc. Petroleum Geologists Bull., v. 89. Program Abstracts (Digital).

Boyer, C., Kieschnick, J., Saurez-Rivera, R., Lewis, R., and Waters, G., 2006: Producing gas from its source, Oilfield Review, v.18, no.3, p. 36-49.

Bramlette, M.N., 1946, The Monterey Formation and the origin of its siliceous rocks: United States Geological Survey Professional Paper 212, 57p.

Byers, C. W., 1977: Biofacies patterns in euxinic basins: A general model: In Cook, H.E. and Enos, P., eds, Deep-water Carbonate Environments: Society of Economic Paleontologists and Mineralogists Special Publication 25, p. 5-17.

Caspers, H., 1957: Black Sea and Sea of Azov. In: *Treatise on Marine Ecology and Paleoecology. Vol. 1, Ecology (Ed. by J. W. Hedgepeth).* Mem. geol. Soc. Am. 67, 801-889.

Chandra, K., Raju, S.N. and Mishra P.K., 1993: Sea level changes, anoxic conditions, organic matter enrichment, and petroleum source rock potential of the Cretaceous sequences of the Cauvery Basin, India. *In* B.J. Katz and L.M. Pratt (eds.), Source rocks in sequence stratigraphic framework. AAPG Studies in Geology 37. Tulsa pp. 131-146.

Cheney, M. G., 1940: Geology of north-central Texas: Am. Assoc. Petroleum Geologists Bull., v. 24, p. 65-118.

Cheney, M.G. and Gloss, L.F. 1952: Tectonics of Central Texas. AAPG Bull. v. 36, no. 12, pp 2237- 2265.

Clark, F.T and Bybee, H.H., 1951: Fort Worth Basin and Muenster arch North-Central Texas. AAPG Bulletin, 35, no.2: 353-356 p.

Clifton, H.E., 1971; Orientation of empty pelecypod shells and shell fragments in quiet water. Journal of Sedimentary Petrology, v. 41, no. 3, pg. 671-682

Cloud, P.E., and Barnes, V.E., 1948: The Ellenburger group of Central Texas, publ. no. 473 p.

Cloud, P.E. Jr. and Barnes, V.E., 1957: Early Ordovician Sea in Central Texas. Geol. Soc. America, v. 67, part 2, p. 163-213.

Cluff, Robert M., 1980, Paleoenvironment of the New Albany Shale Group (Devonian-Mississippian) of Illinois, Journal of Sedimentary Petrology Volume: 50 Issue: 3 Pages: 767-780

Coveney, R.M., Jr, Watney, W.L. & Maples, C.G. 1991. Contrasting depositional models for Pennsylvanian black shale discerned from molybdenum abundances. *Geology* 19, 147-150.

Craig, L.C., and Connor C. W., 1979: Paleotectonic Investigations of the Mississippian System in the United States. Part I. Introduction and Regional Analyses of the Mississippian System: Geol. Survey, Prof. Paper 1010, 559p.

Curtis, J. B., 2002: Fractured shale - gas systems: AAPG Bulletin, v. 86, p. 1921-1938.

Davies, D.K., and Vessell, R.K. 2003, Gas production from shale. In: E.D. Scott, A.H. Bouma, and W.R. Byrant (Eds.), Siltstones, Mudstones and Shales: Depositional Processes and Characteristics. SEPM/GCAGS Joint Publication, p.112-125.

Dawson, W. C., 2000: Shale microfabrics; Eagle Ford Group (Cenomanian-Turonian) north-central Texas outcrops and subsurface equivalents: Gulf Coast Association of Geological Socities Transactions, v. 50, 607-621.

Demaison, G.J. and Moore, G.T. 1980: Anoxic environments and oil source bed genesis. AAPG Bulletin, 64: 1179-1209

Dewhurst, D. N. and Aplin, A. C., 1998: Compaction-driven evolution of porosity and permeability in natural mudstones: An experimental study: Journal of Geophysical Research, v. 103, p. 651– 661.

Dorr, J.A., Jr. and Eschman, D.F., 1970: Geology of Michigan: Ann Arbor, Michigan, University of Michigan Press.

Durham, L.S., 2007, Barnett 'Hits' don't rule out misses still a 'statistical' play: AAPG Explorer, October 2007.

Dyni, J.R., 2005: United States oil-shale deposits. United States Geological Survey Scientific investigations report 2005. http://geology.com/usgs/oil-shale/united-states-oil-shale.shtml (accessed September 16th 2008)

Ece, O. I., 1987: Pertrology of the Desmoinesian Excello black shale of the midcontinent rejoin of the United states. Clays and Clay Minerals, v. 35. no. 4, p.262-270.

Edwards, B.D., 1985 Bioturbation in a dysaerobic, bathyal basin: California borderland. *In* Biogenic structures: their use in interpreting depositional environments, SEPM special Publication 35, p. 309-331.

EIA (Energy Information Administration) http://www.eia.doe.gov/oil_gas/natural_gas/data_publications/crude_oil_natural_gas_reserves/cr.html (accessed on January 15th, 2007)

EIA (Energy Information Administration), 2004, Annual energy outlook 2004 with projections to 2025: U.S. Department of Energy, Energy Information Administration report DOE/EIA-0383 (2004), 278 p.

Embry, A., 2007: Six Impossible Sequence Boundaries Before Breakfast: A 50 year saga of unworkable methods and wishful thinking. A 2007 Ashton Embry presentation. Calgary, Canada http://wildhorse.insinc.com/embry2007/ accessed on 23rd July 2008.

Emery, K. O., 1968, Positions of empty pelecypod valves on the continental shelf. Jour. Sed. Petrology, v. 38, p. 1264-1269.

Ettensohn, F. R.1998: Compressional tectonic controls on Epicontinental black shale deposition: Devonian-Mississippian examples from North America. In: J. Schieber, W. Zimmerle, and P. Sethi (editors), *Shales and Mudstones (vol. 1): Basin Studies, Sedimentology and Paleontology,* Schweizerbart'sche Verlagsbuchhandlung, Stuttgart, p. 109-128.

Fang, H., Jianyu, C., Yongchuan, S., and Yaozong, L., 1993: Application of organic facies studies to sedimentary basin analysis: a case study from the Yitong Graben, China: Organic Geochemistry, v. 20(1), p.27-42.

Fisher, K., 2006: Barnett Shale fracture fairways aid E&P. World Oil, v. 227 no. 8 p. 83-86.

Frantz, J. Jr and Jochen, V., 2005: Shale Gas. White Paper 9p.

Gale, J., Reed, R.M. and Holder, J., 2007: Natural fractures in the Barnett Shale and their importance for hydraulic fracture treatments. AAPG Bull., v. 91, no. 4. p. 603-622.

Gebrehiwet, T.A., Philp, R.P., 2008: Geochemical characterization of Barnett Shale, Fort Worth Basin, TX. Unpublished Annual report to Devon Energy

Gipson, M. Jr., 1966: A study of the relations of depth, porosity and clay mineral orientation in Pennsylvanian shales. Journal of Sedimentary Petrology, vol. 36, no. 4, p. 888-903.

Gonzalez, R., 2004: A GIS approach to the geology, production and growth of the Barnett Shale play in Newark East field: GIS Masters Project: POEC 6386, University of Texas at Dallas. Master's thesis. Link: http://charlotte.utdallas.edu/mgis/prj_mstrs/2004/Summer/Gonzalez/jegonzalez.htm (accessed December, 2006).

Gulbrandsen, R.A., 1960: Petrology of the Mead Peal phpdphatic shale member of the Phospharia Formatuib at Coal Canyon, Wyoming: U.S.G.S. Bull. 1111C, p.71-146.

Halabura, S., Buatois, L., Angula, S., and Piche, L., 2007: From source to trap: A review of the Bakken Petroleum systems, Upper Devonian-Mississippian, Southeastern

Saskatchewan *in* summary of investigations 2007, v. 1 Saskatchewan Geological Survey, Sask. Industry resources, paper A-4, 8p. http://www.er.gov.sk.ca/adx/aspx/adxGetMedia.aspx?DocID=5420,3442,3440,3385,5460,2936,Documents&MediaID=16801&Filename=halabura.pdf (accessed September 16th 2008)

Handford, C.R., 1984: facies and bedding sequences in shelf-storm-deposited carbonates – Fayetteville shale and Pitkin limestone (Mississippian), Arkansas. Journal of sedimentary petrology, v. 56, no.1, p.123-137. Over, D.J., 1992: Conodonts and the Devonian-Carboniferous boundary in the Upper Woodford shale, Arbuckle mountains, South-Central Oklahoma, J. Paleont., v. 66, no. 2, p. 293-311

Hass, W.H., 1959: Conodonts from the Chappel limestone of Texas: U.S. Geol. Survey, Prof. Paper 294-J, p. 365-399, pls. 46-50.

Hayden, J. and Pursell, D., 2005. The Barnett Shale, Visitors Guide to the Hottest Gas Play in the US: Pickering Energy Partners, Inc., October 2005, http://info@pickeringenergy.com (accessed January, 2007).

Henry, J. D., 1982: Stratigraphy of the Barnett Shale (Mississippian) and associated reefs in the northern Fort Worth basin: Dallas Geological Society paper, 21 p.

Herbin, J.P., Muller, C., Geyssant, J.R., Melieres, F., Penn, I.E., and Group, Y., 1993: Variation of the distribution of organic matter within a transgressive system tract: kimeridge clay (Jurrasic), England. *In* B.J. Katz and L.M. Pratt (eds.), Source rocks in sequence stratigraphic framework. AAPG Studies in Geology 37. Tulsa, pp. 67-100.

Hildenbrand, A. and Urai, J.L. 2003 Investigation of pore space in mudstone – first results. Marine and Petroleum Geology v.20, p. 1185-1200.

Jarvie, D. 2005: Shale gas Potential of Source rocks along the Ouachita Thrust Front: EMGI Barnett Shale symposium III, June 8-9, 2005, p. 3. http://www.pttc.org/workshop_presentations/texas_060805/2005barnettshalesymp..pdf (accessed December 14, 2007).

Javier, P., 2006: High resolution facies analysis of the Barnett Shale, Newark field, Fort Worth basin, North-central Texas. Unpublished Master's thesis, University of Oklahoma, Norman, Oklahoma, 51 p.

Jenkins, C.D. and Boyer, C.M., 2008: Coalbed- and Shale-Gas Reservoirs. Jour. Petr. Technology, v.60, no.2, p.92-99.

Kaminski M.A., Boersma A., Tyszka J., and Holbourn A.E.L. 1995. Response of deep-water agglutinated foraminifera to dysoxic conditions in the California Borderland Basins. In: Kaminksi, M. A., Geroch, S., Gasinski, M. A., Eds., *Proceedings of the Fourth International Workshop on Agglutinated Foraminfera, Kraków Poland*. Grzybowski Special Publication no. 3, p.131–140.

Kier, R. S., 1972, Carboniferous stratigraphy of eastern San Saba County and western Lampasas County, Texas: University of Texas, Austin, Ph.D. dissert, 437 p.

Kier, R. S., Brown, L. F., Jr., and McBride, E. F., 1979: The Mississippian and Pennsylvanian (Carboniferous) Systems in the United States: Texas (Reprinted by Bureau of Economic Geology, Geological Circular 80-14), *in* Matthew J. Avcin and Donald L. Koch (editors), The Mississippian and Pennsylvanian (Carboniferous) Systems in the United States: Washington, D. C., U.S. Geological Survey, Professional Paper 1110, p. 51–545.

Knies, J., 2005: Climate-induced changes in sedimentary regimes for organic matter supply on the continental shelf off northern Norway. *Geochimica et Cosmochimica Acta, Vol. 69(19) p.*4631-4647

Kochenov, A.V. and G. N. Baturin, 2002, The paragenesis of organic matter, Phosphorous and Uranium in Marine sediments: Lithology and Mineral Res. v. 37, no. 2, p. 107-120

Koutsoukos, E.A.M., Leary, P.N. and Hart, M.B. 1990. Latest Cenomanian-earliest Turonian low-oxygen tolerant benthonic foraminifera: a case study from the Sergipe Basin (N.E. Brazil) and the western Anglo-Paris (southern England). Palaeogeography. Palaeclimatology, Palaeocology, 77, 145-177.

Krushin, J. T., 1997. Seal capacity of nonsmectite shale, in R. C. Surdam, ed., Seals, traps, and the petroleum system: AAPG Memoir 67, p. 31– 47.

Land, S. L., 1985: The origin of Massive Dolomite. Journal of Geological Education, v. 33, pp 112-125.

Leckie, D.A., Singh, C., Goodarzi F., and Wall J.W. 1990. Organic-rich, radioactive marine shale: A case study of a shallow-water condensed section, Cretaceous

Shaftesbury Formation, Alberta, Canada. Journal of Sedimentary Petrology, v. 60, p. 101-117.

Lorenz, J.C., 1982: Sedimentology of the Mesaverde formation at Rifle Gap, Colorado and implications for gas-bearing intervals in the subsurface, 44p. http://www.osti.gov/energycitations/servlets/purl/5313562-nnG2lH/5313562.PDF (accessed September 16th 2008)

Loucks, R.G. & Ruppel, S. C., 2007: Mississippian Barnett Shale: Lithofacies and Depositional Setting of a Deepwater Shale-Gas Succession in the Fort Worth Basin, Texas. AAPG Bull. Vol. 91, no. 4, p. 579-601.

Macquaker, J.H.S., Gawthorpe, R.L., Taylor, K.G. and Oates, M.J., 1998: Heterogeneity, Stacking Patterns and Sequence Stratigraphic interpretation in Distal Mudstone Successions: Examples from the Kimmeridge Clay formation, U.K. In: J. Schieber, W. Zimmerle, and P. Sethi (editors), Shales and Mudstones (vol. 1): Basin Studies, Sedimentology and Paleontology, Schweizerbart'sche Verlagsbuchhandlung, Stuttgart, p. 163-185.

Mapel, W.J., Johnson, R.B., Bachman, G.O. and Varnes, K.L., 1979: Southern Midcontinent and southern Rocky Mountains Region, *in* L.C. Craig, and C. W. Connor (editors), Paleotectonic Investigations of the Mississippian System in the United States. Part I. Introduction and Regional Analyses of the Mississippian System: Geol. Survey, Prof. Paper 1010, p. 161-187.

Mcgookey, D.P. 2005: Geologic Wonders of West Texas, 210 p

Meckel. L.D., Smith D.G., and Wells, L.A., 1992: Ouachita Foredeep Basins: Regional Paleogeography and habit of hydrocarbons: Foreland Basins and Fold Belts, AAPG Memoir 55, p 427-444.

Milliken, K., S. Choh, P. Papazis, and J. Schieber, 2007, 'Cherty' stringers in the Barnett Shale are agglutinated foraminifera: Sedimentary Geology. 198, p. 221-232.

Mongomery, S., 2005: Barnett Shale: A new Gas Play in the Fort Worth Basin: Petroleum Frontiers, v. 20, no.1.

Montgomery, Scott L., Daniel M. Jarvie, Kent A. Bowker, and Richard M. Pollastro, 2005: Mississippian Barnett Shale, Fort Worth Basin, North-Central Texas: Gas-

Shale Play with Multi-Tcf Potential, AAPG Bull., E&P Note, Vol. 89, No. 2, p. 155-175.

Morgan, C.D. and Chidsey, T.C., 1991: Horizontal drilling potential of the Cane Creek Shale, Paradox Formation, Utah, AAPG Bull. v. 75:6. http://www.osti.gov/energycitations/product.biblio.jsp?osti_id=6011841 (accessed on Jan, 2008)

Namy, J.N., 1982: Stratigraphy and Hydrocarbon production of the Marble Falls Group Southern part if the Fort Worth basin: Petroleum Geology of the Fort Worth basin and Bend Arch area, DGS. p 213-222.

O'Brien and Slatt, 1990: Argillaceous Rock Atlas. Springer Verlag. 141p.

Obid, J., 2008 upper Jurassic sequence stratigraphy, onshore to offshore Alabama, eastern gulf of Mexico. http://www.searchanddiscovery.net/documents/2008/08071GCAGS2005/abstracts/obid.htm (accessed September 16th 2008)

Olausson, E., 1961: Studies of Deep-Sea Cores. Reports of the Swedish Deep-Sea Expedition, 1947 - 1948, 8:353-391.

Omarzai, S.K. 1992. Monterey Formation of California at Shell Beach (Pismo Basin): Its Lithofacies, Paleomagnetism, Age, and Origin. In Sequence Stratigraphy in fine-grained rocks: Examples from the Monterey Formation. Pacific Section – SEPM v 70, p. 47-67

Papazis, P.K., 2005, Petrographic characterization of the Barnett Shale, Fort Worth Basin, Texas, Master's Thesis, University of Texas at Austin, Austin, Texas, 142 p.

Parrish, J. T. 1982: Upwelling and petroleum source beds, with reference to Paleozoic. AAPG Bull. 66, p.750-774.

Pashin, J.C., 1994 Cycles and stacking patterns in Carboniferous rocks of the Black Warrior Foreland basin. GCAGS Transactions, v. 44, p. 555-563

Pederson, T. F., and Calvert, S.E. 1990: Anoxia vs. productivity: What controls the formation of organic-carbon rich sediments and sedimentary rocks? AAPG Bull., 74, p. 454-466.

Peppard-Sounders, 1975: The structural and stratigraphy of the Fort Worth Basin. Unpublished Report.

Pollastro, R.M., Jarvie, D.M., Ronald J.H., and Adams, C.W., 2007: Geologic framework of the Mississippian Barnett Shale, Barnett-Paleozoic total petroleum system, Bend arch-Fort Worth Basin, Texas. AAPG Bull. 91. no. 4 p. 405-436.

Pollastro, R.M., Ronald J.H., Jarvie, D.M. and Henry, M.E. 2003: Assessing Undiscovered Resources of the Barnett-Paleozoic Total Petroleum System, Bend Arch–Fort Worth Basin Province, Texas: Online adaptation of presentation at AAPG Southwest Section Meeting, Fort Worth, TX, March, 2003.

Potter P.E. Maynard, J.B. and Pryor, W.A., 1980. Sedimentology of Shale. Springer Verlag New York Inc. 305p.

Provo, L. J., Kepferle, R. C., Potter, P.E., 1978: Division of Black Ohio Shale in Eastern Kentucky. AAPG Bull. 62, no. 9 p. 1703-1713.

Raiswell, R., 1988. Chemical model for the origin of minor limestone-shale cycles by anaerobic methane oxidation: Geology, v.16 p. 641-644.

Rhoades, D. C., and Morse, I. W. 1971. Evolutionary and ecologic significance of oxygen-deficient marine basins. Lethaia 4. p 413-428.

Rhoades, D. C., Mulslow, S.G., Gutschik, R., Baldwin, C. T., and Stolz, J. F. 1991: The dysaerobic zone revisited: a magnetic facies? In: R.V. Tyson and T. H. Pearson (editors), *Modern and ancient continental shelf anoxia*. Geological Soc. Spec. Publication 58, p. 187-199.

Robinson, W.E. 1976: Origin and characteristics of Green River Oil shale. In "oil Shale" (G.V. Chilingarian and T.F. Yens, eds.), pp. 61-80. Elsevier, Amsterdam.

Robison V.C., Engel M., 1993: Characterization of the source horizons within the Late Cretaceous Transgressive sequence in Egypt. In: Katz BJ, Pratt LM (eds) Source Rocks in a Sequence Stratigraphic Framework. AAPG Studies in Geology 37:101–117

Rodriguez, N., 2007: Geochemical characterization of gases from the Barnett Shale, Fort Worth basin, Texas: Unpublished Master's thesis, University of Oklahoma, Norman, Oklahoma, 123 p.

Ross, D. J. K., and Bustin, R. M., 2007: Shale gas reservoir systems: Insights from north of the border. Adaption from poster presentation at AAPG Annual Convention.

Ruedemann, R., 1935: Ecology of black shales of eastern New York, Jr. Paleontology, v. 9, no. 1, p. 79-91.

Ruppel, S. C., 1989: Summary of Mississippian stratigraphy in north and north-central Texas, *in* Mear, C. E., McNulty, C. L., and McNulty, M. E., eds., A symposium on the petroleum geology of Mississippian carbonates in north-central Texas: Fort Worth Geological Society and Texas Christian University, p. 49–55.

Schieber, J. & Ellwood, B.B. 1993: Determination of basinwide paleocurrent patterns in a shale sequence via anisotropy of magnetic susceptibility (AMS): A case study of the Mid-Proterozoic Newland Formation, Montana. – Jour. Sed. Petrology. 63, p. 874 – 880.

Schieber, J., 1998, Developing a sequence stratigraphic framework for the Late Devonian Chattanooga Shale of the southeastern US: relevance for the Bakken Shale, *in* J.E. Christopher, C.F. Gilboy, D.F. Paterson, S.L. Bend, eds., Eight International Williston Basin Symposium, Saskatchewan Geological Society, Special Publication No. 13, p. 58–68.

Schmoker, J. W., Quinn, C. J., Crovelli, R. A., Nuccio, V.F., and Hester, T. C., 1996: Production characteristics and resource assessment of the Barnett Shale continuous (unconventional) gas accumulation, Fort Worth Basin, Texas: U.S. Geological Survey Open-File Report 96-254, 20 p.

Schutter, S. R., 1998, Characterization of shale deposition in relation to stratigraphic sequence systems tracts, *in* J. Schieber, W. Zimmerle, and P. Sethi, eds., Shales and mudstones I: Stuttgart, Germany, E. Schweizerhbart'sche Verlagsbuchhandlung, p. 79–108.

Selley, R. C., 1998: Elements of Petroleum Geology. Second Edition, Academic Press 463 p.

Souders P, 1975: The Structure and Stratigraphy of the Fort Worth Basin. Peppard-Souders consultant study

Stein, R. 1991. Accumulation of organic carbon in marine sediments. *In* Lecture Notes in Earth Sciences, Springer Verlag, Berlin Heidelberg. 214 p

Stow, D.A.V., H.G. Reading, and J.D. Collinson, 1996, Deep seas, *in* H.G. Reading, eds., Sedimentary environments: processes, facies and stratigraphy, Blackwell Scientific, Oxford, p. 395–454

Stow, D.A.V., Huc, A.–Y., and Bertrand, P., 2001, Depositional processeses of black shales in deep water: Marine and Petroleum Geology, v. 17, no. 4 p. 491-498.

Stucker, J.D., Rowe, H., Rimmwe, S., Ruppel, S. and Loucks, R., 2008: Geochemical constraints on the depositional environment of the Barnett formation, Permian Basin, West Texas, USA. GCACS Joint Meeting (Abs.), Oct. 2008, http://gsa.confex.com/gsa/2008AM/finalprogram/abstract_151672.htm (accessed on September, 16, 2008)

Sutton, S.J, Ethridge, F.G, Almon, W.R, Dawson, C. D and Edwards, K.K., 2004 Textural and sequence stratigraphic controls on sealing capacity of Lower and upper cretaceous shales, Denver basin, Colorado. AAPG Bulletin, Vol.88, No.8 p.1185-1206.

Theede, H., 1973: Comparative studies on the influence of oxygen deficiency and hydrogen sulphide on marine invertebrates. Netherlands Journal of Sea Research, 7, 224-252

Tissot, B.P. 1977. The application of the results of organic chemical studies in oil and gas exploration. *In* "Developments in petroleum geology", Vol. 1, p. 53-82. Applied Science Publishers, London.

Tissot, B.P. & Welte, D.H. 1978: Petroleum formation and Occurrences: A New Approach to Oil and Gas Exploration. Springer-Verlag, Berlin.

Tomlinson, C. W. 1916: The origin of red beds: Amer. Jour. Sci., v. 24, p. 153-179.

Tubb, R. 2007, P&GJ 2007: Worldwide Pipeline Construction Report, p. 17. http://www.oildom.com/PGJ/pgjarchive/Jan07/pipereport1-07.pdf (accessed April 29, 2008)

Turner, G. L., 1957: Paleozoic Stratigraphy of the Fort Worth Basin: in "Lower Penn and Miss Rocks of the NE llano Uplift. Abilene and Fort Worth Geological: Joint Field Trip Guidebook-1 cross section. p. 57-77

U.S. Geological Survey National Oil and Gas Resource Assessment Team, 1995, 1995 national assessment of United States oil and gas resources: U.S. Geological Survey Circular 1118, 20 p.

Van Wagoner, J.C., R.M. Mitchum, K.M. Campion, and V.D. Rahmanian, 1990, Siliciclastic sequence stratigraphy in well logs, cores and outcrops: concepts for high resolution correlation of time and facies: AAPG Methods in Exploration Series, no.7, 53 p.

Walker, R.G. and James, N. P., 1992: Facies Models Response to Sea Level Change, Geological Association of Canada, p. 1-12.

Walper, J.L., 1982: Plate tectonic evolution of the Fort Worth basin: Dallas Geological Society.

Weeks, L.G., 1953, Environment and mode of origin and facies relationships of carbonate concretions in shales: Journal of Sedimentary Petrology, v.23, no. 3, p. 162-173.

Wignall, P.B., 1994, Black Shales: Oxford Science Publication, 127 p.

Zachry, D.L., Jr., 1969: Carboniferous stratigraphy of the Chappel area, San Saba County, Texas: University of Texas, Austin, Ph.D. dissert, 353 p.

Appendix

Appendix A.1.

Upward decreasing Gamma Ray Parasequence
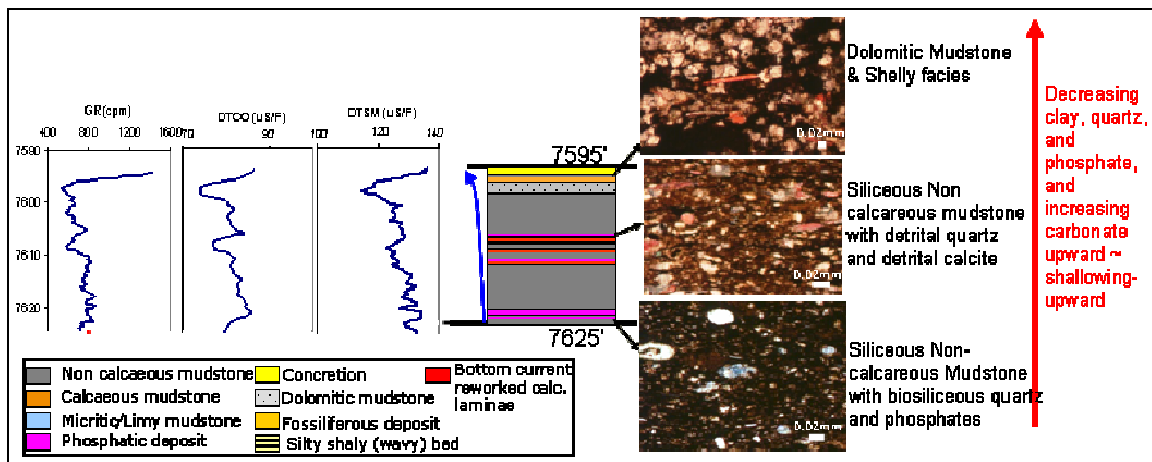
Appendix A.2.

Upward increasing Gamma Ray Parasequence
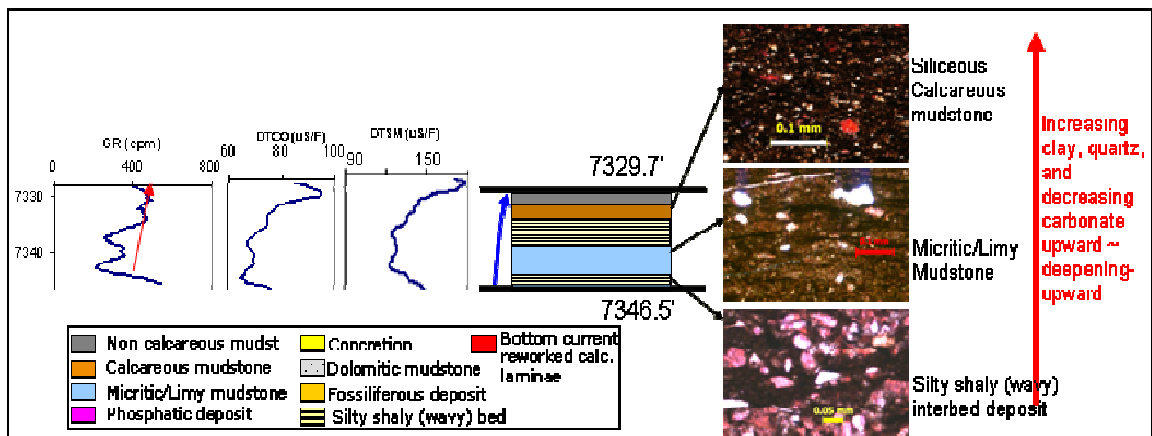
Appendix A.3.

Upward constant Gamma Ray Parasequence
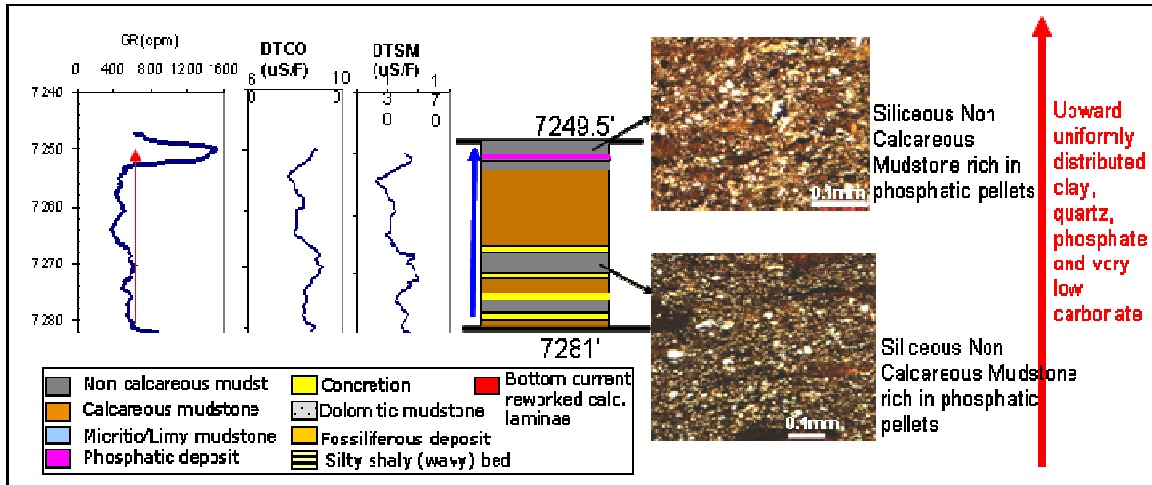
Gas content of the Lower Barnett Shale of Sol Carpenter H#7
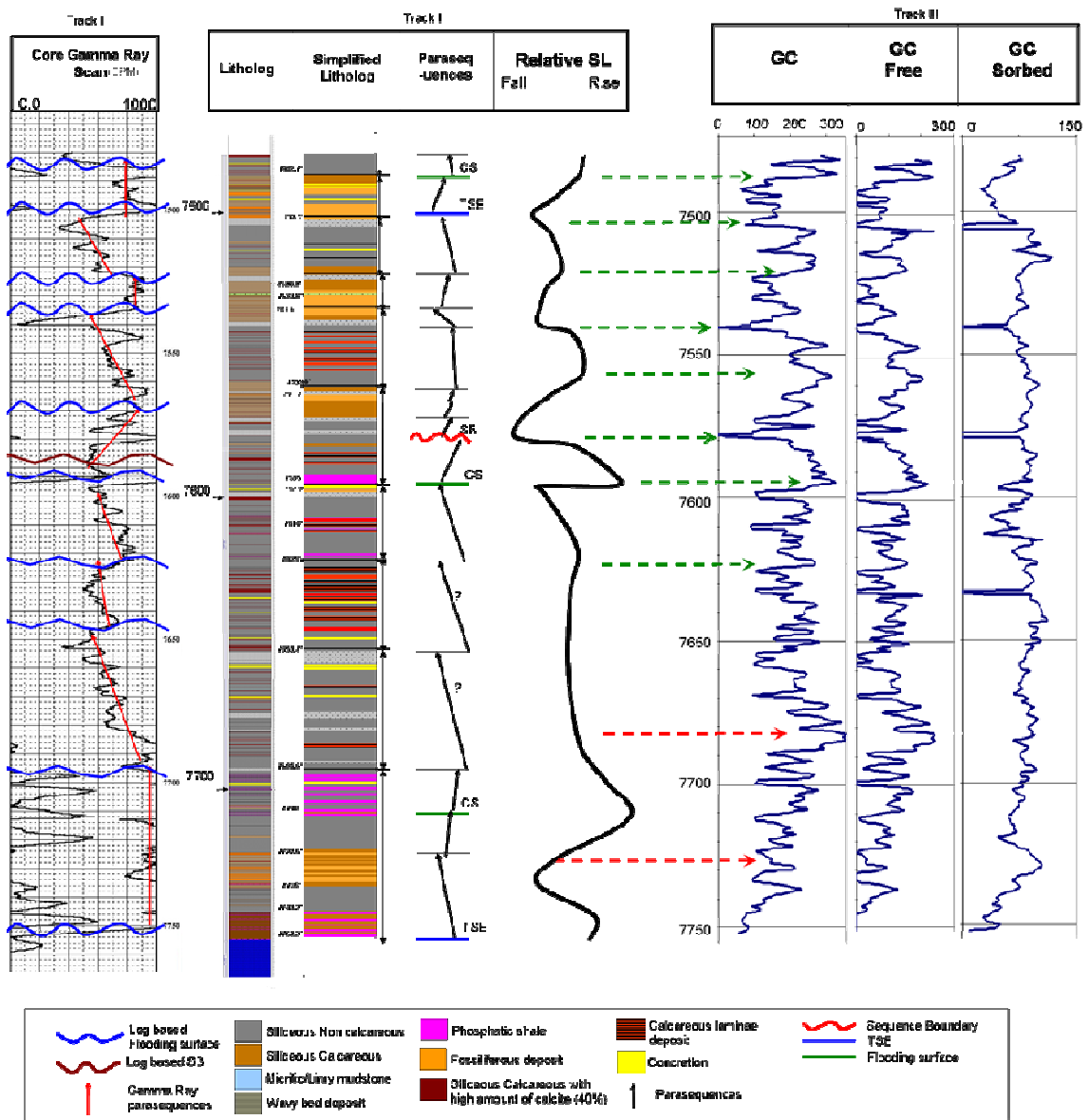
Gas content of the Lower Barnett Shale of John Porter #3
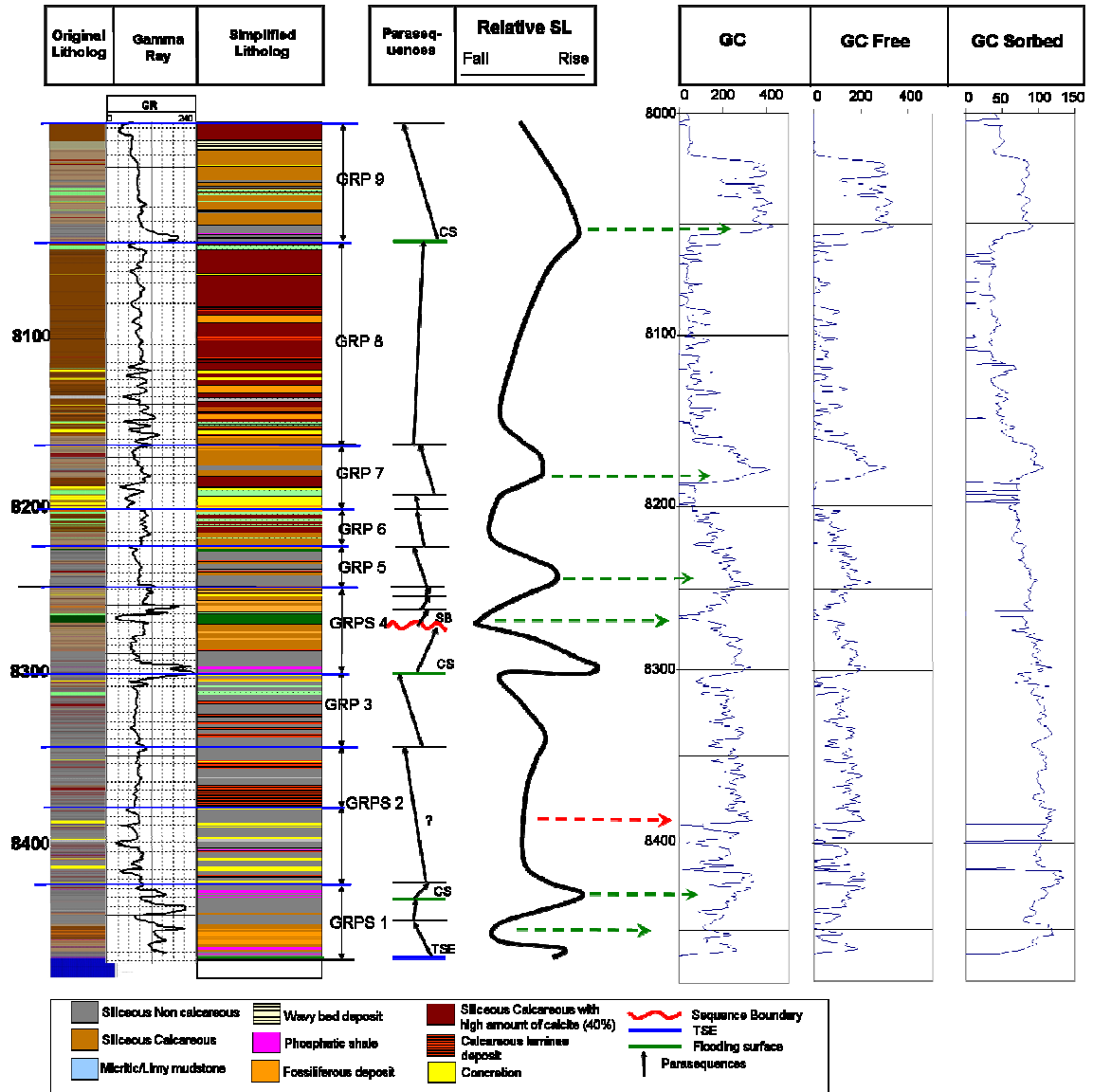
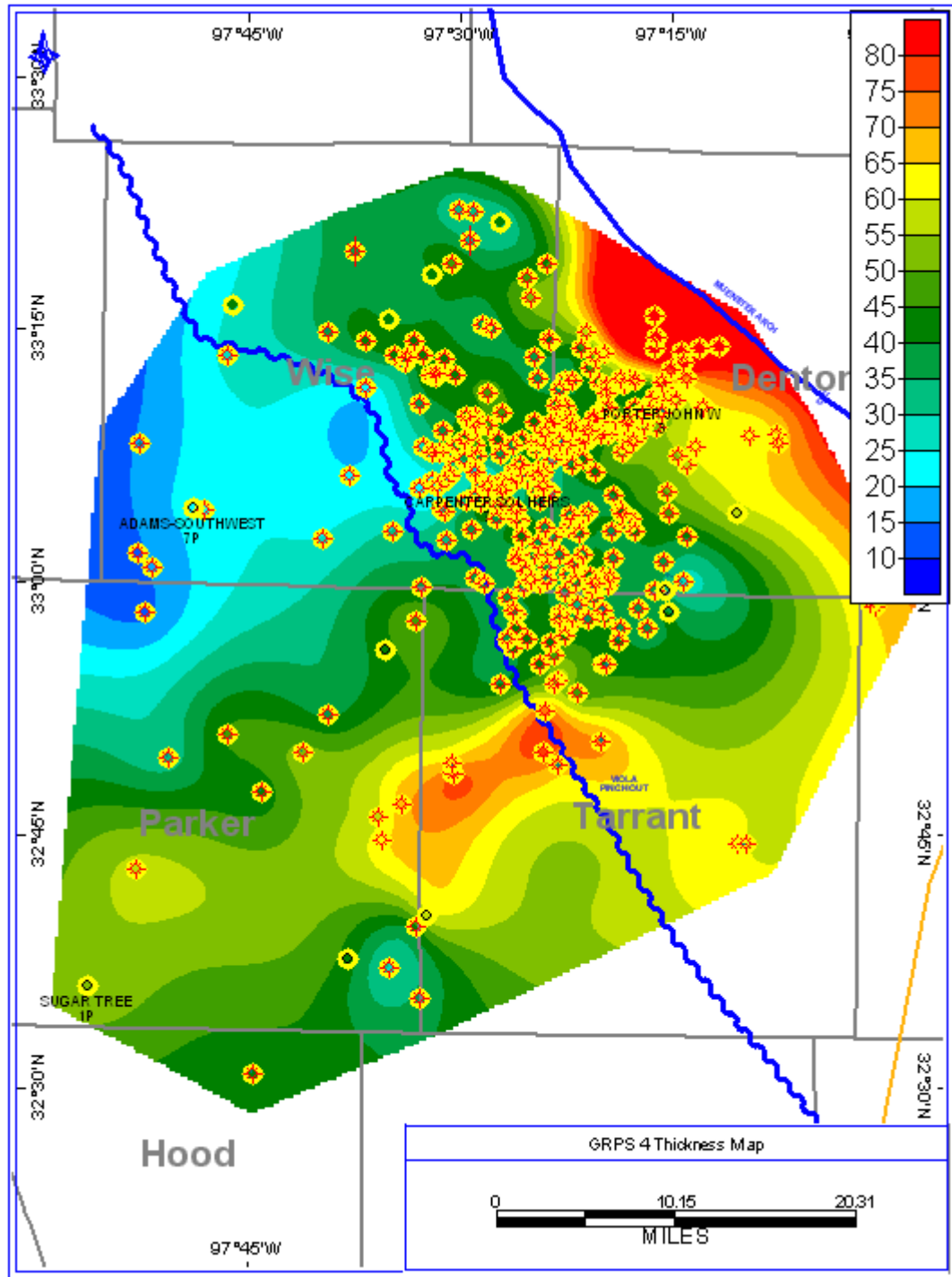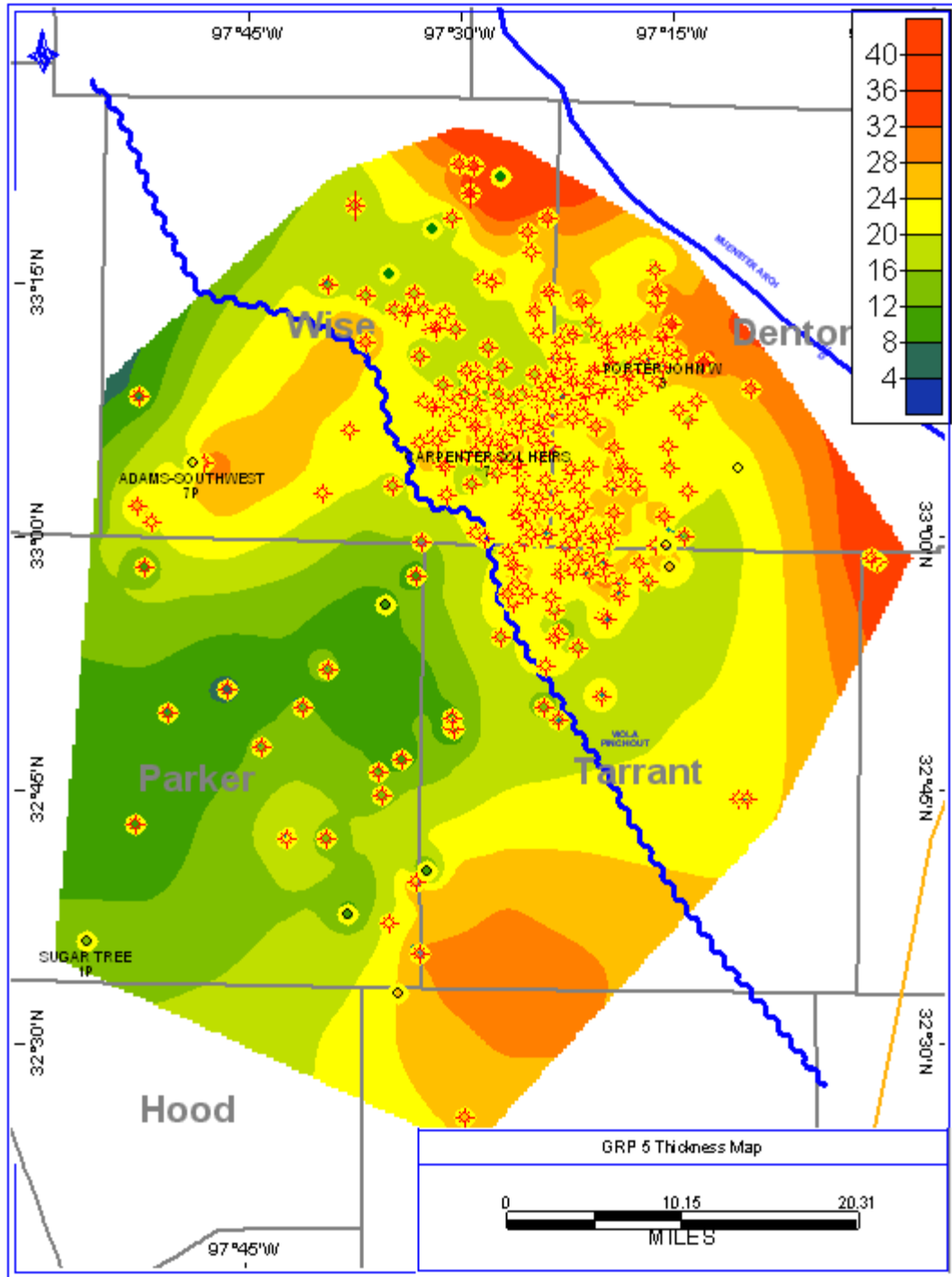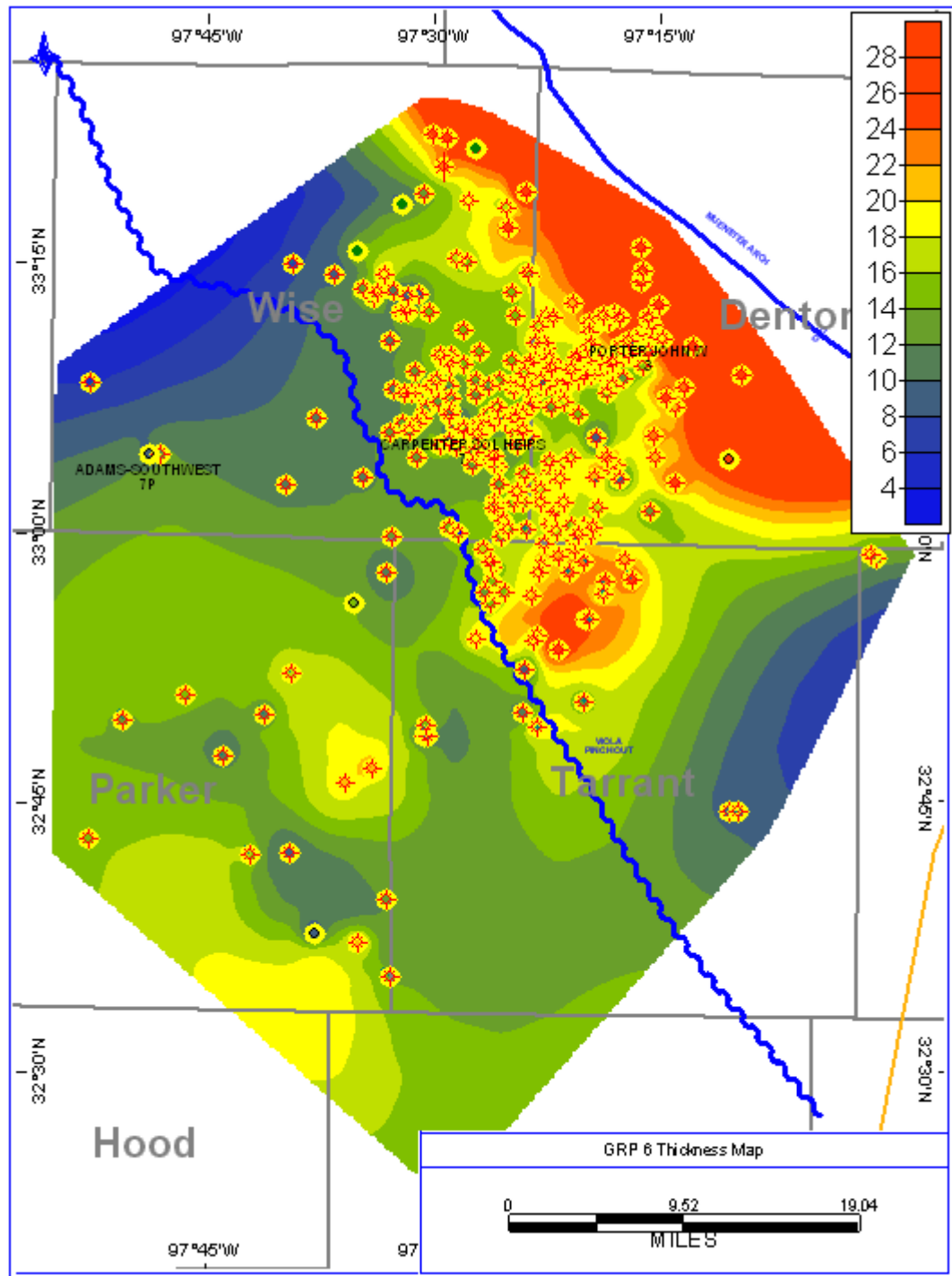## Appendix A.6.

Thickness maps of GRP and GRPS with well control locations
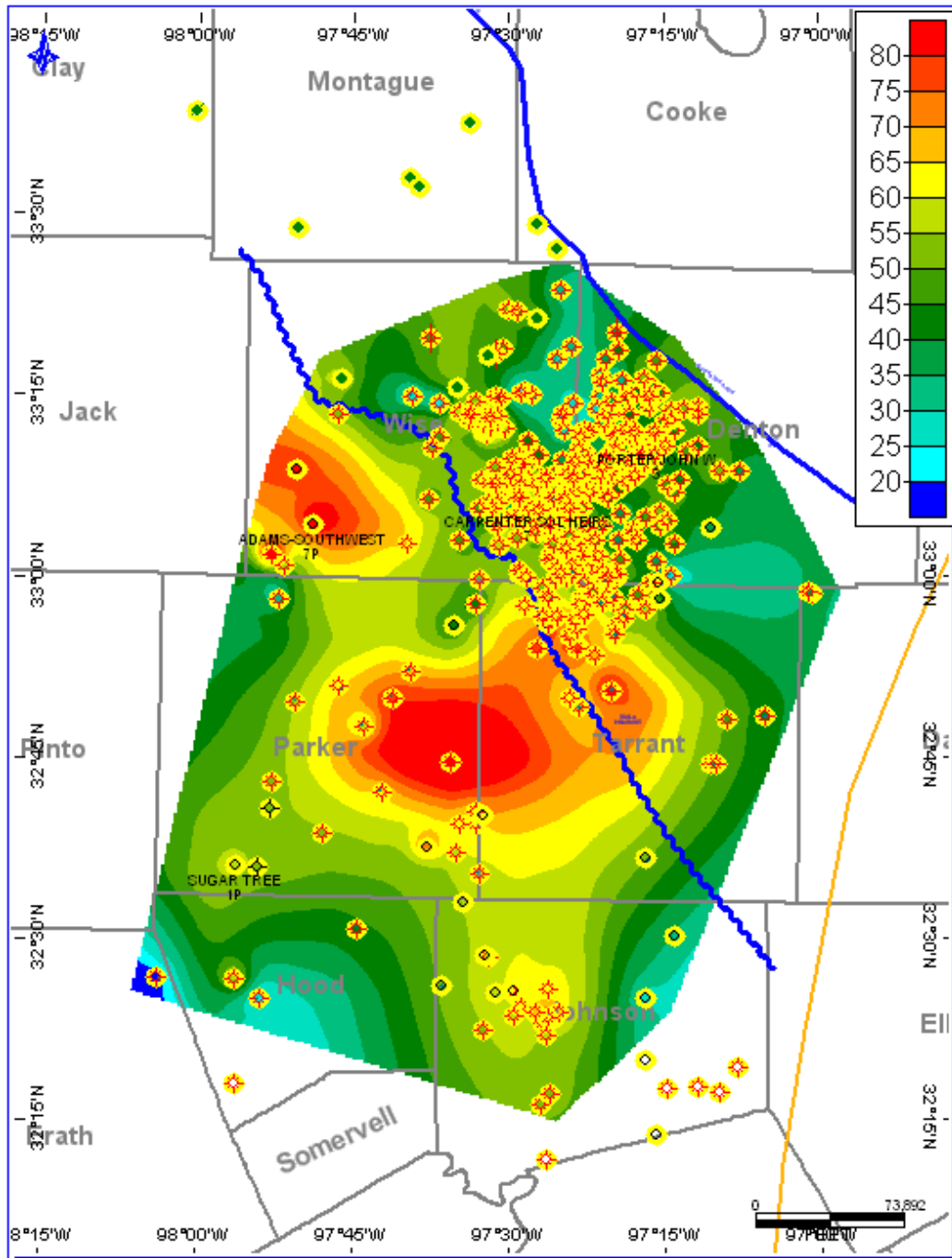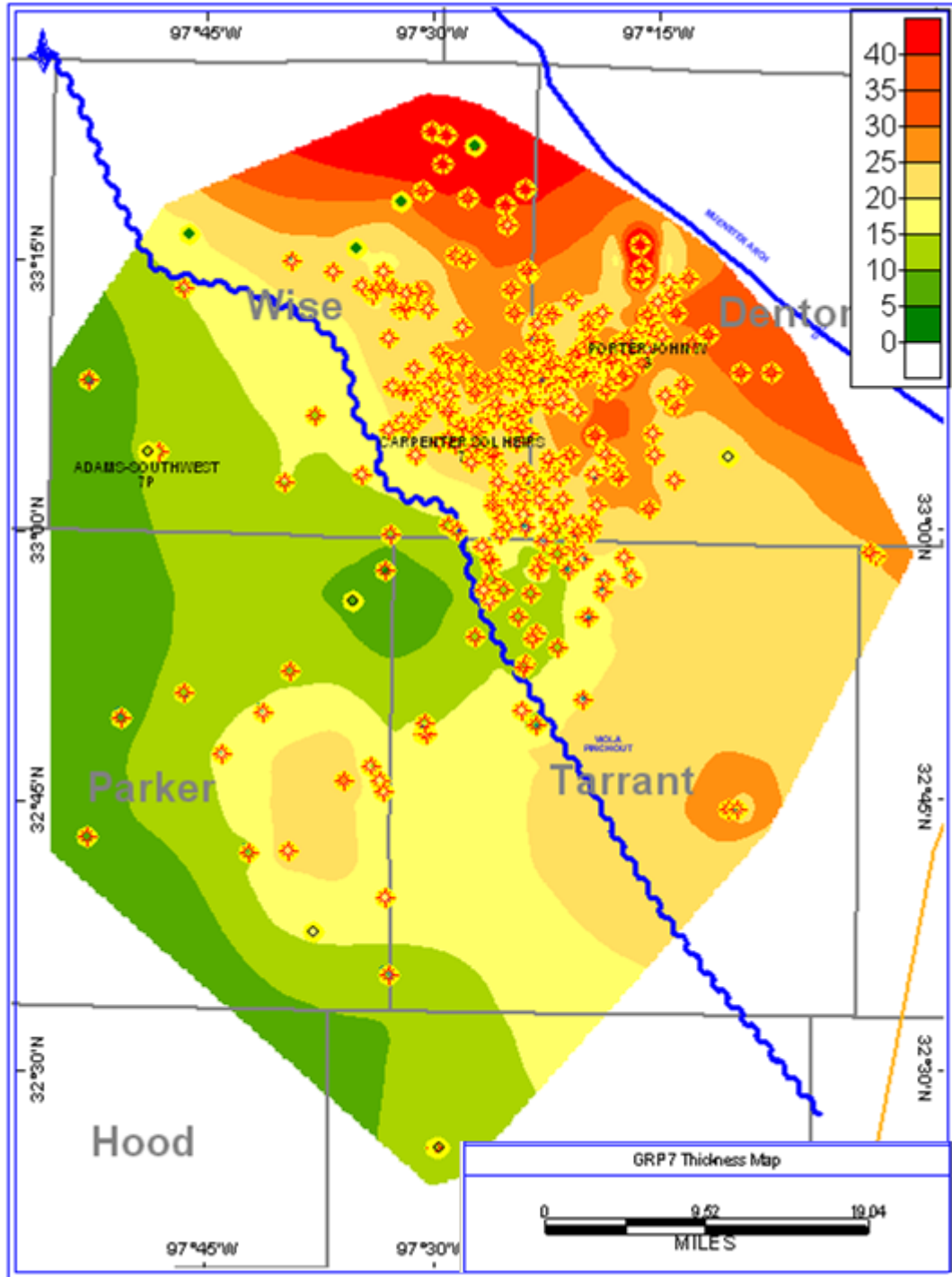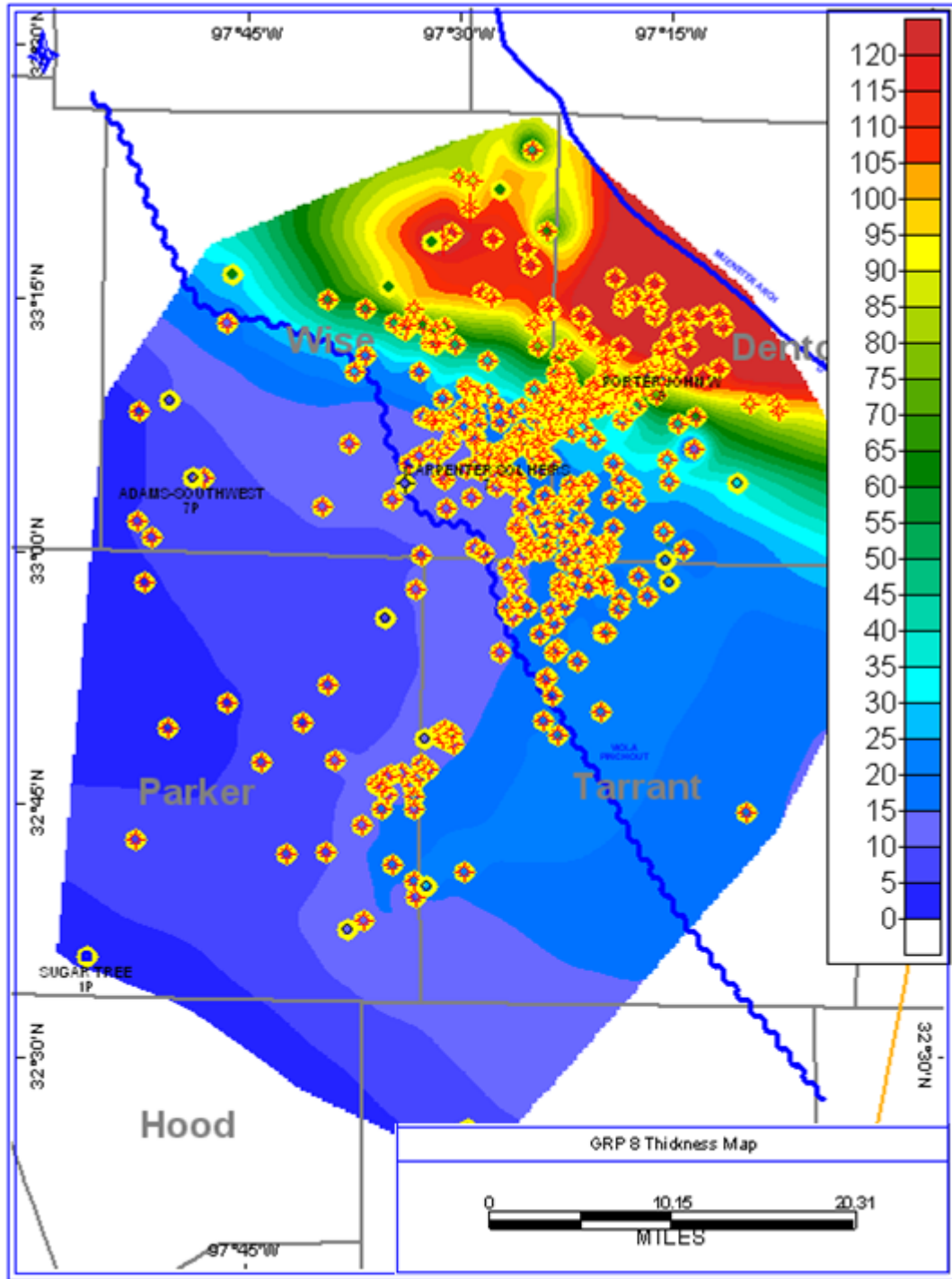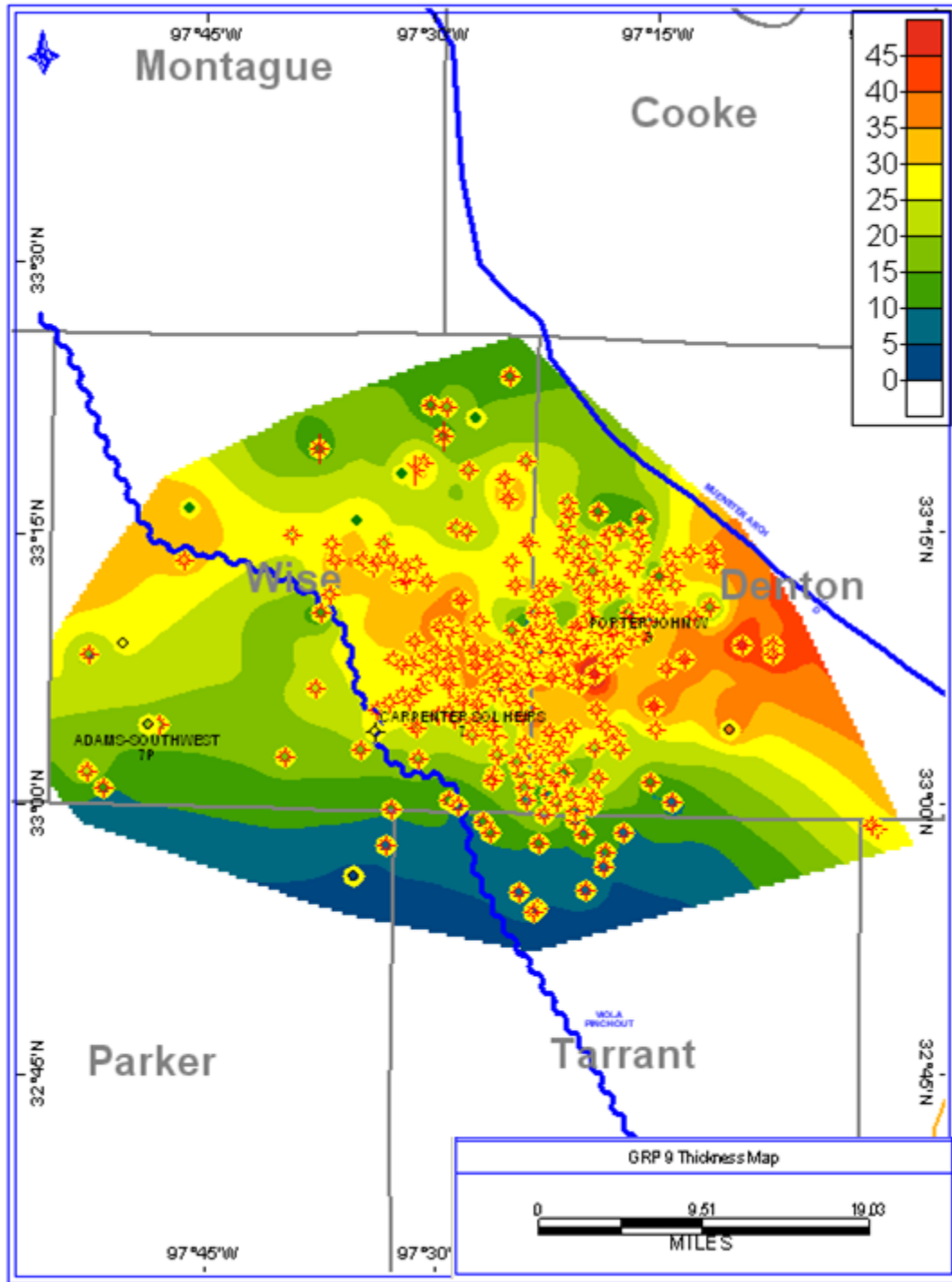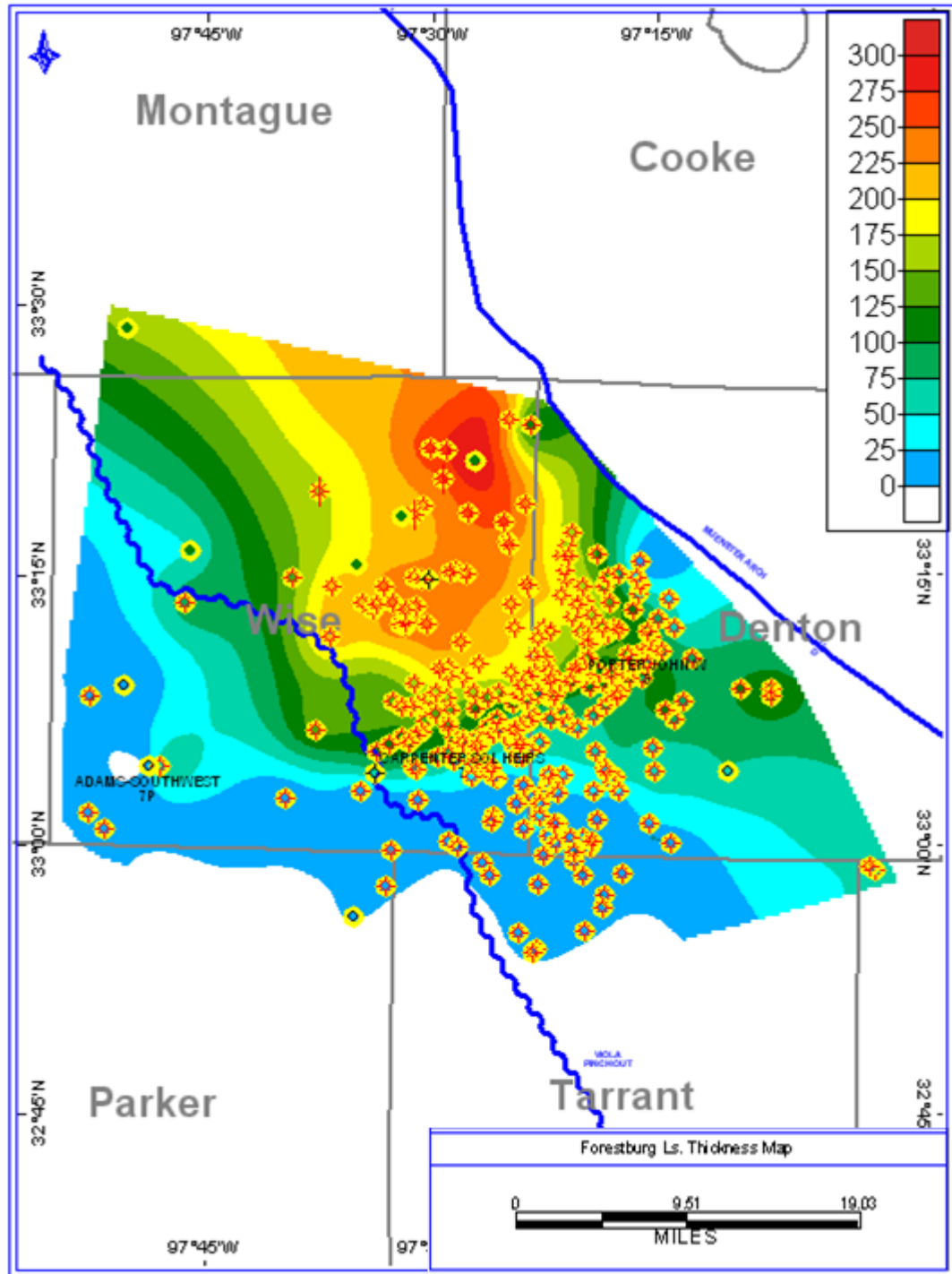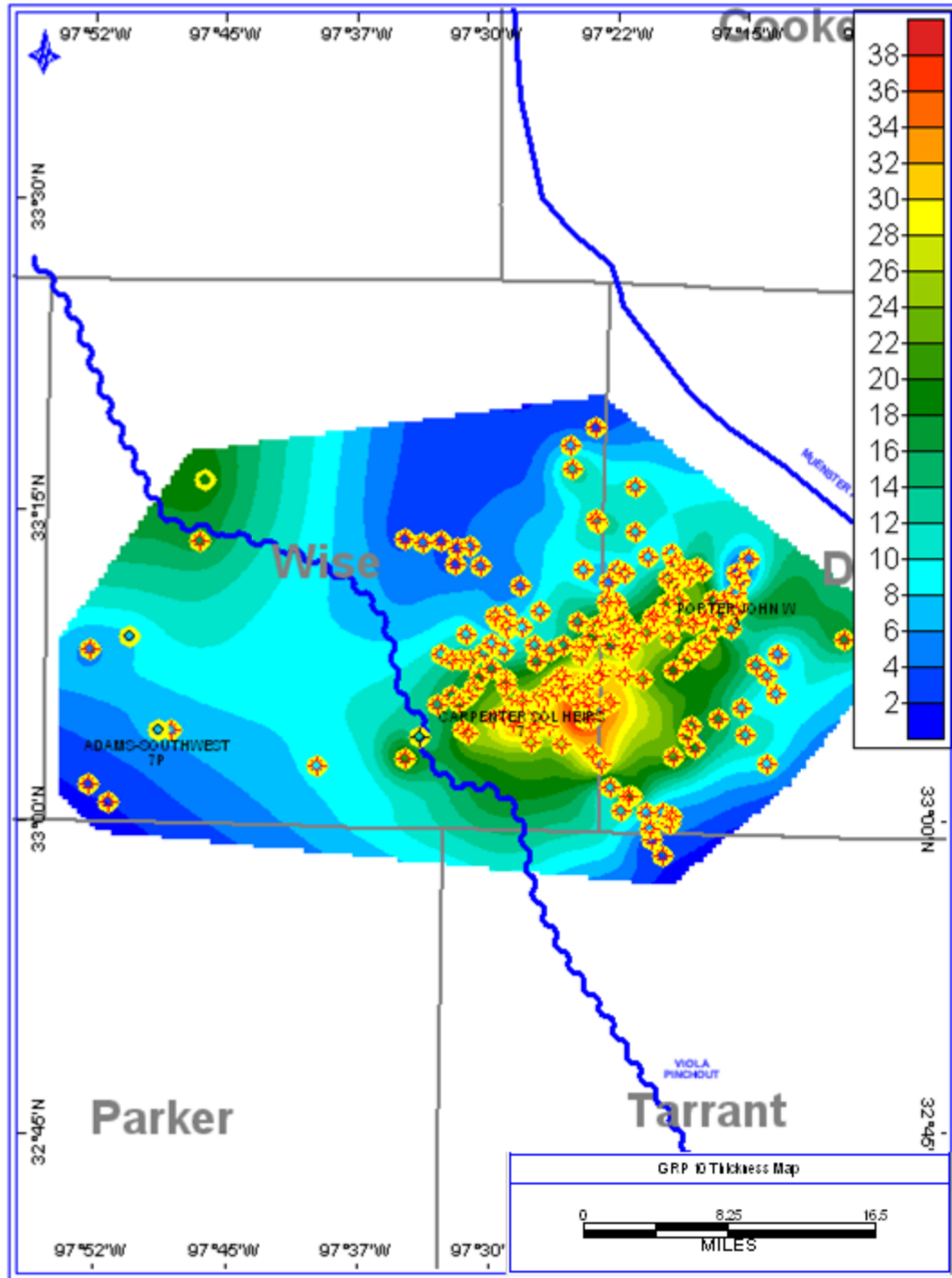

GRPS 1 Thickness map
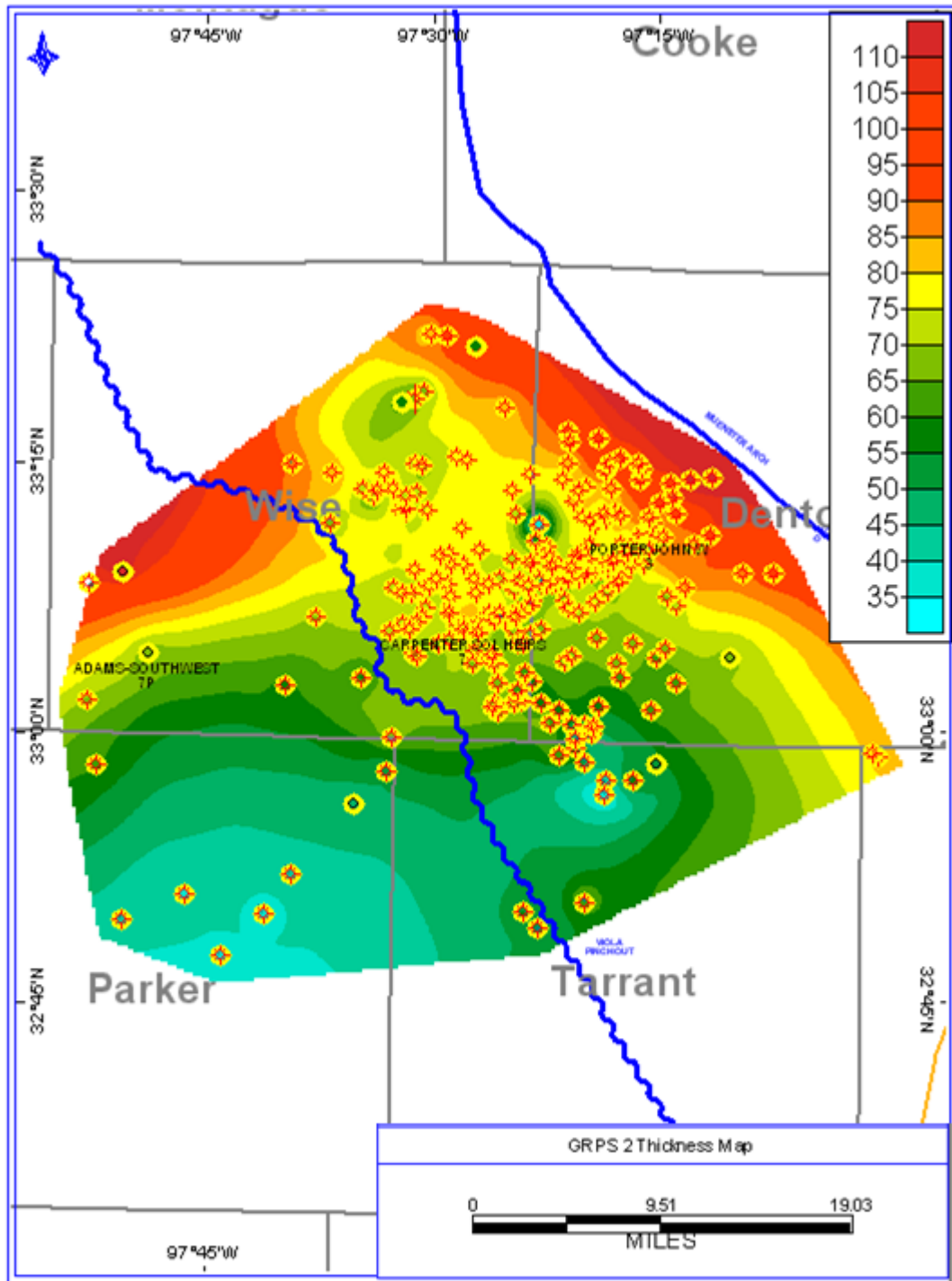
GRPS 2 Thickness map
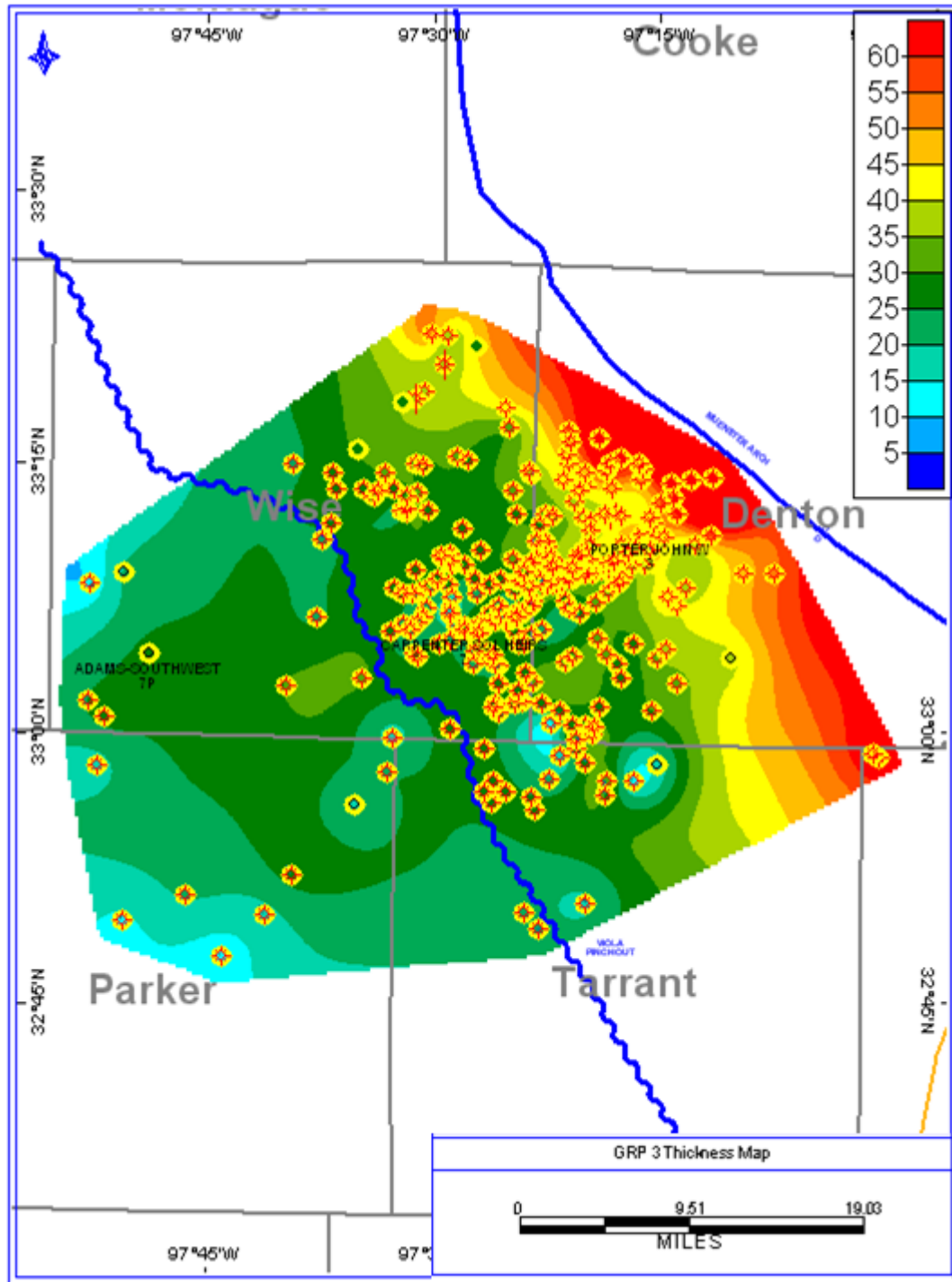
GRP 3 Thickness map

GRPS 4 Thickness map

170

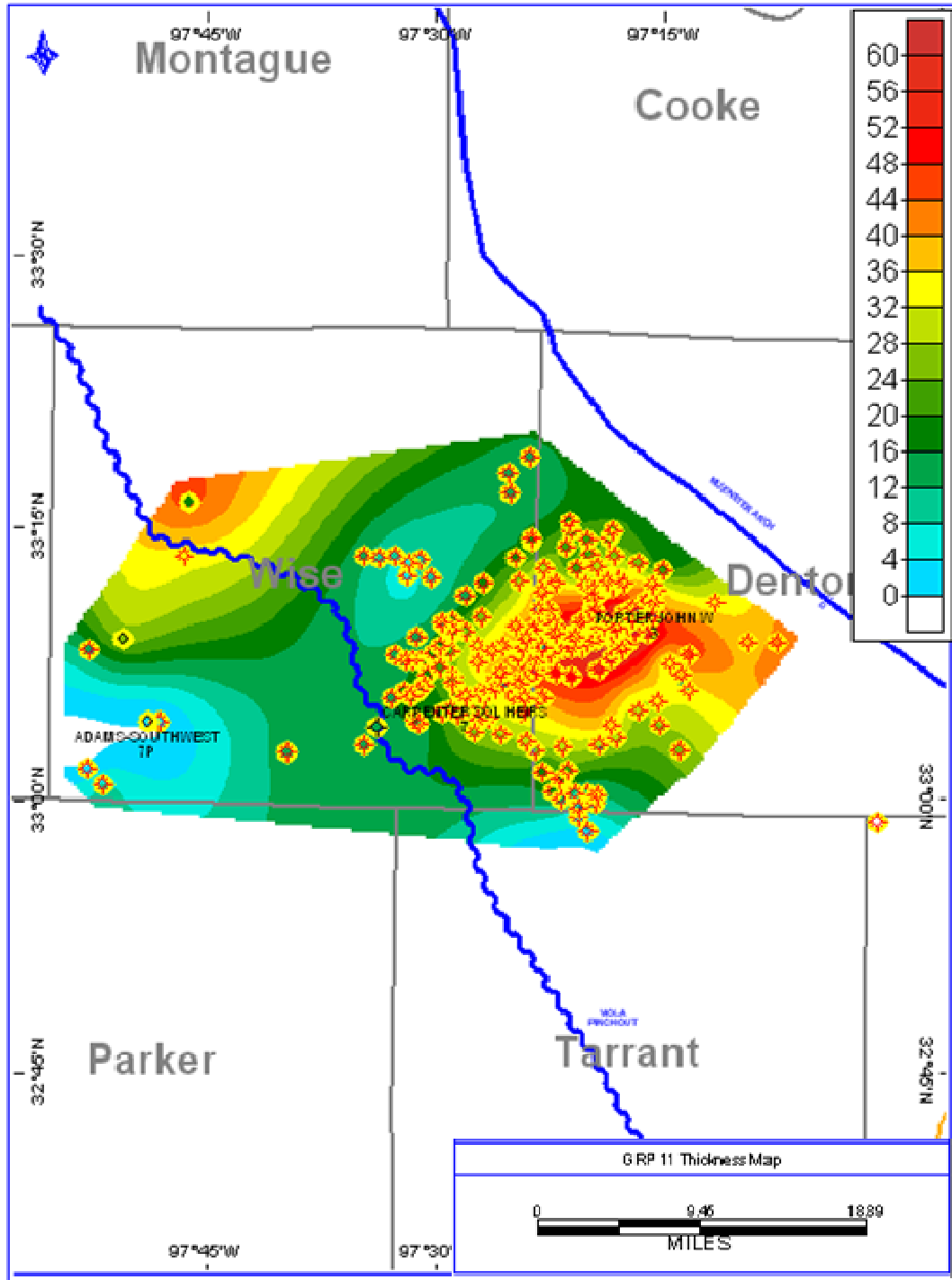GRP 5 Thickness map

GRP 6 Thickness map

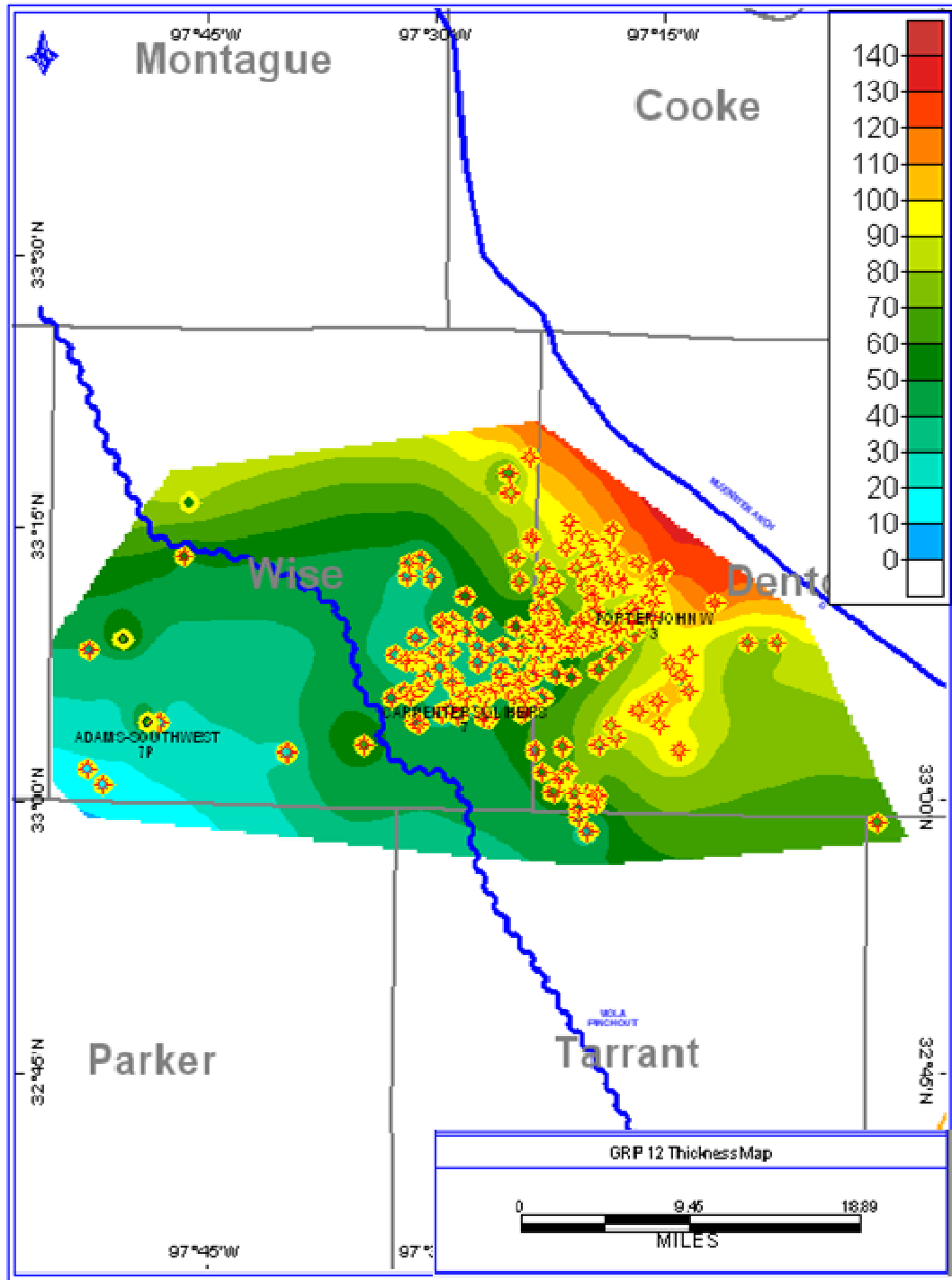GRP 7 Thickness map

GRP 8 Thickness map

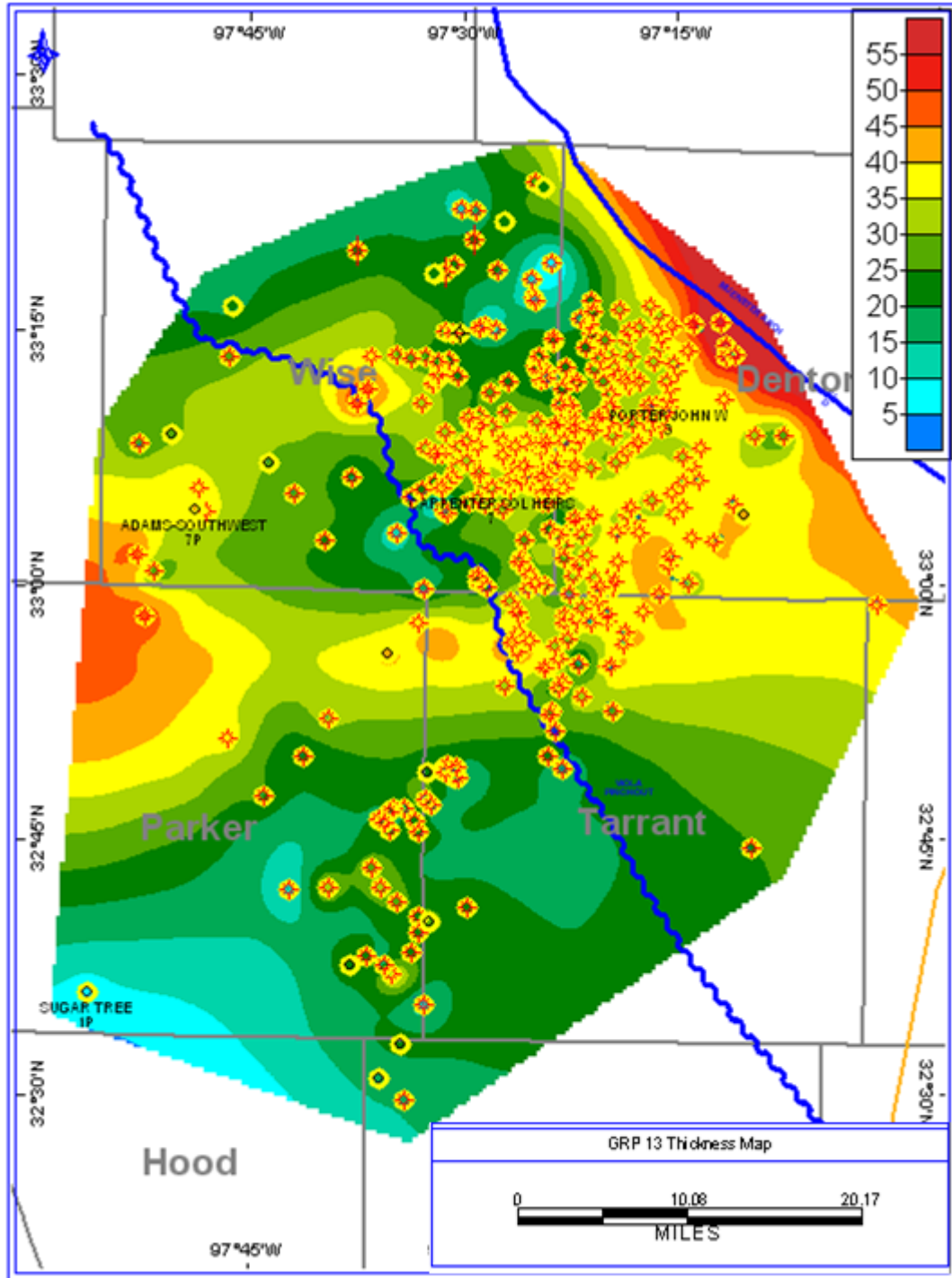GRP 9 Thickness map

Forestburg Limestone Thickness map
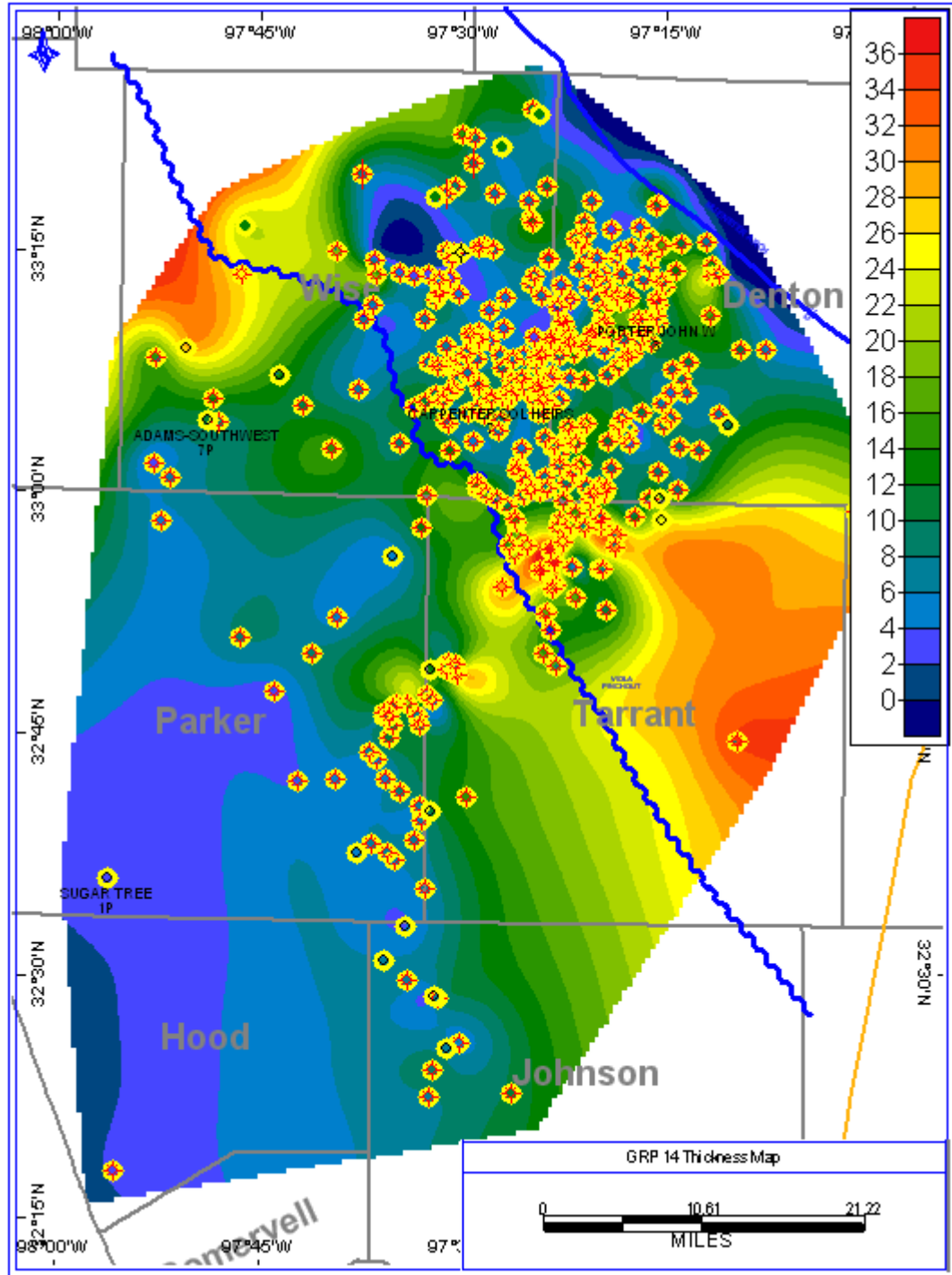
GRP 10 Thickness map

GRPS 11 Thickness map

GRP 12 Thickness map

GRP 13 Thickness map

GRP 14 Thickness map